

An interrogation into the role of p62 in the pluripotent state.

LOUISE FRANCES BULLEN

PhD 2020

Interrogation into the role of p62 in the pluripotent state.

LOUISE FRANCES BULLEN

A thesis submitted in partial fulfilment of the requirements of Manchester Metropolitan University for the degree of Doctor of Philosophy

Manchester Metropolitan University
School of Healthcare Science
Centre for Bioscience

PhD 2020

Acknowledgments

First, I would like to express my deepest thanks and respect to my Director of Studies, Professor Tristan McKay, for welcoming me into his research group 6 years ago and

continuing to give me opportunity, support, guidance and advice over the next several years. Thank you for believing in me even when I did not believe in myself and for encouraging me to do what I thought impossible. I will be eternally grateful. On a more personal note: I would never have moved to Manchester had I not worked with you, and my life has been forever changed for the better because of it.

Secondly, my sincere thanks to every member of the McKay lab, both past and present, but a special mention to Dr Lorna FitzPatrick, Dr Christopher Thornton and Alysha Burrows who have been there every step of the way. Thank you all for the academic support and advice, but mostly for sharing the highs and the lows, the laughs, commiserations, quizzes, McKay lab conference trips, dinners and wine!

Thank you also to every other colleague (and friend) at MMU and beyond who has ever given advice, provided materials, or encouraged my research, particularly Dr Stephen White at MMU and Dr Richard Harbottle and Dr Alicia Roig-Merino at DKFZ.

Finally, thank you to my wonderful family and friends for your unwavering love and support, as well as your kindness and understanding when I had to miss yet another important occasion to spend my time in the lab. A very special thank you to Tom, without whom I would have been writing this thesis while homeless. Words cannot express my gratitude and love; I could not have done any of this without you.

Contents

Chapter 1. 14

1.1. Stem cells

16

1.2. Embryonic Stem Cells (ESCs)	17
1.3. Introduction to induced pluripotent stem cells (iPSCs)	19
1.4. Methods of iPSC reprogramming	20
1.5. Benefits and drawbacks of using iPSCs in disease modelling	23
1.5.1. Disease modelling and clinical application for lysosomal storage disorders	26
1.6. Clinical application of iPSC	28
1.7. Mechanism of iPSC reprogramming.	30
1.8. Differences in mouse and human pluripotency	32
1.9. Autophagy	34
1.9.1. Introduction to Autophagy	34
1.9.2. Macro-autophagy	35
1.9.3. mTOR	36
1.9.4. p62 in autophagy	37
1.10. The role of autophagy in iPSC reprogramming	38
1.11. SQSTM1/p62 biology	41
1.12. p62 domains and mutations	42
1.12.1. Truncated human p62	43
1.12.2. PB1 domain.	44
1.12.3. ZZ-type zinc finger region	45
1.12.4. TRAF6 binding region	46
1.12.5. LC3 Interacting region	47
1.12.6. KEAP-1 Interacting region	47
1.12.7. UBA domain.	48
1.13. p62 in health and disease	50
1.13.1. Paget disease of the bone	50
1.13.2. Metabolic and cardiac disorders	51
1.13.3. p62 in cancer	52
1.13.4. Neurodegenerative disease	53
1.13.5. p62 and cancer stem cells	56
1.13.6. p62 in stem cells and pluripotency	57
1.14. Research statement and aims	58
1.15. Project aims and objectives:	61

2.1. Cell Culture	65
2.1.1. Primary fibroblast cell culture	65
2.1.2. Pluripotent stem cell culture	67
2.1.3. Cryopreservation of cells.	67
2.1.4. Thawing of cells	68
2.1.5. Preparation of gelatin and matrigel for coating cell culture plates.	68
2.1.6. Human iPSc Reprogramming	68
2.1.7. Reprogramming of inducible MEFs	70
2.1.8. Reprogramming of WT MEFs	70
2.2. Stem cell validation	71
2.2.1. Tri-lineage Differentiation of iPS cells	71
2.2.2. Immunostaining	71
2.2.3. Alkaline Phosphatase staining	73
2.2.4. Analysis of AP staining using ImageJ	73
2.3. Western blot	74
2.3.1. Western blot	74
2.3.2. Densitometry analysis of western blots using ImageJ	75
2.4. MitoTracker Red™ and LysoTracker Green™ live cell staining	76
2.5. Cloning	76
2.5.1. PCR amplification of mouse and human p62 genes to clone into pENTR1a	76
2.5.2. shRNA	79
2.5.3. Additional cloning vectors	80
2.5.4. Cloning: restriction digest and gel extraction	84
2.5.5. Cloning: Ligation	85
2.5.6. Cloning: Recombination	87
2.5.7. Cloning: Transformation and recovery.	87
2.5.8. Qiagen Mini and Midi-Prep DNA preparation.	88
2.5.9. Cloning: In-Fusion® cloning for site specific mutations	88
2.6. Transfection; virus production and quantification; and transduction.	90
2.6.1. Production of VSV-G psuedotyped lentivector using PEI.	90
2.6.2. Large- scale viral preparation	90
2.6.3. Small-scale viral preparation	91
2.6.4. Virus quantification	92

Chapter 3.	90	
3.1. Introduction		94
3.2. Objectives:		95
3.3. Inducible MEF reprogramming		95
3.4. WT-MEF reprogramming		101
3.5. hDF reprogramming		105
3.6. Conclusions		117
Chapter 4.	115	
4.1. Introduction		119
4.2. Objectives:		120
4.3. Human shRNA		121
4.3.1. Human shRNA design		121
4.3.2. Cloning and validation		124
4.3.3. Transfection and Transduction of sh(h)p62 in Hek293T cells.		128
4.3.4. Transduction into nhDFs		132
4.3.5. Conclusions		136
4.4. Human p62 overexpression		136
4.4.1. Design, cloning and validation of human p62 overexpression construct.		136
4.4.2. Conclusions		141
4.5. pBABE-puro HA-p62 and pBABE-puro HA-p62-LIR		141
4.6. pBMN mCherry- p62 retroviruses.		144
4.7. Truncated- hp62 overexpression plasmid		152
4.8. Mouse p62 cloning		159
4.8.1. Introduction		159
4.8.2. Mouse shRNA design		159
4.8.3. Cloning and validation		160
4.9. Mouse p62 overexpression.		163
4.9.1. Design, cloning and validation of mouse p62 overexpression construct.		163
4.9.2. Infusion cloning to create specific functional mutants of mouse p62.		164
4.9.3. Recombination into SFFV-lentiviral vector.		170
4.10. Conclusions		175
Chapter 5.	174	
5.1. Introduction		178

5.2. Objectives	178
5.3. Characterisation of hDF-p62 ^{-/-}	179
5.4 iPSC reprogramming	193
5.4. Conclusions	210
Chapter 6.	209
6.1. Introduction	212
6.2. Objectives	212
6.3. iPSC reprogramming and colony analysis	213
6.4. Tri-lineage differentiation	229
6.5. Discussion	234
Chapter 7.	234
References.....	258
Appendices.....	27

List of Figures

Figure	Title	Page no.
--------	-------	----------

Figure 1.1	Deviation of ESCs	17
Figure 1.2	ESCs are capable of differentiating into cells from all three germ layers	19
Figure 1.3	Summary of the three phases of iPSC reprogramming	30
Figure 1.4	Overview of autophagic processing with the selective autophagy adaptor, p62	35
Figure 1.5	The role of p62 in autophagy	37
Figure 1.6	The role of autophagy in iPSC reprogramming	40
Figure 1.7	Basic protein structure of p62	45
Figure 1.8	Overview of project aims and objectives	63
Figure 2.1	Brief outline of the McKay Lab hDF reprogramming protocol	70
Figure 2.2	ImageJ iPSC colony analysis	75
Figure 2.3	Mouse p62 overexpression plasmid	78
Figure 2.4	Truncated human p62 overexpression plasmid	79
Figure 2.5	pENTR1A minimal cloning vector	79
Figure 2.6	pEX-A128 minimal vector containing p62 shRNA sequences	80
Figure 2.7	pLL 3.7 shRNA destination lentivector	81
Figure 2.8	pUMVC packaging plasmid for producing MuLV retroviral particles	82
Figure 2.9	pCMV-VSV-G envelope protein for producing lentiviral and MuLV retroviral particles	83
Figure 2.10	pBABE-puro-HA-p62 and pBABE-puro-HA-p62-LIR	84
Figure 2.11	pBMN-mCherry-p62 (Δ UBD) and pBMN-mCherry-p62 (W340A/ Δ UBD)	85
Figure 2.12	Basic schematic of cut-and-paste based cloning	87
Figure 2.13	Basic principle of In-fusion® cloning	90

Figure 3.1	The STEMCCA multicistronic 2A-OKSM cassette was stably transduced into 'reprogrammable mice'	97
Figure 3.2	iPSC reprogramming of JB7 & JB8 MEFs	99-100
Figure 3.3	Immunofluorescent cell staining for SSEA1, a key marker of pluripotency in mouse	101-102
Figure 3.4	Reprogramming of WT-MEFs to miPSCs	103-104
Figure 3.5	Immunofluorescent cell staining for key markers of pluripotency in miPSC colonies	105-106
Figure 3.6	Control hDF throughout iPSC reprogramming and at an early passage	108
Figure 3.7	CLN6 Batten's disease patient hDFs throughout iPSC reprogramming and at an early passage	109
Figure 3.8	CLN7 Batten's disease patient hDFs throughout iPSC reprogramming and at an early passage	110
Figure 3.9	P10 CLN7 iPSC colonies are well established & morphologically typical	111
Figure 3.10	Immunofluorescent cell staining in P10 CLN7 iPSC to confirm pluripotency (Tra160 + Oct4)	113
Figure 3.11	Immunofluorescent cell staining in P10 CLN7 iPSC to confirm pluripotency (Tra181 + Sox2)	113
Figure 3.12	Immunofluorescent cell staining in P10 CLN7 iPSC to confirm pluripotency (Nanog)	115
Figure 4.1	Design of miRNA sequences for sh(h)p62 lentiviral construct	117
Figure 4.2	Construction of 'triple-hit' shRNA sequence for human p62 and the overall design concepts	124
Figure 4.3	Cloning of shRNA for human p62 into PLL3.7 destination vector	126
Figure 4.4	Successful cloning of sh(h)p62 constructs into pLL3.7 lentiviral vector	127-128
Figure 4.5	Validation of the sh(h)p62 construct in Hek293T cells	130-131
Figure 4.6	p62 protein knock-down in Hek293Ts using sh(h)p62 shRNA	133
Figure 4.7	Transduction of nhDFs with sh(h)p62 lentivirus & p62 protein knock-down	136
Figure 4.8	Cloning of hp62 overexpression cassette into PENTR1A minimal vector	138
Figure 4.9	Sequencing of hp62 pENTR1A clones demonstrates successful cloning	139

Figure 4.10	Sequencing of hp62 SFFV clones demonstrates successful cloning	141
Figure 4.11	Preparation of pBABE-puro-HA-p62 and pBABE-puro-p62-LIR retroviral plasmids	143
Figure 4.12	Puromycin selection of retrovirus transduced hDF-p62 ^{-/-}	145
Figure 4.13	Retroviral pBMN-mCherry-p62 vectors	147
Figure 4.14	Transfection & transduction of Hek293T cells with pBMN-mCherry-p62 retroviruses	149
Figure 4.15	iPSC reprogramming of hDF-p62 ^{-/-} + p62 overexpression mutant retroviruses	151
Figure 4.16	iPSC reprogramming of hDF-p62 ^{-/-} + p62 overexpression mutant retroviruses	152
Figure 4.17	Truncated human p62	154
Figure 4.18	Transfection, and transduction of hp62-trunc in Hek293Ts	156-157
Figure 4.19	hDF-p62 ^{-/-} transduced with hp62-trunc-GFP lentivirus	159
Figure 4.20	Cloning of shRNA for mouse p62 into pLL3.7 destination vector	162
Figure 4.21	Cloning of sh(m)p62 constructs into pLL3.7 lentiviral vector	163
Figure 4.22	Mouse p62 overexpression vector is cloned into PENTR1A minimal cloning vector	165
Figure 4.23	Desired functional mutations of mouse p62 as they relate to the domain architecture of the protein	166
Figure 4.24	(A-C) Successful mouse p62 mutation In-Fusion® cloning in PENTR1A	167
Figure 4.25	(A-D) Successful cloning of mp62 in SFFV lentiviral vectors	168-170
Figure 4.26	Successful cloning of mp62 in SFFV lentiviral vector- mp62-SFFV	172-175
Figure 5.1	p62 and LAMP1 immunofluorescent cell staining in WT-MEFs (40x)	181
Figure 5.2	p62 and LAMP1 immunofluorescent cell staining in WT-MEFs (63x)	182
Figure 5.3	p62 and LAMP1 immunofluorescent cell staining in hDF-p62 ^{-/-} fibroblasts (40x)	184
Figure 5.4	p62 and LAMP1 immunofluorescent cell staining in hDF-p62 ^{-/-} fibroblasts (63x)	185

Figure 5.5	p62 and LAMP1 immunofluorescent cell staining in nhDFs (40x)	186
Figure 5.6	p62 and LAMP1 immunofluorescent cell staining in nhDFs (63x)	187
Figure 5.7	No primary antibody negative controls	188
Figure 5.8	Western blot analysis of various fibroblasts for p62 protein	189
Figure 5.9	MitoTracker™ staining on early passage hDFs	191-192
Figure 5.10	MitoTracker™ and p62 staining on early passage hDFs	193
Figure 5.11	nhDF vs hDF-p62 ^{-/-} iPSC reprogramming	197
Figure 5.12	Primary colony analysis of hDF-p62 ^{-/-} reprogramming.	199-200
Figure 5.13	Comparison of nhDF and hDF-p62 ^{-/-} iPSC primary colony formation (P0).	202-204
Figure 5.14	iPSC reprogramming of nhDF and hDF-p62 ^{-/-} , Passage 1	206-207
Figure 5.15	Analysis of P1 nhDF and hDF-p62 ^{-/-} iPSC colonies	208
Figure 5.16	hDF-p62 ^{-/-} colonies rapidly lose pluripotency.	210
Figure 6.1	nhDF and sh(h)p62 nhDF comparative reprogramming experiments.	215
Figure 6.2	nhDF vs p62 null hDF reprogramming. Day 25, primary (P0) iPS colonies stained with Alkaline Phosphatase	217
Figure 6.3	nhDF and nhDF-shp62 comparative reprogramming experiments (P0)	219
Figure 6.4	iPSC reprogramming of nhDF-shp62 cells and nhDF controls (P1)	221
Figure 6.5	nhDF and nhDF-shp62 comparative reprogramming experiments (P1)	223
Figure 6.6	Phase and fluorescence imaging of nhDF and nhDF-shp62 derived iPS cells at passage 2	225
Figure 6.7	Phase and fluorescence imaging of nhDF and nhDF-shp62 derived iPS cells at passage 3.	226
Figure 6.8	Phase imaging of nhDF and nhDF-shp62 derived iPS cells at passage 5	228
Figure 6.9	Phase and fluorescence imaging of nhDF and nhDF-shp62 derived iPS cells at passage 9	229

Figure 6.10	Phase and fluorescence imaging of nhDF-shp62 embryoid bodies (EBs) after 8 days in suspension culture.	231
Figure 6.11	Phase imaging of nhDF-shp62 embryoid bodies (EBs) after replating onto adherent plates and 8 days of outgrowth	231
Figure 6.12	nhDF-shp62 'iPS' cells subjected to 16 days of a spontaneous differentiation protocol and stained for β III-Tubulin	233
Figure 6.13	nhDF-shp62 'iPS' cells subjected to 16 days of a spontaneous differentiation protocol and then stained for Sox17	234
Figure 6.14	nhDF control iPSC were subjected to 16 day spontaneous differentiation protocol stained positive for both β III-Tubulin and Sox17	235

List of Tables

Table	Title	Page no.
Table 1.1	An overview of iPSC reprogramming methods	21
Table 1.2	Key mutations in mouse and human p62	49
Table 2.1	Primary antibodies used in ICC experiments	72
Table 2.2	Secondary antibodies used in ICC experiments	73
Table 2.3	Plasmids for cloning and transduction experiments	80
Table 2.4	Restriction enzymes used in cloning experiments	85
Table 4.1	miRNA sequences predicted by the SplashRNA algorithm to induced potent p62 knock-down in human cells	122
Table 4.2	miRNA sequences predicted by the SplashRNA algorithm to induced potent p62 knock-down in mouse cells	160

NB. A list of abbreviations can be found at Appendix 1

Abstract

The reprogramming of somatic cells to induced pluripotent stem cells (iPSC) has huge potential for disease modelling, drug screening and regenerative medicine, and is an extremely important area of

research and development across the globe. The inefficiency of the reprogramming process from somatic cell to pluripotency using established gold-standard methodologies is a major roadblock to realising the full potential of iPSC in cell therapy. The sequestosome protein p62 is an evolutionarily highly conserved scaffolding protein with roles in a range of crucial cell regulatory processes including autophagy, nutrient sensing and inflammation as well as being involved in the pathology or causation of various diseases. The canonical role of p62 is to aggregate ubiquitinated proteins to form the sequestosome, a precursor to the autophagosome, in the induction of autophagy under conditions of stress or starvation, but it has six known functional domains with a range of binding partners including NRF2, NF- κ B, Traf6 and LC3. In addition, p62 directly binds to ubiquitinated proteins involved in the anti-oxidant response and inflammation and mediates mitophagy. There is an emerging role for autophagy in iPSC reprogramming, and a growing body of evidence for the role of p62 in maintaining stemness in cancer stem cells. As yet, the role of p62 in establishing or maintaining pluripotency in iPSCs has not been elucidated. I have created a 'genetic-manipulation toolbox' including overexpression, shRNA and functional mutants of p62 in order to assess the mechanistic role of p62 in iPSC reprogramming and maintenance of pluripotency. Utilising p62 null patient fibroblasts, and lentiviral based shRNA to create a stable p62 knock-down cell line, I have established a novel role for p62 in the maintenance of the pluripotent state. Future works will further utilise the tools and cell lines I have created to elucidate the mechanisms by which p62 exerts its effects on the pluripotent state.

Chapter 1. Introduction

Chapter 1: Introduction

1.1. Stem cells

A stem cell is defined as a cell with the capacity for unlimited self-renewal, coupled with the ability to differentiate into one or more cell types. Stem cells exist in the developing embryo and in the adult (Zakrzewski, *et al*, 2019). In the first days of embryonic development, the one-cell zygote begins to undergo a series of cell divisions: these cells are totipotent, meaning they are capable of differentiating into every cell of the body and the extra-embryonic tissues required to support the developing embryo and later fetus (Zakrzewski, *et al*, 2019). At around Day 2-3 in mice, and Day 5 in humans, the early blastocyst forms, made up of an outer layer of trophoblast that goes on to form extraembryonic tissues such as the placenta; and an asymmetric ball of cells called the inner cell mass (ICM) (Figure 1.1) (Chagastelles and Nardi, 2011; Rossant and Tam, 2017). Cells within the ICM are pluripotent stem cells that have the capacity to go on to differentiate into the three germ layers: ectoderm, endoderm and mesoderm. These three germ lineages then go on to further differentiate into all cell types in the human body (Chagastelles and Nardi, 2011; Mado, 2008). As the cells of the developing fetus begin to differentiate and become more specialised, their potency becomes more limited. Multipotent cells, such as those in each of the three germ layers, can differentiate into multiple cell types, but only within a specific lineage. For example, ectoderm cells go on to differentiate into the cells of the central nervous system; the endoderm gives rise to the internal organs such as the liver and pancreas; and the mesoderm differentiates into cells comprising the skeleton and muscles (Kiecker *et al*, 2016; Elshazzy *et al*, 2021).

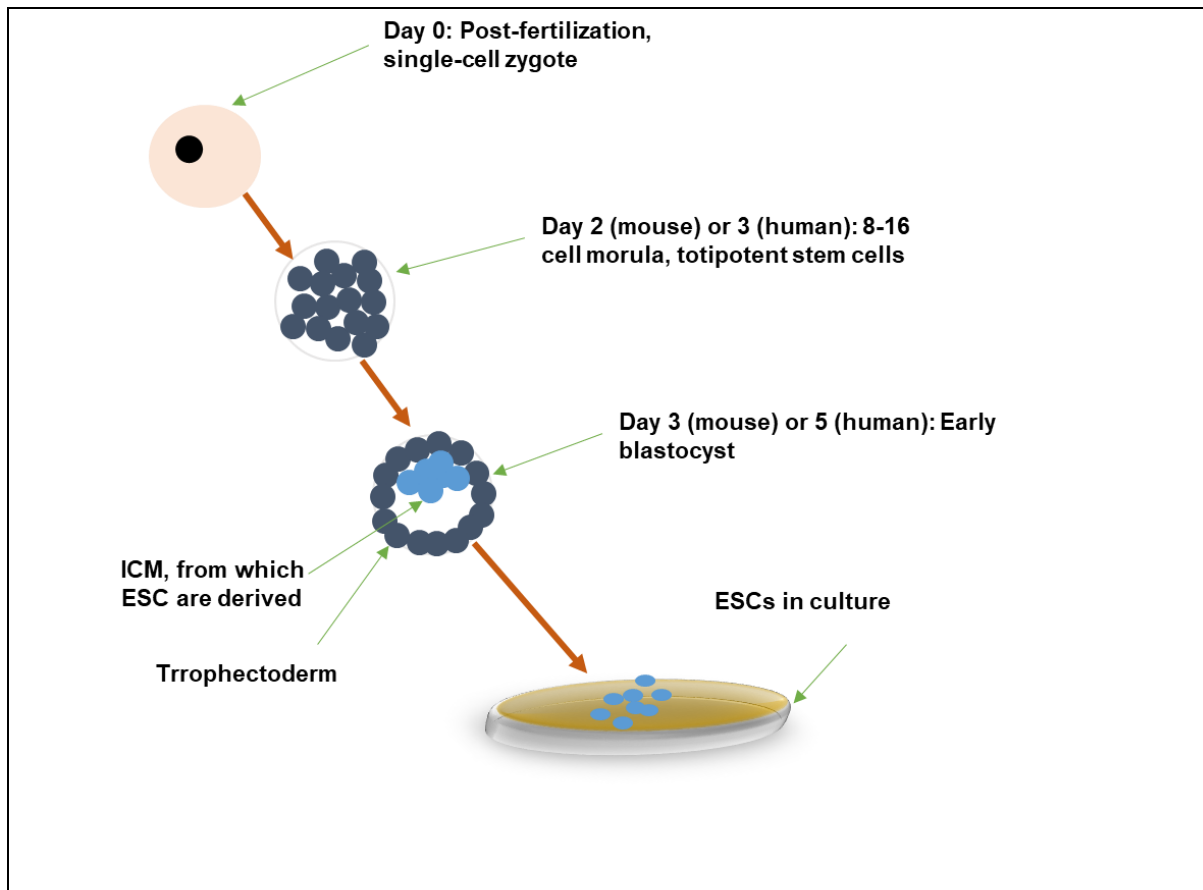


Figure 1.1: Derivation of ESCs. The totipotent cells of the zygote form an early blastocyst at around embryonic Day 3 in mice and Day 5 in humans. The blastocyst is made up of the trophectoderm, which goes on to form extra-embryonic tissues including the placenta and the ICM, which goes onto form all cells of the body. ESCs are pluripotent cells derived from the ICM of a blastocyst that can be maintained in culture in the lab.

1.2. Embryonic Stem Cells (ESCs)

ESCs are pluripotent stem cells derived from the ICM of the blastocyst and maintained in culture. ESCs can be cultured long-term, whereby they demonstrate the defining characteristics of pluripotent stem cells: the ability to proliferate indefinitely and the capacity for differentiation into cells from all three germ layers (Figure 1.2) (Gepstein, 2002; Vazin and Freed, 2010). The first mouse ESCs (mESCs) were derived in 1981 by culturing cells directly from the ICM in media conditioned by an established embryonal carcinoma cell line (Martin, 1981). Thompson *et al.* first derived human ESCs (hESCs) in the lab in 1998, by disrupting the human blastocyst and maintaining colony-forming pluripotent cells in long-term

culture. These cultured ESCs were able to form teratomas containing cells from all three germ layers when injected into immunodeficient mice and expressed key markers of pluripotency such as alkaline phosphatase, SSEA3, Tra-160, and Tra-181. This opened up a completely new field of developmental biology, the potential for regenerative medicine, and the expansion of the scope of research into human disease. These hESCs cells could, *in vitro*, broadly recapitulate the process of human embryonic development; having the ability to spontaneously differentiate into cells from all three germ layers, or undergo a directed differentiation towards a multitude of somatic cell types including cardiac cells, neurons and vascular cells (reviewed in Ludwig et al, 2018).

However, the use of hESC in research has always caused some ethical concerns since the derivation of hESCs from the ICM of an embryo thus destroys the embryo. Many nations worldwide still preclude the use of hESC in research or therapy due to moral or religious objections. In the UK, there is a well-regulated governance and ethical approval process for the use of hESC in research or regenerative medicine. All activities of the 'UK Stem Cell Bank and all UK research involving established hESC lines is overseen by the UK Stem Cell Bank Steering Committee' in association with the Department of Health, the Human Fertilisation and Embryology Authority (HFEA), the Human Tissue Authority (HTA) and the Medicines and Healthcare Products Regulatory Agency (MHRA) (MRC/UKRI, 2021: online).

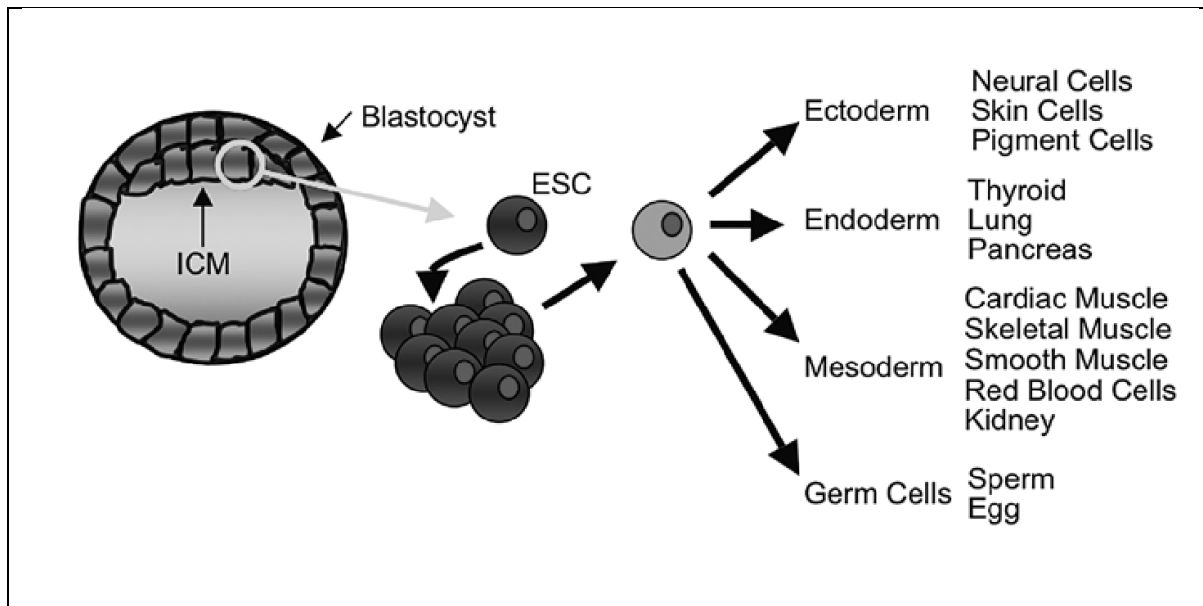


Figure 1.2: ESCs are capable of differentiating into cells from all three germ layers, the germ cells, and from there can be further specialised and differentiated into multiple different cells types, recapitulating the characteristics of the ICM cells *in vitro*. (Modo, 2008)

1.3. Introduction to induced pluripotent stem cells (iPSCs)

The next huge leap in the field of stem cell research came when, in 2006, Shinya Yamanaka described the reprogramming of mouse embryonic and adult fibroblasts to a state that mimicked that of pluripotent embryonic stem cells (Takahashi et al, 2006). These embryonic-like cells were named induced pluripotent stem cells (iPSC). Yamanka and colleagues, after a rigorous trial and error of dozens of factors, had used four key 'reprogramming factors': Oct4 (Octamer-binding transcription factor 4); SOX2 (Sex determining region Y-box 2); KLF4 (Kruppel-like factor 4) and c-MYC (myc proto-oncogene) (collectively known as OKSM) in retroviral vectors for the iPSC reprogramming. The successful reprogramming of human adult fibroblasts using the same OKSM iPSC reprogramming factors was achieved a year later by the same group (Takahashi et al, 2007). At around the same time, the Thompson group achieved similar results reprogramming human fibroblasts using a slightly different

combination of factors in a lentiviral system: Oct4, SOX2, NANOG and Lin28 (Yu et al, 2007). Thus, patient derived cells, for example skin fibroblasts isolated from a small skin biopsy or cells derived from a blood sample, can be returned to an embryonic-like state by the forced expression of a small number of key genes (Okita et al, 2013).

The derivation of patient-specific iPSC has created a brand new platform for personalised medicine in disease modelling and drug screening because, unlike mouse and other animal models, which often do not entirely recapitulate human disease, iPSC share a genetic background and cellular phenotype with the patients (Ellit et al, 2018; Farkhondeh et al, 2019). For example, patient fibroblasts reprogrammed to pluripotency and then subjected to directed differentiation to neurons would share genetic and phenotypic characteristics with the patients' neurons. The potential of induced pluripotent stem cells (iPSC) for use in disease modelling, drug screening and regenerative medicine is enormous and the full extent of this potential is not yet fully realised.

1.4. **Methods of iPSC reprogramming**

Since the first description of iPSC reprogramming in 2006, a number of methods for iPSC reprogramming have been developed, including the use of adenovirus (Stadtfield et al, 2008), Sendai virus (Fuscaki et al, 2009), lentivirus (Sommer et al, 2009), recombinant protein (Zhou et al, 2009) and mRNA (Anokye-Danso et al, 2011). Additionally, various modifications have been made to the exact combination of genes used to trigger reprogramming. These methods have varying degrees of safety and efficiency (Table 1.1), with one often coming at the expense of the other. For example, genome integrating oncoretroviruses or lentiviruses are the most efficient at producing iPSC, but the risks of deleterious insertional mutagenesis and

the potential downstream effects associated with this preclude their application in clinical therapies. In contrast, small molecules and mRNA do not carry the same risks, but are either far less efficient at iPSC production, expensive or extremely labour intensive (Moradi et al, 2019, Singh et al, 2015).

Table 1.1: An overview of iPSC reprogramming methods, seminal papers, reprogramming factors used, reprogramming efficiencies typically achieved and the key pros and cons associated with these methods.

O, Oct3/4; K, Klf4; S, Sox2; M, c-myc
(Schlaeger et al, 2015; Singh et al, 2015)

	Method	Factors	Cell type	Efficiency (%)	Pros and cons
I n t e g r a t i n g m e t h o d s	Retroviral transduction (Takahashi and Yamanaka, 2006)	OKSM	Mouse fibroblasts	0.0001-1	<ul style="list-style-type: none"> • Can be highly efficient • Genomic integration carries a risk of insertional mutagenesis • Viral protein has the potential to trigger innate immune response – limited clinical translation potential
	Lentiviral (Huangfu et al, 2008)	OKSM	Human fibroblasts	1	<ul style="list-style-type: none"> • Highly efficient • Able to transduce multiple cell types • Genomic integration carries a risk of insertional mutagenesis • Viral protein has the potential to trigger innate immune response – limited clinical translation potential
N o n - i n t e g r a t i n g m	Sendai virus (Fusaki et al, 2009)	OKSM	Human fibroblasts	~0.1	<ul style="list-style-type: none"> • High reprogramming efficiency • Non-integrating • Single transduction and relatively low workload • Virus persists in iPSCs for many passages, a problem for clinical translation • Expensive
	oriP-EBNA episomal plasmids (Yu et al, 2009, Bang et al 2018)	OKS, l-myc, LIN28 +shp53	Fibroblasts	~0.01-0.017	<ul style="list-style-type: none"> • Non-integrating, and non-viral • EBNA1 protein tethers the plasmid to the host chromosome allowing replication simultaneously to mitosis • Transient expression

e t h o d s					<ul style="list-style-type: none"> ● Inexpensive and easy to store and produce ● Single nucleofection required ● Effective in multiple cell types ● Use of shp53 is potentially tumourigenic, limiting clinical translation ● EBNA1 viral protein can persist and potentially cause an immune response
	PiggyBAC transposon (Woltjen et al, 2009)	OKSM	Mouse and human embryonic fibroblasts	0.01	<ul style="list-style-type: none"> ● Doxycycline inducible, easy excision ● Transient expression of non-viral reprogramming factors ● 'Footprint' free, leaves no trace ● Reprogramming takes approximately 14-28 days ● Doxycycline independence takes several weeks
	RNA modified synthetic mRNA (Warren et al, 2010)	OKSML	Human fibroblasts	0.6-4.40	<ul style="list-style-type: none"> ● Highly efficient ● Non-integrating ● Modifications ensure evasion of anti-viral response ● iPSC colonies form rapidly (14-17 days) ● Labour intensive and requires multiple transfections over 17 days ● Repeated transfections means mRNA could be reverse transcribed into DNA and integrate into the genome of the transfected cells ● Lower overall success rate than other methods

A couple of years after the publication of Yamanaka's seminal paper the Thomson lab developed the OriP/EBNA episomal plasmids containing SOX2, KLF4, L-MYC, LIN28, Oct3/4 and an shRNA (short hairpin RNA) for p53 alongside transient expression of EBNA1 (Eptein Barr Nuclear Antigen 1); both of which improve iPSC reprogramming efficiency (Yu et al, 2009, Okita et al, 2011, Okita et al, 2013). The

oriP/EBNA episomal plasmid is the current gold standard of iPSC reprogramming, particularly for a clinical setting, because they do not integrate into the host genome and are relatively safe and cost effective. These non-integrating episomal plasmids provide a good balance between safety and efficiency (Moradi et al, 2019). The McKay lab utilise these OriP/EBNA episomal plasmids as standard in our iPSC reprogramming experiments. iPSC, like ESCs, have the potential for both unlimited self-renewal as well as the potential for differentiation into any mature cell type.

1.5. **Benefits and drawbacks of using iPSCs in disease modelling**

Animal models have provided a vast wealth of information relating to human development, health and disease over centuries of scientific research and discovery, beginning in ancient Greece in the 6th Century BCE (Ericsson et al, 2013). In particular, the use of rodents as animal models have been exceedingly popular since the twentieth century because they are relatively cheap to house and easy to handle when compared to other animals. Rodents have short lifespans and fast reproduction rates; and, perhaps most importantly, are resistant to repeated inbreeding (Franco, 2013). As a result of the use of animal models for studying human diseases an enormous range of medical breakthroughs have been achieved including the discovery of insulin as a treatment for type 1 diabetes and the development of many vaccines including for smallpox and polio (Barre-Sinoussi and Montagnutelli, 2015). In addition, cancer treatments, pioneering surgical techniques such as balloon angioplasty for cardiovascular disease and treatments for AIDs have all been developed due to the use of animal models (National Academy of Sciences and Institute of Medicine; 1991).

However, the use of animals as models for human diseases has many limitations.

First and foremost, there are obvious genetic differences between humans and other

animals, even closely related ones such as chimpanzees and other non-human primates (Doncheva et al, 2021). Even where genes are conserved across species, there are differences in gene regulatory networks and epigenetic profiles (Barre-Sinoussi and Montagutelli, 2015), creating an entirely different genetic background upon which diseases are modelled and drugs are tested. There are often important differences in the presentation of diseases between species: for example, genetically engineered mouse models of Cystic Fibrosis have similar intestinal disease to those seen in humans, but lack the pulmonary effects (Ericsson et al, 2013). In addition, drugs can have vastly different reactions in different species including pharmacokinetics, drug metabolism and immune responses. One devastating example of this was when six human volunteers in Phase 1 clinical trial received an immunomodulatory drug called TGN1412 and all suffered severe adverse reactions and multiple organ failure due to a cytokine storm. This drug had been tested on mice, rats, rabbits and non-human primates with no similar effects (Attarwala, 2010; Akhtar, 2015). Lastly, there are obvious ethical and moral objections to the use of animals in medical research and the NC3Rs framework of reducing, replacing and refining the use of animals in research to make it more humane aims to address these concerns in the UK (NC3Rs, accessed 2021).

IPSCs are one major way in which the use of animal models in research can be reduced, since IPSCs can provide a new platform with which to model human diseases. In particular, iPSCs have been particularly well utilised in the study of neurological diseases, where appropriate animal models have been lacking to date (Volpato and Webber, 2020). IPSCs derived from human donor somatic cells possess the exact same genetic and epigenetic background, providing a more suitable context in which to study disease (Bragança et al, 2019). Cells

reprogrammed from a patient with a disease caused or influenced by genetic mutations or variants can be differentiated into cells or even tissues affected in that disease and studied *in vitro* and have been shown to recapitulate key phenotypic features (Bragança et al, 2019; Sharma et al, 2020; Volpato and Webber, 2020). For example, iPSC derived neurons are capable of releasing neurotransmitters and firing action potentials: fundamental functions of this cell type (Volpato and Webber, 2020).

One major benefit of the use of iPSC derived cell lines for disease modelling is the ability to differentiate iPSCs into cell types that are ordinarily difficult to obtain directly from human or culture, such as primary neurons (Borger et al, 2017). In addition, it is possible to expand and freeze iPSC lines, thereby creating a large supply of these cells (Borger et al, 2017). Further, patient derived iPSCs have the identical genetic background at the somatic cells from which they are derived, and all other cells in that particular patient: This is a major benefit of the use of iPSC-based cell models over other primary or immortalised cell line models. Even using gene-editing techniques such as shRNA to reduce the expression of a particular gene, or CRISPR-Cas9 mediated genetic modification to induce a specific gene mutation does not recapitulate the genetic and epigenetic background seen in human patients (Luciani et al, 2020).

However, there are potential pitfalls when considering the use of iPSC derived cell models. Firstly, variability can be introduced at multiple points during the collection of somatic cell samples; the culturing of the primary cells; the iPSC reprogramming process and culturing of resultant iPSC clones; and the differentiation process to other cell types such as NSCs or neurons (Luciano et al, 2020). Isogenic control lines can be utilised in order to try to overcome these barriers, whereby disease-causing mutations are artificially introduced in a cell line and the unedited line serves

as a control with an identical genetic background (Wang et al, 2014). This can also be performed 'in reverse' whereby a patient derived iPSC line with a known disease causing mutation can be genetically 'corrected' using gene editing techniques such as CRISPR-Cas9 or TALENS to create a 'healthy' isogenic control line (Merkert et al, 2017).

1.5.1. Disease modelling and clinical application for lysosomal storage disorders

Lysosomal storage disorders (LSD) are a group of inherited, usually progressive, metabolic diseases caused by lysosomal deficiencies of various enzymes that result in a build up of waste products that cannot be degraded (Sun, 2018). There are a range of clinical manifestations and disorders including the mucopolysaccharidoses, Gaucher's disease and the neuronal ceroid lipofuscinoses (Sun, 2018). There are a number of mucopolysaccharidoses with various gene associations and enzyme deficiencies and these disorders are mostly inherited in an autosomal recessive manner (apart from MPS-II, which is x-linked) (Sun 2018).

Gaucher's disease is caused by mutations in the GBA gene, resulting in a deficiency of the glucocerebrosidase enzyme (Sun, 2018) and is the most common LSD, with a prevalence of approximately 1 in 40,000 (Mehta, 2006). Gaucher's disease can cause a range of symptoms including hepatosplenomegaly, bone pain and poor growth, seizures, severe developmental delay and cognitive regression depending on the type (Sun, 2018).

The neuronal ceroid lipofuscinoses (NCL) are a group of disorders caused by mutations in the CLN genes (currently there are 13 or 14 genes known to cause NCLs) and are progressive neurodegenerative disorders (Nita et al, 2016; Sun, 2018). NCLs are characterised by an accumulation of lipopigments in and around

neuronal cells (Nita et al, 2016) and many NCLs manifest in infancy or childhood and typical clinical manifestations include seizures, blindness and loss of language and motor skills; most patients do not survive past adolescence (Sun, 2018). The functions of several of these genes remains unknown, limiting research into potential therapeutics (Nita et al, 2016).

Overall, there are over fifty types of LSD, and together there is a prevalence of up to 1 in 4000 live births and most are lacking effective treatments options due to the diverse array of gene associations, causative enzyme deficiencies and clinical manifestations (Borger et al, 2017). iPSC based disease models of these diseases have changed the way that researchers can study these diseases: Since they are rare and caused by specific gene mutations, appropriate animal models have been lacking and human iPSC derived cell models are able to more accurately mimic LSDs (Borger et al, 2017).

iPSC derived neuronal stem cells (NSC) are multipotent, and express key neural markers such as Pax6 and Nestin and have the potential to be differentiated into neurons, oligodendrocytes and astrocytes, meaning they have the potential to recapitulate the pathologies seen in neurodegenerative LSDs (Luciani et al, 2020). iPSCs derived from skin or blood cells of patients with LSDs have the exact same genetic mutations and genetic background; hence, when reprogrammed to pluripotency and differentiated into neuronal cell types these mutations remain, providing an ideal platform for understanding the mechanisms of these rare disorders and developing novel therapeutics (Luciani et al, 2020).

As an example, patient specific iPSC lines from a patient with NCL caused by mutations in the CLN3 gene have been used to create a model of the blood-brain-

barrier, which showed phenotypic features, associated with CLN3 disease including the accumulation of lipofuscin and mitochondrial dysfunction (Kinarivala et al, 2020). This novel model system was then used to screen previously identified potential therapeutic compounds for their ability to reduce the phenotype seen (Kinarivala et al, 2020). Another publication described the use of an iPSC derived neuronal cell model to elucidate the mechanism of disease in Gaucher's disease and identify mTORC1 as a potential therapeutic target due to its control of the defective autophagolysosome pathway in Gaucher's disease patient derived cells (Brown et al, 2019). Dysregulation of autophagy is a key feature of LSDs due the fundamental role of lysosomes in the autophagy pathway (See sections 1.9 and 1.10 for further information).

1.6. **Clinical application of iPSC**

Although the potential for the use of human iPSC in regenerative medicine is enormous, to date this potential has not been reached. There are clear advantages to the use of human iPSC over hESC cells in a clinical setting: firstly, iPSC avoid the ethical concerns around the use of hESC. Secondly, the use of autologous iPSC-derived from a patient's own cells avoids any kind of immune rejection (Vanneaux, 2019). The basic premise of these regenerative therapies is thus: iPSC are differentiated into any desired cell or tissue type and transplanted into the patient to replace lost or damaged cells (Moradi et al, 2019). Of course, this is particularly relevant to degenerative diseases, which are characterised by cell loss.

The first clinical trial utilising autologous human iPSC was launched in 2014, in Japan, with the aim of treating age-related macular degeneration (AMD). However, this study was suspended shortly after due to safety concerns regarding some copy-number alterations in the iPSCs and iPSC derived RPE cells in one patient: it could

not be determined if these changes may be potentially tumourigenic and so the trial was aborted (Mandai et al, 2017). The use of allogenic stem cells (coming from a healthy donor and undergoing extensive safety testing), was then deemed to be safer and quicker (Vanneaux et al, 2019). The first successful Phase 1 clinical of an allogenic iPSC derived mesenchymal stem cell product was initiated in 2016 and completed in June 2020 by Cynata Therapeutics, this is now moving into Phase 2 trials (Clinical Trials, 2021: [NCT02923375](#); Bioinformant, 2021). In 2019, eleven clinical trials using iPSC had been approved, for a range of diseases including AMD, Parkinson's disease and spinal cord injury (Vanneaux et al, 2019, Wiegand and Bannerjee, 2019).

However, there has not yet been the explosion of human iPSC based trials that one might expect and as of September 2020 no pluripotent stem cell- based therapy (including both ESC and iPSC derived cells) is in routine clinical use (Deinsberger et al, 2020). This is partly due to safety concerns regarding potential immunogenicity and oncogenicity (Garretta et al, 2018) and partly because derivation of the number of cells required for clinical application, manufactured according to current Good Manufacturing Practise (GMP) is extremely difficult to achieve (Wiegand and Banerjee, 2019). This is because the exact mechanisms, cell signalling and timing of the iPSC reprogramming process remains elusive and the process is still highly inefficient.

1.7. **Mechanism of iPSC reprogramming.**

The forced expression of 'reprogramming genes' confer a wide range of morphological, epigenetic, transcriptomic and metabolic changes in adult somatic

cells in a process which is not yet mechanistically or temporally clearly understood (Jackson and Sridharan, 2013; David and Polo 2014). iPSC reprogramming of adult somatic cells such as fibroblasts is widely considered to consist of three main phases, a stochastic initiation phase, maturation and a hierarchical stabilisation phase (Samarvachi-Tehrani, et al, 2010; Buganim, et al, 2012; David and Polo, 2014) (Figure 1.3)

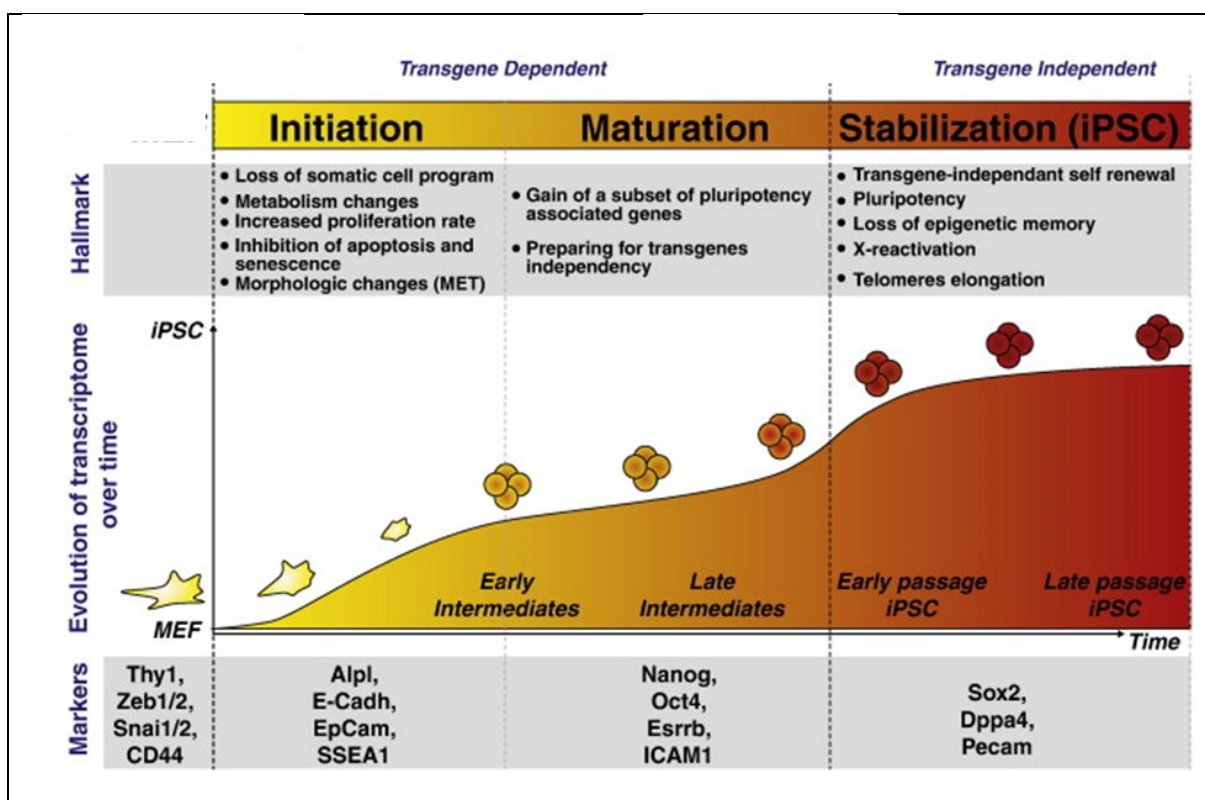


Figure 1.3: Summary of the three phases of iPSC reprogramming- initiation, maturation and stabilisation. Image adapted from David and Polo, 2014.

During the initiation phase, cells undergo a range of changes including the loss of somatic cell programming by epigenetic gene methylation; further epigenetic changes including histone modification; increased proliferation rate; metabolic changes from oxidative to glycolic energy production; and clear and easily visible

morphological changes from a mesenchymal to epithelial (MET) phenotype. During MET, cells gain polarity and begin to express E-Cadherin (Hawkins et al, 2014).

In the maturation phase, cells begin to 'switch on' transcription of a programme of pluripotency genes including *Nanog* and *OCT4* in preparation for independence from transgenes (David and Polo, 2014). An upregulation of genes driving and regulating glycolysis is also associated with the maturation phase of iPSC reprogramming (Jackson and Sridrahan, 2013) This phase of reprogramming completes the shift in glucose metabolism from oxidative phosphorylation to glycolysis, rapidly providing energy for the reprogramming and proliferating cells and potentially facilitating chromatin remodelling related to pluripotency (Jackson and Sridrahan, 2013).

Finally, in the stabilisation phase cells gain this transgene independence, lose the epigenetic memory of the somatic cells from which they were derived, and achieve stable pluripotency (David and Polo, 2014). During transition from the maturation to the stabilisation phase of reprogramming, cells unable to down regulate transgene expression cannot proceed to the stabilisation phase (Jackson and Sridrahan, 2013). Most cells that enter the reprogramming process are not 'stabilisation competent' (i.e. cannot reach or maintain the stabilisation phase) (Golipour et al, 2012) and the activation of endogenous pluripotency genes is essential to enter the stabilisation phase (Hawkins et al, 2014).

Current methods for reprogramming cells to pluripotency are largely inefficient; usually much less than 1% of gene-modified cells successfully progress to a state of stable pluripotency (Bragança, et al, 2019). In addition, the quality of the resultant pluripotent stem cells can be highly variable as the process is long, occurring over 25-30 days with stabilisation of iPSC colonies taking much longer. Hence, analysis of

this variable and temporal process is challenging. This variability and lack of quality-controlled stages limits the potential for producing the quantity and quality of reproducible iPSC needed for application in research and therapy. Elucidating the exact mechanisms and cellular pathways of reprogramming to pluripotency could be extremely useful for improving the efficiency and reproducibility of iPSC production and therefore their use in disease modelling, drug screening and regenerative medicine.

1.8. **Differences in mouse and human pluripotency**

Although mouse and human iPSC can be reprogrammed using the same set of reprogramming factors and are defined by the same properties of self-renewal and multi-lineage differentiation potential (Schnerch et al, 2010), there are some fundamental differences in the pluripotent states of cells from the two species. Both species rely upon the central self-regulatory network of Oct4, Sox2 and Nanog in order to gain and maintain pluripotency (Schnerch et al, 2010; Hawkins et al, 2016), but the wider gene regulatory networks and signalling pathways are not identical. For example, the cell surface antigens SSEA3 and SSEA4 are key markers of pluripotency in human cells, whereas SSEA1 is a key pluripotency marker in mouse cells: expression of SSEA1 is associated with early differentiation in human cells. In addition, the process of iPSC reprogramming takes significantly longer in human cells than in mouse cells (For example within the McKay lab an human iPSC reprogramming experiment takes approximately 25 days, whereas a mouse iPSC reprogramming experiment takes around 14 days.). During the initiation phase of iPSC reprogramming, Sox2 suppresses EMT (epithelial to mesenchymal transition) via Snail, while Klf4 induces E-Cadherin expression, which in turn promotes MET

(Hawkins et al, 2016). In mouse, BMP (bone morphogenic protein) is also essential for promoting MET in the early stages of iPSC reprogramming (Hawkins et al, 2016). In later stages, FGF2 (fibroblast growth factor) has been reported as essential for the maintenance of the pluripotent state in human pluripotent cells (Schnerch et al, 2010). In contrast, Stat3/LIF (Leukemia inhibitory factor) signalling is essential for maintenance of pluripotency in mouse cells (Schnerch et al, 2010) and LIF is an essential component in mouse iPSC and ESC culture media (Ginis et al, 2004; Abradijev et al, 2012).

In mice embryos, there exist two distinct pluripotent states: naïve (cultured mESCs recapitulate this state) and primed (mouse epiblast stem cells (mEpiSCs convey the characteristics of the primer pluripotent state in culture) (Kumari, 2016). Naïve and primed states of pluripotency have some key distinguishing features including colony morphology, growth factor requirements and, in females, chromosome-X activation status (Kumari, 2016). During the stabilisation phase of mouse iPSC reprogramming, chromosome-x is reactivated, meaning they exist in the naïve state (Hawkins et al, 2016). In contrast, X-reactivation does not occur in human iPSC reprogramming in the presence of FGF2, meaning that human iPSC typically exist in the primed state (Hawkins et al, 2016). However, in the presence of LIF, human fibroblasts have been shown to be reprogrammed to a naïve state, suggesting that the state of pluripotency is context dependent (Hawkins et al, 2016). Mouse ESCs derived from the ICM of pre-implantation embryos are naïve, whereas mEpiSCs derived from the epiblast of post-implantation embryos are primed (Kumari, 2016). Human ESCs derived from the ICM of pre-implantation embryos and human iPSCs typically exemplify a primed pluripotent state and are similar to mEpiSCs (Kumari, 2016). One key difference between naïve and primed pluripotent cells is that naïve cells use both oxidative

phosphorylation and glycolysis to produce energy, whereas primed cells use primarily glycolytic energy production (Kumari, 2016). In addition, suppression of autophagy has been demonstrated during the transition from naïve to primed pluripotency in mouse embryos via activation of mTOR (Kalkan et al, 2017).

1.9. **Autophagy**

1.9.1. Introduction to Autophagy

Autophagy is the process by which cells remove and recycle misfolded or aggregated proteins, damaged organelles and even pathogens as well as conserving and balancing energy sources during cell stress or starvation (Glick et al, 2010). Autophagy can be divided into three sub-categories: macro-autophagy, chaperone-mediated autophagy and micro-autophagy; although all three types share the common function of the facilitation of proteolytic degradation of cytosolic components in the lysosome (Glick et al, 2010, Parzych and Klionsky, 2014). Chaperone mediated autophagy involves the degradation of soluble proteins, transported directly to the lysosome by way of a chaperone (Parzych and Klionsky, 2014). Microautophagy is the process by which cytosolic components are sequestered directly into the lysosome by the invagination of the lysosomal membrane (Mizushima et al, 2008).

1.9.2. Macro-autophagy

During macro-autophagy, cytosolic components such as aggregated proteins and organelles are engulfed with a newly formed double-membrane structure known as the autophagosome. Ultimately, the autophagosome fuses with the lysosome to form the autophagolysosome and components are degraded (Yu et al, 2018) (Figure 1.4).

Macro-autophagy is the most well understood, and the classically thought-of form of autophagy (Parzych and Klionsky, 2014), and the form that will henceforth be referred to as ‘autophagy’. A whole host of autophagy related genes (Atg) have been identified which control every stage of autophagic processing (Wu et al, 2015).

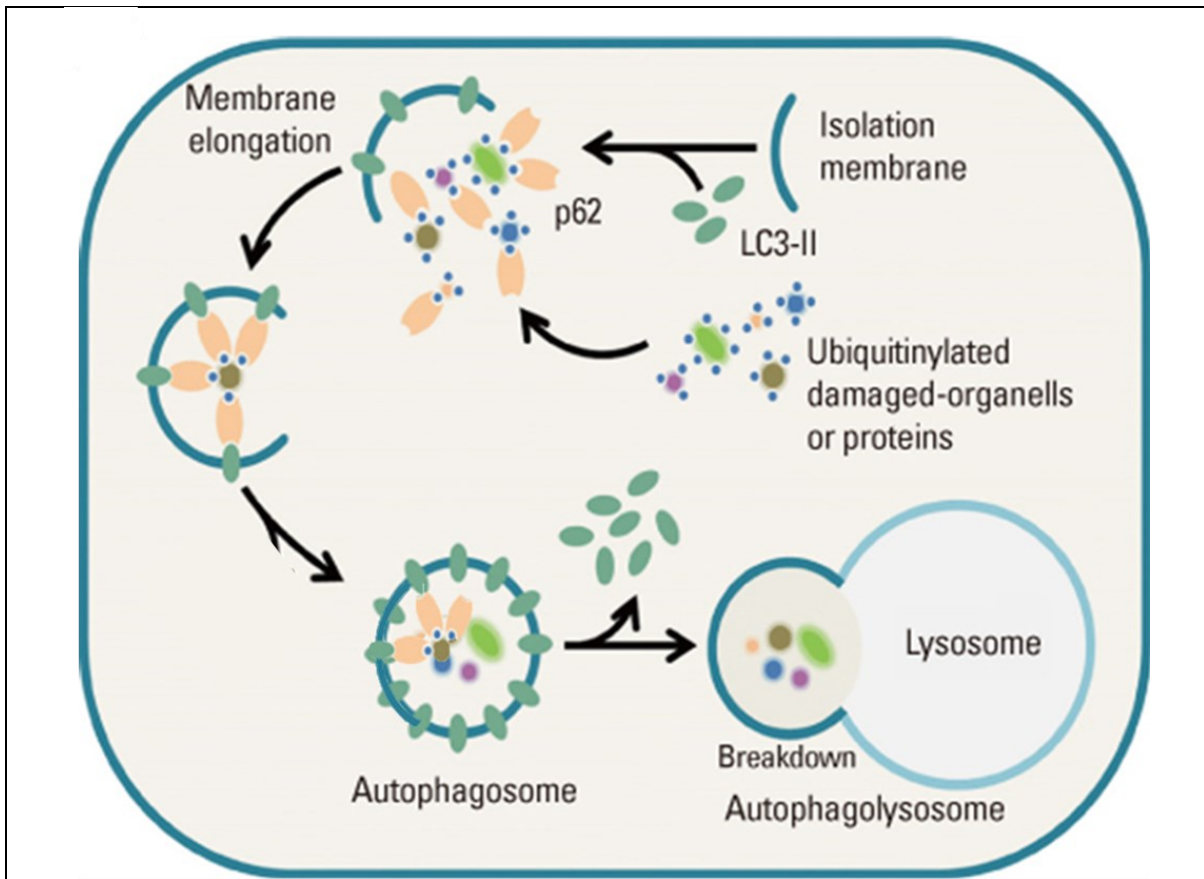


Figure 1.4: Overview of autophagic processing with the selective autophagy adaptor, p62. An autophagosome is formed from the elongation of an isolation membrane. Damaged proteins and organelles are ‘marked’ for degradation by the process of ubiquitination and targeted to the autophagosome by p62, which then binds to LC3-II on in the cytoplasmic membrane of the autophagosome. The autophagolysosome binds to a lysosome, forming an autophagolysosome where damaged proteins and organelles are degraded. Image adapted from Choi and Kim, 2013.

1.9.3. mTOR

mTOR (mammalian target of rapamycin) is ubiquitously required for the regulation of cell growth and survival. mTOR integrates various nutrient and hormone signals, which are distributed between different protein complexes: mTORC1 and mTORC2,

which have distinct functions and interacting partners (Pollizi et al, 2015). mTORC1 is better characterised and understood, and is sensitive to rapamycin via the PI3K (Phosphoinositide-3-kinase)-Akt (Protein kinase B)-mTOR pathway (Feldman et al, 2009). mTORC2 is not sensitive to rapamycin (Fan et al, 2012).

Under conditions of nutrient starvation, autophagy is induced in organisms from yeast to mammals. In mammals, mTORC1 (also known as mechanistic target of rapamycin complex 1) is inactivated leading to activation of the ULK1/2 (Unc-51 like kinase) pathway, increasing the ability of the cell to form autophagosomes (Lane et al, 2017). Autophagy is initiated by the formation of an intracellular isolation membrane, which expands and invaginates to form the autophagosome (Yu et al, 2018), engulfing cytosolic components within the double-membraned organelle (Glick et al, 2010). Ubiquitinated proteins are destined for degradation via the 18s proteasome or via autophagy and the multi-domain, multi-function autophagy receptor protein p62 (also known as SQSTM1 (Sequestosome 1)) has a triple role in this process as described below and summarised in Figure 1.5.

1.9.4. p62 in autophagy

Phosphorylation of p62 enables the binding of ubiquitinated proteins via its UBA (Ubiquitin associated) domain (Liu et al, 2016). p62 complexes are tethered to the autophagosome through interaction between the LIR (LC3-interacting region) domain of p62 and microtubule-associated protein light chain 3 (LC3-II) on the autophagosome membrane. Finally, the p62 PB1 domain allows for oligomerisation of p62 and the associated autophagy targets (Lane et al, 2017). In the last step of autophagy, the autophagosome fuses with a lysosome to form an autophagolysosome where material is degraded (Mizushima, 2007). Conversely, the

process of autophagy constantly feeds back to autoregulate p62 levels, as p62 is degraded by autophagy (Ichimura et al, 2008).

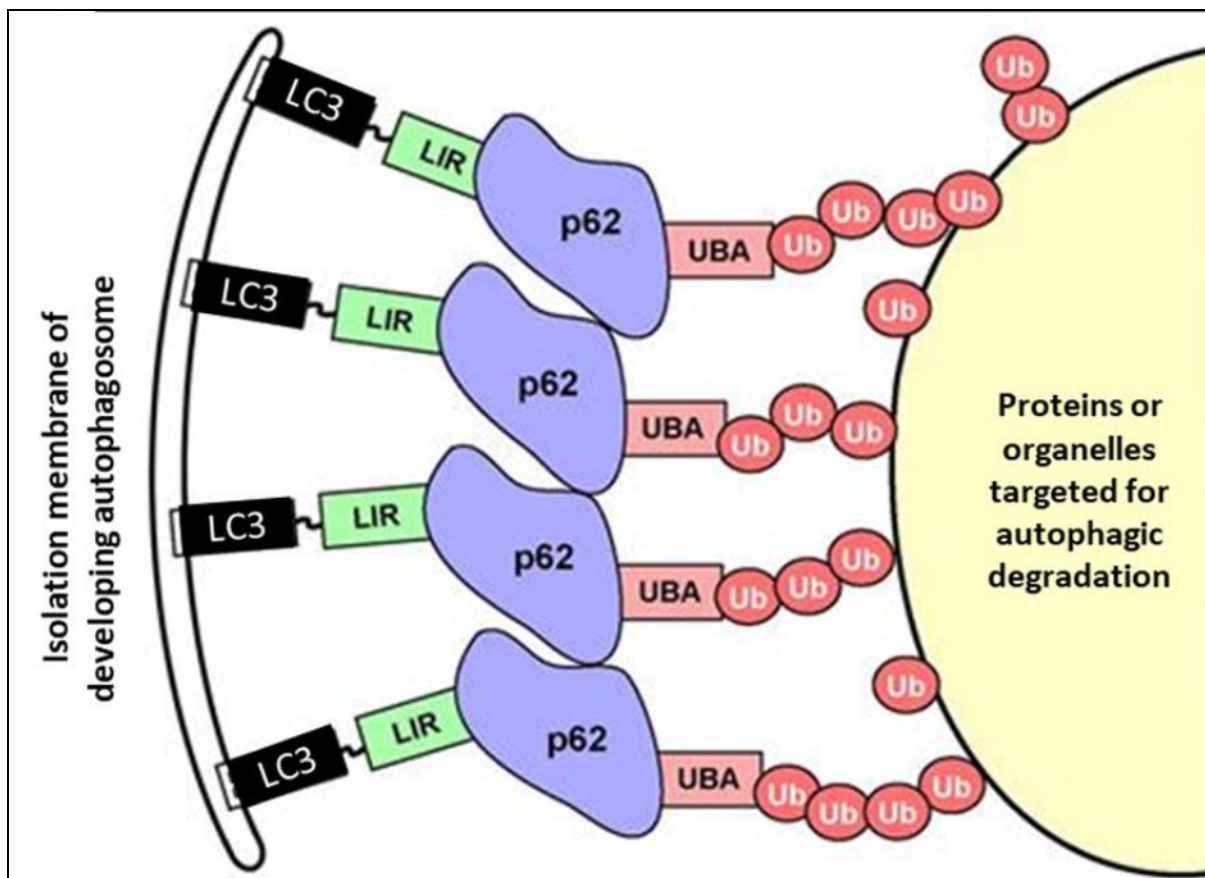


Figure 1.5: The role of p62 in autophagic processing. P62 has three key roles during autophagy. Firstly, p62 binds to ubiquitinated cargoes for the UBA domain. Secondly, p62 forms dimers and oligomers by homodimerising via its PB1 domain. Finally, p62 targets ubiquitinated targets to the autophagosome where it binds to LC3-II via its LIR domain on the elongating isolation membrane and tethers the proteins or organelles to the forming autophagosome. Image adapted from Lane et al, 2017).

1.10. The role of autophagy in iPSC reprogramming

Autophagy plays a crucial role in iPSC reprogramming, namely the stochastic initiation phase. Early in iPSC reprogramming, autophagy is upregulated. Some of the key iPSC reprogramming factors (SOX2, OCT4, KLF4 and c-MYC) work to inhibit mTORC1, which in turn induces autophagy (Wu et al, 2015). In particular, SOX2 expression early in iPSC reprogramming transiently downregulates mTORC1, and

iPSC reprogramming cannot occur without this event (Wang et al, 2013). Enhanced autophagy has also been seen in early embryonic development and iPSC efficiency can be improved by the addition of mTOR inhibitor rapamycin early in reprogramming (Wang et al, 2013).

It is possible that inhibition of mTORC1 during the initiation phase of iPSC reprogramming enhances MET or prevents cellular senescence; thereby improving iPSC reprogramming outcomes (Menendez et al, 2011). Furthermore, inhibition of both mTORC1 and mTORC2 has been shown to induce MET in cancer cells (Menendez et al, 2011). As previously discussed, during the initiation phase of successful iPSC reprogramming, an enormous amount of cell proliferation occurs. Therefore, the prevention of cellular senescence by inhibition of mTORC1 is likely a crucial factor in the initiation of iPSC reprogramming. Interestingly, KLF4 and c-MYC increase expression of autophagy related genes whereas SOX2 and OCT4 downregulate them leading to temporal and context dependent modulation of autophagic processing (Menendez et al, 2011). In addition, mTORC1 promotes mitochondrial remodelling, which is essential for iPSC reprogramming, due to the essential switch from oxidative to glycolytic energy production in the initiation phase (Menendez et al, 2011). Atg-5-independent autophagy has been shown to be essential in the regulation of mitochondrial clearance, which facilitates the metabolic switch and allows iPSC reprogramming to occur (Ma et al, 2015). The induction of autophagy for a prolonged period is detrimental to reprogramming efficiency (Wu et al, 2015). Finally, autophagy leads to the degradation of the p62 protein inside the autophagolysosome but iPSC-reprogramming efficiency is increased in cells where p62 is accumulated due to a deficiency in autophagy (Wu et al 2015). It is important

to understand that p62 is a fundamental component of autophagy but elevated levels of p62 accumulation is indicative of a block in autophagy or “autophagic shunting”. The role of p62 in iPSC reprogramming remains unclear and unstudied. Figure 1.6 provides a graphical summary of the role of autophagy in iPSC reprogramming.

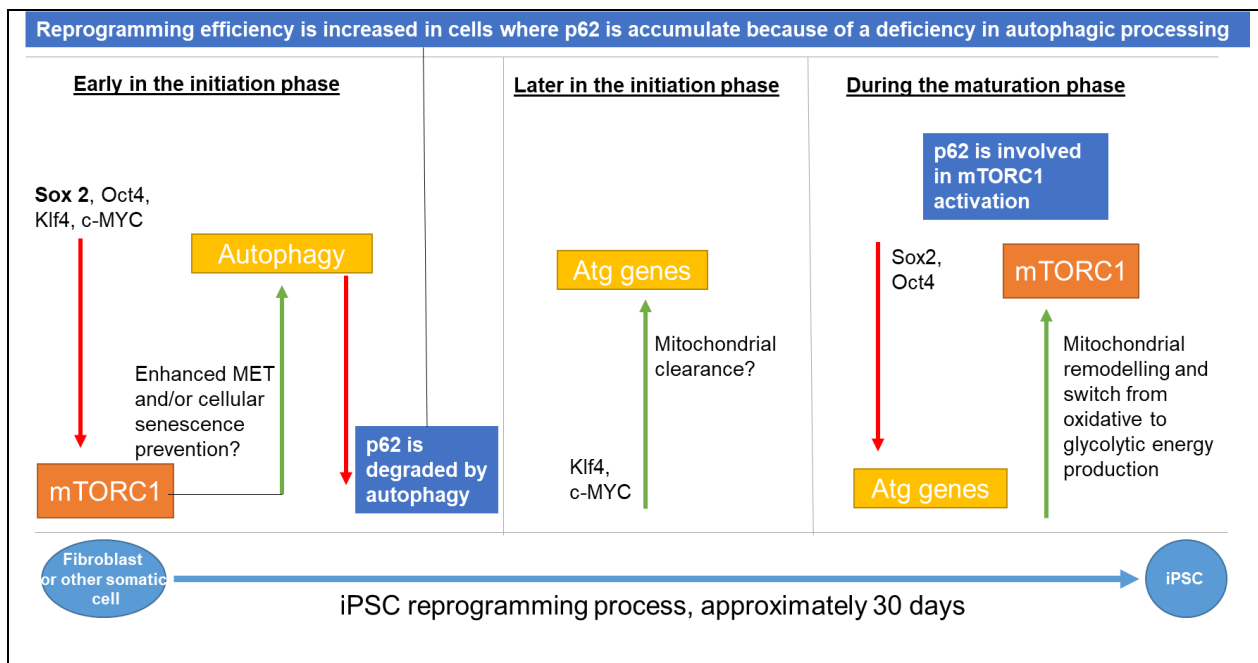


Figure 1.6: The proposed role of autophagy in iPSC reprogramming. During the early part of the initiation phase or iPSC reprogramming key reprogramming factors, in particular Sox2 inhibit mTORC1 signalling, an event which is essential for iPSC reprogramming. The downregulation of mTORC1 leads to an upregulation of autophagy. mTORC1 inhibition is also hypothesised to play a role in enhancing MET or preventing cellular senescence. Later in the reprogramming process, in a temporal and context dependent manner that is not entirely understood, Klf4 and c-MYC expression results in an upregulation of Atg genes. Autophagic processing is essential for mitochondrial clearance during iPSC reprogramming. Sox2 and

Oct4 are later responsible for the downregulation of autophagy genes, which could then lead to an upregulation of mTORC1 signalling. mTORC1 is known to promote mitochondrial remodelling, which is essential for the switch from oxidative to glycolytic energy production that occurs during the maturation phase of iPSC reprogramming. The specific role of p62 in iPSC reprogramming has, to the best of my knowledge, never been studied. However, in physiological conditions p62 is degraded during autophagic processing. p62 is also known to be involved in the activation of mTORC1. In cells where p62 is accumulated due to a deficiency in autophagy iPSC reprogramming efficiency is increased. In contrast, if autophagy is upregulated for a prolonged period of time iPSC reprogramming efficiency is reduced. It is clear that a fine balance of the levels of autophagy is maintained throughout iPSC reprogramming, and given the essential roles that p62 plays in autophagy, it is hypothesised that p62 has a potential undiscovered role in the maintenance of pluripotency.

1.11. **SQSTM1/p62 biology**

p62 is a multi-domain; multi-function protein encoded by the SQSTM1 gene but will be referred to as p62 throughout this report. Vadlamudi and Shin first described the SQSTM1 gene in 1998. SQSTM1 is located on the fifth chromosome, and has eight exons, spanning ~16kb in total (Sanchez-Martin et al, 2018). p62 is highly conserved across species including fish, birds, amphibians, reptiles and mammals (Katsuragi et al, 2015), and is best known for its role as an autophagy adaptor protein. However, p62 has many other roles defined to specific protein structural moieties, including activation of mTORC1 in nutrient sensing (mTORC1 is active when bound to lysosomes) (Lippai and Low, 2014; Alegre et al, 2018) and the activation of NF- κ B (Nuclear Factor kappa-light-chain-enhancer of activated B cells) in response to inflammation (Lippai and Low, 2014; Fan et al, 2018). p62 is also involved in the activation of the antioxidant response via upregulation of the NRF2-KEAP1 (nuclear factor erythroid 2-related factor 2, Kelch like ECH Associated Protein 1) interacting pathway (Sanchez-Martin et al, 2018). It is also well known as a scaffold protein for PKC (atypical protein kinase C) and ERK (extracellular signal related kinase) signalling (Katsuragi et al, 2015).

The p62 protein localises in both the cytoplasm and the nuclei of cells, is ubiquitously expressed, and is able to shuttle between the nucleus and the cytoplasm. Under conditions of cellular stress, p62 is translocated to autophagy substrates (Katsuragi et al, 2015). p62 directly mediates autophagy via interaction with LC3-II on autophagosomal membranes (Ichimura et al, 2018), and by targeting ubiquitinated proteins to the autophagosome as previously discussed (Ma et al, 2019).

1.12. **p62 domains and mutations**

The SQSTM1 gene encodes for a protein that, in human, is 440 amino acids in length (Chen et al, 2020) and in mouse is 443 amino acids in length (Richard et al, 1995). The p62 protein has multiple functionally distinct domains that each have different binding partners and interactions (Figure 1.7). p62 has a Phox-BEM1 (PB1) domain at its N-terminal which can form both p62 oligomers and heterodimers with other PB1 domain containing proteins such as atypical protein kinase C (aPKC) and NBR1 (Neighbour of BRCA 1) (Lippai and Low, 2014). A central zinc finger region (ZZ) and a Tumour necrosis factor (TNF) receptor-associated factor 6 (Traf6) binding region (TB) which, in combination with the PB1 domain, play a role in NF- κ B signalling pathways (Pun and Park, 2017) are further functional domains within the p62 protein. p62 also has an LC3-II interacting region (LIR) which facilitates the delivery of ubiquitinated protein cargo to the autophagic pathway (Liu et al, 2016).

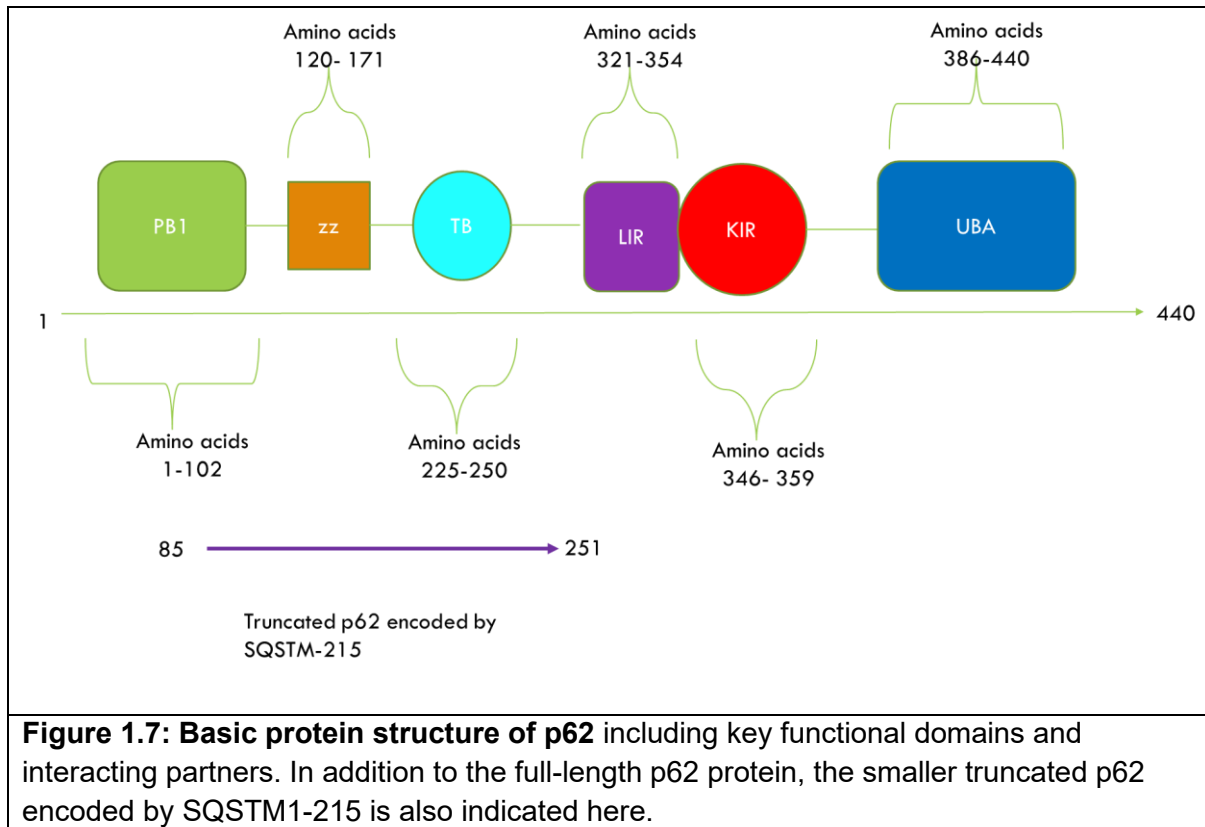
The p62 protein is involved in the anti-oxidant response via its KEAP1 interacting region (KIR) which binds and regulates KEAP1, the primary inhibitor of the NRF2 transcription factor and master regulator of the anti-oxidant response (Kansanen et al, 2012). KEAP1 binds and ubiquitinates NRF2 labelling it for proteasomal degradation (Sun et al, 2007). Finally, p62 has a clearly defined role as a selective autophagy receptor via the UBA domain, targeting ubiquitinated proteins to the

autophagosome for subsequent lysosomal breakdown (Katsuragi et al, 2015; Pun and Park, 2017). In addition to its six key functional domains, p62 also has two small nuclear localisation signals (NLS) and a nuclear export signal (NES) responsible for facilitating shuttling of p62 between the cytoplasm and the nucleus (Chen et al, 2020). The role of p62 within the nucleus is not clearly understood but there is some evidence that nuclear p62 is deleterious and interferes with the BRCA1 (breast-cancer 1)-mediated DNA damage response (Pankiv et al, 2010) resulting in the accumulation of genomic DNA damage. There are a huge number of post-translational modifications of p62, such as phosphorylation and ubiquitination (Lane et al, 2017), which can affect its function in time and context dependent ways which are not yet entirely understood. These modifications can also be exploited in order understand better the functionality of p62 as individual domains, and as a whole. The domains of p62 are summarised in graphical form in Figure 1.7 and discussed in further detail in the following sections.

1.12.1. Truncated human p62

p62 is a multi-domain, multi-functional protein 440 amino acids in length, encoded by the SQSTM1 gene: specifically the SQSTM1-202 transcript. However, another commonly expressed transcript exists- SQSTM1-215. This transcript encodes a much shorter protein, only 167 amino acids in length. These 167 amino acids constitute a central portion of p62, since there are two locations in the p62 coding sequence where a methionine (M) amino acid is followed immediately by an alanine (A): at the very beginning of the human p62 sequence, and at the 255th base (Figure 1.7) The protein translated from SQSTM1-215 constitutes amino acids 85- 251 of the 440 amino acid complete human p62. This corresponds with a small portion of the

PB1 domain, a ZZ-type zinc finger domain, and the Traf6 binding region (TB) only (Ensembl, SQSTM1, Transcript ID: [ENST00000514093.5](#)) (Figure 1.7).



1.12.2. PB1 domain.

There are several proteins that contain PB1 domains including p62, NBR1, aPKC and Mitogen Activated protein kinase 3 (MEKK3) (Sumimoto et al, 2007). PB1 domains can contain two different types of highly conserved protein motif which allows for interaction with other PB1 domains. The OPCA type motif is highly acidic (also known as A-type), whereas the B-type motif contains a lysine residue and is basic; the acidic and basic motif types interact with each other (Lim et al, 2019). The N-terminal PB1 domain of p62 comprises approximately amino acids 20-102 (Chen and White, 2011) and has both an A-type and B-type domain, meaning that it can

interact with other p62 molecules to form homodimers and oligomers (Sumimoto et al, 2007; Christian et al, 2014,). Of course, p62 is also able to form heterodimers and oligomers with other PB1 domain containing proteins as previously described (Lippai and Low, 2014).

Most protein interactions so far identified between p62 and other PB1 domain interacting domains happen between the basic B-type motif of p62 and acidic A-type motif of the interacting partner. MEKK3, however, interacts in the opposite fashion, allowing the selective activation of canonical NF- κ B signalling (Nakamura et al, 2010, Christian et al, 2014). Similarly, Phosphodiesterase-4 (PDE4) interacts with the A-type motif of p62, autophagy receptors p62 and NBR1 can work independently or together through heterodimerisation at PB1 domains to recruit targeted proteins to the autophagosome (Peng et al, 2017). Localisation of p62 to the membranes of autophagosomes is dependent on self-oligomerisation of its PB1 domains (Itukara and Mizushima, 2011). Further, cAMP dependent protein kinase (PKA) phosphorylates p62 at Serine 24 (S24) (conserved in human and mouse) and prevents hetero-oligomerisation with other PB1 domain containing interacting partners (Christian et al, 2014) while enabling homodimerisation (Christian et al, 2014). Thus, mutating S24 to a non-reactive alanine (S24A) will prevent homodimerisation but enable heterodimerisation. p62 interacts with MEKK3 and Traf6 to activate NF- κ B, while also activating mTOR (Linares et al, 2015). In addition, mutating human amino acid K7 to an Alanine (K7A) will also prevent homodimerisation of PB1 but not heterodimerisation, (Nakamura et al, 2010).

1.12.3. ZZ-type zinc finger region

The ZZ-type zinc-finger region of p62 is not well characterised or studied, but it comprises amino acids 128-163 (Lippai and Low, 2014). Some studies have shown that the ZZ-type zinc finger region binds to Receptor-interacting serine/threonine-protein kinase 1 (RIP1) and forms a signalling complex with aPKC (Lin et al, 2013). The interaction of the ZZ-type zinc finger region and RIP1 then works with the TRAF6 binding region and TRAF6 to activate canonical NF-KB signalling (Lippai and Low, 2014). In addition, the ZZ- domain works to mediate the aggregation of p62 into oligomers (Zhang et al, 2018).

1.12.4. TRAF6 binding region

The TB region of p62 has several complex and context dependent interactions. The TB region of p62 comprises amino acids ~228-254 (Wooten et al, 2005) (although some important TRAF6 interactions happen beyond this, at amino acids 269 and 272). When human p62 is phosphorylated at amino acid residues T269 and S272 (t272 in mouse) in response to the presence of amino acids, TRAF6 is recruited to p62 and mTORC1 is activated and translocated to the lysosome, later followed by polyubiquitination and activation of mTOR (Linares et al, 2015). Downstream, activation of mTORC1 and mTOR regulates autophagic processing. In starvation conditions, phosphorylation of T269 and S272 does not occur. Mutating residues T269 and T272 to non-reactive alanine (A) residues prevents phosphophorylation occurring and therefore blocks recruitment of TRAF6 (Linares et al, 2015).

The TRAF6 binding region of p62 has also been implicated in initiating apoptosis, whereby p62 interacts with TRAF6 and caspase-8 to activate downstream caspase activity (Schimmack et al, 2017; Islam et al, 2018). Furthermore, the TRAF6 binding

region (TB) binds to TRAF6, an important signalling molecule in inflammation (Moscat et al, 2007). p62 homodimerises in response to Receptor Activator of NF- κ B ligand (RANKL) and Interleukin-1 (IL-1), leading to ubiquitination of TRAF6, activation of NF- κ B and a whole cascade of pro-inflammatory events (Wooten et al, 2005; Abbot et al, 2007; Manley et al, 2013). p62 also interacts with TRAF6 to regulate signalling of tumour necrosis factor- α (TNF- α), IL-1 β , and nerve growth factor (NGF) (Sanz et al, 2000; Duran et al, 2004; Zotti et al, 2014).

1.12.5. LC3 Interacting region

LC3 interaction is necessary to facilitate p62 degradation by autophagy (Ichimura et al, 2008). The LC3 interacting region (LIR) of p62, consists approximately of amino acids 321-344, although the specific amino acid LC3 recognition sequence (LRS) is amino acids 334-344 (Pankov et al, 2007; Ichimura et al, 2008). LC3 is the human homologue of ATG8, an evolutionarily conserved autophagy gene. Within the p62 LRS there are three consecutive aspartate residues (DDD), which are also highly conserved, and essential for binding to LC3, followed by WxxL amino acids (Ichimura et al, 2008; Johansen et al, 2011; Lin et al, 2013). The tryptophan residues at human p62 amino acid positions 338/340 (W338/W340) are essential for binding to LC3 and mutation of either of these amino acid to an alanine (W338A/W340A) has significantly reduced LC3 binding (Ichimura et al, 2008).

1.12.6. KEAP-1 Interacting region

The KIR region of p62 was determined by Komatsu et al (2010) to be comprised of amino acids 346- 359. p62 is involved in the anti-oxidant response via the KIR, whereby p62 forms a positive feedback loop by competing with NRF2 to bind with

KEAP1 under oxidative stress conditions (Liu et al, 2016). Amino acid 349 in human, and 351 in mouse, is phosphorylated in response to mTORC1, leading to regulation of the oxidative stress response, and host defence mechanisms (Ichimura et al, 2013; Lane et al, 2017). Mutation of these residues in both mouse and human prevents this phosphorylation occurring, thus preventing binding of the KIR (Ichimura et al, 2013). In both mouse and human, amino acid residues P350, S351, T352, E354 and L355 are essential in the interaction with KEAP1 (Komatsu et al, 2010, Lau et al, 2010).

Phosphorylation on p62 KIR aa349 in human induces binding of KEAP1, which in turn leads to Cullin-3 ubiquitination of aa420 in the UBA domain. This ubiquitination of aa420 prevents UBA dimer formation and increases UBA binding to ubiquitinated targets (Lane et al, 2017, Sanchez-Martin and Komatsu, 2018). KEAP1 is degraded by selective autophagy alongside p62. KEAP1 usually works to inhibit NRF2 activity, and so in times of cell stress, competitive binding of KEAP1 by p62 frees NRF2 to translocate to the nucleus, leading to transcription of oxidative response genes including SQSTM1, in a competitive positive feedback loop (Komatsu et al, 2010, Liu et al, 2016, Lane et al, 2017, Islam et al, 2018). NRF2 is essential for the neutralisation of reactive oxygen species (ROS) (Komatsue et al, 2010). p62 cannot bind with LC3 and KEAP1 at the same time, due to the proximity of the LIR and KIR domains (Jain et al, 2010).

1.12.7. UBA domain.

The UBA domain of p62 comprises amino acids ~386 to 434 (Seibenhener et al, 2004). The UBA domain of p62 directly interacts with poly-ubiquitinated proteins, with a preference for the higher molecular weight chains (K48 and K63) (Liu et al,

2016). The UBA domain of p62 can also homodimerise, and does so in times of p62 inactivity, preventing interaction with ubiquitinated proteins (Sanchez-Martin and Komatsu, 2018). Upon phosphorylation of Serine 407 (S407) p62 is released from dimerisation, followed by a further phosphorylation event at serine 403 (S403) which facilitates binding to polyubiquitinated proteins (Long et al, 2010; Sanchez-Martin and Komatsu, 2018). Phosphorylation of Serine 403 (S403) by Casein Kinase 2 (CK2) in the UBA domain, allows for efficient binding of ubiquitinated proteins, and increase recruitment of polyubiquitinated proteins to autophagy (Matsumoto et al, 2011). Furthermore, phosphorylation of S403 increases the rate of turnover of p62 (Matsumoto et al, 2011) Mutation of the serine at 409 to alanine s409a will prevent UBA domain binding to Unc-51 like kinase (ULK) (a serine/threonine kinase involved in autophagy) (Lim et al, 2015). Mutating p62 at S403A/s405a or S407A/s409a reduces binding affinity of p62 to ubiquitinated proteins (Matsumoto et al, 2011; Lim et al, 2015). A summary of some of the key mutations found in p62 domains can be found in Table 1.2.

p62 domain	Mutation	Effect	Disease model	Key reference
PB1	K7A	Prevents homodimerisation/ oligomerisation of p62	Human	Nakumura et al 2010
PB1	S24A	Prevents homodimerisation but enables heterodimerisation of p62	Human, mouse and rat	Christian et al, 2014
TB	T269A	Prevents mTORC activation in conjunction with S/t272A/a	Human and mouse	Linares et al, 2015
TB	S272A/t272a	Prevents mTORC activation in conjunction with T/t269A/a	Human (S272A) and mouse (t272a)	Linares et al, 2015
LIR	d337/338/339a	Prevents p62/LC3-II interaction	Mouse	Ichimura et al, 2008

LIR	W338A/ W340A	Reduces LC3-II binding capability	Human and mouse	Ichimura et al, 2008; Chen et al, 2013
LIR	I343a	Reduces p62/LC3-II interaction	Mouse	Itakura and Mizushima, 2011
KIR	S349A/ s351a	Prevents binding to Keap1	Human (S349A) and Mouse (s351a)	Ichimura et al, 2013
UBA	S403A/ s405a	Reduces binding affinity to ubiquitinated proteins	Human (S403A) and mouse (s405a)	Matsumoto et al, 2011
UBA	S407A/ s409a	Prevents binding to ILK	Human (S407A) and mouse (s409a)	Lim et al, 2015

1.13. p62 in health and disease

1.13.1. Paget disease of the bone

Paget disease of the bone is a chronic disorder, and the second most common skeletal disease after osteoporosis, characterised by increased and uncontrolled bone turnover. Osteoclasts in Paget disease are larger than normal and multinucleated with inclusion bodies (Lu et al 2017; Zach et al, 2018). Symptoms of Paget disease include bone pain, frequent fractures and bone deformity (Lu et al, 2017, Shaw et al, 2019). p62 mutations are causative of Paget disease, particularly mutations in the UBA domain, whereby UBA is either truncated or non functional (Chamoux et al, 2009; Geetha et al, 2012). In Paget disease, mutations in the UBA domain lead to impaired phosphorylation of TRAF6, which leads to NF- κ B activation and increased osteoclastogenesis (Komatsu et al, 2012; Zach et al, 2018). The most common mutation of p62 in patients with Paget disease is P392L, accounting for up to 50% of familial cases and ~16% of sporadic cases (Geetha et al, 2012; Lu et al, 2017).

1.13.2. Metabolic and cardiac disorders

p62 binds to the insulin receptor substrate 1 (IRS-1) and is involved in insulin signalling (Long et al, 2017). As previously described, p62 plays a key role in autophagy, induced by nutrient depletion and is important in metabolism. Mice with abnormal p62 expression display abnormal lipid and glucose metabolism and p62^{-/-} mice develop mature onset obesity (Rodriguez et al; Long et al, 2017). p62 levels are lower than normal in the visceral fat of obese and type 2 diabetic patients (Rodriguez et al, 2006). p62 is known to regulate adipogenesis and insulin resistance (Long et al, 2017; Sanchez-Martin and Komatsu, 2018). p62 deficiency has been associated with inhibited respiration due to a lack of substrates for mitochondrial complex 1 and decreased mitochondrial membrane potential (Bartolome et al, 2017). Additionally, p62 deficiency causes an increase in reactive oxygen species (ROS) (Bartolome et al, 2017). p62 may play a role in gout and thyroid disease (Kim et al, 2016; Long et al, 2017). As previously discussed, p62 is important in NF-κB signalling, and therefore inflammation. Atherosclerosis is an inflammatory disease, and studies have shown that p62 can prevent atherosclerosis (Sergin et al, 2016; Liang and Guan, 2017). Furthermore, p62 aggregates have been found in atherosclerotic plaques (Long et al, 2017), and p62 is increased in response to atherogenic signalling (Ishii et al, 2013). While this may seem contradictory, it is important to remember the complexities of the roles of p62. p62 aggregation or accumulation is indicative of a failure of autophagy (Wu et al, 2020) and thus its abundance is indicative of a pathological state. In contrast, in healthy physiological conditions, p62 levels will increase and decrease as a result of autophagic flux (We et al, 2020), and so its presence in general is not detrimental. A fine balance of p62 levels can be protective in the case of atherosclerosis (Sergin et

al, 2016; Liang and Guan, 2017), but in the case of deficient autophagy and an accumulation of p62 atherosclerotic processes may be in play (Ishii et al, 2013; Long et al, 2017).

1.13.3. p62 in cancer

p62 is implicated in tumourigenesis and cancer, due, at least in part, to its role in mTORC1 and NF- κ B activation and signalling (Sanchez-Martin and Komatsu, 2018). p62 plays a role in the development of hepatic carcinoma via NRF2 and mTORC 1 signalling and p62 is the main component of Mallory-Denk bodies, which are found in pre-malignant liver disease (Umemura et al, 2016). p62 seems to be important in the initiation of tumourigenesis in hepatic carcinoma, and is strongly predictive of recurrence in this cancer type as well as worse patient survival rates (Umemura et al, 2016; Denk et al, 2018). In hepatocellular carcinoma, p62 enhances malignancy through NRF2 signalling, which leads to metabolic reprogramming, and by upregulating inflammatory signalling pathways (Kessler et al, 2015; Saito et al, 2016).

p62 has been implicated in the oncogenesis of renal cell carcinoma through activation of mTORC1, and is accumulated in endometrial cancer (Iwadate et al, 2015; Umemura et al, 2016). p62 expression is increased in malignant prostate cancer tumours (Kitamura et al, 2005). Dysregulation of NRF2 (which is of course at least partly controlled by p62), is known to play a role in renal cancer (Li et al, 2013). Furthermore, p62 accumulation is predictive of poor prognosis in lung cancer patients, and contributes to malignancy and metastatic tendency in cancer through NF- κ B signalling (Inoue et al, 2012).

Furthermore, p62 plays a role breast cancer tumour progression (Rolland et al, 2007), and p62 overexpression in triple-negative breast cancer (TNBC) is associated with a high level of metastases (Luo et al, 2013). 31.3% of TNBC cases showed p62 overexpression in one study, and patients with p62 overexpression have shorter disease-free survival rates (Luo et al, 2013). p62 can act as a tumour enhancer, or a tumour suppressor, depending on context and expression levels. Again, it is the fine balance of an appropriate level of autophagic flux which is essential to the regulation of homeostasis (Valencia et al, 2014).

p62 also regulates resistance of ovarian cancer to cisplatin, a chemotherapeutic agent, via it's NRF2-KEAP1 interactions (Xia et al, 2014). In multiple myeloma, the p62-KEAP1-NRF2 signalling pathway also regulates resistance to proteasome inhibitor drug treatment, and p62 inhibitors have been suggested as an add-on to treatment in some multiple myeloma patients (Riz et al, 2016). p62 has also been implicated in glioblastoma, gastric adenocarcinoma, colorectal and colon cancer, (Polonen et al, 2019; Kim et al 2019; Roy et al, 2019; Zhang et al, 2019)

1.13.4. Neurodegenerative disease

p62 protein has been implicated in a variety of diseases, particularly neurodegenerative diseases including Alzheimer's disease (Salminen et al, 2012), Parkinson's disease (Geisler et al, 2010) and lysosomal storage diseases such as Batten's disease (Chandrachud et al, 2015). Batten's disease is a rare, fatal neurodegenerative disorder affecting children. Batten's disease is the most common type of neuronal ceroid lipofuscinosis (NCL) and numerous mutations in 16 different genes have been identified so far as causative of NCL. Mutations in the CLN3 gene are most prevalent and cause NCL with juvenile onset. The McKay lab has

previously engaged in research surrounding the development of iPSC-derived cellular models for NCLs caused by mutations in CLN3, CLN6 and CLN7 genes. The key pathological features of Batten's disease are the accumulation of autofluorescent, electron dense lipopigment lipofuscin or ceroid as well as the progressive loss of neurons in the cerebral and cerebellar cortex and the retina (Haltia and Goebel, 2012). This Batten's disease pathology causes a gradual onset of blindness and seizures, and later neurodegeneration resulting in mental and motor deterioration. There is no cure for Batten's disease and current treatments can only hope to alleviate symptoms and prolong survival.

The Storch lab in Hamburg, Germany recently demonstrated that p62 and autophagic flux was elevated in Batten's disease cells with mutations CLN6 and CLN7 genes (Brandenstein et al, 2016). As yet unpublished experiments from the McKay lab have demonstrated that Batten's disease patient derived dermal fibroblasts (hDFs) carrying CLN6 and CLN7 mutations consistently and reproducibly reprogram to iPSc with higher efficiency than age-matched wild-type controls.

Neurodegeneration and accumulation of hyperphosphorylated tau protein has also been documented in a p62^{-/-} mouse model (Babu et al, 2008). Alzheimer's disease pathology is characterised by accumulation of Amyloid- β and neurofibrillary tangles containing hyperphosphorylated tau, and these neurofibrillary tangles have been shown to co-localise with accumulations of both p62 and aPKC (Babu et al, 2008). In normal conditions, tau is transferred to proteasomes for degradation by p62 in neurons, but in the absence of p62, tau is accumulated (Babu et al, 2008). As p62 is so crucial in the trafficking of proteins and other cellular materials for degradation, it makes sense that any defect in the function, processing or accumulation of p62

would result in aberrant degradation or accumulation of proteins, a key hallmark of many neurodegenerative diseases.

Serine-403 phosphorylation in p62 has been associated with Alzheimer's disease and Amyotrophic Lateral Sclerosis (ALS) (Kurosawa et al, 2016); and a lack of p62 protein has been shown to alter signalling pathways in Alzheimer's disease, with p62 protein expression shown to be lower in the frontal cortex of Alzheimer's disease patients compared to controls. (Du et al, 2009; Salminen et al, 2012). p62 has also been shown to co-localise with ubiquitin in Parkinson's disease and Lewy body Dementia, and may be able to regulate synaptic plasticity (Salminen et al, 2012). Furthermore, p62 has an important role in mitophagy (autophagic clearance of mitochondria), along with PINK1/Parkin: Parkin is also heavily implicated in the pathogenesis of Parkinson's disease (Salminen et al, 2012). p62 overexpression has also been shown to accelerate ALS disease onset (Mitsui et al, 2018).

The Carroll group in Helsinki, Finland have observed that fibroblasts derived from patients with loss of p62 expression have been shown to be extremely difficult to reprogram with a considerably lower efficiency and decreased autophagic flux compared to wild-type controls (conversation with Prof Chris Carroll). Interestingly, both elevated p62 and p62 depletion result in a neurodegenerative pathology. Exome sequencing of a small number of patients from four families with undiagnosed childhood or adolescent onset neurodegenerative disease revealed a number of mutations in SQSTM1 that led to a complete absence of p62. These patients had a range of phenotypes, but all had gait abnormalities and ataxia, as well as other varying neurodegenerative symptoms (Haack et al, 2016).

1.13.5. p62 and cancer stem cells

Cancer stem cells (CSC) are a small sub-population of cells found in cancerous tumours. Cancer stem cells, like all stem cells, have the potential for unlimited proliferation and the ability to differentiate into multiple cell types (Yu et al, 2012). CSC are capable of seeding tumours in animal hosts, and are like the cause of metastatic activity in cancer (Yu et al, 2012). In ESC, iPSC and adult stem cells, self-renewal occurs in a tightly regulated manner, and genetic mutations cannot, and must not occur. In contrast, CSC are able to acquire genetic mutations, which could confer the success of a tumour to be resistant to treatment, and to spread (Shackleton, 2010). CSC are involved in all stages of oncogenesis and tumourigenesis from initiation and progression, to metastasis, treatment resistance and recurrence (Rahman et al, 2016).

p62 overexpression has been noted in breast cancer stem cells, and positively correlated with MYC expression (Xu et al, 2016). MYC is a strong oncogene, but is also common in the genetic overexpression cocktail used to induce iPSC reprogramming. p62 may even be essential for the stem-like properties of CSC in breast cancer (Xu et al, 2016). CD44 (cluster of differentiation 44), is a key CSC marker, and high levels of CD44 have been shown to increase p62 expression. In turn, high levels of p62 expression results in increased NRF2 signalling which is linked to treatment resistance and poorer prognosis in breast cancer patients (Ryoo et al, 2018).

Furthermore, p62 is known to regulate metabolic reprogramming and energy metabolism in glioblastoma stem cells. In p62 knock-down glioblastoma stem cells, cell migration and invasion was reduced, suggesting that p62 may play an important role in tumour formation and migration (Galavotti et al, 2012). p62 overexpressing

transgenic mice displayed more CSC-like properties, had a more aggressive phenotype and had more chromosomal genetics which were pro-oncogenic than controls (Galavotti et al, 2012). p62 may also play a role in CSC differentiation in hepatic cancer, via activation of mTORC1 in response to amino acids (Sugiyama et al, 2016).

In mesenchymal stem cells (also known as stromal cells) within prostate tumours, p62 reduction leads to higher levels of tumourigenesis (Valencia et al, 2014). In this instance, p62 acts as a tumour suppressor by reducing inflammatory signalling. p62, along with other markers of autophagy including LC3-II and Beclin1 have also been found to be upregulated in colon CSC (Roy et al, 2019). Finally, in ovarian cancer stem cells, p62 inhibition led to decreased NRF2 expression which in turn reduced the CSC-like properties. Conversely, high p62 and NRF2 levels enhanced CSC-like properties of ovarian cancer cells (Kim et al, 2018).

1.13.6. p62 in stem cells and pluripotency

To date, there is very little published research about the role of p62 in adult stem or pluripotent stem cells, their differentiation, reprogramming or maintenance. Despite a wealth of evidence to suggest p62 has an important role in several key cell regulatory pathways including metabolic reprogramming and energy production via its amino acid sensing and regulation of mTOR signalling; role in inflammation and anti-oxidant responses, and of course its three vital roles as an autophagy adaptor. It stands to reason, that in iPSC reprogramming or in differentiation to specialised cell types, processes which require massive phenotypic, epigenetic, and metabolic changes, p62 would play important regulatory roles.

Wang et al (2016), found that in autophagy deficient mice (various Atg gene knock-outs), p62 accumulation was increased in neural stem cells (NSC) in the absence of Fip200 (a key autophagy inducer), but not mature neurons. Furthermore, removal of these p62 aggregates rescued defective NSC maintenance and differentiation in autophagy deficient mice (Short, 2016; Wang et al, 2016). p62 has also been implicated in mediating autophagic cell death in adult hippocampal neural stem cells, because of phosphorylation of S294 by 5' AMP-activated protein kinase (AMPK) (Ha et al, 2017). Finally, increased p62 and NRF2 was found to mediate the CSC properties and treatment resistant nature of ovarian cancer cells (Kim et al, 2018). NRF2 has been demonstrated to be a key regulator of the metabolic switch from oxidative to glycolytic energy production during iPSC reprogramming (Hawkins et al, 2016). As previously discussed, p62 is a key signalling partner of NRF2 via KEAP1 signalling and so perhaps p62 affects iPSC reprogramming via NRF2. There is no published literature about the role of p62 in iPSC reprogramming or the maintenance of pluripotency.

1.14. **Research statement and aims**

p62 is multi-domain, multi-functional protein with myriad roles in cell signalling and regulation. Many of these roles and interactions have been discussed here, but this is by no means an exhaustive list of the ways in which p62 regulates cells. p62 plays a key role in autophagy, inflammation, anti-oxidant responses, and cell metabolism. Aberrant expression or processing of p62 has been implicated in a range of diseases, and is particularly important in regulating and maintaining the self-renewal and differentiation potential of cancer stem cells. p62 levels must be tightly controlled in order to maintain cellular balance: overexpression or protein loss both contribute equally to pathogenesis depending on the context.

In combining all of the evidence about the ways in which p62 is so crucial for controlling cell states in both health and disease we began to hypothesise that p62 may also be important in iPSC reprogramming or in pluripotency. The role of autophagy in iPSC reprogramming is broadly understood, although the specific time and context dependent roles of reprogramming factors in influencing the levels of mTORC1 and autophagy are yet to be elucidated. However, p62 specifically has never been studied in this regard. Unpublished observations from our colleagues in the Carroll lab in Helsinki suggested that human fibroblasts from patients with bi-allelic SQSTM1 mutations resulting in a complete lack of p62 protein were refractory to iPSC reprogramming. In addition, unpublished observations from within the McKay lab suggested that CLN7 Batten disease patient fibroblasts may reprogram with higher efficiency than controls. p62 protein has been shown to be highly elevated in CLN7 mice (Brandenstein et al, 2017) and the added strength to the hypothesis that p62 levels could play a role in regulating the reprogramming process, or the maintenance of pluripotency.

Given that there was evidence of an association between p62, CLN7 mutations, and/or iPSC reprogramming in human cell models, human patients, and mouse models, I planned to utilise both mouse and human cell models to try and elucidate this connection, if any. Further, as discussed in earlier sections, a wide range of loss of function mutations have been described in the p62 protein: some of these have been characterised in human, some in mouse, and some in both species, further adding to the rationale to use both species in my experiments. Further, there are well established differences between the gene regulatory networks involved in the reprogramming of mouse and human fibroblasts, and in the maintenance of pluripotency in these cells, and so to truly understand the role of p62, a gene which

is highly conserved across species, it will be important to elucidate similarities and differences in its functions in mouse and human systems.). Further, I have acquired doxycycline inducible Mouse Embryonic Fibroblasts (MEFs) from the Hochedlinger lab at Harvard Medical School, USA (Statdfeld et al, 2008). This cellular reagent will enable the study of key regulators of reprogramming efficiency, including p62 because induction is synchronised in all cells at the same time by doxycycline induction. For example, p62 levels could be assessed at multiple points during reprogramming experiments to determine if there is a clear upregulation or downregulation of p62 (or associated factors such as Atg genes, mTORC1, LC3-II) at key milestones of reprogramming.

This research, for the first time, suggests a potential role for p62 in iPSC reprogramming and the maintenance of pluripotency using p62^{-/-} fibroblasts and shRNA mediated p62 knock-down in normal fibroblasts. Cells lacking p62 appear able to initiate reprogramming, but fail to complete the maturation or stabilisation stages of iPSC reprogramming, and do not display capacity for indefinite self-renewal. In addition, a whole 'tool-kit' of genetic modification plasmids has been created to enable further study of the exact way in p62 has the effect on iPSC reprogramming and pluripotency maintenance.

1.15. **Project aims and objectives:**

Overarching project aim:

-To determine whether p62 plays a role in iPSC reprogramming and the pluripotent state in order to better to understand the reprogramming process. The translation of iPSC to clinical utility depends upon the ability to produce safe, stable and well characterised cell products efficiently and reproducibly.

Project objectives (summarised in Figure 1.8):

- To characterise p62 null, control and CLN6 and CLN7 mutation patient fibroblasts for p62 localisation, levels, and associations
- To refine and develop McKay lab iPSC reprogramming protocols in both mouse and human cells
- To compare the efficiency of cellular reprogramming to induced pluripotent stem cells (iPSC) using human p62 null, control, and p62 overexpressing (CLN6 and CLN7 Batten's disease) patient fibroblasts.
- To perform iPSC reprogramming experiments in mouse doxycycline inducible MEFs
- To undertake a qualitative and quantitative characterisation of autophagy in p62 null, control, and p62 overexpressing human dermal fibroblasts and resultant iPSC.
- To use genetic modification techniques including lentiviral expression vectors and shRNA to modify expression of p62 in mouse and human cells
- To assess the specific molecular function that affects iPSC reprogramming using human fibroblasts expressing p62 functional deletion mutants on a p62 null background.

- To assess key markers of pluripotency in the context of p62 using doxycycline inducible MEFs and the resultant iPSCs
- To interrogate the molecular role of autophagy and p62 during the maintenance of pluripotency.
- To use shRNA's to induce p62 RNA knockdown in both mouse and human cells to assess the impact on iPSC reprogramming and the maintenance of pluripotency

NB. Many experiments had to be curtailed or were unable to be completed due to the Covid-19 pandemic and the resultant closure of the labs.

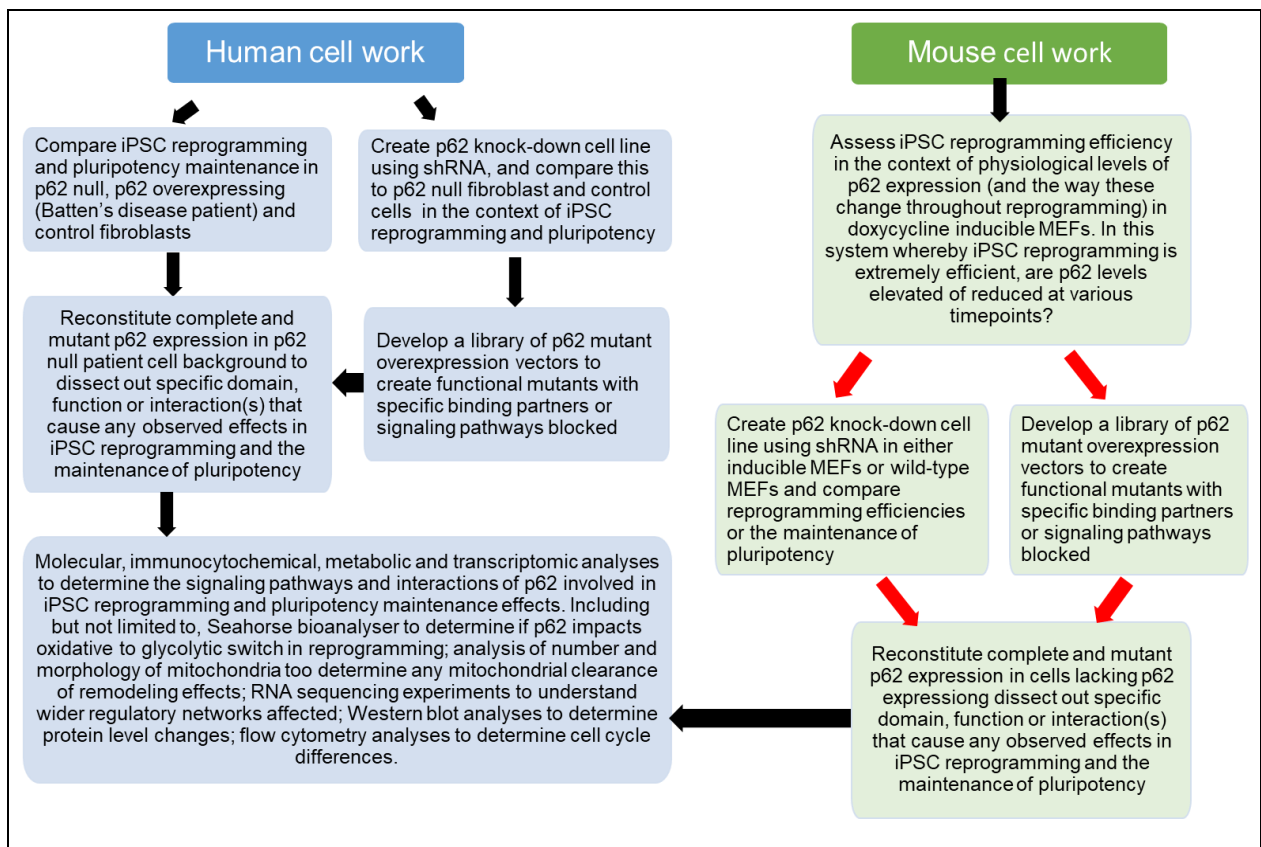


Figure 1.8: Summary of intended objectives and parallel assessments of the role of p62 in iPSC reprogramming and the maintenance of pluripotency in mouse and human derived iPSC cells. Please note this is also included in landscape larger format in Appendix 2

Chapter 2. Materials and Methods

Chapter 2. Materials and Methods

2.1. Cell Culture

2.1.1. Primary fibroblast cell culture

- p62 null human dermal fibroblasts (hDFs) were a kind gift from Dr. Christopher Carroll, St. George's University of London.
- Control neonatal human dermal fibroblasts (nhDF) were purchased from Fisher Scientific ([C0045C](#)).
- MEFs for inactivation were purchased from Cambridge Bioscience (CBA-310).
- CLN6 and CLN7 Batten's Disease hDFs were acquired from Prof. Sara Mole at Laboratory for Molecular Cell Biology, UCL as part of the McKay lab BATCure Horizon2020 consortium collaboration.
- Doxycycline inducible mouse embryonic fibroblasts (MEFs) were a kind gift from Professor Konrad Hochedlinger, Harvard Medical School, USA.
- mESC were a kind gift from Juan Pedro Martinez Barbera at ES cell and chimera production service at UCL ICH.
- WT MEFs were a kind gift from Dr Simon Waddington, UCL.
- Shef3 hESCs were obtained from the UK Stem Cell Bank under the project SCSC10-48.

All hDFs and MEFs were cultured in hDF media (Appendix 3) Cell culture media components). Media was refreshed every 48h and cells were routinely passaged approximately once per week (1:4) using TrypLE (Gibco, [12605028](#)), and centrifugation at 1200 rpm (Eppendorf centrifuge 5804 R) for five minutes before being resuspended in a volume of fresh culture media appropriate to the size of plate

or flask and seeded in new culture flasks or plates. For example, in a six-well plate format, approximately 2 mL of media was added; in a T75 cm² flask, approximately 10 mL of media was added.

MEFs designated for use as feeder layers for iPS cells (iMEFs) were mitotically inactivated by incubation with mytomyacin C (Sigma Aldrich, [m4287](#)) at a concentration of 0.1 µg/mL for 3 hours before washing with PBS (Gibco, [10010023](#)) and dissociating with Tryple. iMEFs were then cryopreserved (2.1.3) in small batches sufficient to cover approximately a full six-well plate when thawed (2.1.4). MEFs were seeded at a density of $\sim 5 \times 10^4$ cells/cm² onto gelatin (Sigma, [C1890](#)) coated plates (2.1.5).

Doxycycline Reprogrammable MEFs were a kind gift from the Hochedlinger lab, who provided me with four vials of MEFs: One vial of 'JB8' MEFs at P2, two vials of 'JB7' MEFs at P2 and one vial of 'JB7' MEFs at P1. 'JB8' MEFs are homozygous for OKSM reprogramming factors, homozygous for rtTA and heterozygous for Oct-4-GFP. These cells were provided as a platform to practise the inducible reprogramming protocol on, before moving on to the 'JB7' cells, which are homozygous for OKSM, rtTA and Oct4-GFP. Cryopreserved vials were thawed into two wells of a six-well plate and passaged 1:4 below P3 and 1:3 beyond P3. Inducible MEFs were grown in a DMEM media, very similar to that for hDFs (Appendix 3), with the addition of β-Mercaptoethanol (BME). Reprogrammable MEFs were thawed as described in 2.1.4 and plated in six-well plates. Cells were passaged when ~ 80 - 90% confluent, and reprogrammed before passage 5 (Reprogramming described in 2.1.7)

2.1.2. Pluripotent stem cell culture

hESC and hiPSC were cultured in HESC media (Appendix 3), which was replenished every day. hESC were maintained on inactivated MEF (iMEF) feeder layers and passaged manually by excision of colonies and dissociation to single cells by pipetting.

On occasion, cells were cultured 'feeder-free', in which case they were seeded onto Matrigel (Corning, [354277](#)) coated plates in mTeSR™ media (Appendix 3). After passaging, the cell media was supplemented with a Rho-associated kinase (ROCK) inhibitor (RI) ([Y-27632](#), Stem Cell Technologies) at 0.5 µL/mL, as this has been shown to significantly improve hESC and hiPSC recovery and growth after thawing, and to 'kick-start' slow growing colonies (Claassen et al, 2009).

Doxycycline Induced mouse iPS cells (miPSC) were cultured in mESC media containing knock-out DMEM and LIF (Gibco™, [A35934](#)) (Appendix 3) and media replenished daily. miPSC colonies were passaged by manual excision as previously described. Other mESC and miPSC were cultured in standard mESC/miPSC media (Appendix 3) on gelatin-coated plates (2.1.5). Media was replenished daily and colonies passaged by manual excision every 3 days.

2.1.3. Cryopreservation of cells.

Cells were passaged as previously described: colonies were manually excised or cells subjected to 3 minutes incubation in TrypLE before centrifugation at 1200 rpm for 5 minutes. Cells were resuspended in freeze media (Appendix 3), stored short-

term in a Mr Frosty at -80°C, and then transferred to liquid nitrogen for long-term storage.

2.1.4. Thawing of cells

Cells were thawed quickly by the addition of 10ml of warmed media, and centrifugation at 1200rpm, before removing supernatant and resuspending cell pellets in fresh media and plating as previously described.

2.1.5. Preparation of gelatin and matrigel for coating cell culture plates.

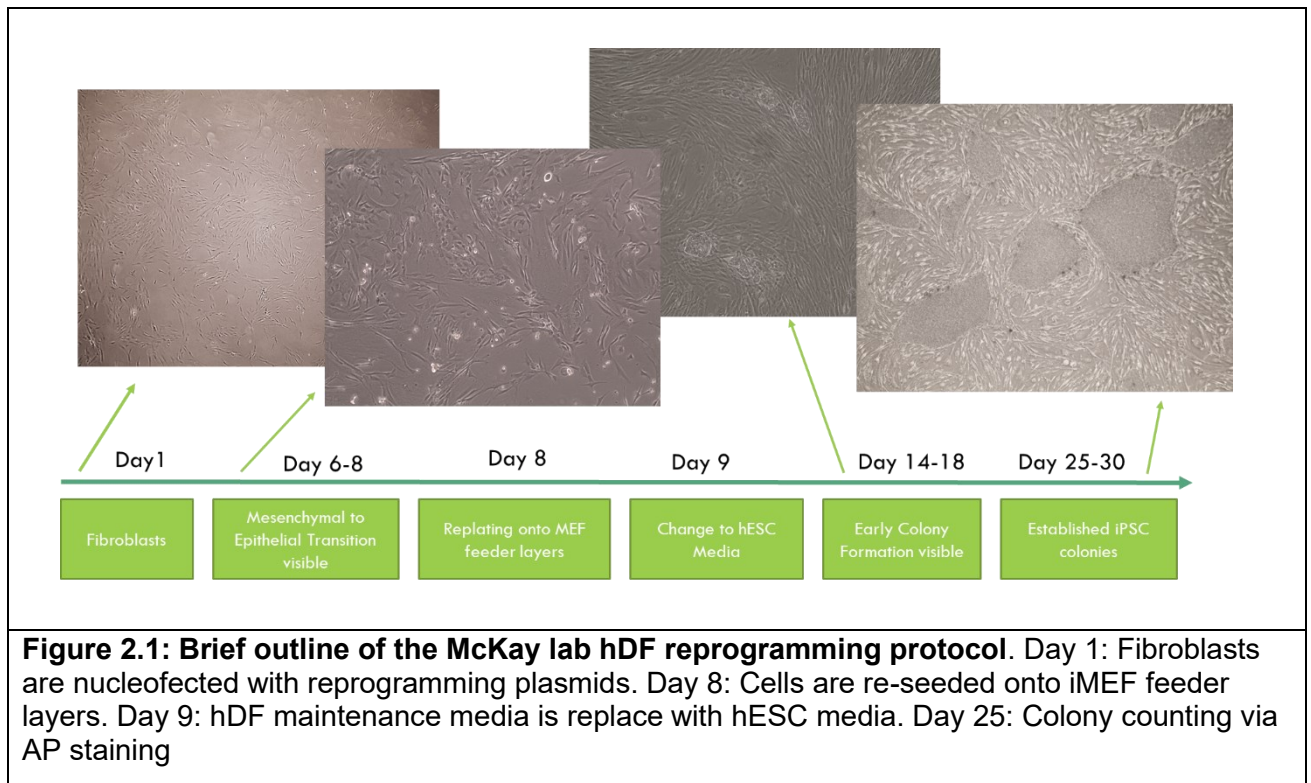
For the culture of iMEFs, plates and flasks were coated in 0.1% gelatin in sterilized ddH₂O. In a six-well format ~1 mL of gelatin was added to each well, and incubated for at least 30 minutes at room temperature, or overnight in the fridge. Gelatin was removed immediately before cells were plated. Matrigel is a solubilised basement membrane preparation based on extracts from Engelbreth-Holm-Swarm (EHS) mouse sarcoma, rich in extracellular matrix proteins such as laminin and collagen, plus growth factors, which provide stem cells with structural and growth support. Matrigel was thawed slowly in the fridge to avoid gelling, and diluted in DMEM/F12 according to the Lot dilution factor (~1:30). Tissue culture plates were coated in enough Matrigel to cover the entire well and incubated overnight in the fridge. Matrigel was removed immediately before seeding cells.

2.1.6. Human iPSc Reprogramming

hDFs were transfected for reprogramming using an Amaxa nucleofector to deliver the reprogramming factors (SOX2, KLF4, L-MYC, Lin28, Oct3/4) as well as shp53 and an additional EBNA expression cassette packaged as OriP/EBNA episomal plasmids. Plasmids are as follows and maps can be found on Addgene:

- pCXLE-hSK ([Addgene ID 27078](#))
- pCXLE-hUL ([Addgene ID 27080](#))
- pCXLE-hOCTshp53 ([Addgene ID 27077](#))
- pCXWB-EBNA1 ([Addgene ID 37624](#))
- These plasmids were a gift from Shinya Yamanaka, via Addgene.

2.0 µg of each plasmid were nucleofected together into 450,000 hDFs resuspended in 90 µL electroporation buffer + 20 µL supplement (LONZA, [VPD-1001](#), Amaxa Nucleofector, program P-022) and seeded into a single well of a six-well plate in standard hDF media. Media was changed the next day and every other day subsequently. On Day 2-4, cells were passaged into a T75 cm² flask, depending on confluence. On Day 8, cells were dissociated using TrypLE and 30,000 cells were re-plated onto iMEF feeder layers in one well of a six-well plate, or 15,000 cells into one well of a twelve-well plate. Media was changed to hESC maintenance media on day 9 and then media changed every other day until Day 25 as a minimum (Figure 2.1).



2.1.7. Reprogramming of inducible MEFs

Doxycycline inducible MEFs were plated at a density of ~30,000 cells per well in a six-well directly into reprogramming media (Appendix 3) Colonies begin to appear at ~8-12D and media can be changed to mESC maintenance media (Appendix 3) at ~14-16D.

2.1.8. Reprogramming of WT MEFs

450,000 cells were transfected with 2 µg of each OriP/EBNA Episomal reprogramming plasmids by electroporation in 90 µl electroporation buffer + 20 µl supplement (LONZA, VPD-1001, Amaxa Nucleofector, program A-30) and seeded into a single gelatin-coated well of a six-well plate in standard MEF media. Media was changed to mESC/miPSC media (Appendix 3) after 48 hours.

2.2. Stem cell validation

2.2.1. Tri-lineage Differentiation of iPS cells

iPSC were subject to a 16-day spontaneous differentiation protocol, which consists of two main phases: Embryoid body (EB) formation; and the subsequent outgrowth of these EBs. A single confluent well of iPSC colonies were manually passaged as previously described (2.1.2) and replated 1:1 into low-attachment cell culture plates in HESC media plus RI at a dilution of 1:1000. Half of this media was replaced after 24 hours. On Day 4, media was changed to hDF media, to encourage spontaneous differentiation. On Day 7, EBs were replated onto gelatin coated tissue culture treated plates and allowed to grow for 8 days.

2.2.2. Immunostaining

hDFs and MEFs were plated directly onto gelatin coated plates as previously described (for fluorescent microscopy), or glass bottomed plates (NUNC glass bottomed confocal dishes, Fisher Scientific UK, [15183728](#)) (for confocal microscopy) and hESC and hiPSC were plated onto iMEF feeder layers for immunostaining. Cells were washed with PBS and fixed using either 4% paraformaldehyde (PFA) in PBS for 2 minutes or ice-cold 100% methanol for 5 minutes. Cells were then blocked for a minimum of 30 minutes using 2% bovine serum albumin (BSA) (Sigma Aldrich, [A2153](#)) + 0.1% Tween (Sigma Aldrich, [P1379](#)) in PBS (Lonza, [BE17-512F](#)).

Antibodies were diluted to an appropriate concentration (see specific antibodies and concentrations in Table 2.1) and incubated overnight at 4°C. Cells were washed with PBS and appropriate secondary antibodies (Alexa Fluor, Abcam: See Table 2.2) were used at a concentration of 1:500 for 1 hour at room temperature in darkness. Cells were washed with PBS again and DAPI (Sigma Aldrich, [D9542](#)) was added at

a 1:1000 dilution in PBS for 1 minute. DAPI containing PBS was replaced with fresh PBS before visualization on either a Leica fluorescent microscope or a Leica SP5 confocal microscope.

Table 2.1: Primary antibodies used in ICC experiments				
Antibody	Ig	Host species	ICC dilution	Supplier, Cat no.
B-III Tubulin	IgG	Rabbit	1:200	Abcam, ab18207
LAMP1	IgG1	Mouse	1:200	Abcam, ab25630
Nanog	IgG	Rabbit	1:66	Abcam, ab80892
Oct4	Recombinant fragment	Rabbit	1:200	Abcam, ab200834
p62	Recombinant full-length protein corresponding to Human SQSTM1/ p62 aa 1-440.	Mouse	1:200	Abcam, ab57416 (discontinued, see Appendix 4 for data sheet)
Sox 2	IgG	Goat	1:100	Biotechne, AF2018
Sox 17	IgG	Goat	1:200	R&D Systems, AF1924
Tra-160	IgM	Mouse	1:200	Abcam, ab16288
Tra-181	IgM	Mouse	1:200	Abcam, ab16289

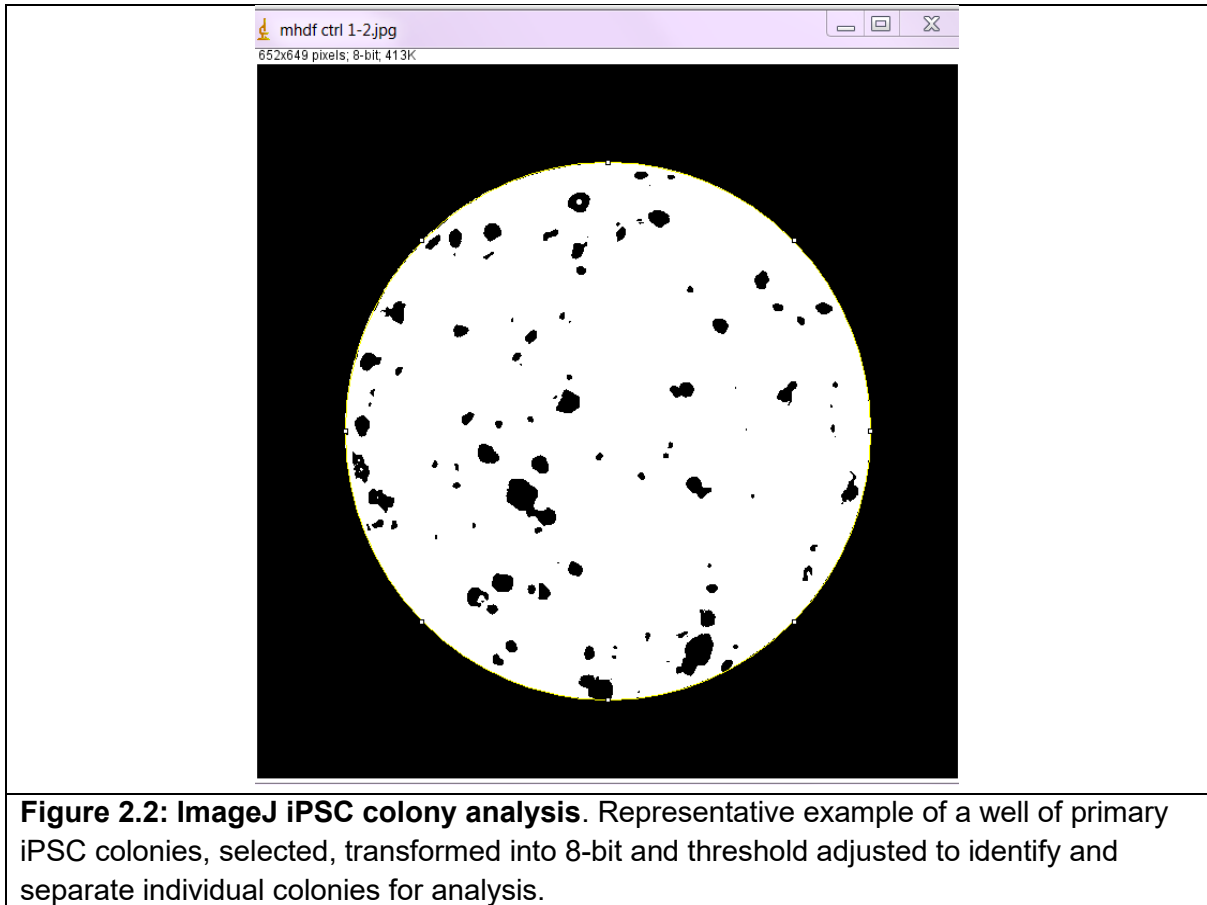
Table 2.2: Secondary antibodies used in ICC experiments		
Antibody	Conjugation	Supplier, Cat. No
Donkey Anti-Goat IgG	Alexa Fluor® 488	Abcam, ab150129
Donkey Anti-Rabbit IgG	Alexa Fluor® 568	Abcam, ab175470
Goat Anti-Rabbit IgG	Alexa Fluor® 488	Abcam, ab150077
Goat Anti-Mouse IgG	Alexa Fluor® 488	Abcam, ab150113
Donkey Anti-Goat IgG	Alexa Fluor® 568	Abcam, ab175474
Goat Anti-Mouse IgG	Alexa Fluor® 568	Abcam, ab175473

2.2.3. Alkaline Phosphatase staining

iPSC colonies were stained for the presence of Alkaline Phosphatase (AP) using SIGMAFAST BCIP®/NBT (Sigma, [B5655](#)). One BCIP/NBT tablet was dissolved in 10ml of ddH₂O, and applied directly to live cells. After 15 minutes of incubation in the dark macroscopic and/or microscopic images were taken ready for analysis

2.2.4. Analysis of AP staining using ImageJ

AP+ colonies were counted and analysed in Image J. Macroscopic images were loaded into the software, and wells selected using the oval selector tool. Images were then converted to 8-bit and the threshold adjusted to create a white background and black colonies (Figure 2.2). Threshold values were kept consistent across matched experiments. Measurements were set in ImageJ and the software analysed colony number, size, shape and area.



2.3. Western blot

2.3.1. Western blot

Cells were lysed for protein using RIPA buffer (Thermo Fisher Scientific, [89900](#)) supplemented with protease inhibitor cocktail (PIC) (Sigma Aldrich, [P8340](#)) at a concentration of 1 μ l/100 μ l. Protein lysates were stored at -80°C. Protein concentration was determined using Bradford reagent (BioRad, [500-0006](#)). Bradford reagent was diluted 1:5 and protein samples diluted 1:10 to minimize interference of RIPA buffer with the Bradford assay. 95 μ l of diluted Bradford reagent was added into each well of a colourless 96-well plate in triplicate for each of the protein standards as well as experimental samples. 5 μ l of each standard and each sample was added to wells and mixed before spectrophotometric quantification at 630 nm.

Later protein samples were quantified using BCA assay, whereby 25 µl of each standard and each unknown sample are added to each well of a colourless 96-well plate. 200 µl of working reagent (diluted according to manufacturer instructions) was added to each well, shaken, and incubated for 30 minutes at 37°C before spectrophotometric quantification at 562 nm.

Proteins were separated using 15% SDS-PAGE. 15-50 µg protein was loaded onto SDS-PAGE gel alongside 5 µl of Precision Plus Protein Kaleidoscope Ladder (BioRad, [1610375](#)) and electrophoresis was carried out at 100 v for 90 minutes in running buffer. Proteins were transferred onto nitrocellulose or PVDF membrane in a semi-dry blotter sandwiched with blotting buffer soaked blotting paper for 1 hour at 15v. Membrane was blocked in 5% milk, 0.1% Tween in PBS for a minimum of 1 hour before adding primary antibody diluted to an appropriate concentration in blocking buffer and incubating overnight at 4°C. Membranes were washed three times in PBS with 0.1% Tween for 5 minutes before blocking in HRP-conjugated secondary antibody (1:5000) for 1 hour at room temperature. Membranes were washed three x 5 minutes in PBS with 0.1% Tween before addition of Amersham ECL Western Blotting Detection Reagent (Fisher Scientific UK, [10340125](#)) for 1 minute and visualisation on a transilluminator.

2.3.2. Densitometry analysis of western blots using ImageJ

Images of western blots developed in a transilluminator were converted to grey scale and loaded into ImageJ. Measurements were set to analyse 'grey mean value'. A 'region of interest' (ROI) was defined for each protein, using the largest protein band in each row. This region of interest was saved for use in all bands for the same protein and each band was measured individually using this pre-defined ROI.

Background measurements for the area immediately outside of the protein bands were also measured using the same ROI frame. Measurements were transported into excel and analysed as a ratio of protein of interest over loading control.

2.4. **MitoTracker RedTM and LysoTracker GreenTM live cell staining**

Cells were seeded in glass-bottomed wells and grown until approximately 80% confluent. MitoTracker Red (Fisher Scientific UK, [M7512](#)) was used at a concentration of 25 nM and cells were incubated for 20-25 minutes; LysoTracker Green (Fisher Scientific UK, [L7526](#)) was used at a concentration of 150 nM and cells were incubated for 2 hours before the stain containing medium was replaced with PBS and cells were viewed using a Leica SP5 confocal microscope.

2.5. **Cloning**

2.5.1. **PCR amplification of mouse and human p62 genes to clone into pENTR1a**

Mouse p62 overexpression vector (mp62) was purchased from Origene (Rockville, MD, USA) (Figure 2.3) and a truncated human p62 overexpression plasmid (hp62 with only the zz and TB regions) was *de novo* synthesized by GeneCopeia (Rockville, MD, USA) in the vector shown in Figure 2.4, with ampicillin resistance. Both of the p62 sequences from these plasmids was cloned into pENTR1a (Figure 2.5) to make later site-specific mutation cloning easier by PCR amplification of the p62 sequences. For the mouse p62, sequence primers were designed with *Bam*HI and *Eco*RI restriction sites added to allow easy re-ligation with the destination vector using complimentary restriction sites. Human p62 primers were designed similarly but with *Kpn*I and *Eco*RI restriction sites. Sequences were amplified using either Q5 high fidelity polymerase (NEB, [M0491S](#)) or Phusion polymerase master mix (NEB,

[M0531S](#)) using appropriate cycling parameters. All primers were purchased from Invitrogen and are listed in Appendix 5

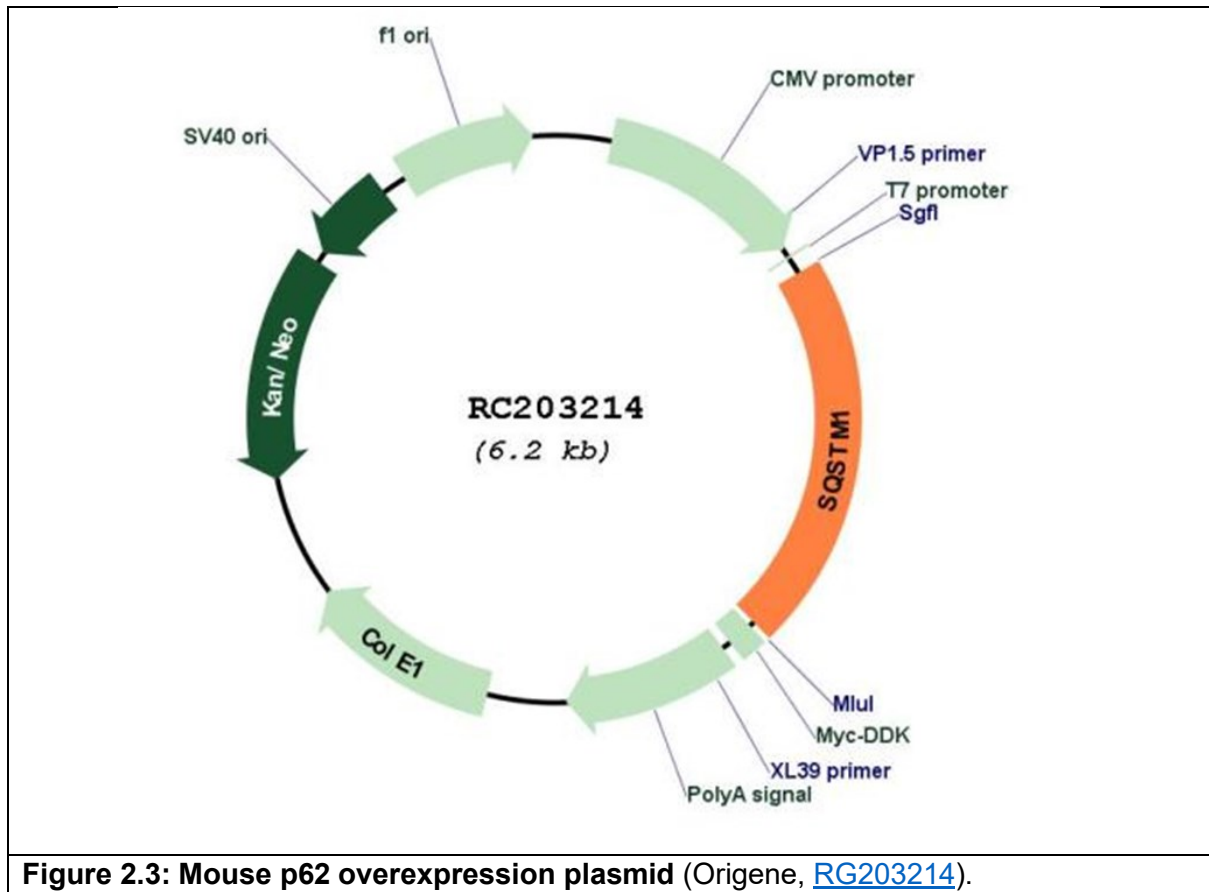


Figure 2.3: Mouse p62 overexpression plasmid (Origene, [RG203214](#)).

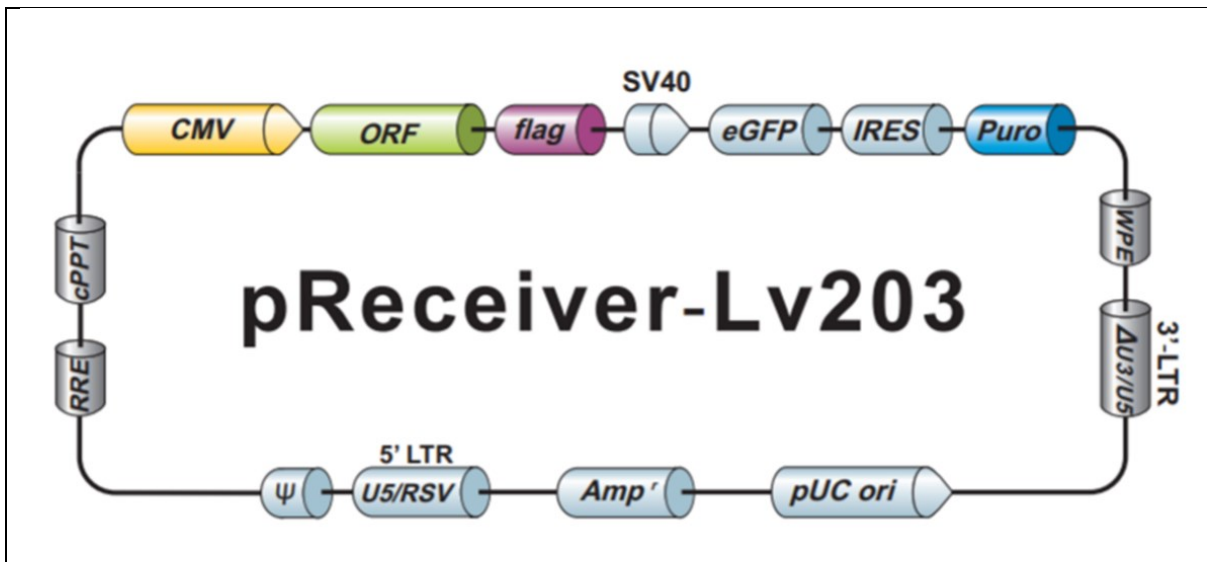


Figure 2.4: Truncated human p62 plasmid (*de novo* synthesised by GeneCopeia, pReceiver- Lv203).

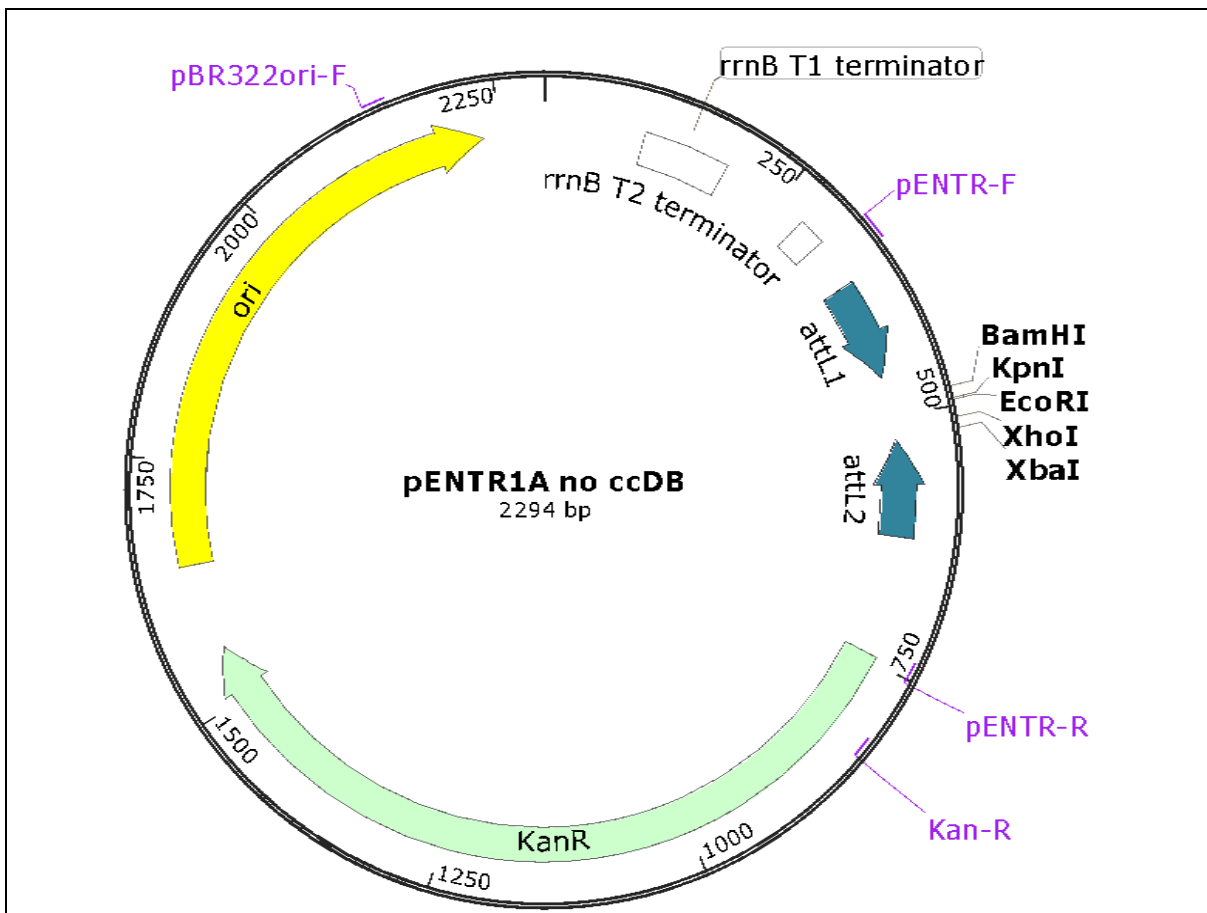


Figure 2.5: pENTR1A minimal cloning vector with select restriction enzymes shown in the multiple cloning site, kanamycin resistance. pENTR1A no ccDB (w48-1) was a gift from Eric Campeau & Paul Kaufman (Addgene, [17398](https://addgene.org/17398/)).

2.5.2. shRNA

shRNA mir sequences were predicted using the SplashRNA algorithm (Pelosof, Fairchild et al, 2017). Dr Stephen White assisted with the design of shRNA constructs (sh(h)p62 and sh(m)p62) and sequences were synthesized by Eurofin Genomics (Ebersberg, Germany) (Figure 2.6). Constructs were designed with inbuilt restriction sites *HpaI* and *XhoI* for ease of cloning into the pLL3.7 destination vector (Figure 2.7) which also contains these restriction sites. shRNA constructs contain three shRNA mir sequences with stem loops, and 60bp between each one to ensure maximum possible efficiency of protein knock-down.

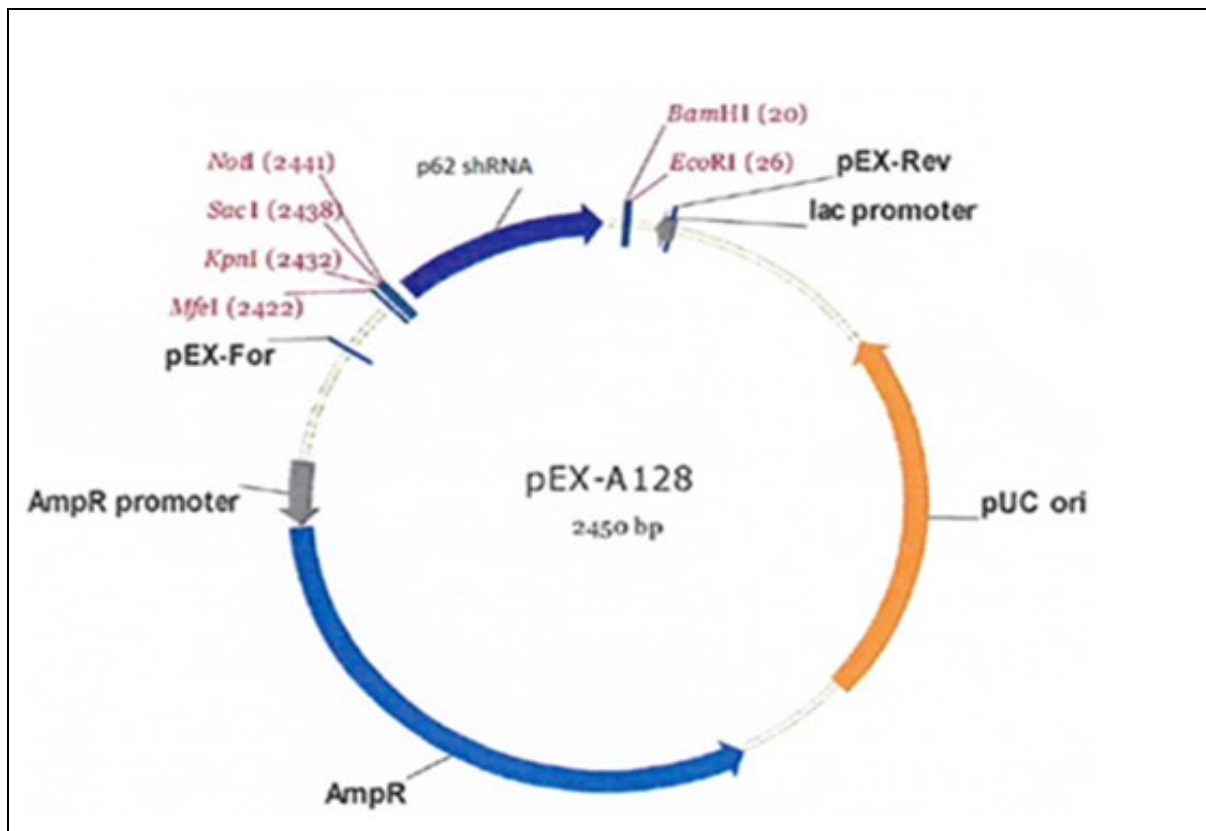


Figure 2.6: pEX-A128 minimal vector containing p62 shRNA sequences. Both human and mouse shRNAs were designed and produced in this minimal vector with selected restriction enzymes for ease of cloning. *De novo* synthesised by Eurofin Genomics.

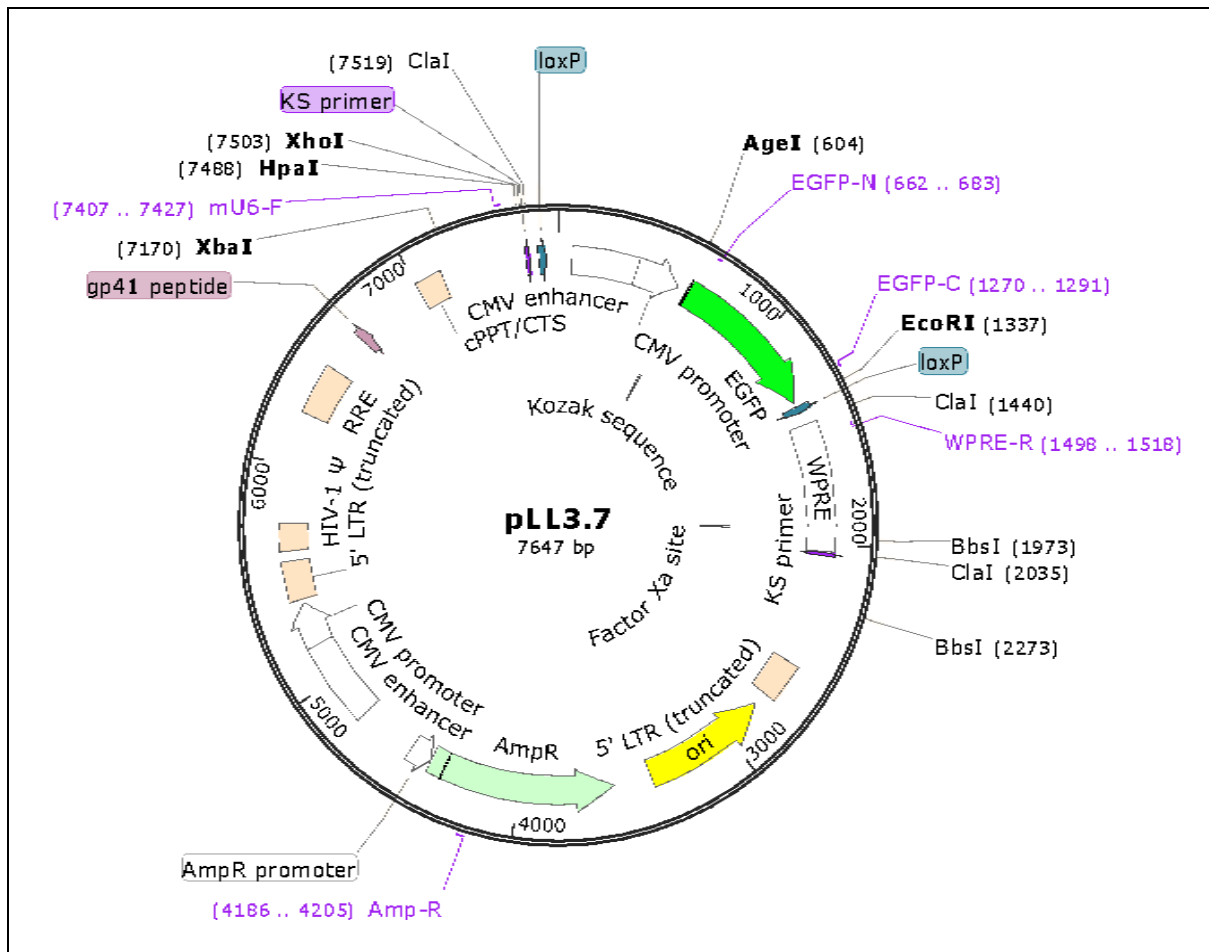


Figure 2.7: pLL3.7 shRNA destination lentivector. pLL3.7 was a gift from Luk Parijs (Addgene, [11795](#))

2.5.3. Additional cloning vectors

Several other vectors were used in either cloning or transduction experiments as listed in Table 2.3.

Table 2.3: Plasmids for cloning and transduction experiments			
Plasmid/Vector	Originating Lab	Addgene ID	Figure
pUMVC	Bob Weinberg	8449	2.8
pCMV-VSV-G	Bob Weinberg	8454	2.9
pBABE-puro-HA-p62	Jayanta Debnath	71305	2.10
pBABE-puro-HA-p62-LIR	Jayanta Debnath	71306	2.10
pBMN-mCherry-p62(ΔUBD)	Michael Lazarou	119687	2.11
pBMN-mCherry-p62 (W340A/ΔUBD)	Michael Lazarou	119688	2.11

pUMVC and pCMV-VSV-G were the packaging and envelope plasmids used for the production of MuLV retroviral particles in Hek293T producer cells (Figures 2.8 and 2.9).

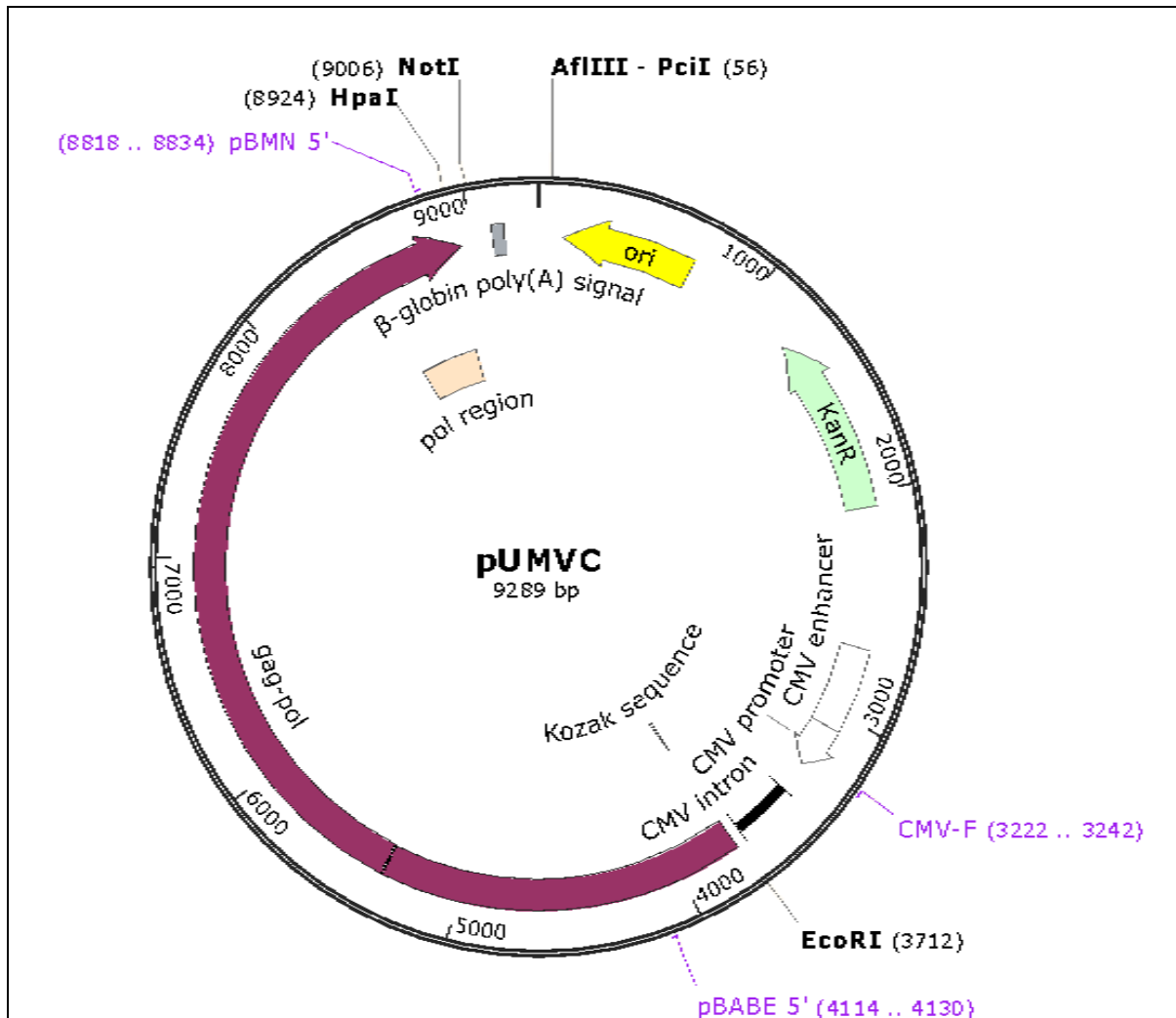
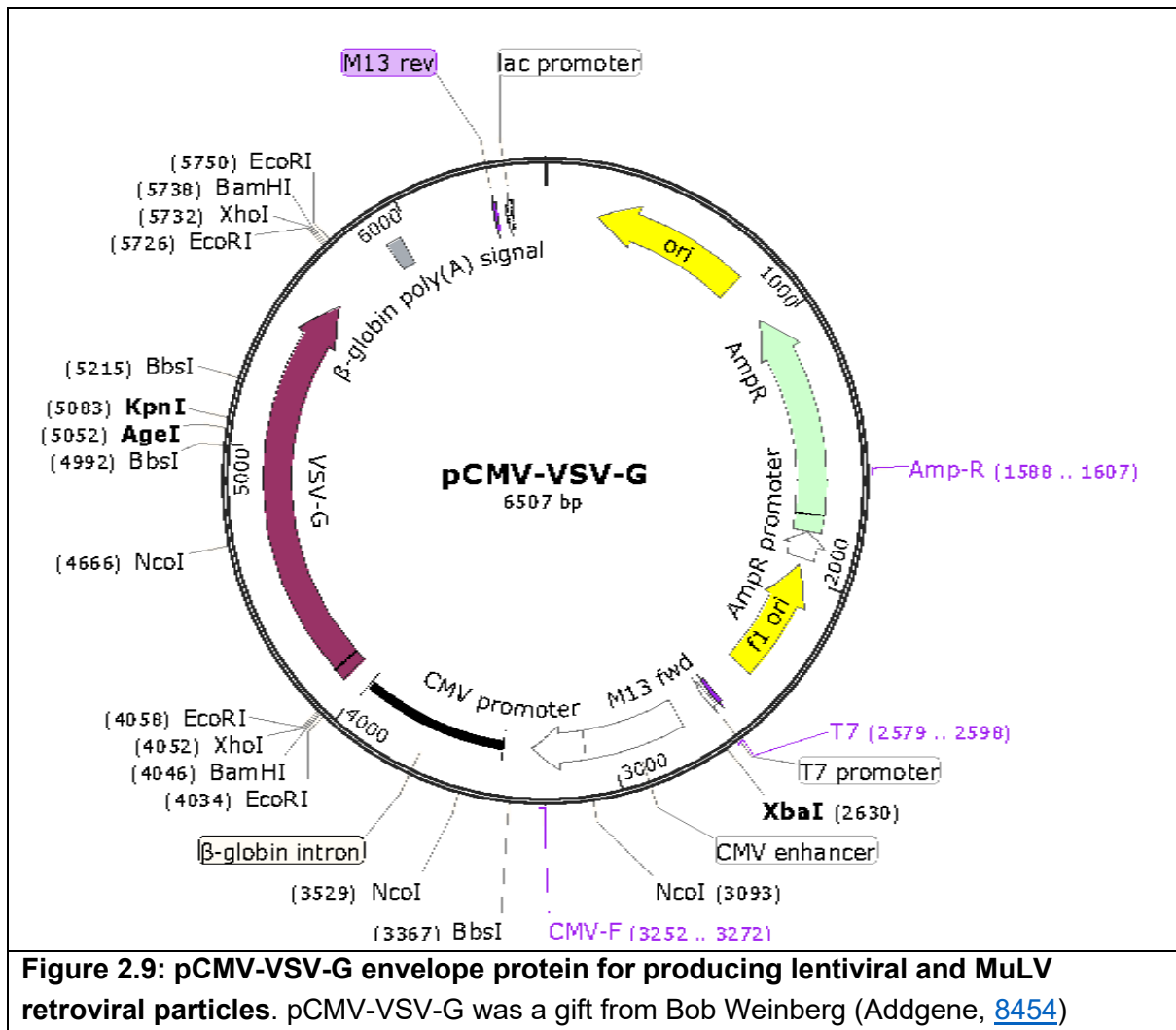


Figure 2.8: pUMVC packaging plasmid for producing MuLV retroviral particles. pUMVC was a gift from Bob Weinberg (Addgene, [8449](#))



pBABE-puro-HA-p62 is a retroviral plasmid for human p62 expression. pBABEpuro-HA-p62-LIR has a DNA point mutation resulting in a single amino acid change at W338A (LIR region). This mutation changes Tryptophan (W) into an Alanine (A): tryptophan can be phosphorylated enabling protein-protein interactions, whereas alanine is non-reactive and cannot be phosphorylated. This means that the function of this particular amino acid in interacting directly with LC3-II is prevented (Figure 2.10).

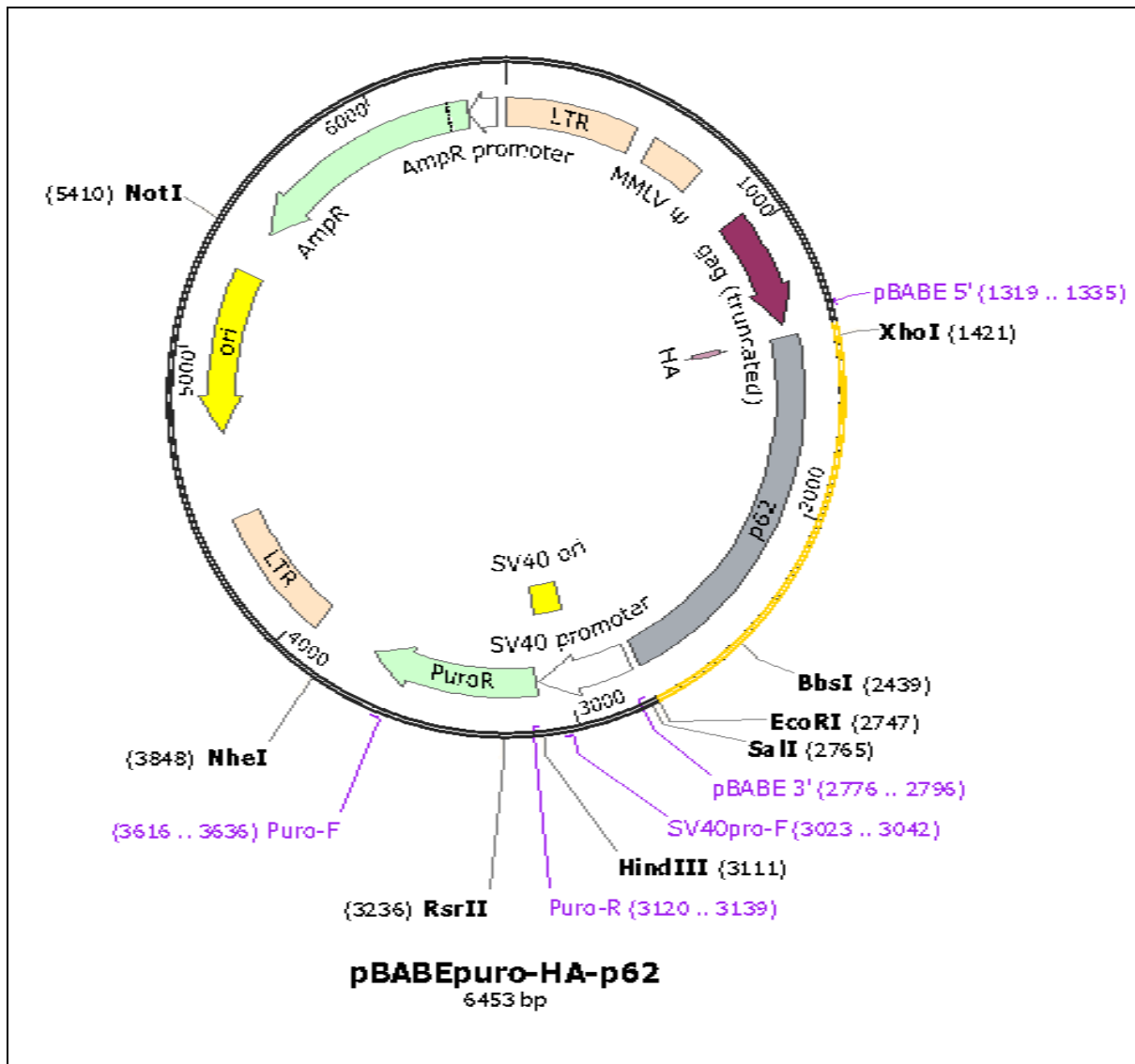
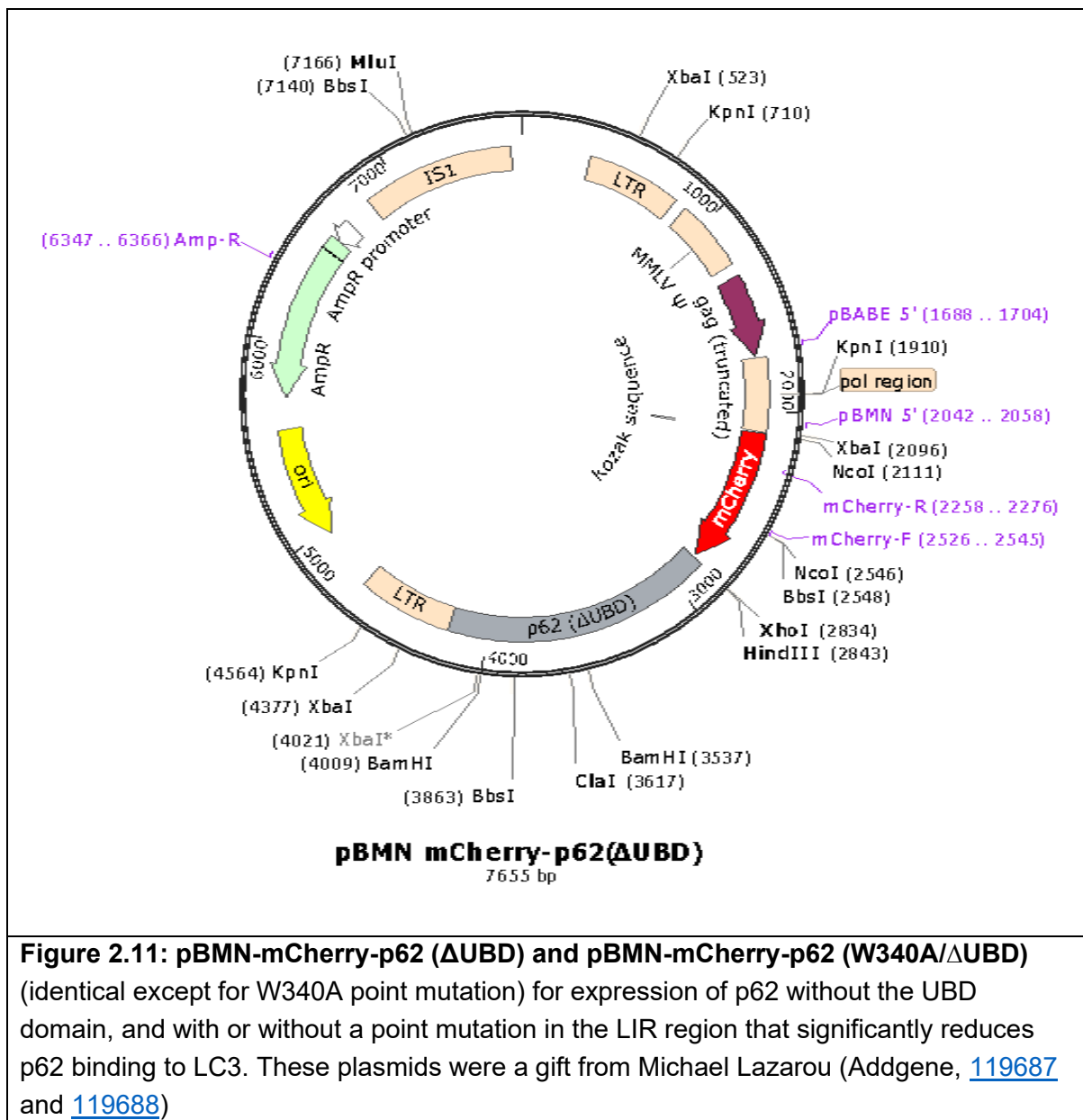


Figure 2.10: pBABEpuro-HA-p62 and pBABEpuro-HA-p62 LIR (identical except for W338A point mutation) for the expression of full-length human p62, and the expression of p62 with a point mutation at amino acid 338 that significantly reduces p62 binding to LC3. pBABEpuro-HA-p62 and pBABEpuro-HA-p62 LIR were a gift from Jayanta Debnath (Addgene, [71305](#) and [71306](#))

pBMN mCherry-p62 (Δ UBD) is a retroviral plasmid for the expression of human p62 without its UBD region: p62 was truncated at residue 385, meaning that the resulting protein could not bind to ubiquitinated proteins, thereby preventing the recruitment of these proteins to the autophagosome. pBMN mCherry-p62 (W340A/ Δ UBD) also has a point mutation leading to an amino acid change at W340A in the LIR region, again

preventing phosphorylation at this site and ameliorating the direct interaction of p62 with LC3B (Figure 2.11).



2.5.4. Cloning: restriction digest and gel extraction

800 ng-1 µg of plasmid DNA was digested with 1 µl of each restriction enzyme (*HpaI* + *XhoI* for cloning shRNA constructs or *BamHI* + *EcoRI* for mp62 overexpression plasmid constructs or *KpnI* + *EcoRI* for hp62 overexpression constructs) and 3 µl of

the appropriate NEB buffer made up to 30 µl with water for 1 hour at 37°C before separation by agarose gel electrophoresis. Alongside, pENTR1a (or other destination vector) was also digested using complimentary restriction enzymes to linearise. Correctly restricted bands were then excised from the gel and gel extraction was performed using columns according to kit instructions (Fisher Scientific, Machery and Nagel, [12303368](#)) before determination of DNA concentration by spectrophotometry using a Nanodrop device (Thermo Fisher). Restriction Enzymes were all purchased from New England Biolabs and are listed in Table 2.4.

Table 2.4: Restriction enzymes used in cloning experiments		
Enzyme	Restriction sequence	Cat. No.
<i>Xho</i> I	C [^] TCGAG	R0146S
<i>Bam</i> HI	G [^] GATCC	R0136S
<i>Eco</i> RI	G [^] AATTC	R3101S
<i>Kpn</i> I	GGTAC [^] C	R0142S
<i>Hpa</i> I	GTT [^] AAC	R0105S
<i>Cla</i> I	AT [^] CGAT	R0197S
<i>Nco</i> I	C [^] CATGG	R0193S

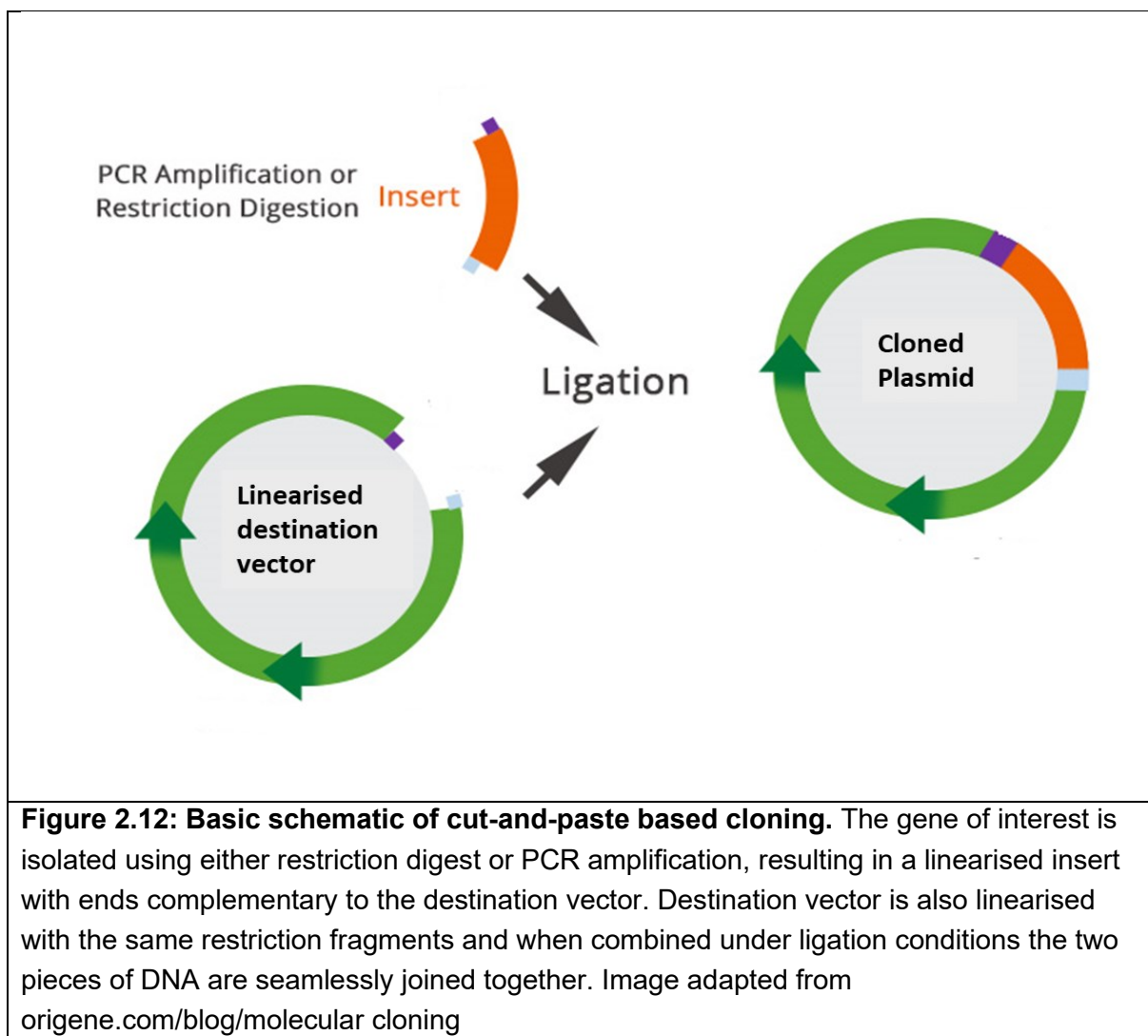
2.5.5. Cloning: Ligation

mp62, truncated hp62 and p62 shRNA constructs were all ligated with destination vectors (pENTR1a or pLL3.7) at three different molar ratios (1:3, 1:5 and 1:10) to maximise efficiency of re-ligation. Ligation reaction was made up with plasmid insert and linearised destination plasmid backbone, 10 µl ligase buffer (NEB, B2200S), 1

µl quick ligase (NEB, M2200L) and H₂O up to 10 µl and incubated at room temperature before transformation. Figure 2.12 provides an overview of cut and paste based cloning and ligation. Ligation reactions were made up with the appropriate amounts of insert and backbone according to the following calculation:

$$\text{Amount of insert (ng)} = \frac{\text{amount of vector (ng)} \times \text{molar ratio} \times \text{size of insert (bp)}}{\text{Size of vector (bp)}}$$

For example: $\frac{50 \text{ ng vector} \times 3 \text{ (molar ratio)} \times 437 \text{ bp insert size}}{7600 \text{ bp vector size}} = 8.63 \text{ ng of insert required}$



2.5.6. Cloning: Recombination

mp62 pENTR1a plasmid was recombined using Gateway™ cloning into SFFV lentiviral plasmid for lentiviral vector production and transduction into cells. 50 ng of SFFV Gateway™ and 50 g mp62 pENTR1a was combined with 3.1 µl TE buffer and 1 µl of LR Clonase (Thermo Fisher Scientific, [11791019](#)) and incubated at room temperature for 1 hour.

2.5.7. Cloning: Transformation and recovery.

Chemically competent Stab13 cells were thawed on ice for approximately 10 minutes. For transformation of existing plasmids 100 ng of plasmid DNA was added to chemically competent cells. For transformation of newly ligated plasmids, the entire ligation reaction was added. Cells were incubated on ice for 30-50 minutes. Cells were then heat-shocked at 42°C for 45 seconds before a further 2 minutes incubation on ice. 500 µl SOC broth (Thermo Fisher Scientific, [15544034](#)) was added and cells underwent recovery for 45-60 minutes in a shaking incubator at 37°C. After recovery, cells were plated onto Agar (Sigma Aldrich, [9002-18-0](#)) plates. For existing plasmids, 100 µl of the comp cell/DNA/SOC mixture was spread onto plates. For newly ligated plasmids the cells were centrifuged (Sigma 1-16k) for 3 minutes at 1000 rpm and the cell pellet resuspended in 100 µl SOC broth and spread onto agar plates with an appropriate antibiotic (Ampicillin or Kanamycin). The next day single colonies were aseptically picked and grown in LB growth medium (Sigma Aldrich, [L3022-1kg](#)) with antibiotic.

2.5.8. Qiagen Mini and Midi-Prep DNA preparation.

Bacterial growth cultures were centrifuged at 4500rpm in a tabletop centrifuge for 30 minutes (midi-prep) or at 13000rpm for 10 minutes in a microcentrifuge (Sigma 1-14k) (mini-prep) before plasmid DNA was extracted and purified using columns according to the kit instructions (Qiagen Mini-Prep Kit, Qiagen, [27106](#), Qiagen Midi-Prep Kit, Qiagen, [12143](#)). DNA concentrations were determined using a Nanodrop.

2.5.9. Cloning: In-Fusion® cloning for site specific mutations

In-Fusion® cloning (Figure 2.13) allows direct cloning of any sequence into any destination vector in a single step. Primers were designed incorporating single nucleotide mutations to create mutations in various different function p62 domains for both mouse and human and can be found in Appendix 6 (with thanks to Dr Alicia Roig-Merino and Dr Richard Harbottle (DKFZ) for help and guidance with In-Fusion® cloning). hp62 and mp62 sequences + restriction sites were amplified from parent or pENTR1a vector with CloneAmp HiFi PCR Premix (Takara Bio, [639298](#)) at appropriate cycling parameters.

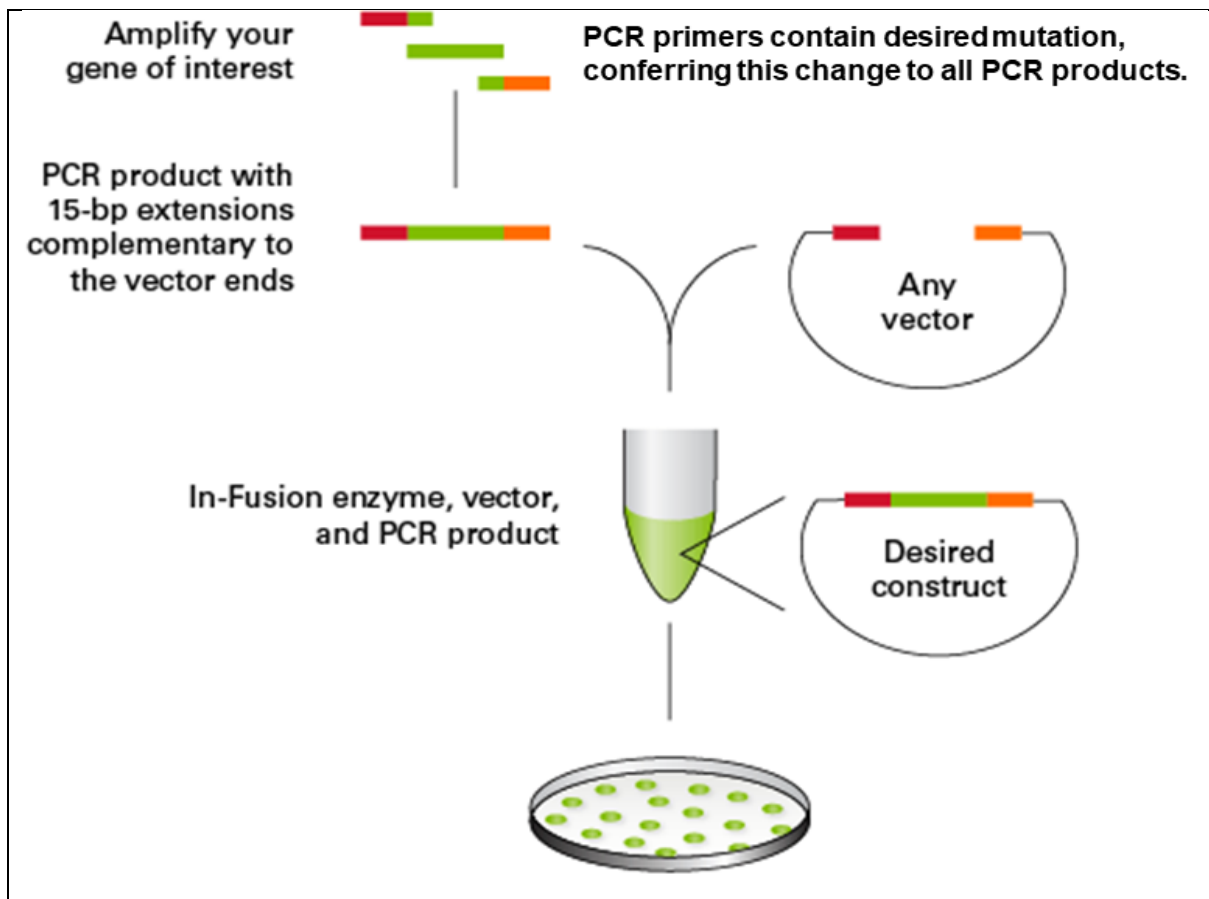


Figure 2.13: Basic principle of In-Fusion® cloning. Primers are designed with ~15bp of complementarity with destination vector ends and the desired DNA mutations. PCR product containing 15bp extensions and newly created DNA mutations are combined with the linearized vector and the In-Fusion® enzyme mix in a single step reaction and transformed into competent cells. Image adapted from <https://www.takarabio.com/learning-centers/cloning/in-fusion-cloning-general-information/in-fusion-cloning-overview>

Concurrently, destination vectors (hp62 pENTR1a or mp62 pENTR1a) were digested with restriction enzymes complementary to those added in to PCR primer sequences (Appendix 6). 3 µg of destination vector (approx. 10 µl) was combined with 3 µl of each restriction enzyme, 5 µl of Fast Digest buffer, and approximately 29 µl H₂O and incubated at 37°C for 1 hour.

Digested destination vector and PCR product were separated by agarose gel electrophoresis (Agarose, Sigma, [A9539](#); GelRed, Biotium, [41003](#)). Vector backbone and hp62 or mp62 sequence with newly introduced mutation were gel extracted

according to manufacturer's instructions (Fisher Scientific, Machery and Nagel, [12303368](#)) before determination of DNA concentration by spectrophotometry using a Nanodrop device. Finally, 100 ng of backbone and 50 ng of insert were combined in an In-Fusion® reaction with 2 µl of infusion mix (Infusion HD Cloning Kit, Takara Bio, [639645](#)) and H₂O up to a total reaction volume of 10µl. This was incubated at 50°C for 15 minutes before 25 µl of the In-Fusion® reaction was transformed into infusion compatible Stellar Competent Cells (Stellar Competent Cells, Takara Bio, [636763](#)) and transformation, recovery and propagation in agar plates was carried out as previously described for all other cloning methods.

2.6. **Transfection; virus production and quantification; and transduction.**

2.6.1. Production of VSV-G psuedotyped lentivector using PEI.

Using plasmid DNA VSV-G psuedotyped lentivirus preps were produced in a small scale (1 well to 1 well format) or large-scale format whereby virus can be concentrated and titred using p24 ELISA. With the small-scale protocol, cells were transduced directly with the filtered conditioned media from transfected Hek293T producer cells at both 48 and 72 hours post transfection and an approximation of transduction efficiency was estimated from GFP expression after 96 hours.

2.6.2. Large- scale viral preparation

Hek293T cells were grown in a T175 cm² flask until 90% confluent. Plasmid DNA mix was made up with 6 mL OptiMEM (Reduced serum medium) (Fisher Scientific UK, [15392402](#)); 50 µg of vector construct; 17.5 µg of VSVg envelope plasmid (pMD2.G) and 32.5 µg of packaging plasmid (pCMVΔ 8.74). pMD2.G and pCMVΔ 8.74 were a gift from Didier Trono (Addgene, [12259](#) and [22036](#))

Separately, 1 μ l of 10 mM PEI was added to 6 mL OptiMEM and this was mixed together 1:1 with the plasmid DNA mixture and incubated at room temperature for 20 minutes to allow DNA complexes to form. Media was removed from Hek293Ts, replaced with the 12ml of DNA mixture, and incubated at 37°C for 3 hours before changing to normal DMEM media. Media was then changed after 24 hours, and cell supernatant harvested at 48 and 72 hours.

Cell supernatant was centrifuged at 5000rpm for 10 minutes at 4°C then passed through a 0.22 μ m filter into a fresh 50 mL falcon tube. To concentrate the virus the filtered cell supernatant was centrifuged at 5000rpm and 10°C for 16-20 hours in a benchtop centrifuge. Supernatant was then carefully removed and discarded and the viral pellet air-dried for 2 minutes. Pellets were resuspended in 50 μ l OptiMEM and incubated on ice for 1 hour before aliquoting and storing at -80°C.

2.6.3. Small-scale viral preparation

Hek293T cells were grown in one well of a six-well plate until 90% confluent. Plasmid DNA mix was made up with 324.5 μ l OptiMEM; 2.75 μ g expression vector construct; 0.96 μ g of VSV-G envelope plasmid (pMD2.G) and 1.79 μ g of packaging plasmid (pCMV Δ 8.74).

Separately, 5.5 μ l of 0.1 mM PEI was added to 324.5 μ l OptiMEM and this was mixed together 1:1 with the plasmid DNA mixture and incubated at room temperature for 20 minutes to allow DNA complexes to form. Media was then removed from HEK293Ts, replaced with the DNA mixture, and incubated at 37°C for 3 hours before changing to normal DMEM media. Media was changed after 24 hours, and cell supernatant harvested at 48 and 72 hours before filtering.

2.6.4. Virus quantification

Concentrated lentivirus was quantified using an HIV-1 p24 antigen ELISA. (Zeptomatrix, [0801111](#)). The *gag* gene in recombinant lentiviruses encodes the viral capsid protein, p24. The amount of p24 in a viral sample is directly correlated to the viral titre. P24 ELISA was carried out according to the manufacturer's [instructions](#). Briefly, wells were pre-coated with Anti-p24, which binds p24 in samples, a biotinylated Anti-p24 and Streptavidin HRP with a colour producing substrate were then added. Samples were quantified by spectrophotometry at 450nm. By utilising a standard curve of known p24 antigen concentrations is possible to determine viral titre of unknown samples in the following formula:

$$\text{Viral Titer} = ((\text{OD} - \text{Intercept})/\text{Slope}) \times 100 \times \text{dilution factor}.$$

The MOI, or volume needed to apply to cells for a desired MOI can then be determined using the following equation:

$$\text{MOI} = (\text{volume of virus applied to cells } (\mu\text{l}) \times \text{titre})/\text{cell number}.$$

Chapter 3. Development of iPS reprogramming protocols and processes.

Chapter 3: Development and refinement of iPS reprogramming protocols and processes.

1.1. Introduction

There are multiple methods for the reprogramming of somatic cells to the pluripotent state, as discussed in detail in the main introduction of this thesis, but the current gold standard is the use of OriP/EBNA episomal plasmids (Yu et al, 2009, Okita et al, 2011, Okita et al, 2013). The OriP/EBNA plasmids strike a reasonable balance between efficiency and safety: Efficiencies of around 0.01-0.02% can be achieved but the episomal plasmids have several safety benefits, predominantly that they are non-integrating and non-viral (Yu et al, 2009; Bang et al, 2018). These plasmids encode the reprogramming factors Oct3/4, L-Myc, Lin28, Sox2, KLF4 as well as components which have been shown to help boost reprogramming efficiency shp53 and EBNA1 (Okita et al, 2011; Okita et al, 2013). These non-integrating, episomal OriP/EBNA reprogramming plasmids are utilised as standard within the McKay lab for the reprogramming of human fibroblasts. The McKay lab does not have a standard reprogramming protocol used in the reprogramming on mouse cells, so one key aim of this chapter is to refine the existing protocols for use in mouse cells.

In order to ensure that valuable patient cells, which had been acquired in very small numbers, were utilised in the best possible way, a series of reprogramming experiments were carried out in other cells types to learn, develop and refine the protocols necessary throughout the process. The reprogramming process is highly inefficient, and inherently has a large number of steps where failure can occur. Ensuring that cells survive nucleofection, are seeded at the right density, are switched to hESC growth media at the correct time, and are analysed and passaged at the optimal time all requires a huge amount of refining.

Further, p62 null patient cells were acquired at P8 from our collaborators in Finland. It is well known that increased time in culture decreases reprogramming efficiency, due to increased levels of cell senescence (Trokovic et al, 2015). Of course, the addition of shp53 in the OriP/EBNA episomal plasmids helps to alleviate this issue due to its suppression of cellular senescence pathways (Rasmussen et al, 2015; Fujita, 2019), but it was important to ensure that other cell types available within the McKay lab (i.e. control hDFs) could also be successfully reprogrammed at later passages as iPSC reprogramming experiments had never previously been carried out in cells beyond passage 5 within the McKay lab.

1.2. **Objectives:**

- Complete iPSC reprogramming experiments in a range of cells types including:
 - WT MEFs
 - Doxycycline inducible MEFs
 - Control hDFs
 - p62 overexpressing CLN6 and CLN7 Batten's disease patient fibroblasts
- Validate iPSC reprogramming experiments by immunocytochemical staining for key pluripotency markers

1.3. **Inducible MEF reprogramming**

We acquired, from the Hochedlinger lab, Harvard Medical School, MA, USA, a doxycycline inducible mouse embryonic fibroblast (MEF) cell line (Stadtfeld et al, 2009). These MEFs were derived from 'reprogrammable mice' in which every cell possesses a single copy of a polycistronic reprogramming cassette containing the OKSM combination of reprogramming factors (Figure 3.1) This cassette is

doxycycline inducible, allowing for the controlled and synchronised induction of pluripotency. This highly efficient system represented the perfect starting point for reprogramming experiments, enabling the understanding of key milestones of pluripotency such as morphological evidence of MET.

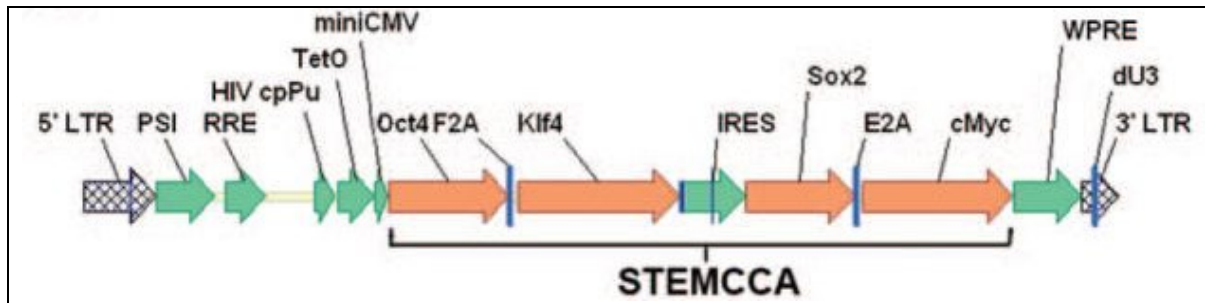


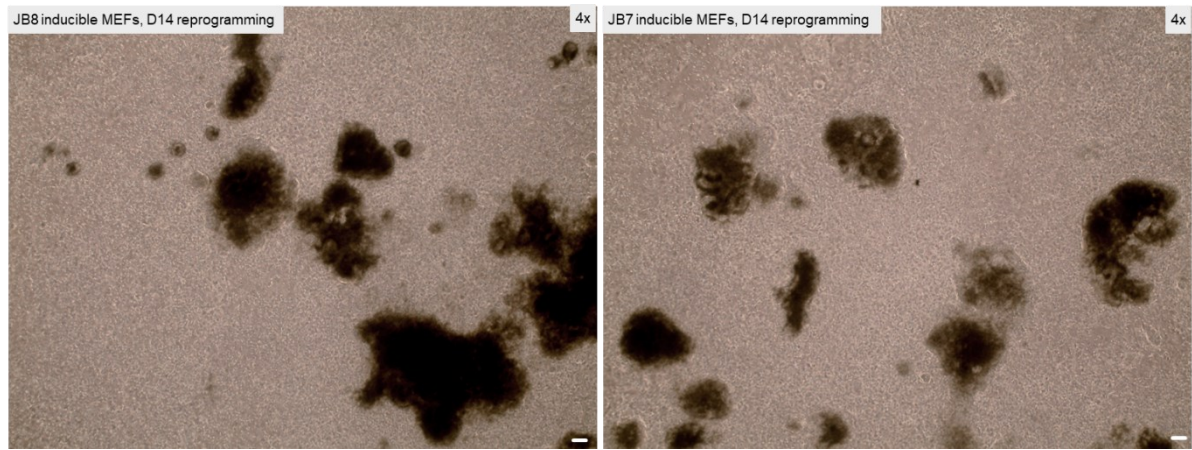
Figure 3.1: The STEMCCA multicistronic 2A-OKSM cassette was stably transduced into ‘reprogrammable mice’ by the Hochedlinger lab. MEFs derived from the embryos of these mice undergo synchronised iPSC reprogramming upon addition of doxycycline. Sommer et al, 2008

Inducible MEFs were thawed as previously described in two wells of a 6-well plate (Methods, 2.1.1 and 2.1.4), and cultured in MEF maintenance media until ready to begin reprogramming. Upon the addition of reprogramming media containing LIF, Ascorbic acid and Doxycycline at a concentration of 2µg/ml, colonies began to appear at ~14d (Figure 3.2, A.). Mouse ES and iPS colonies are typically smaller than human ES and iPSC colonies, and require passaging more frequently. Both the JB7, and JB8 lines supplied are homozygous for the OKSM cassette, but the JB8 line may be heterozygous for Oct4-GFP. This has no effect on reprogramming efficiency as this construct is in place purely as a marker of pluripotency in the resulting iPSC cells.

At ~16d, doxycycline and ascorbic acid containing media was removed and replaced with mESC maintenance media as previously described (Appendix 3) and allowed to

acclimatise for 3 days before AP staining was carried out on ~d20 (Figure 3.2, B). AP staining shows a large number of colonies in both JB7 and JB8 reprogramming experiments. It was not possible to count individual colonies because there were too many to distinguish between them either manually or in ImageJ. Although not quantified, it is clear looking by eye at the AP staining that far more colonies were formed in JB7 cells than JB8, possibly because JB7 MEFs were reprogrammed at P3 whereas JB8 MEFs were reprogrammed at P5. Notably, the polycistronic OKSM reprogramming cassette in these cells does not contain shp53, unlike the OriP/EBNA plasmids used for other reprogramming experiments in this study. This could mean that the later passage JB8 MEFs had undergone some level of cell senescence, resulting in a lower reprogramming efficiency in these cells compared to the JB7. Primary JB7 and JB8 miPSC colonies were serially passaged and imaged at P2 (Figure 3.2.C). JB7 and JB8 miPSC colonies are morphologically very similar and grow in similar numbers after passaging.

A.



B.



Figure 3.2: iPSC reprogramming of JB7 and JB8 inducible MEFs.

A. Primary (P0) miPSC colonies at ~14d, Images taken at 4x magnification. Scale bars represent 100 μ M **B.** AP staining of P0 colonies at ~20d showing extremely high reprogramming efficiency (evidenced by the density of AP positive stained areas) in both JB7 and JB8 miPSC reprogramming experiments

C.

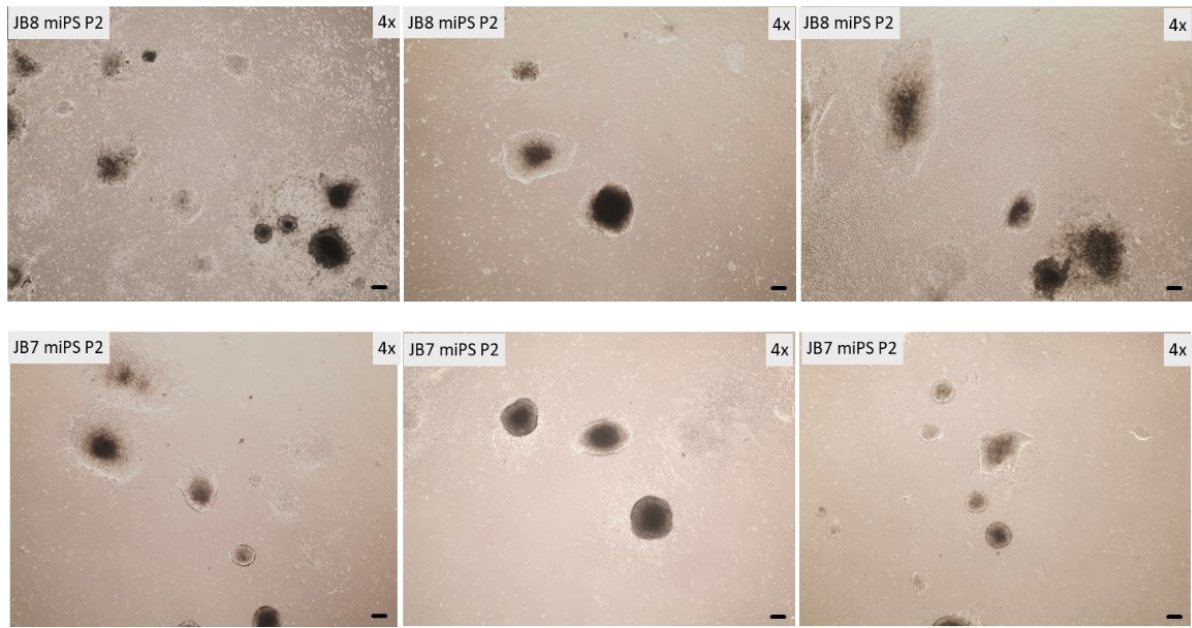


Figure 3.2: iPS reprogramming of JB7 and JB8 inducible MEFs.

C. JB7 and JB8 miPSC colonies after two passages. Several iPSC colonies with clearly defined borders and a typical rounded shape can be seen. Scale bars represent 100 μ M

Finally, JB7 and JB8 were passaged again, fixed with 4% PFA and immunostained for SSEA1, a marker of pluripotency in mice (and of early differentiation in human cells) , and imaged for this, and constitutive OCT4-GFP expression (Figure 3.3). Both JB7 and JB8 miPSC are Oct4-GFP positive and SSEA1 positive, confirming pluripotency in these cells.

A.

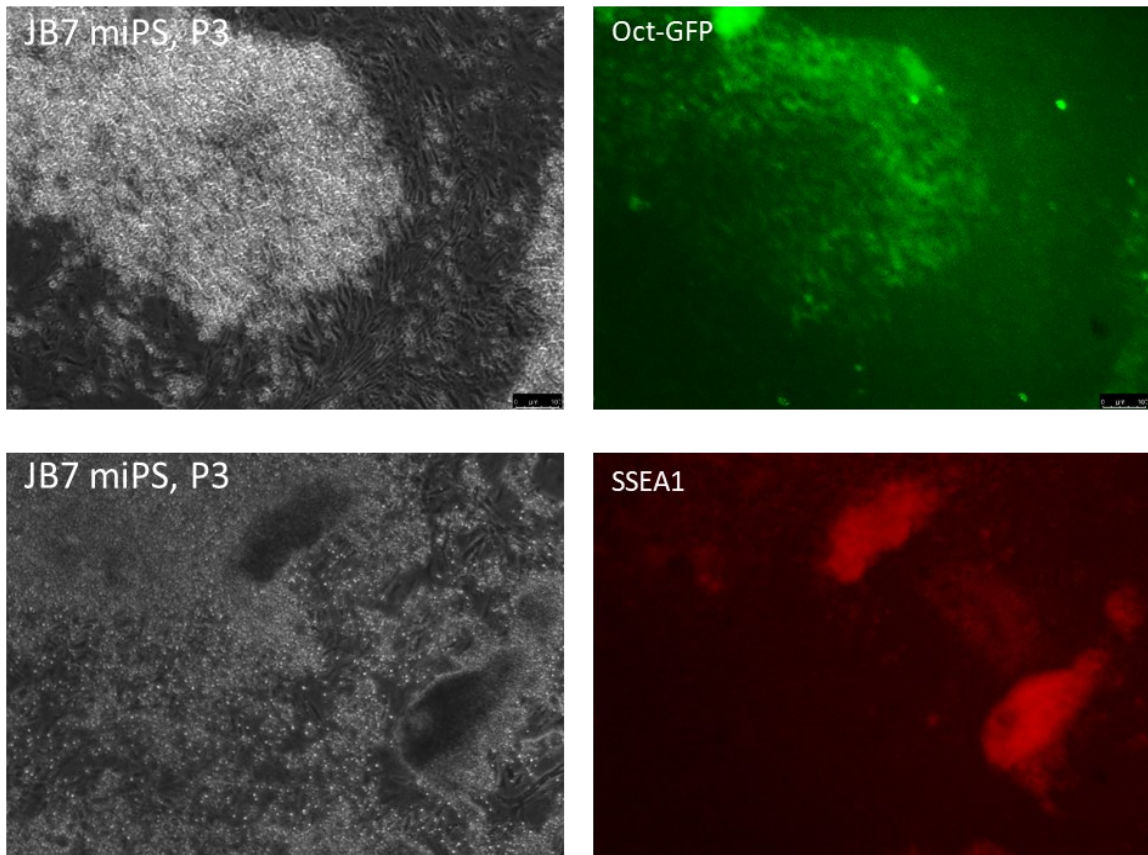
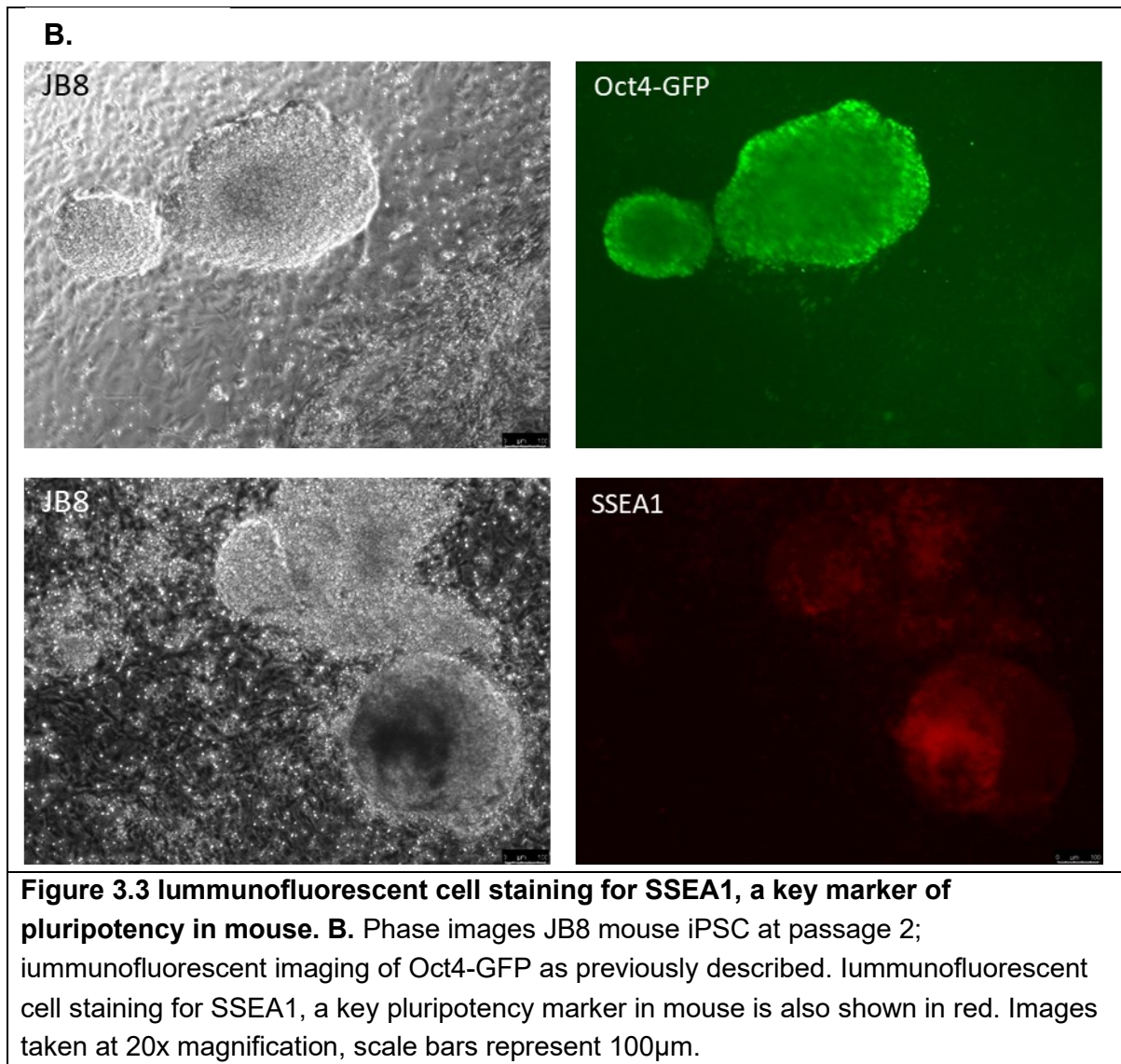


Figure 3.3 Immunofluorescent cell staining for SSEA1, a key marker of pluripotency in mouse.

A. Phase images JB7 mouse iPSC at passage 2; immunofluorescent imaging of Oct4-GFP (Green). The 'reprogrammable mice' from which these cells are derived contain the gene for enhanced GFP in the Oct4 locus, creating a marker for the acquisition of pluripotency as cells are GFP positive when endogenous Oct4 is being expressed. Immunofluorescent cell staining for SSEA1, a key pluripotency marker in mouse is also shown in red. Images taken at 20x magnification, scale bars represent 100 μ m.



1.4. WT-MEF reprogramming

Having successfully achieved iPSC reprogramming with doxycycline inducible MEFS, I next progressed to subjecting Wild-Type Mouse Embryonic Fibroblasts (WT-MEF) to iPSC reprogramming using an adapted version of the established McKay lab hDF reprogramming protocol. Mouse iPSC reprogramming happens slightly quicker than human iPSC reprogramming, and there is no need for MEF feeder layers, as the initial starting cells (MEFs) provide all the necessary structural support and growth factors. For this reason, media was changed to mESC media on day 2 instead of day 9, and cells were plated directly onto gelatin-coated plates

where they remained for the duration of the reprogramming experiment.

Furthermore, primary iPSC colonies in hDF reprogramming experiments are generally analysed and passaged at ~25d, whereas in mouse reprogramming experiments colonies are analysed and passaged earlier, at around ~16-20d. Figure 3.4.A shows WT-MEF at 10d and 16d of a reprogramming experiment. At 10d an early 'pre-ipsc' colony can be seen, and at 16d a well formed primary (P0) colony. At 16d newly formed miPSC colonies were passaged by manual excision, pipetted to a single cell suspension, centrifuged at 1200rpm and reseeded at a density of 1:10 on inactivated MEF feeder layers. miPSC colonies are passaged every 3 days. Figure 3.4.B shows P4 WT-miPSC colonies compared with mESC colonies as a positive control. miPSC colonies, even at this very early passage where they are not yet mature and transgene free are morphologically similar to mESC colonies.

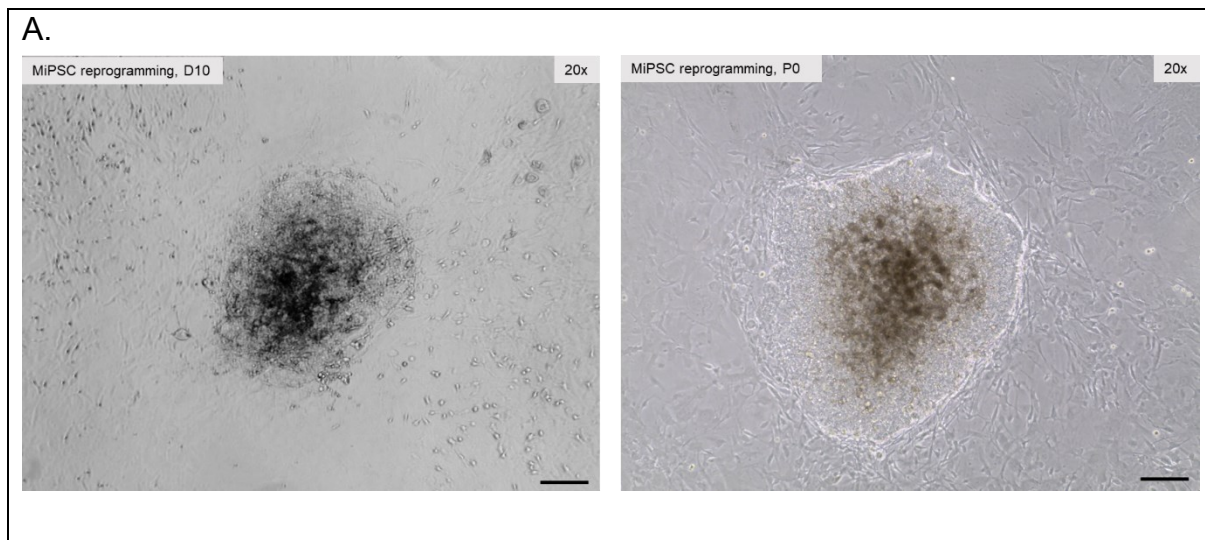


Figure 3.4 Reprogramming of WT-MEFs to miPSC.

A. WT-MEFs at D10 (left) and D16 (P0) (right) of miPSC reprogramming experiments. At D10, early colony formation can be seen, the cells in the colony like structure are small, round and lacking cytoplasm but the colony itself has not yet gained the well-defined border expected in an established iPSC colony. Phase images taken at 20x magnification. At ~16-18d primary (P0) colonies are passaged. Scales bars represent 100µM

B.

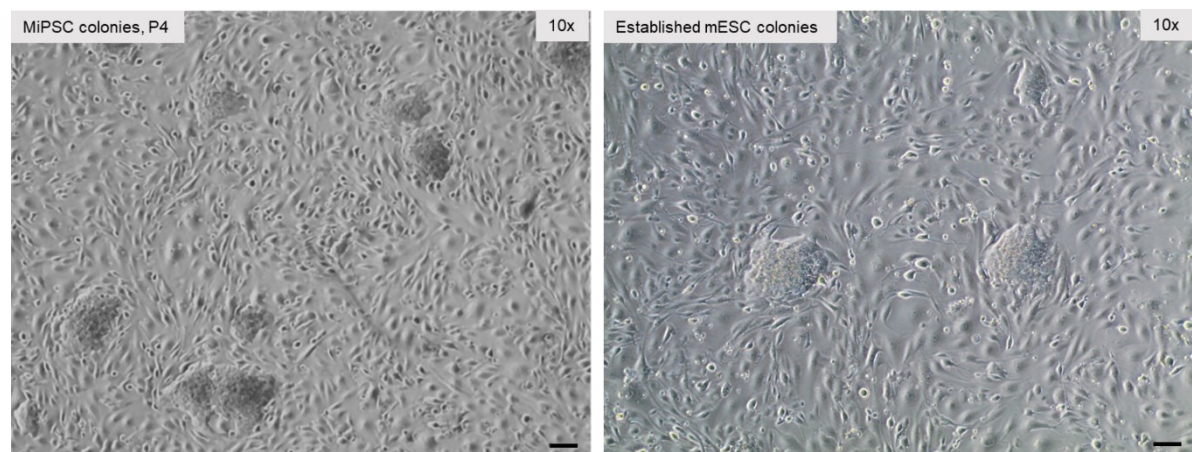


Figure 3.4 Reprogramming of WT-MEFs to miPSC. B. miPSC colonies after 4 passages (left) compared to established mESC colonies (right). Clear morphological similarities can be seen: colonies are of a similar size and have the same rounded appearance with well-defined borders. miPSC colonies are typically smaller than human and require passaging more frequently. miPSC colonies are cultured on iMEF feeder layers after initial passage, mESC are cultured on iMEF feeder layers. Phase images taken at 10x magnification, scale bars represent 100 μ M

At P6 miPSC were fixed with 4% PFA and immunostained for key markers of pluripotency in mouse cells: Lin28, Nanog and E-Cadherin alongside mESC positive controls and MEF negative controls (Figure 3.5). miPSC were positive for Lin28, Nanog and E-Cadherin, like mESC positive controls, suggesting pluripotency. As expected, MEFs are negative for Lin28, Nanog and E-Cadherin.

A.

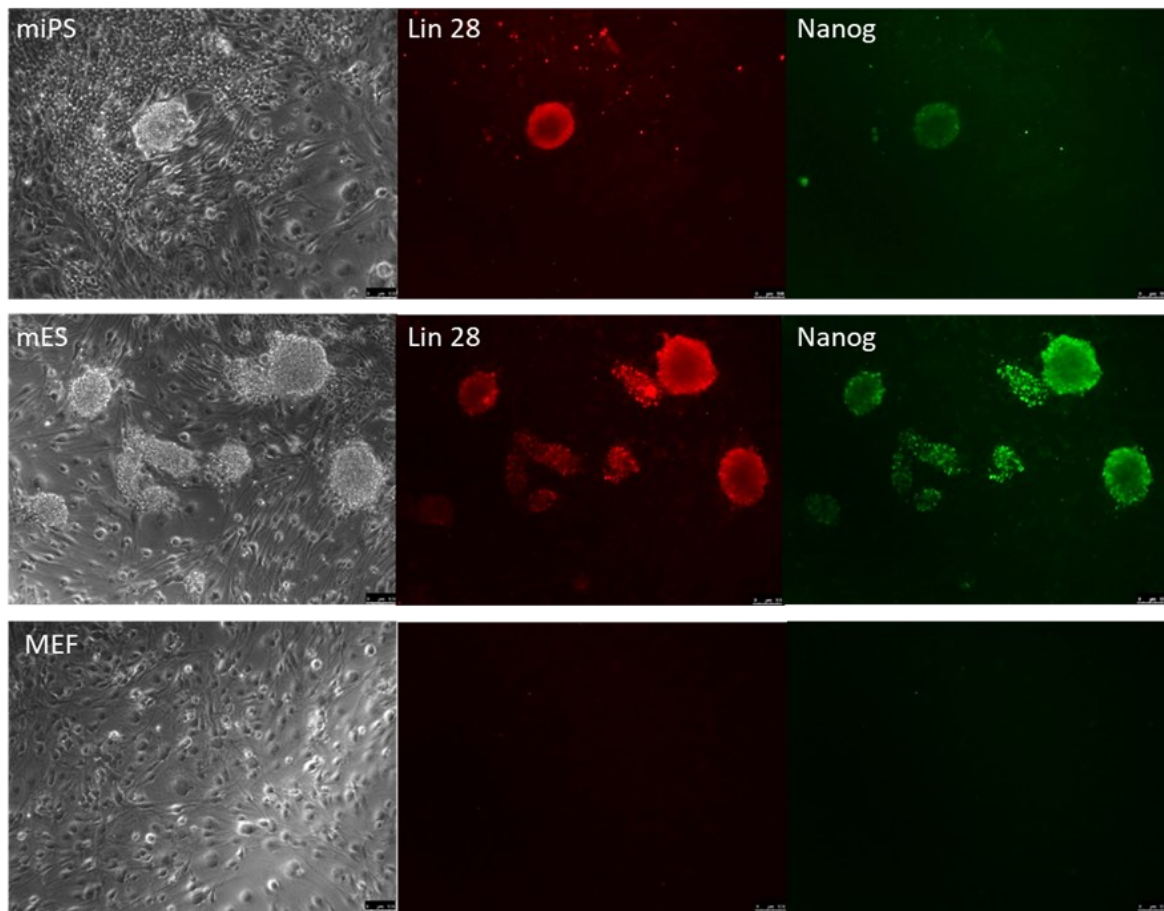


Figure 3.5 Immunofluorescent cell staining for key markers of pluripotency in miPSC colonies at P6.

A. miPSC were derived from WT-MEFs. miPSC (top), mESC (positive control, middle) and MEFs (negative control, bottom) stained for Lin28 and Nanog. miPSC are positive for both Nanog and Lin28 and share a similar morphology to mESC positive controls, strongly suggesting pluripotency in these cells. Images taken at 10x magnification, scale bars represent 100 μm.

B.

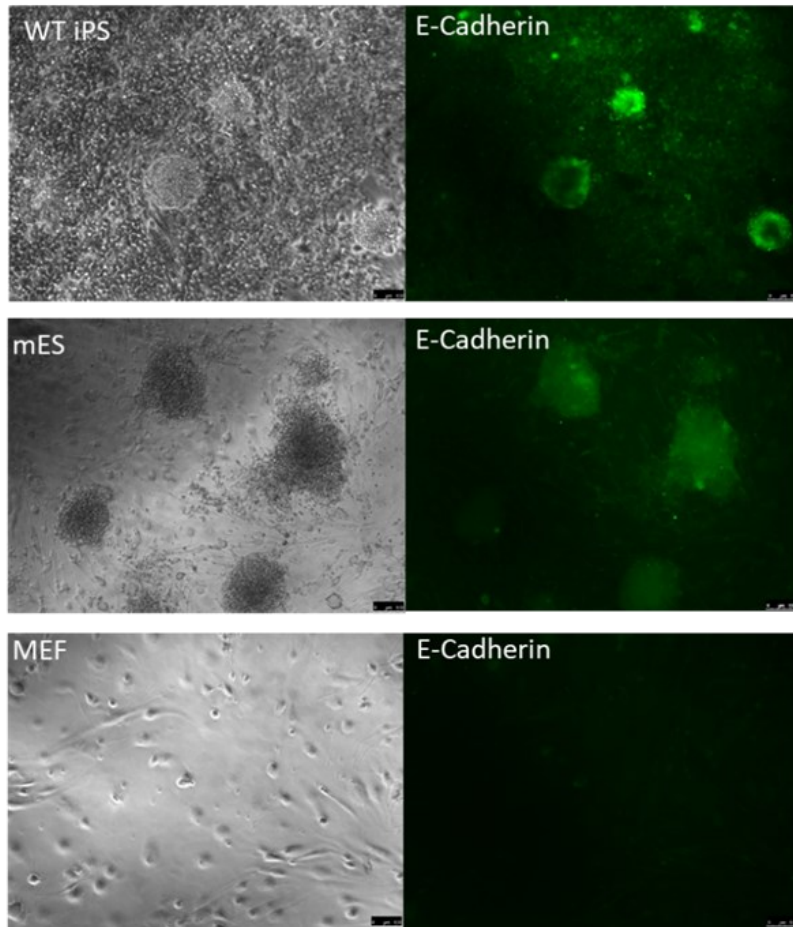


Figure 3.5: Immunofluorescent cell staining for key markers of pluripotency in miPSC at P6, compared to positive (mESC) and negative (MEF) controls.

B. miPSC (top), mESC (positive control, middle), and MEFs (negative control, bottom) stained for E-Cadherin. miPSC colonies are positive for pluripotency marker E-Cadherin, along with the positive results in 3.5.A above, this suggests that reprogramming of WT-MEFs has been successful and these cells are pluripotent. Images taken at 10x magnification, scale bars represent 100 μ m.

1.5. hDF reprogramming

Once MEF iPSC reprogramming protocols had been established and miPSC had been expanded and frozen for future use, I moved on to develop and refine the McKay lab standard human iPSC reprogramming protocol on a number of human dermal fibroblasts. The McKay lab iPSC reprogramming protocol is described in detail in the introduction but, briefly: Cells are nucleofected with the four OriP/EBNA

episomal plasmids (pCXLE-hSK, pCXLE-hUL, pCXLE-hOCT3/4-shp53-F and pCXWB-EBNA1) and seeded at high density in hDF maintenance media. Cells are passaged if/when ~85% confluent, and on D8 are re-seeded at low density onto iMEF feeder cells. At D9, media is changed to hESC media. Typically, at ~D14-18 small colony like structures begin to appear, and at D25, wells are analysed for primary colony number (Refer back to section 2.1.6 for further detail).

Firstly, control hDFs (nhDFs) were reprogrammed using the above described protocol. Figure 3.6 shows nhDFs at D7, D16 and at an early passage (P3).

Typically, we would expect to see evidence of MET at ~D7, and this is not evident in these cells. However, these cells are at a relatively low confluency, which is likely the reason for the lack of visible MET and is not necessarily indicative of a failing in the reprogramming experiment. In the D16 image, there is evidence of early colony formation (red arrow) in the nhDF cells. Finally, at P3, nhDF derived iPSC colonies are well established, with colonies displaying typical iPSC morphology including very small cells, with almost no cytoplasm, tightly packed cells beginning to form a rounded 3D shape, and a defined and well demarcated border around the iPSC colony. All phase images are representative examples of the whole experimental well and are taken at 10x magnification.

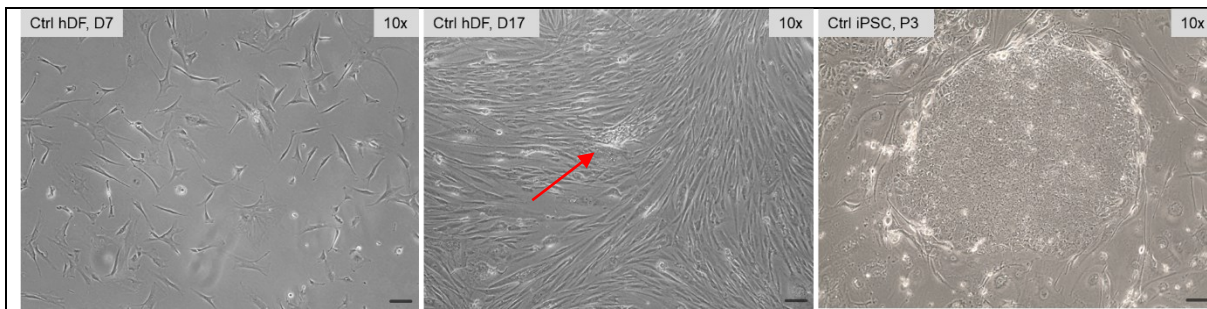


Figure 3.6 Control hDF (nhDF) throughout iPSC reprogramming and at an early passage.

Left, nhDFs at D7, just before being re-seeded onto iMEF feeder layers. Middle, nhDFs at D16 of a reprogramming experiment, the red arrow shows the emergence of a very early colony forming. Finally, right, established and stabilised nhDF derived iPSC at P3, showing a well rounded and clearly demarcated iPSC colony, typical of pluripotent stem cell colonies. Wells show representative examples of 3 experiments. Images taken at 10x magnification, scale bars represent 100 μ M

The McKay lab has ready access to Batten disease patient-derived fibroblasts from a repository held at University College London. Batten disease is a collection of rare, childhood neurodegenerative disorders that leads to blindness, epilepsy and dementia caused by mutations in CLN6 and CLN7 genes (among others) (Nita et al, 2016). Other members of the McKay lab have been investigating new cellular models for Batten disease, and as such we acquired many vials of patient fibroblasts. In 2016, Brandenstein *et al* showed hugely upregulated levels of p62 protein in the brains of CLN7 KO mice. Within the McKay lab, pilot experiments suggested that CLN6 and CLN7 patient fibroblasts may have been reprogrammable with a higher efficiency than other cell types. In order to assess CLN6 & CLN7 patient fibroblast reprogramming in my hands, I applied our standard reprogramming methodology.

Figure 3.7 shows CLN6 batten disease patient fibroblasts (CLN6 hDFs) at D7 and D16 of a reprogramming experiment, as well as at P3. As observed in the nhDF experiment there is no clear evidence of MET at D7 in these cells. However, the

CLN6 batten patient fibroblasts are also at a relatively low density at this stage and typically cells would need to be in closer proximity to each other in order to display these clear morphological signs of MET. At D16 early colony formation is visible (red arrow). At P3 the image shows an iPSC colony displaying all the typical hallmarks of a pluripotent stem cell colony. At P3 CLN6 iPSC colonies are round with a clearly defined border, and cells that are tightly packed with very little cytoplasm. All phase images were taken at 10x magnification and are representative examples of the whole experimental well, CLN6 iPSC reprogramming experiments were performed multiple times, although quantification was not performed at this stage.

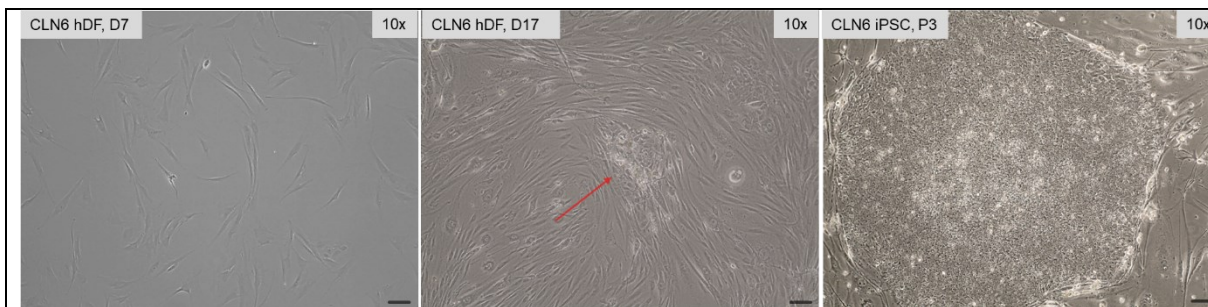


Figure 3.7 CLN6 Batten’s disease patient hDF throughout iPSC reprogramming and at an early passage.

Left, CLN6 hDFs at D7, just before being re-seeded onto iMEF feeder layers. Middle, CLN6 hDFs at D16 of a reprogramming experiment, the red arrow shows the emergence of a very early colony forming. Finally, right, established and stabilised CLN6 hDF derived iPSC at P3, showing a well-rounded and clearly demarcated iPSC colony, typical of pluripotent stem cell colonies. Wells show representative examples of at least 3 experiments. Images taken at 10x magnification, scale bars represent 100µM

Figure 3.8 shows CLN7 hDFs at D7 and D16 of a reprogramming experiment, as well as at P3. In the phase image taken at D7, there is clear evidence of MET occurring in CLN7 hDFs (left panel, red arrows). In contrast to the nhDF and CLN6 experiments, the CLN7 hDFs are more confluent at D7, which is likely the reason for this MET morphology. At D16 there is clear evidence of early colony formation

(middle panel, red arrow). The image taken at P3 shows a morphologically typical iPSC colony derived from CLN7 hDFs, with a well-defined border and a rounded shape. All phase images were taken at 10x magnification, and are representative of the whole experimental well. Experiments were repeated multiple times but quantification was not carried out at this stage.

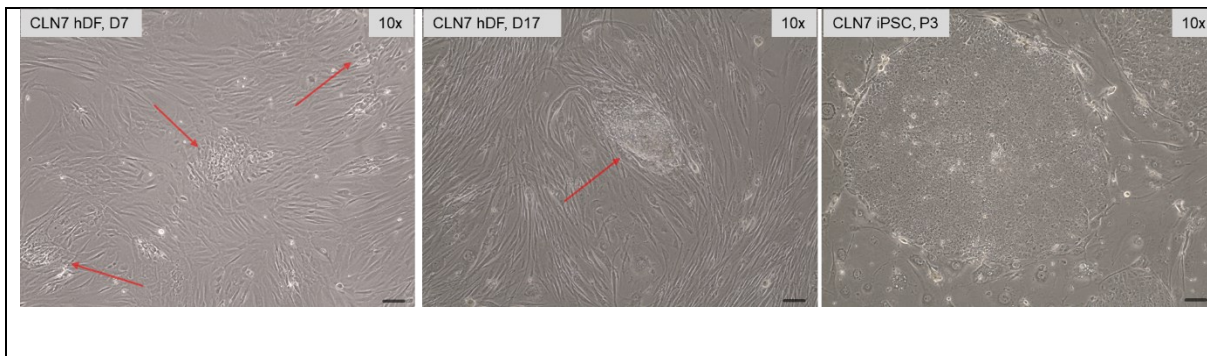


Figure 3.8 CLN& Batten’s disease patient hDF throughout iPSC reprogramming and at an early passage.

Left, CLN7 hDFs at D7, just before being re-seeded onto iMEF feeder layers. The red arrows show clear areas where MET can be seen, cells change morphology during this transition, becoming more compact and close packed together, cytoplasm reduces. Middle, CLN7 hDFs at D16 of a reprogramming experiment, the red arrow shows the emergence of an early colony forming. Finally, right, established and stabilised CLN7 hDF derived iPSC at P3, showing a well-rounded and clearly demarcated iPSC colony, typical of pluripotent stem cell colonies. Wells show representative examples of at least 3 experiments. Images taken at 10x magnification, scale bars represent 100µM

Additionally, CLN7-iPSC were routinely passaged and expanded until P10 (Figure 3.9). At this point, iPSC colonies would likely be losing episomal reprogramming plasmid expression and heading towards transgene independency. Research has shown that episomes are lost at a rate of approximately 2-8% per cell (Drozd et al, 2015) and iPSCs divide rapidly, more than once per passage. Cruvinel and colleagues demonstrated doubling times of between 28.3 and 33.9 hours in various human iPSC clones (Cruvinel et al, 2015). As shown in the images, at P10 CLN7-

iPSC are well established and morphologically typical of human pluripotent stem cell colonies. All images were taken at 4x magnification.

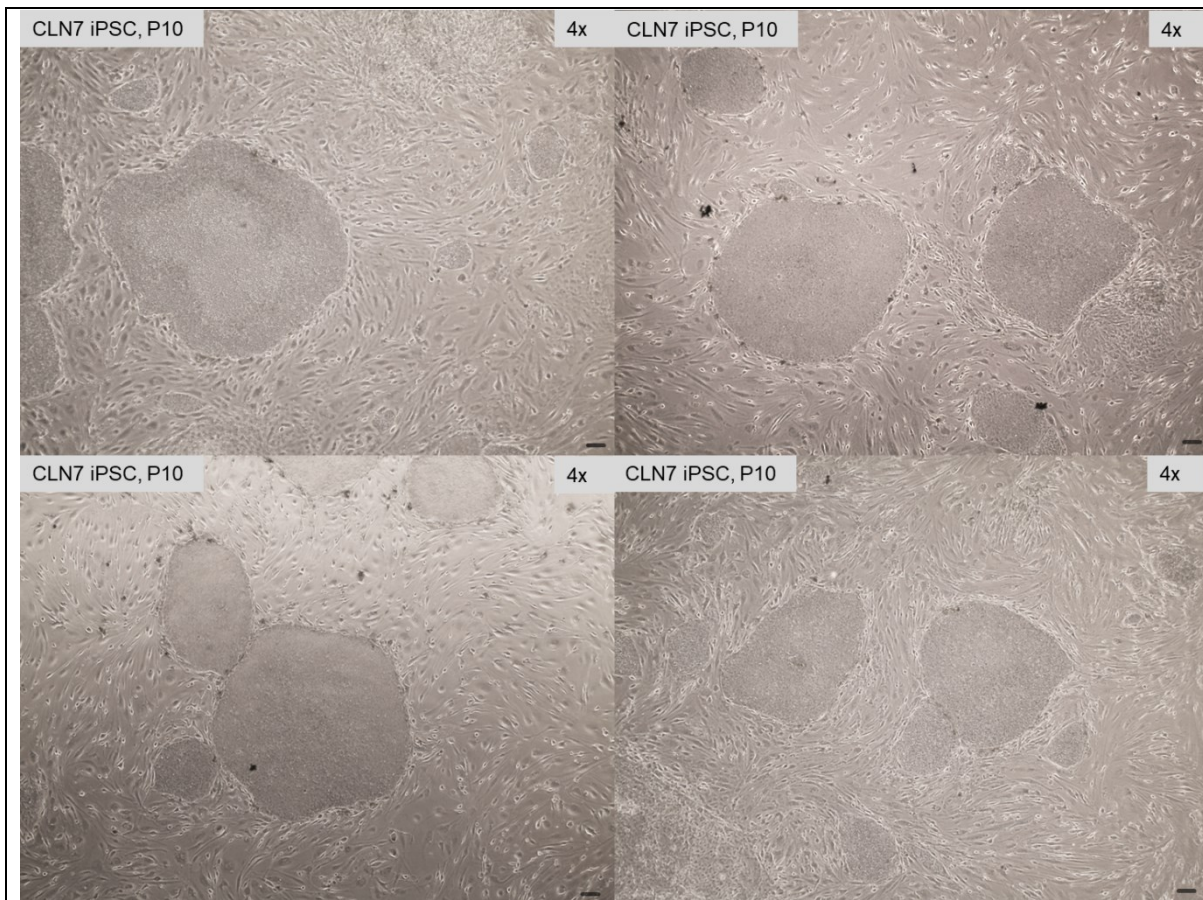


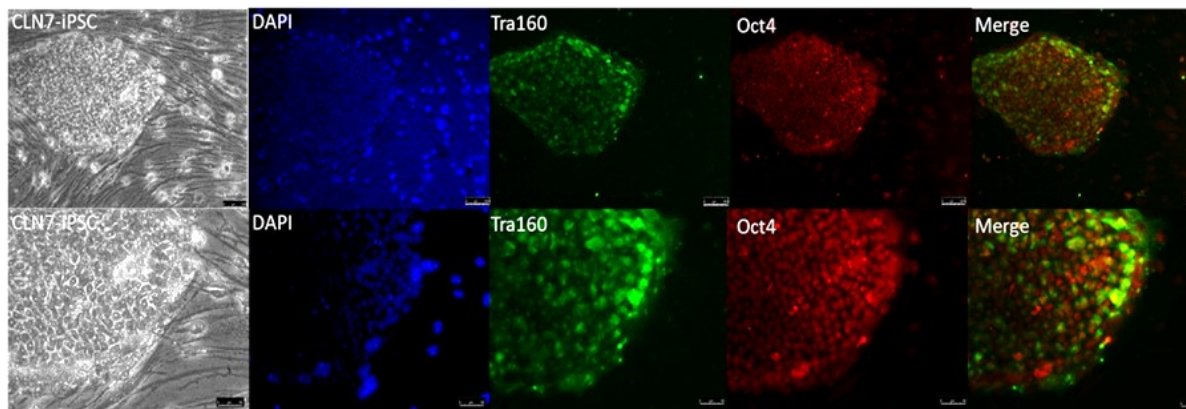
Figure 3.9 P10 CLN7 iPSC colonies are well established and morphologically typical.

CLN7 iPSC derived from Batten's disease patient fibroblasts, with known disease causing mutations in the CLN7 gene at P10 and approaching transgene independency. iPSC colonies are morphologically typical of established iPSC colonies, individual cells are small, lacking in cytoplasm and very round. iPSC colonies are also rounded, with cells closely packed together and well defined borders. Images taken at 4x magnification, scale bars represent 100 μ M

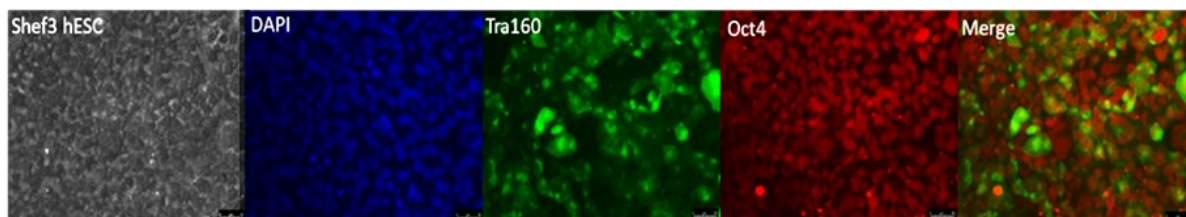
CLN7-iPSC colonies were fixed using 4% PFA and immunostained for a range of key human pluripotency markers, and compared to both positive (Shef3-hESC) and negative (hDF) controls. Shef3-hESC are a research-grade human embryonic stem cell line derived and characterised as karyotypically normal by Aflatoonian and colleagues at the University of Sheffield between 2003 and 2007 (Aflatoonian et al,

2010). These cells were obtained from the UK Stem Cell Bank and serve as a control for iPSC experiments. Firstly, P10 CLN7-iPSC colonies were stained for Tra160 and Oct4, two key markers of pluripotency (Figure 3.10.A). The top panel shows images taken at 10x magnification and the bottom panel shows images taken at 20x magnification on a fluorescent microscope. Positive and negative controls are shown Figure 3.10.B and C. As expected, Shef-3-hESC cells are positive for stem cell markers and hDFs are negative for stem cell markers. Shef3-hESC images are taken at 20x magnification and hDFs images are taken at 10x magnification.

A.



B.



C.

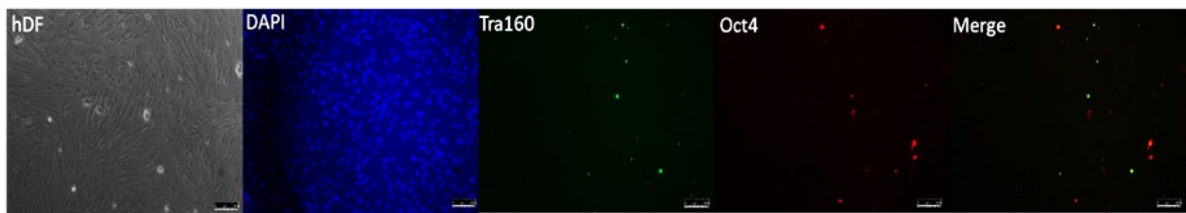
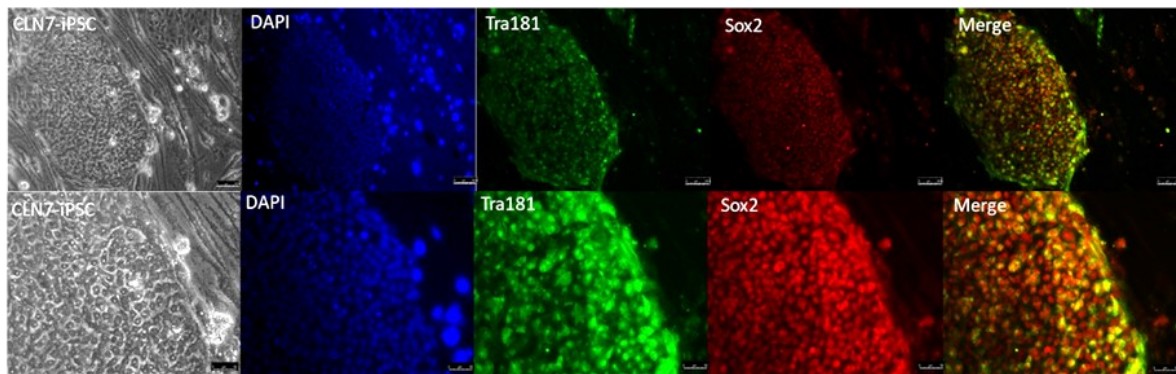


Figure 3.10. Immunofluorescent cell staining in P10 CLN7 iPSC to confirm pluripotency.

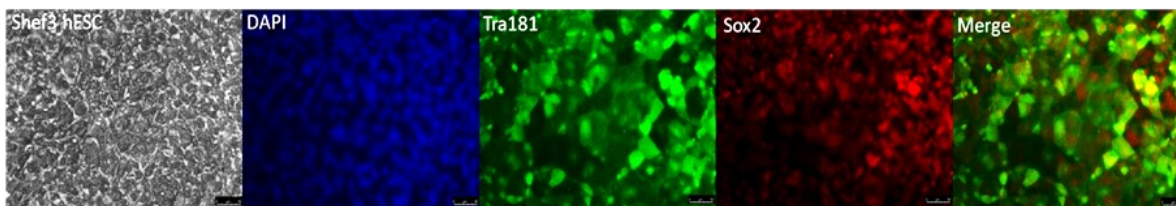
A. CLN7 iPSC stained for key pluripotency markers. From left to right images show: Phase, DAPI (nuclear stain), Tra160, Oct4 and Tra160/Oct4 Merge. CLN7 iPSCs are positive for pluripotency markers Tra160 and Oct4. Tra160 is particularly important for confirming pluripotency as it is not present in OriP/EBNA reprogramming plasmids, suggesting that the cells endogenous pluripotency gene networks have been 'switched on'. Top panel images taken at 10x magnification with scale bars representing 100µm, bottom panel images taken at 20x magnification, with scale bars representing 50µm. B. Shef3-hESC positive controls. From left to right: Phase, DAPI, Tra160, Oct4 and Tra160/Oct4 Merge. Images taken at 20x magnification, scale bars represent 50µm. C. hDF negative controls. From left to right images show: Phase, DAPI (nuclear stain), Tra160, Oct4 and Tra160/Oct4 Merge. Images taken at 10x magnification, scale bars represent 100µm.

CLN7-iPSC colonies were immunostained for Tra181 and Sox2, two further key markers of pluripotency (Figure 3.11.A). The top panel shows images taken at 10x magnification and the bottom panel shows images taken at 20x magnification on a fluorescent microscope. Positive and negative controls are also shown in Figure 3.11.B and C. As expected, Shef-3-hESC cells are positive for stem cell markers and hDFs are negative for stem cell markers. Shef3-hESC images are taken at 20x magnification and hDFs images are taken at 10x magnification.

A.



B.



C.

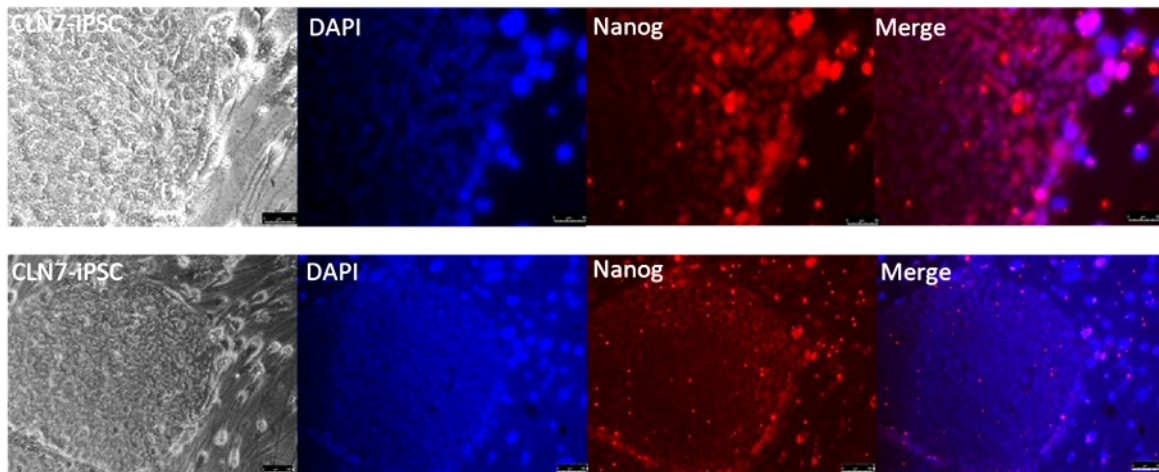


Figure 3.11 Immunofluorescent cell staining of P10 CLN7 iPSC to confirm pluripotency.

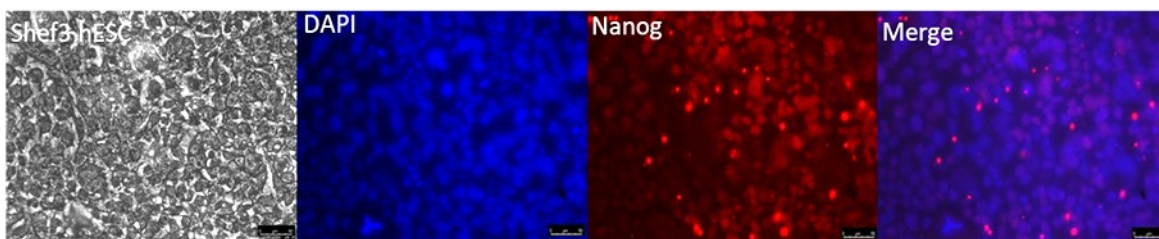
A. CLN7 iPSC stained for key pluripotency markers Tra181 and Sox2. From left to right images show: Phase, DAPI, Tra181, Sox2 and Tra181/Sox2 Merge. CLN7 iPSC are positive for both of these key markers of pluripotency in human cells. Tra181 is not present in the OriP/EBNA episomal reprogramming plasmids, indicating that the cells own pluripotency gene regulation networks have been switched on. Top panel images taken at 10x magnification with scale bars representing 100 μ m, bottom panel images taken at 20x magnification, with scale bars representing 50 μ m. B. Shef3-hESC positive controls. From left to right: Phase, DAPI, Tra181, Sox2, and Tra181/Sox2 Merge. Images taken at 20x magnification, scale bars represent 50 μ m. C. hDF negative controls. From left to right images show: Phase, DAPI (nuclear stain), Tra181, Sox2 and Tra181/Sox2 Merge. Images taken at 10x magnification, scale bars represent 100 μ m.

Finally, CLN7-iPSC colonies were immunostained for Nanog (Figure 3.12.A.). The top panel shows images taken at 20x magnification and the bottom panel shows images taken at 10x magnification on a fluorescent microscope. CLN7-iPSC colonies were positive for Nanog, a marker of pluripotency in human stem cells. Positive and negative controls are shown in Figure 3.12.B and C. As expected, Shef-3-hESC cells were positive for stem cell markers and hDFs are negative for stem cell markers. Shef3-hESC images are taken at 20x magnification and hDFs images are taken at 10x magnification.

A.



B.



C.

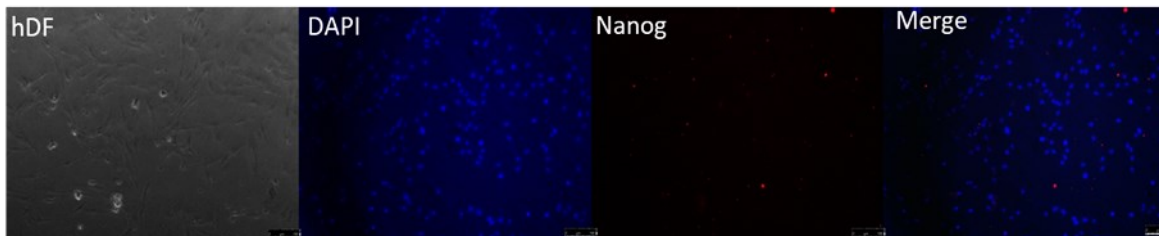


Figure 3.12 Immunofluorescent cell staining of P10 CLN7 iPSC to confirm pluripotency.

A. CLN7 iPSC stained for Nanog, a key pluripotency marker. From left to right images show: Phase, DAPI, Nanog and DAPI/Nanog Merge. CLN7 iPSC are positive for Nanog. Top panel images taken at 20x magnification with scale bars representing 50 μ m, bottom panel images taken at 10x magnification, with scale bars representing 100 μ m. B. Shef3-hESC positive controls, positive for Nanog. From left to right: Phase, DAPI, Nanog, and DAPI/Nanog Merge. Images taken at 20x magnification, scale bars represent 50 μ m. C. hDF negative controls, negative for Nanog. From left to right images show: Phase, DAPI, Nanog and DAPI/Nanog Merge. Images taken at 10x magnification, scale bars represent 100 μ m

CLN7-iPSC cells at P10 express multiple key markers for pluripotency. Importantly, not only do they positively express Oct4 and Sox2, which are both present in the episomal reprogramming plasmids; they also express Tra160, Tra181 and Nanog, key markers of pluripotency which are not in the reprogramming plasmids. This indicated that the cells own pluripotency regulatory machinery has been switched on, suggesting that these cells will retain pluripotency even when transgene free.

1.6. **Conclusions**

Overall, these data suggest that the McKay lab iPSC reprogramming protocols are effective at reproducibly producing a variety of different mouse and human iPSC lines that express key endogenous markers of pluripotency, and in the case of the CLN7 iPSC, this is true at a passage where transgene independency should be approaching. In order to confirm pluripotency further, RT-PCR experiments using primers that included part of the 3'UTR region could have been carried out to show that the cells were actively transcribing pluripotency genes such as Oct4 and Sox2. By including the 3'UTR region in PCR primer design, the amplification of any transgene sequences is prevented as this region is absent from the episomal plasmids. Unfortunately, time constraints meant these experiments could not be completed.

Chapter 2.

Chapter 3.

Chapter 4.

Chapter 5. Design, cloning and validation of a genetic manipulation toolkit for interrogating the role of p62 in iPSC reprogramming and the maintenance of pluripotency.

Chapter 4: Design, cloning, and validation of a genetic manipulation toolkit for interrogating the role of p62 in iPSC reprogramming and the maintenance of pluripotency

5.1. Introduction

As discussed at length in the Introduction, p62 is a multifunctional, multi-domain scaffolding protein with numerous roles. p62 is an autophagy adaptor; is involved in the anti-oxidant response via NRF2/KEAP1 signalling; in the activation of mTORC1 in the presence of amino acids; in the inflammatory response via the activation of NFκB and more (Lippai and Low, 2014; Katsuragi et al, 2015; Fan et al, 2018; Sanchez-Martin et al, 2018). Due to the many roles of p62 and its myriad of interacting partners, I decided to attempt to assess several of these functions in isolation in the context of iPSC reprogramming and the maintenance of pluripotency. Many of the signalling pathways p62 is involved in are also crucial for the iPSC reprogramming process including autophagy, mitochondrial clearance, energy production and utilisation and the clearance of huge amount of debris from protein and organelles that are remodelled or no longer required as cells so from somatic to pluripotent cell types.

Further, because p62 is highly conserved across species (Katsuragi et al, 2015), I wanted to determine if any effects of p62 on iPSC reprogramming or pluripotency maintenance are also conserved across mouse and human, and so cell lines from both species were employed throughout the course of this investigation. By introducing point mutations and thereby changing a single amino acid, it is possible to prevent phosphorylation of a protein moiety and alter a defined function of p62 whilst preserving all others. This should allow us to gain valuable insight into the

exact mechanisms and binding partners by which p62 has its p62 reprogramming effects, if any.

In order to assess the role of possibility of a role p62 in iPS reprogramming and in the state of pluripotency, a range of tools for the genetic manipulation of p62 expression were designed, created and validated. These tools included lentivirus shRNA expression vectors for both human and mouse p62 (sh(h)p62 and sh(m)p62), respectively; complete human and mouse p62 overexpression lentivirus; and a range of p62 deletion mutants to change specific functions of p62. These unique tools were verified and utilised to varying degrees in a range of cell types throughout this project; and the vectors and viruses themselves, as well as the novel cell lines they have created have enormous potential for further use in future experiments. By introducing point mutations and thereby changing a single amino acid, it is possible to prevent phosphorylation of a protein moiety and alter a defined function of p62 whilst preserving all others. This should allow us to gain valuable insight into the exact mechanisms and binding partners by which p62 has its p62 reprogramming effects.

5.2. **Objectives:**

- To design, clone and validate human p62 shRNA (sh(h)p62)
- To transduce nhDFs with sh(h)p62 and determine the level of protein knock-down achieved
- To design, clone and validate a human p62 overexpression construct
- To clone human p62 overexpression construct into lentiviral vector
- To design, clone and validated a library of human p62 mutant overexpression vectors and transduce into p62 null patient fibroblasts

- To validate the Addgene purchased human p62 mutant overexpression vectors in p62 null fibroblasts (As described in Table 2.3).
- To clone and validate a truncated p62 human overexpression construct
- To transduce p62 null fibroblasts with truncated p62 overexpression construct
- To design, clone and validate a mouse p62 shRNA (sh(m)p62)
- To transduce WT-MEFs with sh(m)p62 and determine the level of protein knock-down achieved
- To design, clone and validate a mouse p62 overexpression construct
- To clone mouse p62 overexpression construct into lentiviral vector
- To design, clone and validate a library of mouse p62 mutant overexpression constructs

5.3. **Human shRNA**

5.3.1. Human shRNA design

Firstly, an shRNA construct for human p62 was designed in order to induce p62-knockdown in nhDF control cells. shRNA sequences were generated using the Splash RNA algorithm (Pelossof et al, 2017), which predicts high-potency, miRNA based shRNA sequences (Table 4.2) whereby a score of over 1.0 suggests a good shRNA sequence. Three sequences can be combined to create a 'triple-hit' effect, thereby increasing efficiency and ensuring a good level of knock-down. Three sequences were selected from the algorithm-generated options. In this case, sequences SQSTM1202_1282_v2; SQSTM1202_1010_v2 and SQSTM1202_694_v2 were selected (highlighted green in Table 4.2); the remaining sequence was excluded (highlighted red in Table 4.2) because it contained significant overlap with one of the other sequences.

Table 4.1: miRNA sequences predicted by the SplashRNA algorithm to induce potent p62 knock-down in human cells		
Label	Antisense Guide Sequence	SplashRNA Score
SQSTM1202_1282_v2	TTTGAATACTGGATGGTGTCCA	1.521
SQSTM1202_1010_v2	TTTTGAAGACAGATGGGTCCAG	1.341
SQSTM1202_1013_v2	TTCTTTTGAAGACAGATGGGTC	1.316
SQSTM1202_694_v2	TTCTTCAGGAAATTCACATCG	1.289

Next, sequences and their complimentary strands are aligned to the p62 sequence (Figure 4.1.A), with mismatches created in the complimentary strand in order to promote duplex unwinding and passenger strand degradation (Figure 4.1.B).

A.

```
TTTGAATACTGGATGGTGTCCA          TGGACACCCATCCAGTATTCAAA
TGTCAAAGTGCTTACAGTGCAGGTAGTGATATGTGCATCTACTGCAGTGAAGGCACTTGTAGCAT

TTTGAAGACAGATGGGTCCAG          CTGGACCCATCTGTCTTCAAAA
TTCFAAGGTGCATCTAGTGCAGATAGTGAAGTAGATTAGCATCTACTGCCCTAAGTGCTCCTTCTGGCAT

TTCTTCAGGAAATTCACACTCG          CGAGTGTGAATTCCTGAAGAA
GTTAGTTTTCATAGTTGCACTACAAGAAGAATGTAGTTGTGCAAATCTATGCAAAACTGATGG
```

B.

```
*234*678***          **          ***876*432*
TTTGAATACTGGATGGTGTCCA          TGGACACCCATCTTGTATTTCAC

*234*678***          **          ***876*432*
TTTTGAAGACAGATGGGTCCAGTGAAGTAGATTAGCATCTAAGGACCCATCTCCCTTATAC

*234*678***          **          ***876*432*
TTCTTCAGGAAATTCACACTCGACAAGAATGTAGTTAAAGTGTGAATTGTCTGGGGAC
```

Figure 4.1 Design of miRNA sequences for sh(h)p62 lentiviral construct.

A. Sequences identified by the SplashRNA algorithm are aligned to the human p62 sequence. B. Mismatches are created in the miRNA sequences in the complimentary strand (in the positions highlighted blue) in order to promote duplex unwinding and passenger strand degradation. For example, note that the bases circled in red have been altered from TG to AA.

Finally, these sequences are combined with restriction sites added at each end (*HpaI* and *XhoI*) for ease of cloning into our destination vector of choice (pIL3.7). This shRNA was designed so that each individual sequence could be used separately or together, so restriction sites are also present between each shRNA sequence (*PvuII* between sequences 1 and 2; *SalI* between sequences 2 and 3) (Figure 4.2.A). The overall design of the shRNA sequence is shown in Figure 4.2.B; sequences have a stem loop between complementary strands, and approximately 60bp between each sequence for maximum effectiveness.

A.

```
.....  
GGATCCATTGTTAAAGTCAGAATAATGTTTGAATACTGGATGGTGTCCATGATATGTGCATCTAAGAC  
ACCATCTTGTAATTCACCATTATGGTGAAGCTGCTCGGGAAGCCAAGTTGGGCCTTAAAGTGCAGGGC  
CTGCTGATGTTGAGTGCTTTTTGTTCTTTTGAAGACAGATGGGTCCAGTGAAGTAGATTAGCATCTAAGC  
ACCCATCTCCCTTATACATAAGAAGTTATGTATTCATCCAATAATTCAAGCCAAGCAAATCGACAGGT  
GTTTTAATAGTTTTGTTTGCAGTCCTCTGTTTCTTCAGGAAATTCACACTCGACAAGAATGTAGTAAA  
GTGTGAATTGTCTGGGACTGGTGGCCTTTTTCCAAAAATGACTGTTCAAAAAAAAAAAAACTCGACAAA  
AAAAATCTAGAGAATCC
```

B.

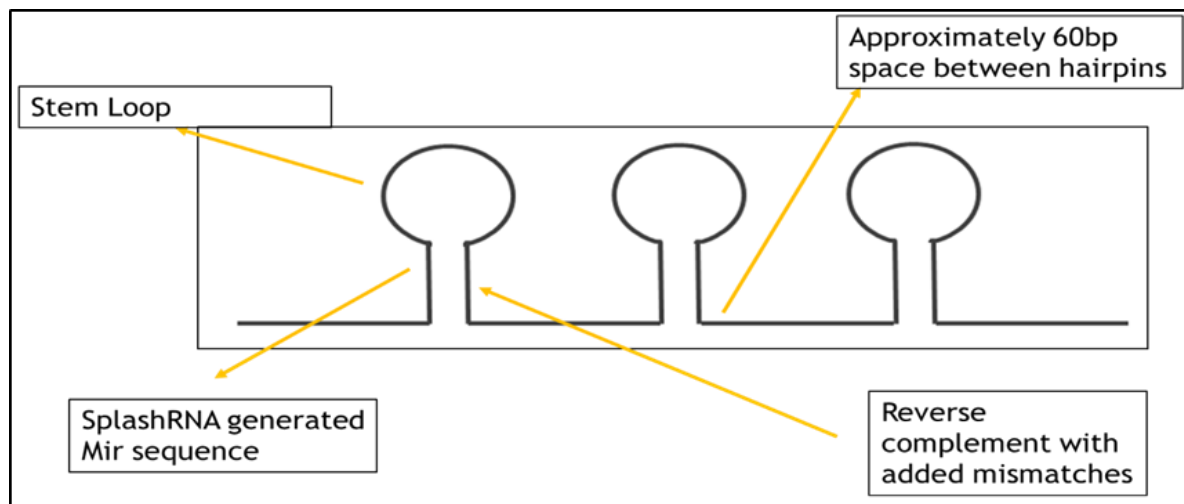


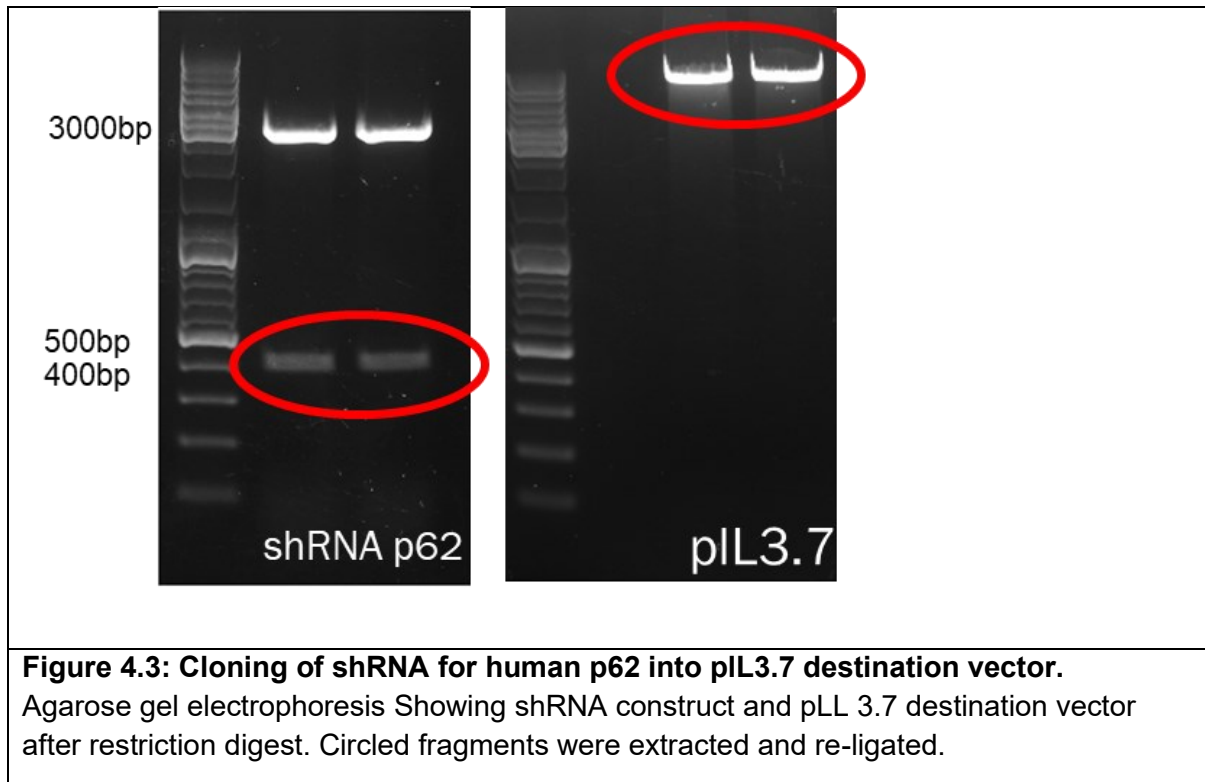
Figure 4.2 Construction of 'triple hit' shRNA sequence for human p62 and the overall design concepts.

A. The three pairs of miRNA sequences (highlighted pink, and with the addition of mismatches highlighted in blue) are strung together separated by approximately 60bp and with restriction enzymes (red) at either end and between individual sequences for ease of cloning. B. Key design elements of the 'triple-hit' shRNA design including the SplashRNA generated Mir sequences, reverse complement strands with mismatches introduced, a stem loop and a spacing of approximately 60bp between each sequence.

5.3.2. Cloning and validation

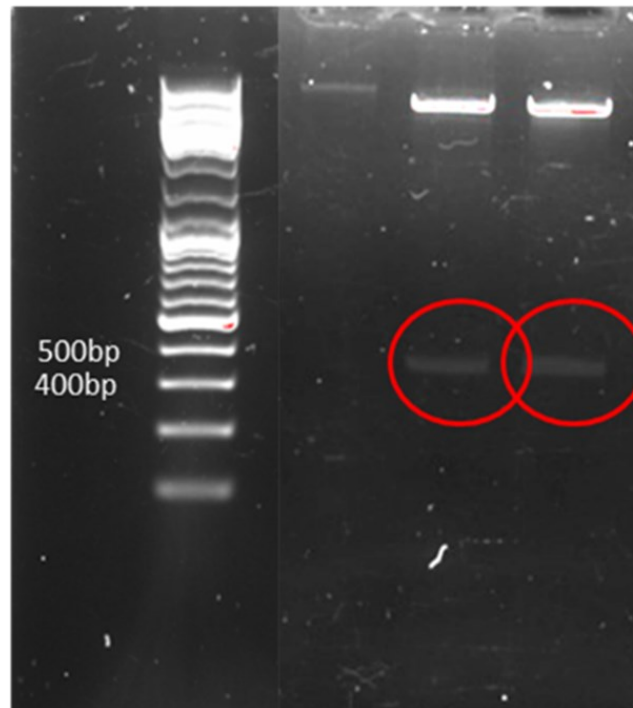
The sh(h)p62 construct was cloned into pL3.7 as described in Materials and Methods. Both the pL3.7 destination vector and the originating plasmid containing the shRNA sequence were subject to restriction digest with *Hpa1* and *Xho1* enzymes. *Hpa1* cuts DNA in a 'blunt' fashion, and *Xho1* leaves a sticky end to help ensure that the shRNA construct is religated into the destination vector in the correct directionality. Digested

plasmids were separated by agarose gel electrophoresis and correct bands were excised and DNA extracted from the gel (Figure 4.3)



The linearised pIL3.7 vector and the shRNA construct are then religated and transformed into *Stbl3* competent cells. (See also Materials and Methods). Individual bacterial colonies were then prepped and subjected to restriction digest with *HpaI* and *XhoI* (the same enzymes used to clone the construct into the vector) in order to check the success of the cloning (Figure 4.4.A.). Clones that appeared correct were sent to Source Bioscience for Sanger sequencing (Figure 4.4.B.) and finally, these sequences were aligned with the designed sequence (Figure 4.4.C.). Both clones were perfectly aligned to the designed sequence.

A.



B.

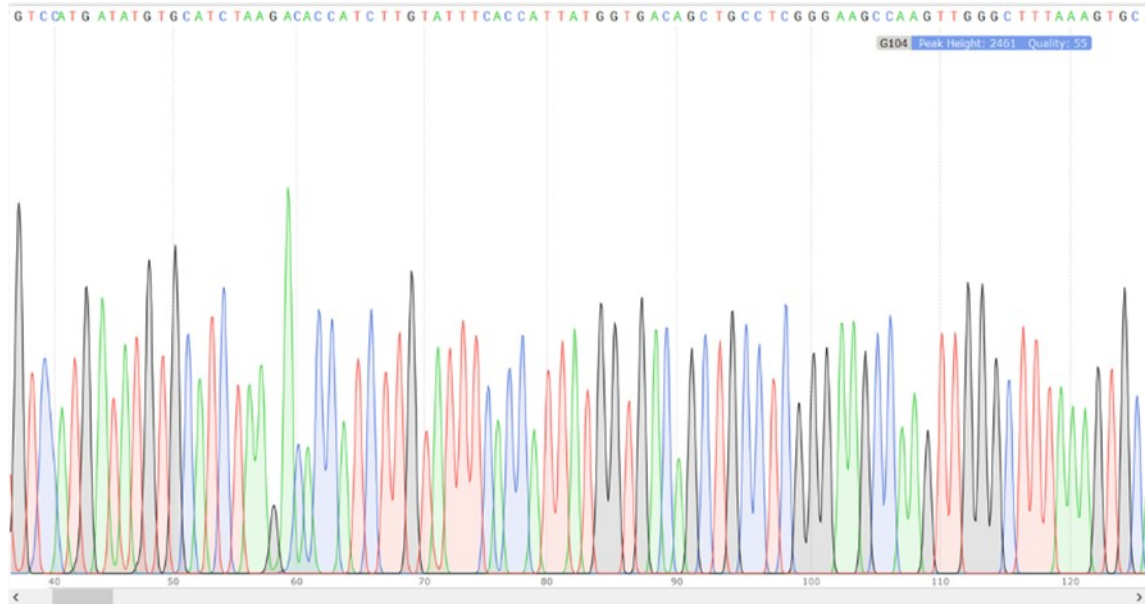


Figure 4.4 Successful cloning of sh(h)p62 constructs into pIL3.7 lentiviral vector.

A.

First stage colony screening was carried out by restriction digest with *HpaI* and *XhoI*.

Lanes 2 and 3 showed correct clones, whereas lane 1 showed an incorrect clone. **B.**

Clones that appeared correct on restriction digest were sent for Sanger sequencing at Source Bioscience.

C. Sequencing results are compared and aligned to the designed sequence using CLC sequence viewer to confirm cloning has been successful. 100% alignment can be seen between both sh(h)p62 clones sent for sequencing (top two sequence sequences) and the sequence as designed.

5.3.3. Transfection and Transduction of sh(h)p62 in Hek293T cells.

After Sanger sequencing results had confirmed the correct cloning and orientation of the sh(h)p62 construct into the pLL3.7 lentiviral vector, a proof-of-principal experiment was carried out to ensure that the expression plasmid was functional. Hek293T cells were transiently transfected with the pLL3.7-sh(h)p62 plasmid as described in the Materials and Methods section. 48 hours after transfection with PEI, approximately 40% of Hek293Ts were GFP+ upon visualisation on a fluorescent microscope (Figure 4.5.A).

Hek293T cells were then co-transfected with a 2nd generation lentiviral envelope plasmid (pCMVR8.74) and a VSV-G envelope expressing plasmid (pMD2.G). These plasmids contain *rev*, *gag* and *pol* lentiviral genes encoding the essential proteins required for producing and packaging lentiviral particles inside Hek293T cells. At 48, 72 and 96 hours the virus containing media was collected, filtered through a 0.22µm filter, concentrated and applied to fresh Hek293Ts at a range of concentrations from 0.125 – 2µl/ 2ml media for transduction (Figure 4.5.B), in order to visually determine the optimum concentration of virus, balancing a high level of transduction efficiency, while still ensuring that cells have only a single integration of virus into the host genome. Since Hek293T cells can be easily clonally expanded from a single cell, it is not necessary to have an extremely high level of transduction efficiency, as GFP+ cells can be clonally expanded to create a homogeneous population.

A.

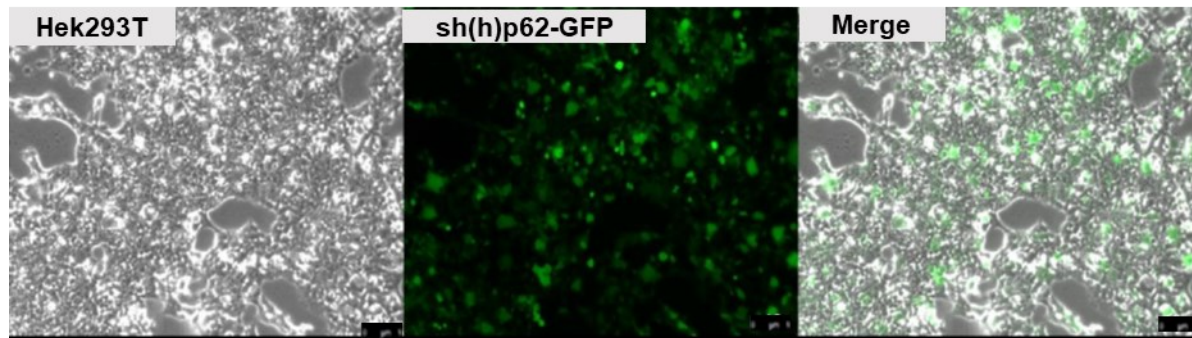


Figure 4.5 Validation of the sh(h)p62 construct in Hek293T cells

A. Transient transfection of sh(h)p62-GFP plasmid in Hek293T cells.

Approximately 40% transfection efficiency was achieved after 48 hours. All fluorescence images were taken at 10x magnification, scale bar represents 100 μ M

B.

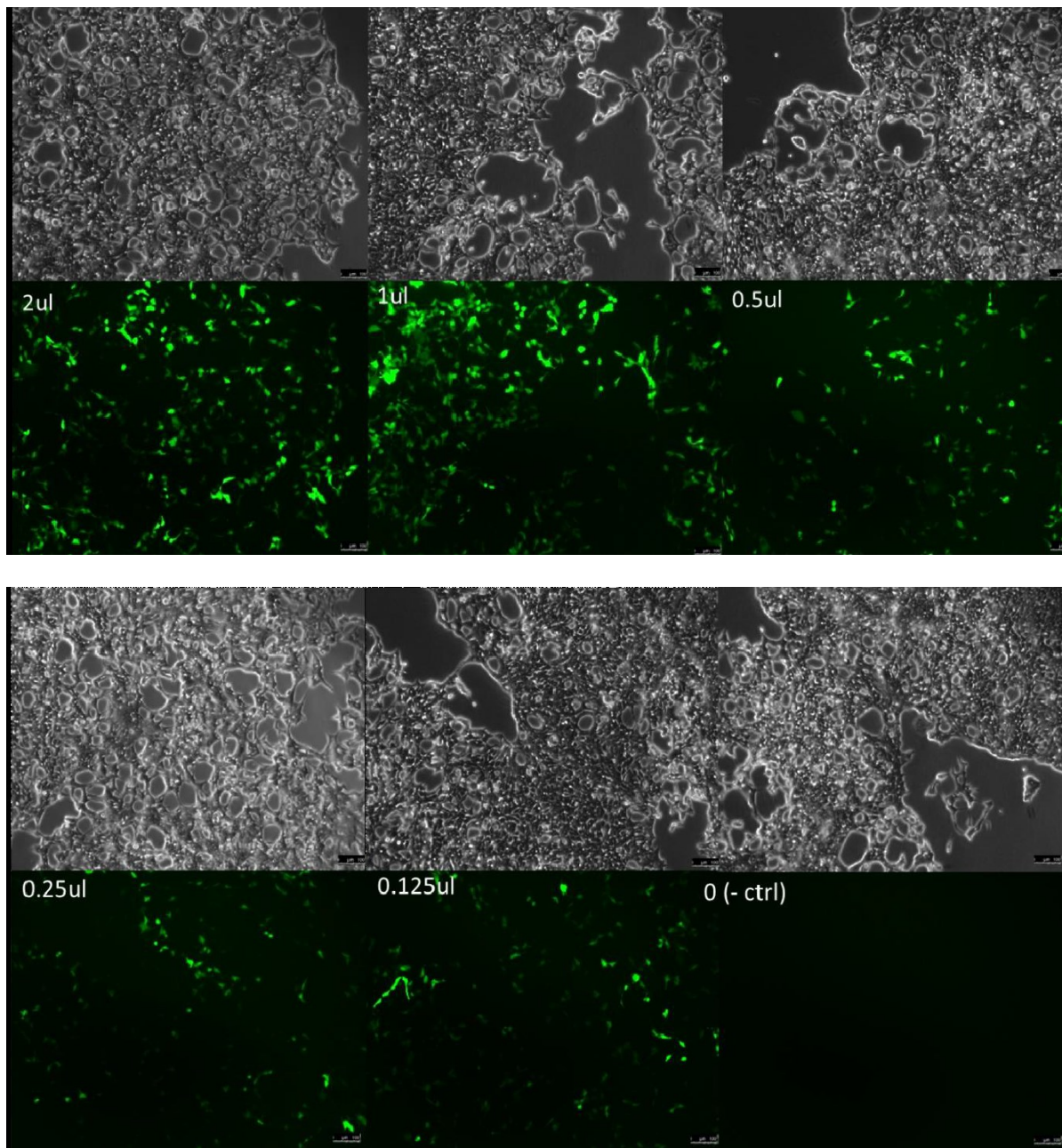
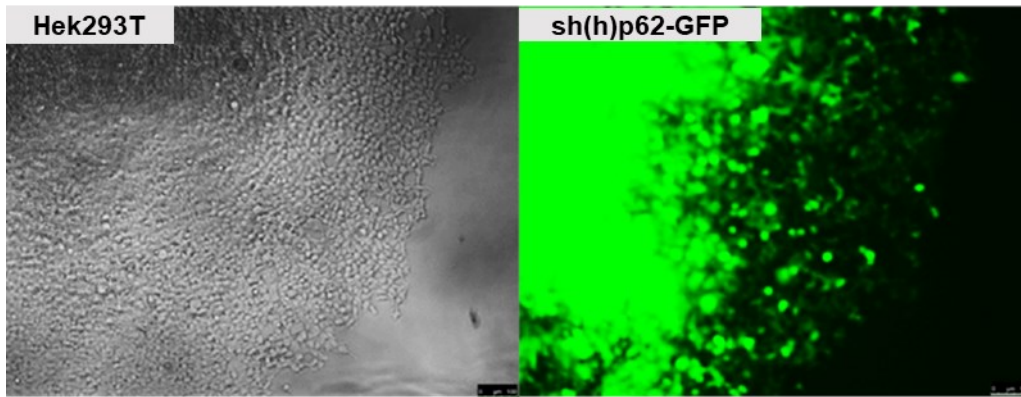


Figure 4.5 Validation of the sh(h)p62 construct in Hek293T cells

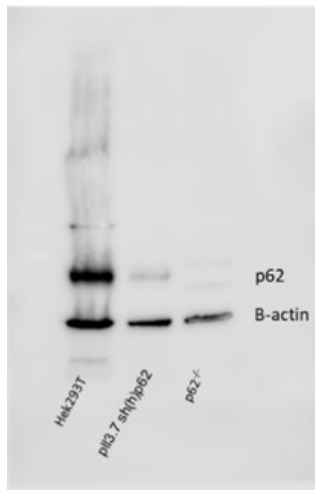
B. Transduction of Hek293T cells with sh(h)p62-GFP virus and at a range of concentrations from 0.125-2 μ l/2ml, with a negative control. Good transduction efficiency is achieved at all concentrations. All fluorescence images were taken at 10x magnification and scale bars represent 100 μ m

Once preliminary fluorescence imaging had showed that the sh(h)p62-GFP was functional, Hek293T-sh(h)p62 cells were plated as single cells in a 96-well format and allowed to clonally expand to create a homogeneous population (Figure 4.6.A.). Individual colonies of Hek293T-sh(h)p62 cells were then continually passaged until an appropriate number of cells were available to lyse for protein extraction. Western blots were carried out to determine the extent to which sh(h)p62 reduces p62 protein levels in Hek293T cells. Figure 4.6.B shows a representative example of three western blots comparing p62 protein levels, normalised to housekeeper β -actin. Untransduced Hek293Ts provide a positive control, while p62 null patient fibroblasts provide a negative control. Densitometry analyses using ImageJ determine that the sh(h)p62 lentivirus results in a ~85% reduction in p62 production levels, on average, across three independent experiments. ($n=3$, $p<0.0001$, p62 protein levels in sh(h)p62-Hek293Ts = $14.79\% \pm 4.35$) (Figure 4.6.C.)

A.



B.



C.

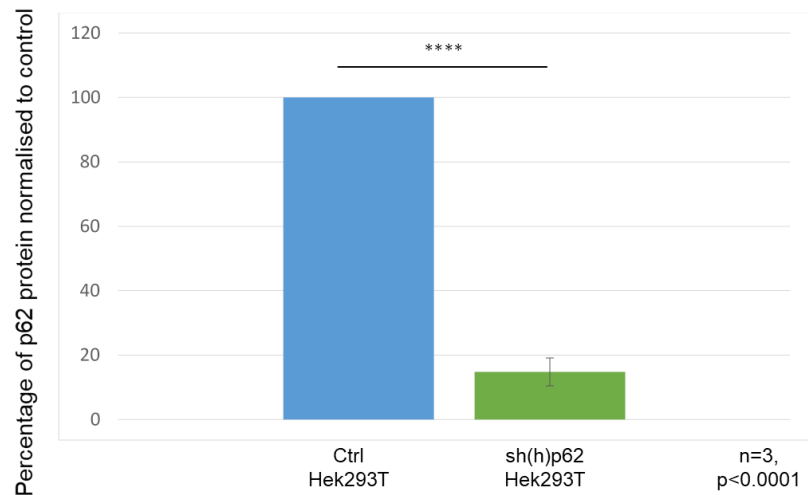


Figure 4.6 p62 protein knock-down in Hek293Ts using sh(h)p62 shRNA

A. Fluorescence imaging of sh(h)p62-Hek293T cells subjected to clonal expansion creating a homogeneous population of sh(h)p62-GFP+ cells. B. Representative example of 3 independent western blots showing p62 protein levels in Hek293T controls, sh(h)p62-Hek293T cells and p62 null patient fibroblasts. Housekeeper is β -actin. C. Densitometry analysis in ImageJ shows a highly significant reduction in p62 protein levels in sh(h)p62-Hek293T cells compared to control. When normalised to both β -actin and Hek293T controls, p62 protein levels are reduced by an average of $\sim 85\% \pm 4.35\%$. ($n=3$, $p<0.0001$, error bar represents S.E.M, statistical analysis = paired t-test). Fluorescence image taken at 10x magnification, scale bars represent $100\mu\text{m}$.

5.3.4. Transduction into nhDFs

These experiments showed that not only is the sh(h)p62 easily transfected and transduced, it also results in reliably and reproducibly high levels of protein knock-

down. The next step was to test the sh(h)p62 lentivirus in our target cells: nhDFs. The concentrated virus was added to approximately 125,000 early passage (P3) nhDFs, in a range of concentrations from 0.25-1µl/ 2ml media. As shown in Figure 4.7.A, a good level of transduction efficiency was again achieved in the nhDFs, particularly at the higher two concentrations. When 0.5µl/2ml of media was added, approximately 40% transduction efficiency was achieved; when 1µl/2ml media was added, approximately 80% transduction efficiency was achieved. Viral titre was estimated in these target cells. Viral titer can be estimated in the following calculation:

$$\text{Titer/ml (TU/ml)} = \text{cell number on the day of transduction} \times \left(\frac{\text{percentage of GFP+ cells}}{100} \right) / \text{dilution factor}$$

Thus, the titre of sh(h)p62 virus produced in this experiment can be estimated as follows:

$$125,000 \times (0.8/0.0005) = 2 \times 10^8 \text{ TU/ml}$$

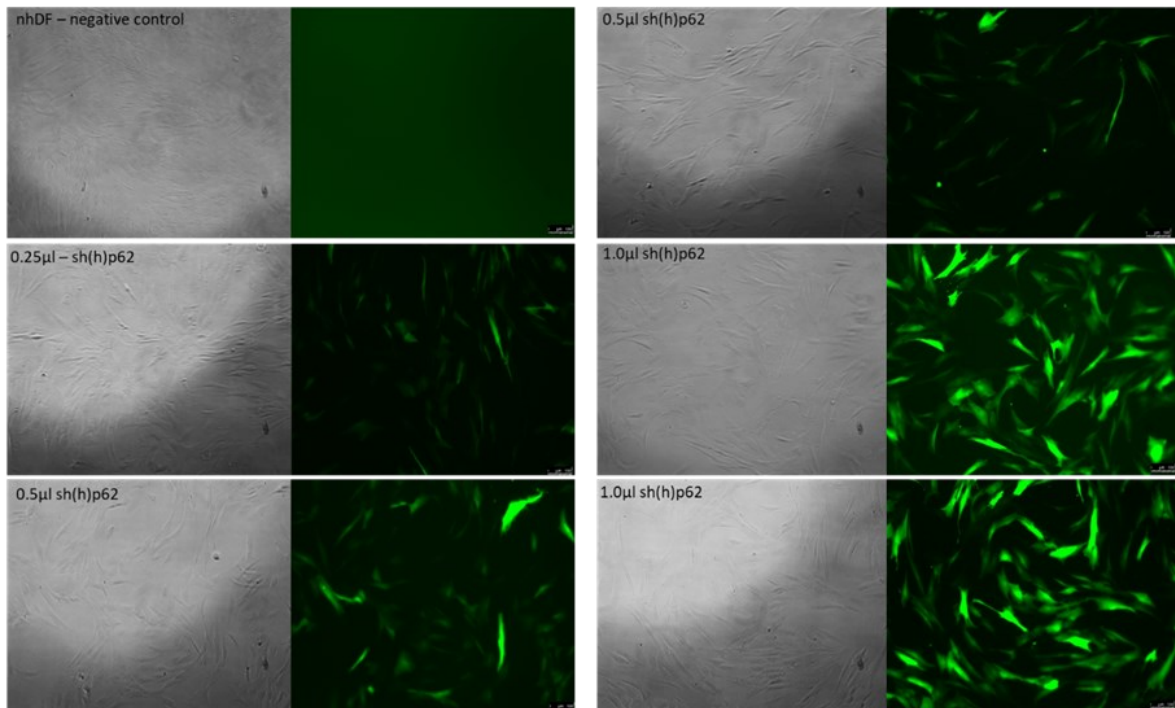
$$125,000 \times (0.4/0.00025) = 2 \times 10^8 \text{ TU/ml}$$

nhDFs stably transduced with sh(h)p62 were then sent to The University of Manchester for fluorescence activated cell sorting (FACS), in their core flow cytometry facilities. Cells were sorted by Dr Gareth Howell, and on his advice, cells transduced with all three MOIs of virus were pooled together, in order to ensure that enough cells were available for sorting (~5million). 62% of all cells (3.1million) sorted were GFP+. The resultant homogeneous population of 100% transduced cells

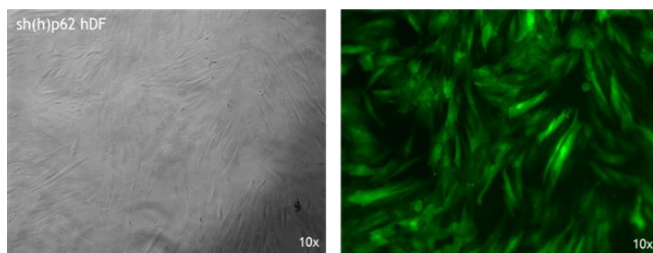
(Figure 4.7.B) were then passaged and expanded until ready to embark upon reprogramming experiments described in Chapter 6.

Approximately 150,000 cells were lysed for protein extraction and a western blot performed as before to determine if the level of protein knock-down achieved in nhDFs was similar to that achieved in Hek293Ts (4.7.C). This was only carried out once and so statistical analysis was not carried out, however, protein knock-down levels achieved appear very similar to that in Hek293Ts

A.



B.



C.

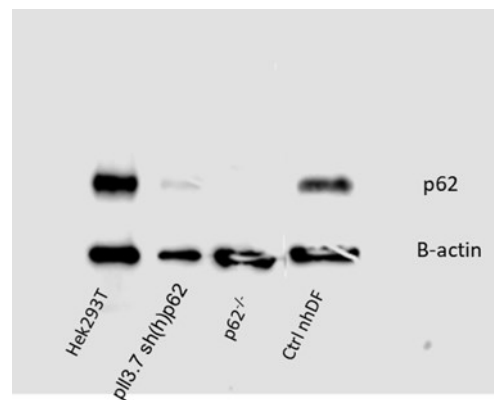


Figure 4.7. Transduction of nhDFs with sh(h)p62 lentivirus and p62 protein knock-down.

A. Transduction of sh(h)p62 lentivirus at concentrations of 0.25, 0.5 and 1 $\mu\text{l}/2\text{ml}$. 1 $\mu\text{l}/2\text{ml}$ sh(h)p62 lentivirus results in an approximately 80% transduction efficiency. B. Cells were sorted using FACS to create a homogenous population of cells, with a single integration of sh(h)p62 virus. Images show the resulting cells with 100% GFP expression. C. Western blot analysis shows that the level of p62 knock-down achieved in nhDFs is very comparable to that achieved in the Hek293T cells when compared to control nhDFs, control Hek293T cells and p62 null patient cells (n=1). Images taken at 10x magnification, scale bars represent 100 μm .

5.3.5. Conclusions

A shRNA construct was designed and cloned into the pL3.7 lentiviral vector, with Sanger sequencing data to support this. The shp62 cassette was then transiently transfected into Hek293T cells to produce lentiviral particles. Fresh Hek293Ts transduced with lentivirus containing media show a high level of transduction efficiency as evidenced by GFP fluorescence. Further, in a homogenous population of Hek293T cells, densitometry analysis of three western blots showed that the sh(h)p62 cassette caused on average 85% reduction in p62 protein levels. Once these proof-of-principle experiments confirmed the effectiveness of the sh(h)p62 construct, our target cells, nhDFs were transduced with sh(h)p62 virus. nhDFs transduced with the virus were then sorted by FACs, and a homogeneous line of nhDF-shp62 cells was created. These cells were then ready to undergo reprogramming experiments (Chapter 6).

5.4. Human p62 overexpression

5.4.1. Design, cloning and validation of human p62 overexpression construct.

A construct for the overexpression of human p62 (hp62) was designed. The construct was designed as the whole of the human p62 coding sequence, which is 1323bp in length and codes for the complete multi-domain p62 protein, which is 440 amino acids in length. This sequence was bookended with *EcoRI* and *XbaI* restriction sites at each end for ease of cloning into the pENTR1A minimal vector. A 4bp buffer between restriction sites and the coding sequence was also added. This construct was de novo synthesised under my instruction by Eurofins Genomics, and provided in a minimal plasmid with Ampicillin resistance.

The hp62 sequence was cloned into the pENTR1A plasmid by cut-and-paste cloning, as described previously; hp62 sequence and the pENTR1A vector are both linearised with restriction enzymes before being re-ligated together. pEX-A258-hp62 plasmid and pENTR1A were both digested with *EcoRI* and *XbaI* restriction enzymes and separated by gel electrophoresis (Figure 4.8.A) and the correct fragments (red circles) were extracted from the gel, re-ligated and transformed into *StbI3* competent cells as previously described. Individual bacterial clones were prepped, and again subjected to restriction digest with *EcoRI* and *XbaI* as a first line of screening. All seven clones showed digested bands of the correct size indicating a successful cloning (Figure 4.8B), and a few were sent to Source Bioscience for Sanger sequencing to confirm (Figure 4.9).

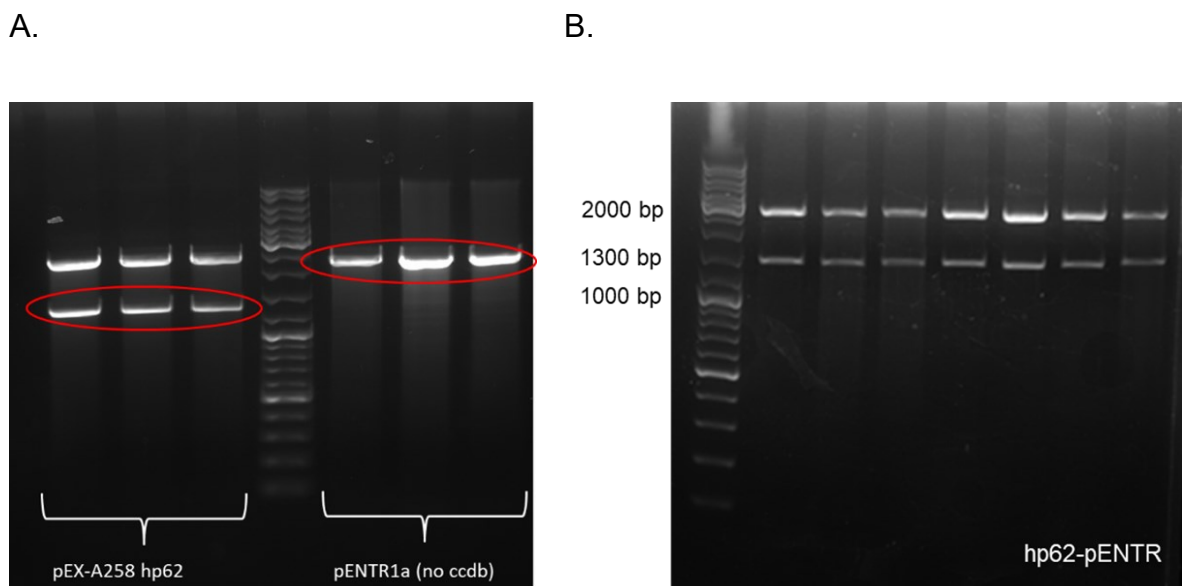


Figure 4.8 Cloning of hp62 overexpression cassette into pENTR1A minimal vector.

A. pEX-A258-hp62 and pENTR1A vectors were both digested with *EcoRI* and *XbaI* restriction enzymes, the correct fragments are ~1340bp long for hp62 and ~2200bp long for pENTR1A (red circles). C. Re-ligated hp62-pENTR is transformed into *StbI3* competent cells, and grown overnight at 37°C. Individual bacterial clones are prepped and once again subjected to restriction digest with *EcoRI* and *XbaI* enzymes to create 2 bands on agarose gel of ~1340bp and ~2200bp.

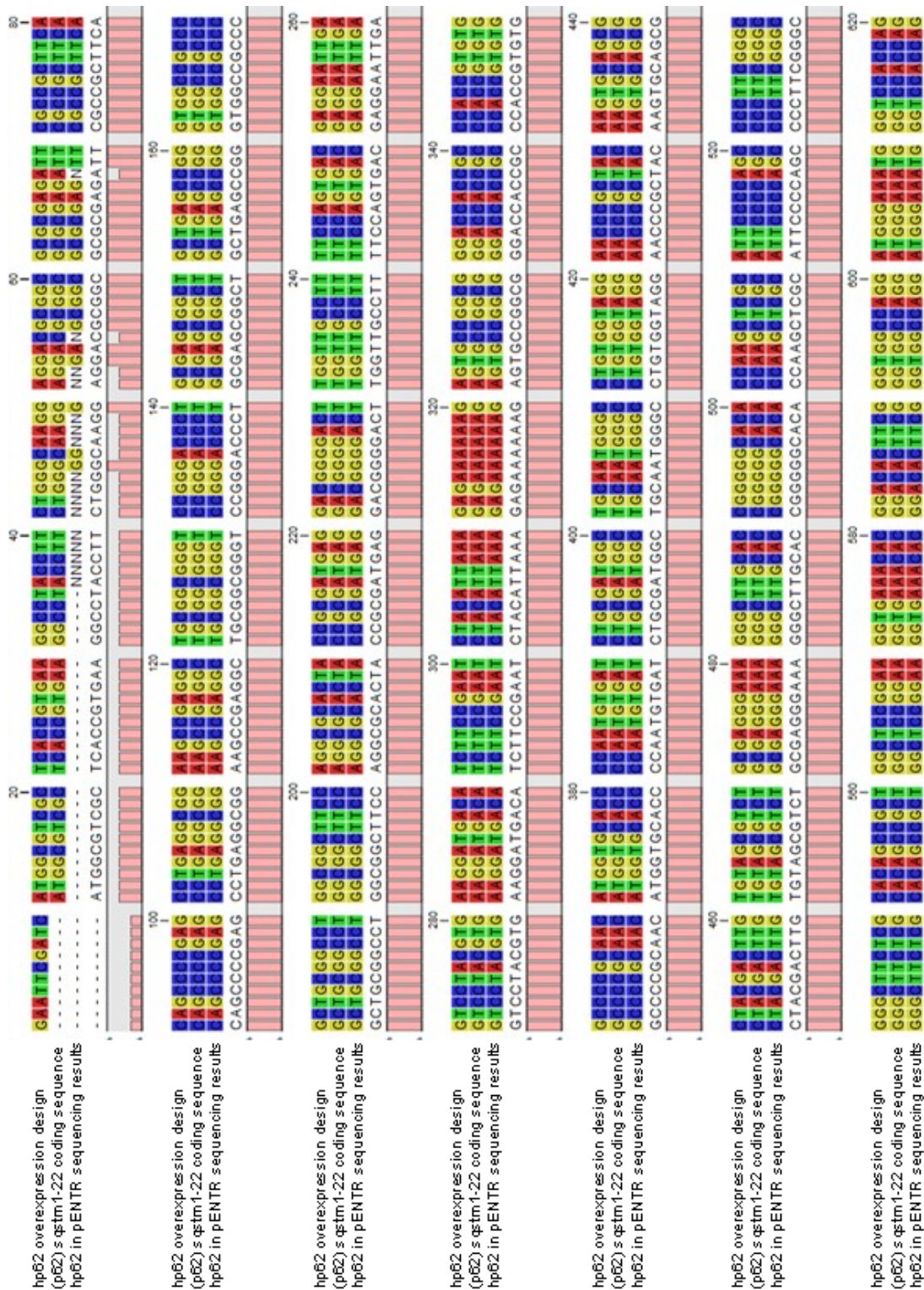


Figure 4.9 Sequencing of hp62 pENTR1A clones demonstrates successful cloning.

Clones that appear correct are sent for Sanger sequencing. Image shows multiple sequence alignment in CLC sequence viewer: 1 – hp62 overexpression sequence as designed. 2- SQSTM1-202 (p62) coding sequence (Transcript ID: ENST0000389805.1).

3. hp62-pENTR 1A sequencing results. All three are perfectly aligned, showing that the hp62 overexpression cassette has been successfully cloned into pENTR1A.

The pENTR1A minimal vector is an ideal intermediate cloning vector: it has a small number of restriction enzymes in a multiple cloning site (MCS), allowing for easy cloning. Further, it contains *attL1* and *attL2* sites, which enable Gateway cloning. Gateway cloning is based on a site-specific recombination system used by phage in order to integrate its DNA into the chromosome of *E.coli*, whereby phage contains an *attP* site and *E.coli* contains an *attB* site, enzymes catalyse a reaction where the sites are recombined and create *attL* and *attR* sites in a reversible process. Gateway cloning allows convenient cloning from an Entry vector (pENTR1A) to a destination vector of choice (in this case SFFV-GW). The *attL* and *attR* sites, as well as any DNA between them are recombined in the LR reaction. hp62 pENTR1A and SFFV-GW vectors were recombined, transformed and grown overnight on ampicillin containing agar plates. Individual bacterial colonies were prepped and sent to Source bioscience for sequencing. SFFV-hp62 clones were not subjected to screening with restriction enzymes as the SFFV vector is very large (~10.5kb) and contains a huge number of restriction items and on this occasion, it was not possible to find suitable enzymes to screen for the success of the cloning. Figure 4.10 shows multiple sequence alignment of SFFV-hp62 sequencing results, along with the hp62 overexpression cassette as designed, and the SQSTM1-202 transcript coding sequence. Perfect alignment can be seen, proving that the hp62 overexpression cassette was successfully cloned into SFFV-lentiviral vector.

5.4.2. Conclusions

The hp62 overexpression cassette was successfully cloned into both the pENTR1A minimal cloning vector and the SFFV lentivector. However, it was later determined that this SFFV lentivector was not the ideal destination vector, as it contained neither a GFP cassette (or similar) or a puromycin selectable cassette. This meant that it would be impossible to determine transfection or transduction efficiency levels with the vector, and that it would not possible to create a homogeneous population of cells, which would be essential for experiments aiming to determine the role of p62 in iPSc reprogramming and pluripotency. Unfortunately, I was not successful in cloning the hp62 overexpression cassette into a more suitable GFP or puromycin containing lentivector within the timeframe of the project, although a suitable vector was identified, the MCS did not allow for the cloning of the p62 overexpression construct. As such, a retroviral vector containing an hp62 overexpression cassette and a puromycin selection marker was purchased from addgene.

5.5. **pBABE-puro HA-p62 and pBABE-puro HA-p62-LIR**

pBABE-puro HA-p62 (Addgene ID: 71305) is a retroviral vector based on Moloney murine leukemia virus (Mo MuLV) (Chen et al, 2013), with a puromycin selectable marker and a human p62 overexpression cassette. This was purchased in addition to pBABE-puro HA-p62-LIR (addgene ID: 71306), which is identical to pBABE-puro HA-p62, except for a mutation in the cDNA corresponding to a single amino acid change (W338A) in the LIR region of p62. This W338A mutation prevents p62 from being broken down by autophagy (Chen et al, 2013). See Materials and Methods for further details regarding these plasmids.

pBABE- puro HA-p62 and pBABE-puro HA-p62-LIR bacterial colonies were prepped and subjected to *Xho*I and *Hind*III restriction digest to confirm (Figure 4.11).

Fragments of ~1700bp and ~4750bp indicate a positive result.

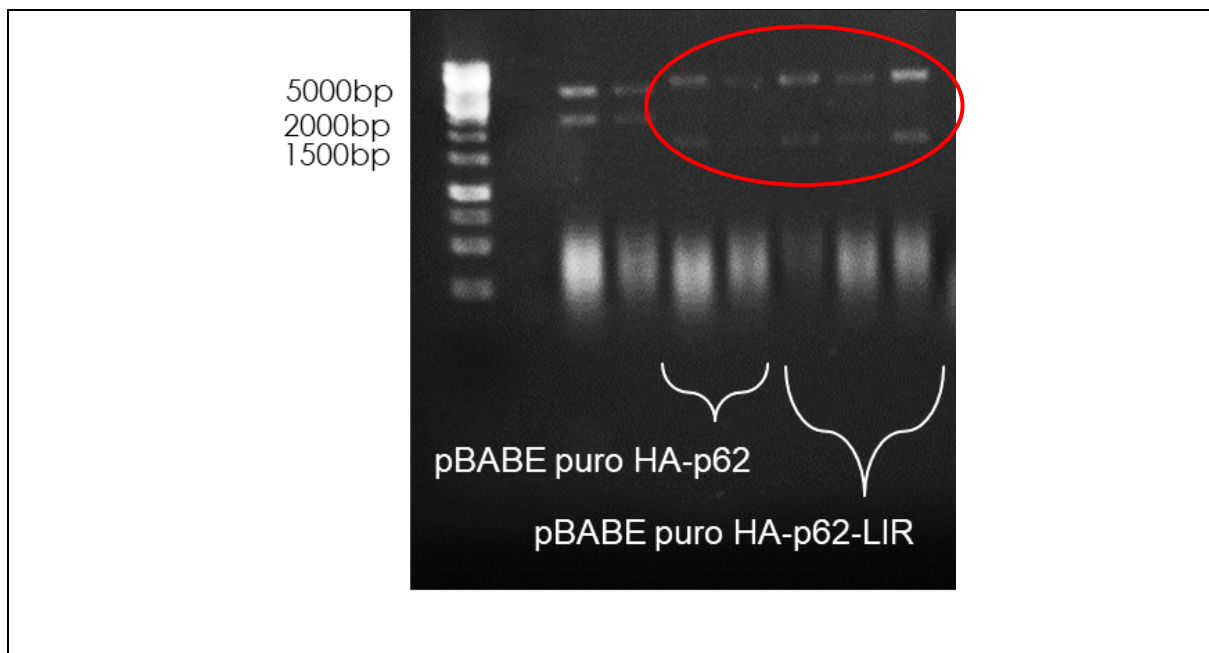


Figure 4.11 Preparation of pBABE-puro-HA-p62 and pBABE-puro-HA-p62-LIR retroviral plasmids.

A. pBABE-puro HA-p62 and pBABE-puro HA-p62-LIR plasmids were subjected to *Xho*I and *Hind*III restriction digest. Fragments of ~1700bp and ~4750bp indicate a positive result, and shown within the red circle.

pBABE-puro plasmid preps were not sent for Sanger sequencing, as no cloning or genetic manipulation had occurred, and so a restriction digest was sufficient.

pBABE-puro HA-p62 and pBABE-puro HA-p62-LIR retroviral plasmids were then transfected into Hek293T cells alongside pUMVC packaging plasmid for producing MuLV retroviral particles, and pCMV-VSV-G envelope protein producing vector (See Materials and Methods). 1.5µg pBABE-puro vector; 1µg pUMVC and 0.5µg VSV-G were co-nucleofected into 1,000,000 Hek293T producer cells per experiment. At 48, 72 and 96 hours, the virus containing cell supernatant was collected, filtered through

a 0.22µm filter and applied directly to hDF-p62^{-/-} 1:1 (one well of virus containing media applied to one well of hDF-p62^{-/-}). Retrovirus cannot easily be concentrated, due to instability of the viral membranes.

hDF-p62^{-/-} stably transduced with pBABE-puro HA-p62 and pBABE-puro HA-p62-LIR were subjected to puromycin (concentration 1.5 µg/ml) selection for 48 hours (2D) (Figure 4.12). Since the pBABE retroviruses have within them a puromycin resistance gene, only cells which have been transduced by the viruses will survive selection; thus creating a homogeneous population of hDF-p62^{-/-} whereby the expression of p62 has been recovered, either in its native form (hDF-p62^{-/-}-HA-p62) or with a mutation in the LIR, preventing degradation of p62 by autophagy (hDF-p62^{-/-}-HA-p62-LIR). These newly created cell lines could be utilised in future iPSC reprogramming experiments.

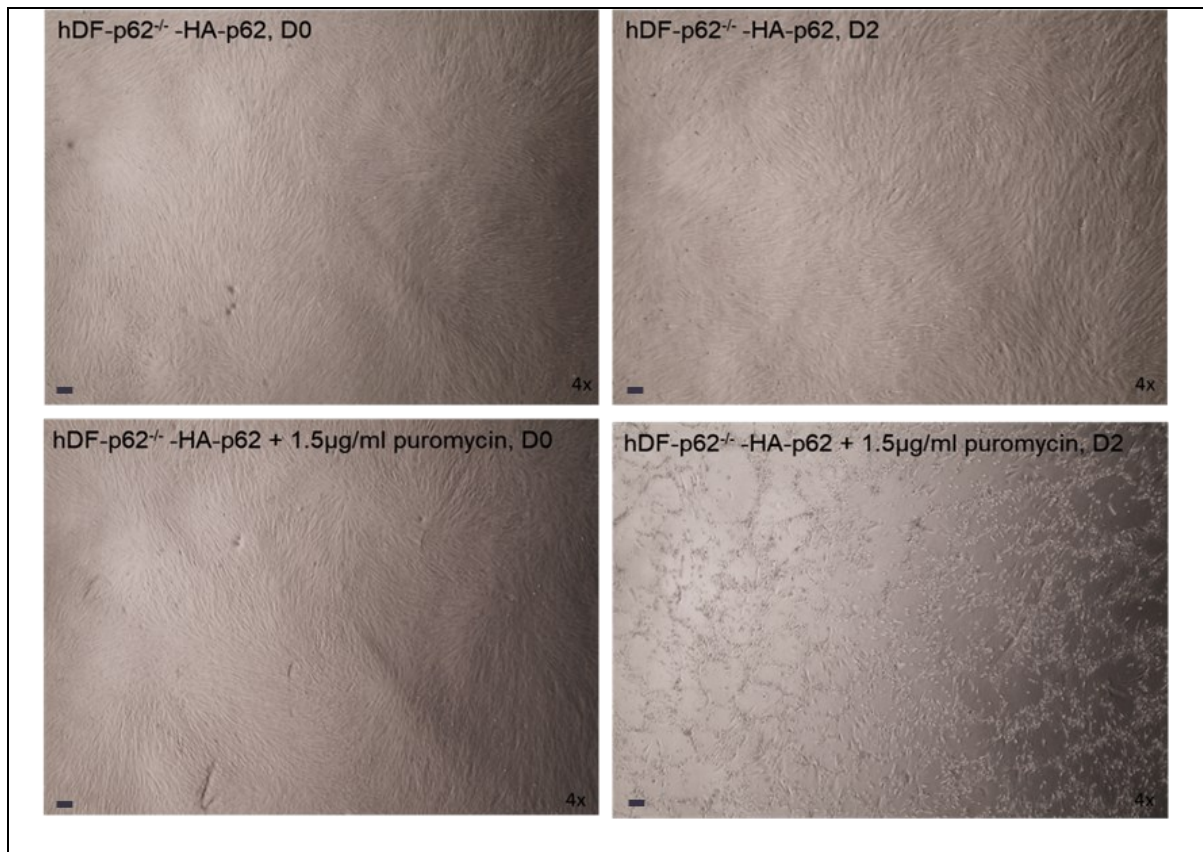


Figure 4.12 Puromycin selection of retrovirus transduced hDF-p62^{-/-}.

hDF-p62^{-/-} cells stably transduced with HA-p62 and HA-p62-LIR retrovirus were subjected to 48 hours of puromycin selection to create a homogeneous cell line. Images show representative example. hDF-p62^{-/-} cells at day 0 and day 2 (48 hours) with and without 1.5µg/ml puromycin. Cells were allowed to recover, expanded and frozen for future iPSC reprogramming experiments. Images taken at 4x magnification, scale bars represent 100µM

5.6. pBMN mCherry- p62 retroviruses.

Two further human p62 overexpression mutant retroviral plasmids were purchased from Addgene: pBMN-mCherry-p62 (Δ UBD) (Addgene ID: 119687) and pBMN-mCherry-p62 (Δ UBD/W340A) (Addgene ID: 119688) (Padman et al, 2019) (See Materials and Methods). pBMN-mCherry-p62 (Δ UBD) is an overexpression plasmid for human p62, without its UBD domain. This mutation will prevent the binding of p62 to ubiquitin tagged proteins, preventing the recruitment of these proteins to the autophagosome. Of course, other proteins besides p62 do contain UBD domains (e.g. OPTN, NBR1 and NDP52) (Padman et al, 2019), so this does not prevent that

targeting of ubiquitin tagged proteins to autophagosome in general, merely, the ability of p62 specifically to enact this function. pBMN-mCherry-p62 (Δ UBD/W340A) has an additional mutation in the LIR region, resulting in a single amino acid change W340A, preventing the interaction of p62 with LC3.

pBMN-mCherry-p62 (Δ UBD) and pBMN-mCherry-p62 (Δ UBD/W340A) plasmids were prepped and plasmids sent to Source bioscience for sequencing, as an appropriate restriction digest could not be found in this instance. Multiple sequence alignment in CLC sequence viewer shows the pBMN-mCherry-p62 (Δ UBD) sequence as provided in Addgene, compared to sequencing results for both pBMN-mCherry-p62 (Δ UBD) and pBMN-mCherry-p62 (Δ UBD/W340A) plasmid preps (Figure 4.13). The blue circle shows the single point mutation in the pBMN-mCherry-p62 (Δ UBD/W340A) sequence. pBMN-mCherry-p62 (Δ UBD) and pBMN-mCherry-p62 (Δ UBD/W340A) retroviral plasmids were co-nucleofected into Hek293T cells along with p-CMV-VSV-G and pUMVC retroviral envelope and packaging plasmids as previously described (See Materials and Methods).

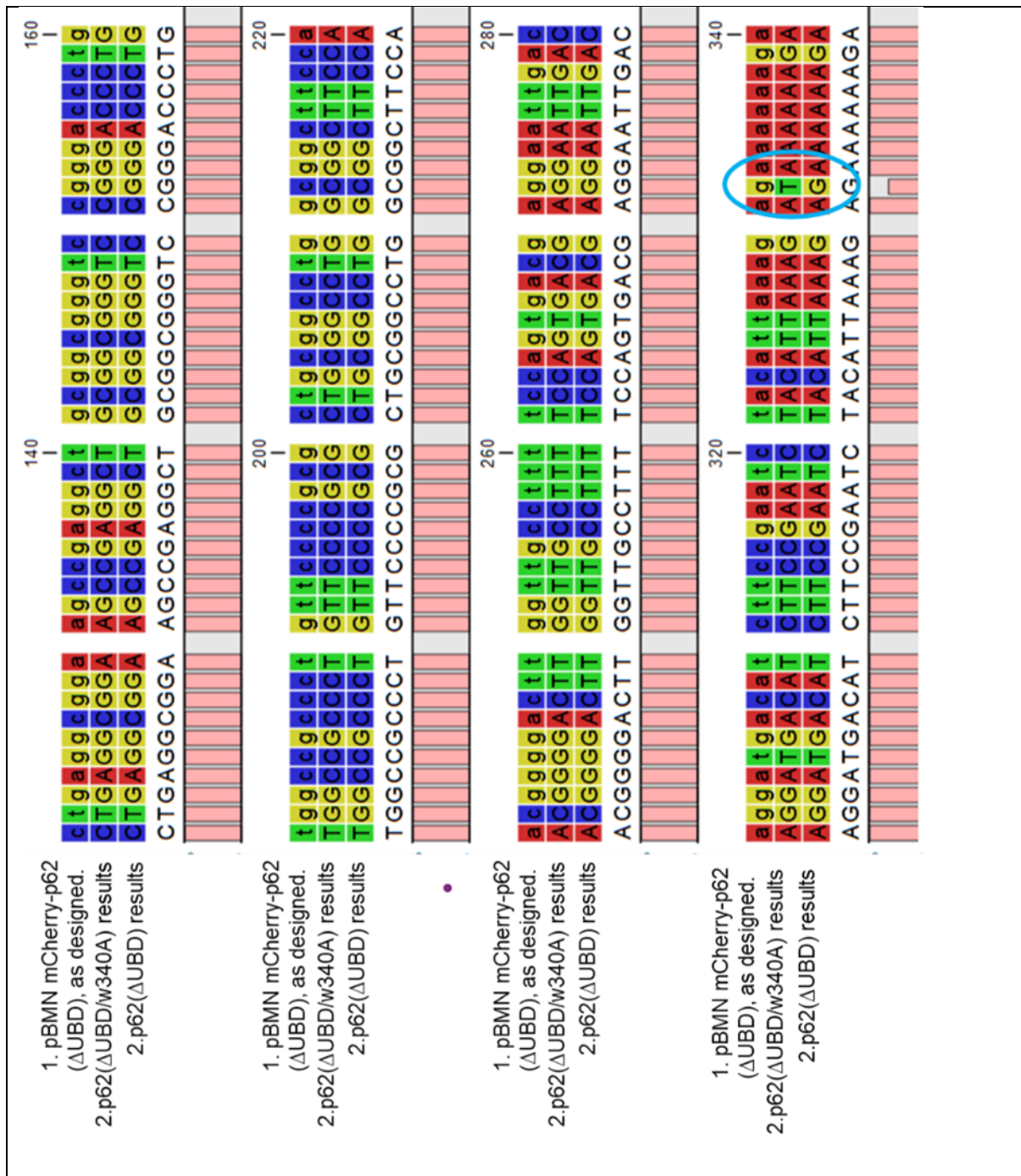


Figure 4.13 Retroviral pBMN-mCherry-p62 vectors.

Multiple sequence alignment in CLC sequence viewer shows sequencing results confirming pBMN-mCherry-p62 (ΔUBD) and pBMN-mCherry-p62 (ΔUBD) sequences, compared to the sequences provided in addgene. The blue circle also shows the single point mutation that results in the W340A amino acid change in pBMN-mCherry-p62 (ΔUBD).

pBMN-mCherry-p62 (Δ UBD) and pBMN-mCherry-p62 (Δ UBD/W340A) were co-nucleofected into Hek293T producer cells with pCMV-VSV-G and pUMVC retroviral packaging and envelope plasmids as previously described. 48 hours after nucleofection Hek293T producer cells were imaged under fluorescence microscopy. Figure 4.14 shows Hek293Ts transfected with pBMN-mCherry-p62 (Δ UBD) (Figure 4.14.A) and pBMN-mCherry-p62 (Δ UBD/W340A) (Figure 4.14.B) alongside p-CMV-VSV-G and pUMVC packaging and envelope plasmids, at 10x (top of each panel) and 20x magnification (at bottom of each panel). Upon visualisation, approximately 50% of Hek293T cells were mCherry+. Since the pBMN-mCherry retroviral plasmids are only very weakly expressed under the gag-pol promoter embedded in the plasmid, transient transfection efficiency with these plasmids is extremely low. Hence, this level of mCherry+ expression is only possible when co-transfected with the packaging and envelope plasmids; thus suggesting that virus is being successfully produced and released into the supernatant in this experiment, and that the mCherry+ expression comes from self-transduction of the Hek293T producer cells, rather than transfection itself. The virus containing cell supernatant was collected at 48, 72 and 96 hours, filtered through a 0.22 μ m filter, and applied directly to target cells.

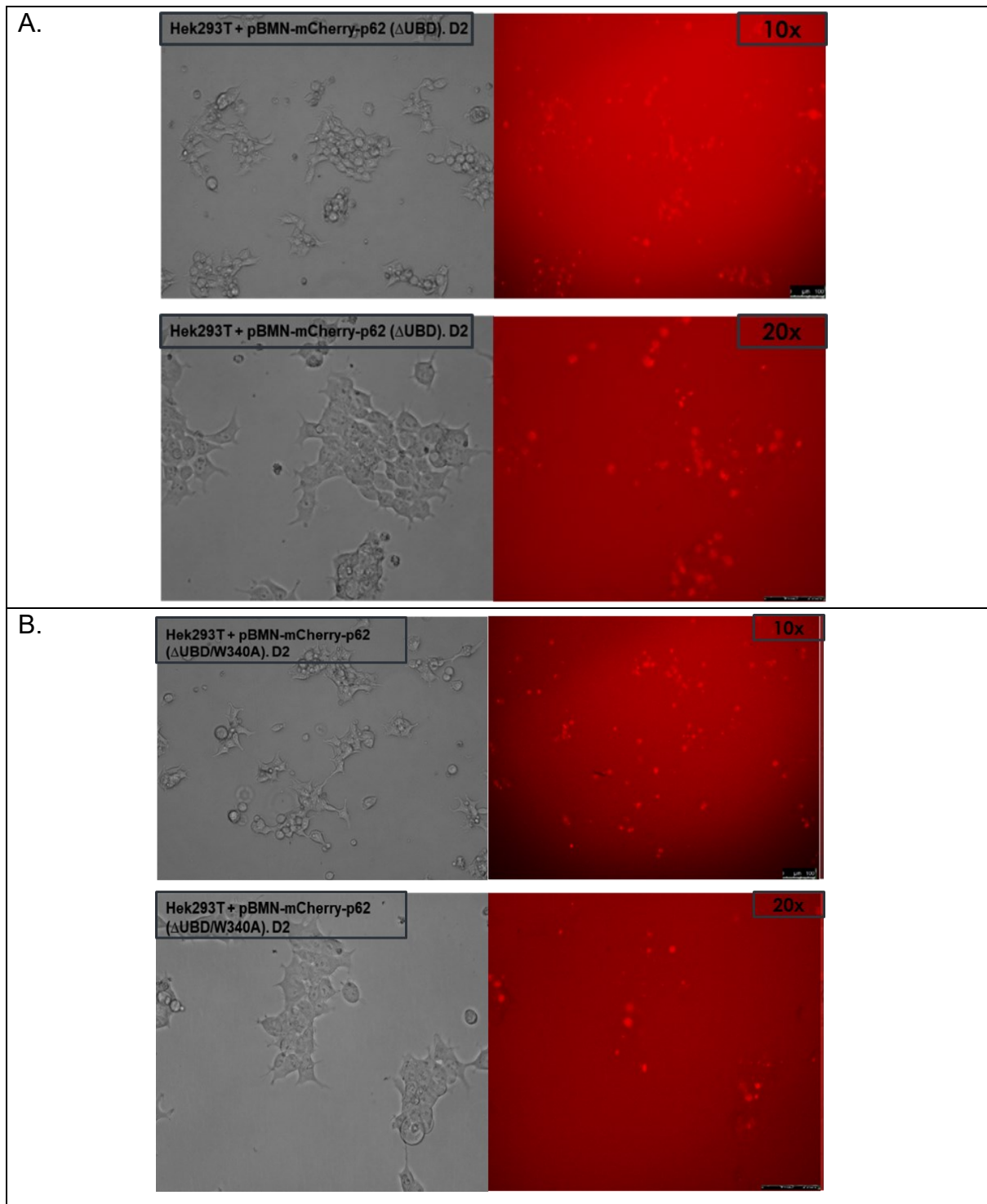


Figure 4.14 Transfection and transduction of Hek293T cells with bBMN-mCherry-p62 retroviruses. A. Hek293T cells imaged 48 hours after transfection with pBMN-mCherry-p62 (Δ UBD) alongside pCMV-VSV-G and pUMVC envelope and packaging plasmids. B. Hek293T cells imaged 48 hours after transfection with pBMN-mCherry-p62 (Δ UBD/W340A) alongside pCMV-VSV-G and pUMVC envelope and packaging plasmids. In both sets of images, approximately 50% of cells are mCherry+, suggesting that viral production has occurred and that these Hek293T cells have undergone some level of self-transduction. Images taken at 10x (top panel) and 20x (bottom panel). Scale bars represent 100 μ M

In this instance, the target cells were hDF-p62^{-/-} cells that had already been nucleofected with iPSC reprogramming OriP/EBNA episomal plasmids (as previously described in Results 1). hDF-p62^{-/-} were nucleofected using the usual McKay Lab iPSC reprogramming protocol, but, on 1D when cell media was usually replaced with fresh hDF maintenance media, instead pBMN-mCherry-p62(Δ UBD) and pBMN-mCherry-p62(Δ UBD/W340A) virus containing media was added. Virus containing media was also added two subsequent days, to ensure that as many cells were transduced as possible. As cell number and density are usually relatively low following nucleofection, a high transduction efficiency was achieved. Figure 4.15 provides a schematic of this modified reprogramming protocol.

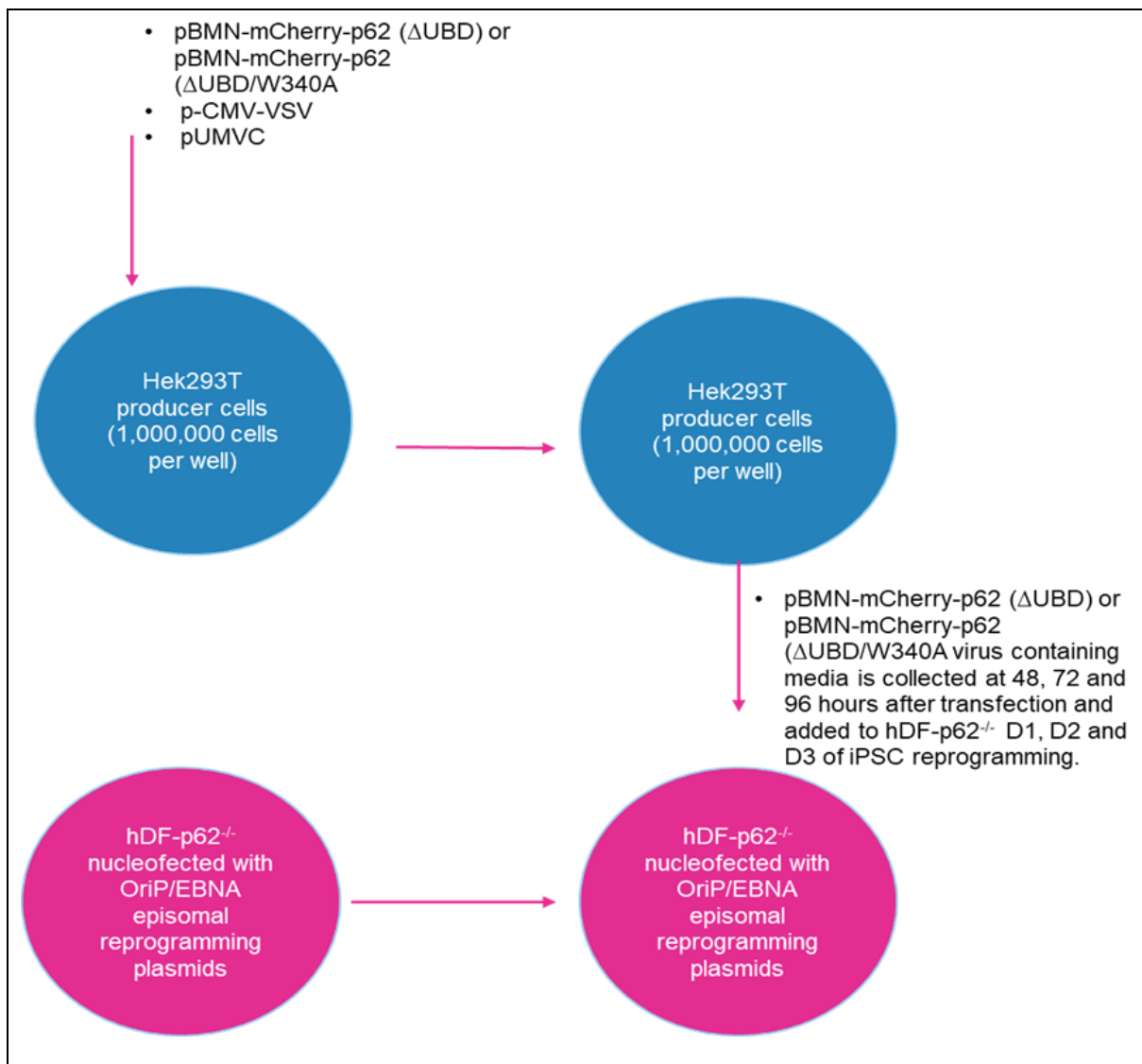
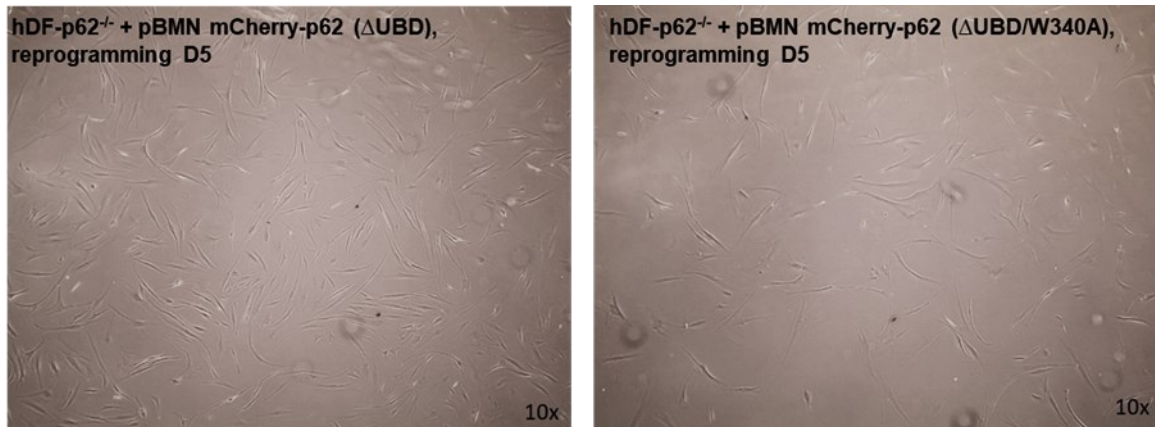


Figure 4.15 iPSC reprogramming of hDF-p62^{-/-} + p62 overexpression mutant retrovirus (pBMN-mCherry-p62 (Δ UBD and pBMN-mCherry-p62 (Δ UBD/W340A)).
Experimental design overview.

hDF-p62^{-/-} cells nucleofected with reprogramming plasmids and transduced with pBMN-mCherry viruses were imaged on D5 of iPSC reprogramming (Figure 4.16). Again, these experiments could not be completed, but fluorescence imaging taken on D5 of iPSC reprogramming experiments indicated a very high level of transduction efficiency in these cells, suggesting that the experimental design was successful and important data could have come from these experiments.

A.



B.

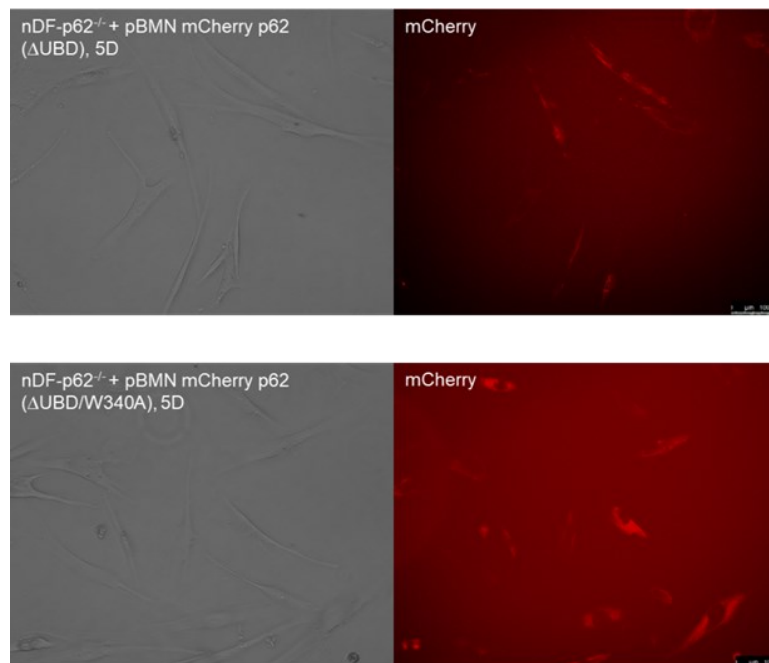


Figure 4.16 iPSC reprogramming of hDF-p62^{-/-} + p62 overexpression mutant retrovirus.

A. Phase images of hDF-p62^{-/-} + pBMN-mCherry-p62 (ΔUBD) (left image) and of hDF-p62^{-/-} + pBMN-mCherry-p62 (ΔUBD/W340A) (right), at D5 of a reprogramming experiment. Cells appeared to have recovered well from nucleofection and three days of transductions and appear healthy. Phase images were taken at 10x magnification. B. Fluorescence imaging of hDF-p62^{-/-} + pBMN-mCherry-p62 (ΔUBD) (left image) and hDF-p62^{-/-} + pBMN-mCherry-p62 (ΔUBD/W340A) at D5 of iPSC reprogramming. A high level of transduction is visible. Fluorescence images were taken at 20x magnification, scale bars represent 50μm.

5.7. **Truncated- hp62 overexpression plasmid**

As previously discussed, p62 is a multi-domain, multi-functional protein 440 amino acids in length, encoded by the SQSTM1 gene: specifically the SQSTM1-202 transcript. However, another commonly expressed transcript exists- SQSTM1-215. This transcript encodes a much shorter protein; only 167 amino acids in length (See further details in Introduction, section 1.12. These 167 amino acids correspond with a small portion of the PB1 domain, a ZZ-type zinc finger domain, and the Traf6 binding region (TB) only. Figure 4.17 shows truncated hp62 (hp62-trunc) aligned to the full-length protein.

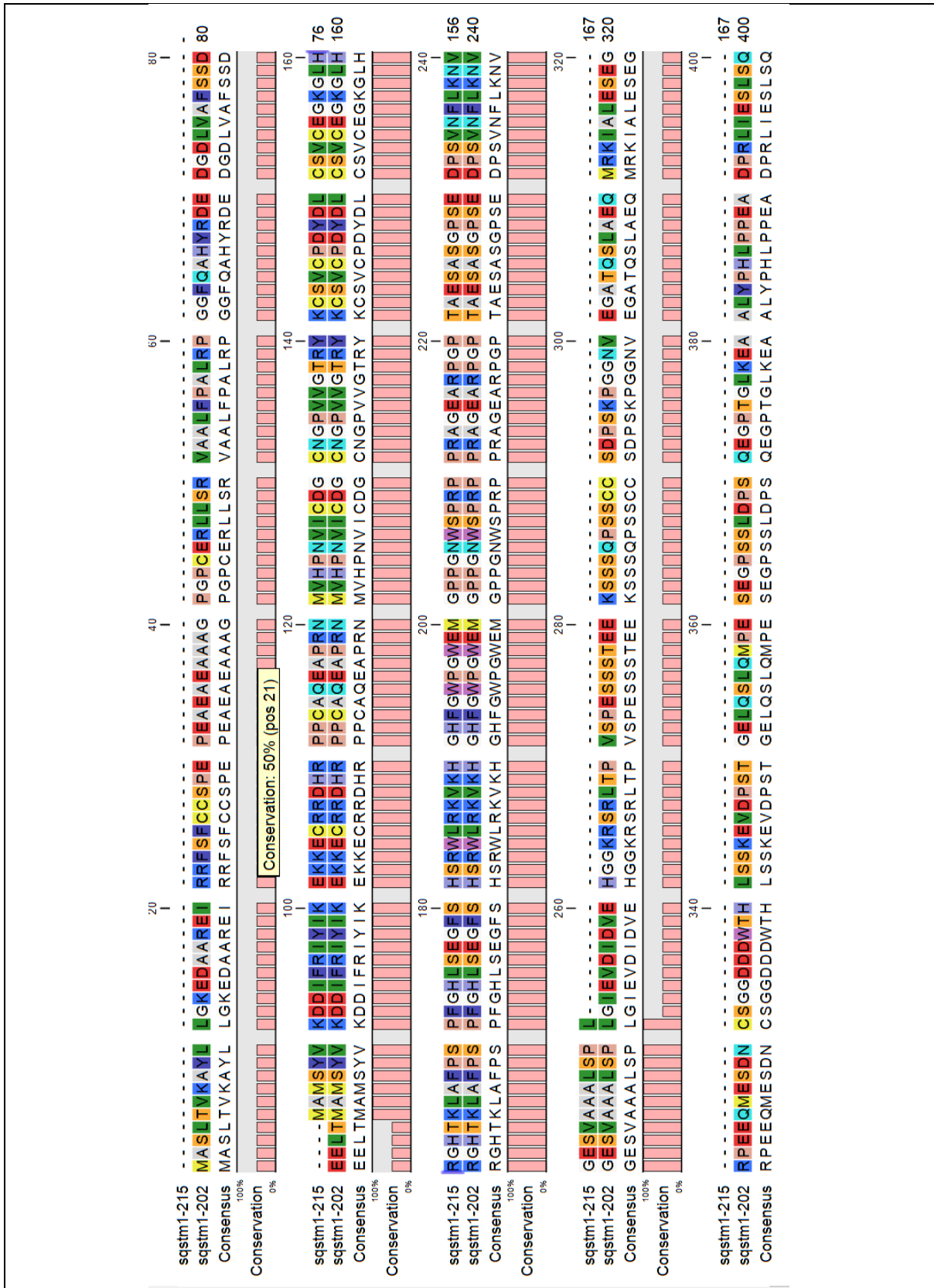


Figure 4.17: Truncated human p62.

A. Multiple sequence alignment in CLC sequence viewer shows the amino acid sequence for full-length human p62 encoded by the SQSTM1-202 transcript compared to truncated human p62 encoded by the SQSTM1-215 transcript.

A lentiviral overexpression vector containing this hp62-trunc expression cassette, controlled by a CMV promoter was purchased from GeneCopeia™, which also contains eGFP and puromycin selection cassettes. This hp62-trunc vector was co-transfected into Hek293T producer cells alongside lentiviral envelope (pCMVR8.74) and VSV-G envelope expressing (pMD2.G) plasmids as previously described.

Figure 4.18.A shows Hek293T cells 72 hours after transfection. Fluorescence imaging shows an extremely high level of GFP+ cells (~70%), suggesting a high level of transfection efficiency. Untransfected Hek293T cells are also shown, confirming that GFP+ expression is directly a result of the Lentiviral production and no auto-fluorescence is occurring. In addition, there was no fluorescence in the red channel (not shown).

Virus containing media was collected at 48, 72 and 96 hours, filtered through a 0.22µm filter and applied directly to fresh Hek293T cells to undergo transduction. Virus containing media was added either 1-well of virus media directly onto 1- well of Hek293T cells (1:1) or 1-well of virus containing media to 2-wells of Hek293T cells (1:2) (Figure 4.18.B). Transduction efficiency is approximately 25% at the higher concentration.

A.

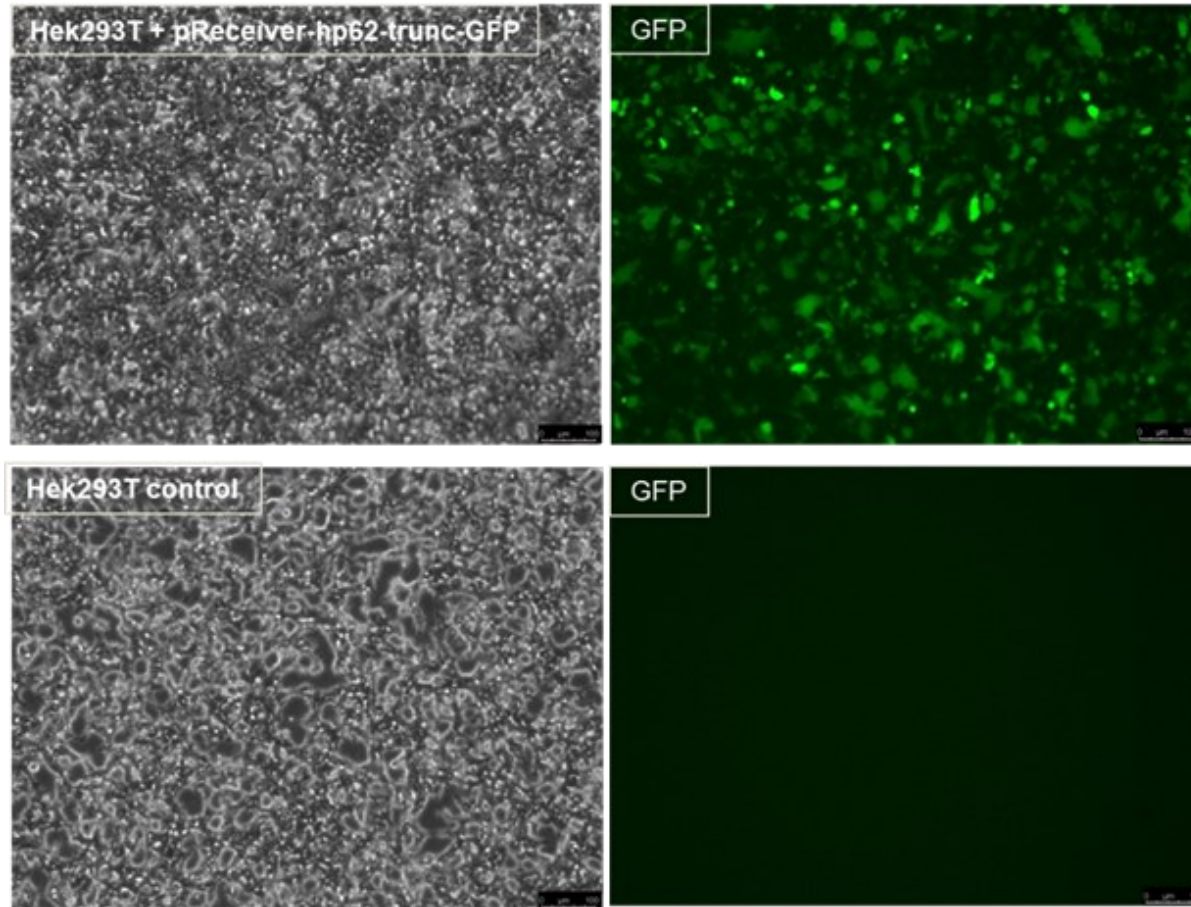


Figure 4.18 Transfection and transduction of hp62-trunc in Hek293Ts.

A. Hek293T cells 72 hours after transfection with p-receiver-hp62-trunc-GFP lentiviral vector alongside envelope (pCMVR8.74) and VSV-G packaging expressing (pMD2.G) plasmids. A very high level of transfection efficiency is achieved.

B.

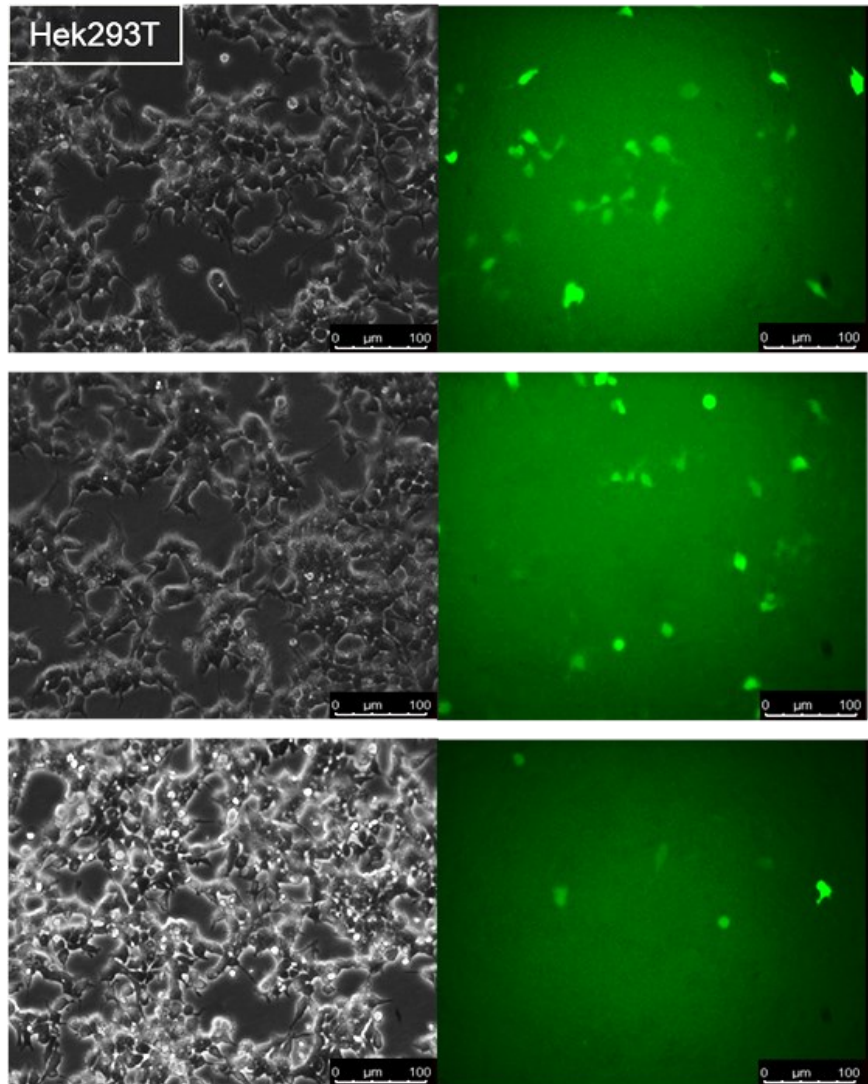


Figure 4.18 Transfection and transduction of hp62-trunc in Hek293Ts.

B. Hek293Ts transduced either 1:1 (top two panels) or 1:2 (bottom panel) with hp62-trunc-GFP lentivirus containing media.

Hek293T cells are not the ideal cell line in which to test this lentivirus, due to the high level of exogenous p62 protein expression. However, the GFP expression in the transduced cells suggested that the overexpression construct was at least actively expressed in Hek293T cells so I decided to test these cells in the hDF-p62^{-/-} target cells.

Hek293T cells were co-transfected with alongside lentiviral envelope (pCMVR8.74) and VSV-G envelope expressing (pMD2.G) plasmids as previously described and imaged under a fluorescence microscope after 72 hours (Figure 4.19.A.). hp62-trunc-GFP lentivirus containing media was collected and filtered through a 0.22 μ m filter at 48, 72 and 96 hours after transfection and applied 2:1 (in order to improve upon the transduction efficiency achieved in the Hek293T experiment) onto hDF-p62^{-/-} in a 6-well plate. hDF-p62^{-/-} were imaged under fluorescence microscopy 72 hours after transduction (Figure 4.19.B) and ~50% of cells are GFP+.

hDF-p62^{-/-}-hp62-trunc-GFP cells were then expanded and subjected to puromycin selection in order to create a homogeneous population of cells. A puromycin titration experiment was performed (Figure 4.19.C) in order to determine the optimum concentration of puromycin for these cells. It was determined that a concentration of 1 μ g/ml puromycin was the optimum concentration to ensure that 100% of cells were GFP+ and therefore stably transduced with the hp62-trunc-GFP lentivirus without causing any toxicity. This brand new cell line of p62 null fibroblasts with a reconstituted, truncated form of p62 (hDF-p62^{-/-}-hp62-trunc-GFP) were expanded and placed in cryopreservation for future iPSC reprogramming experiments.

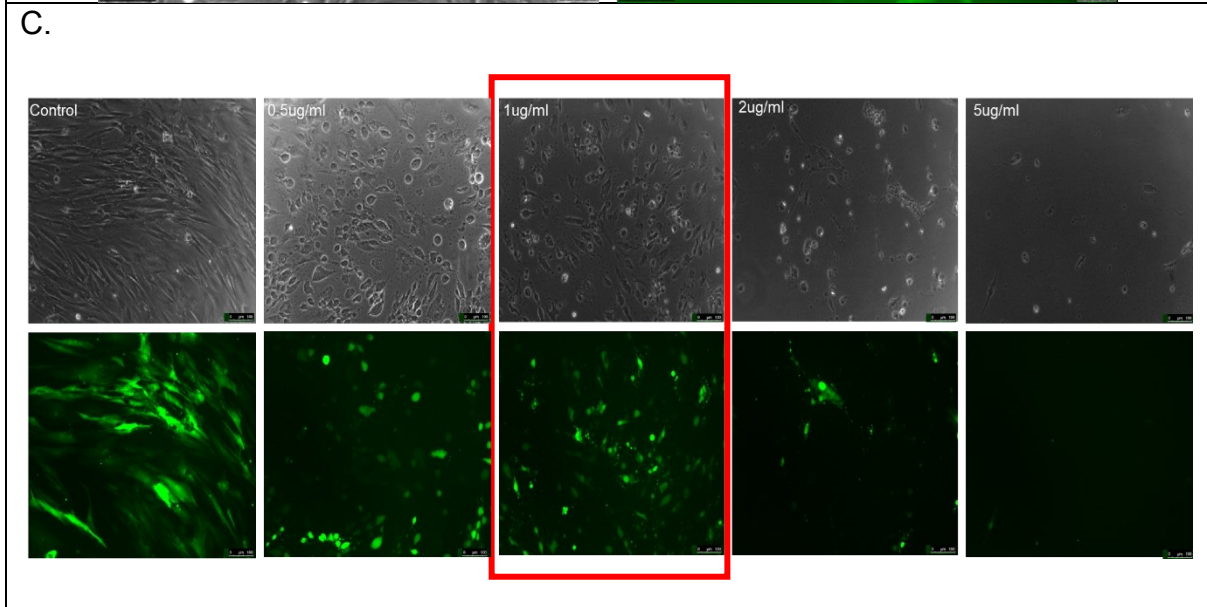
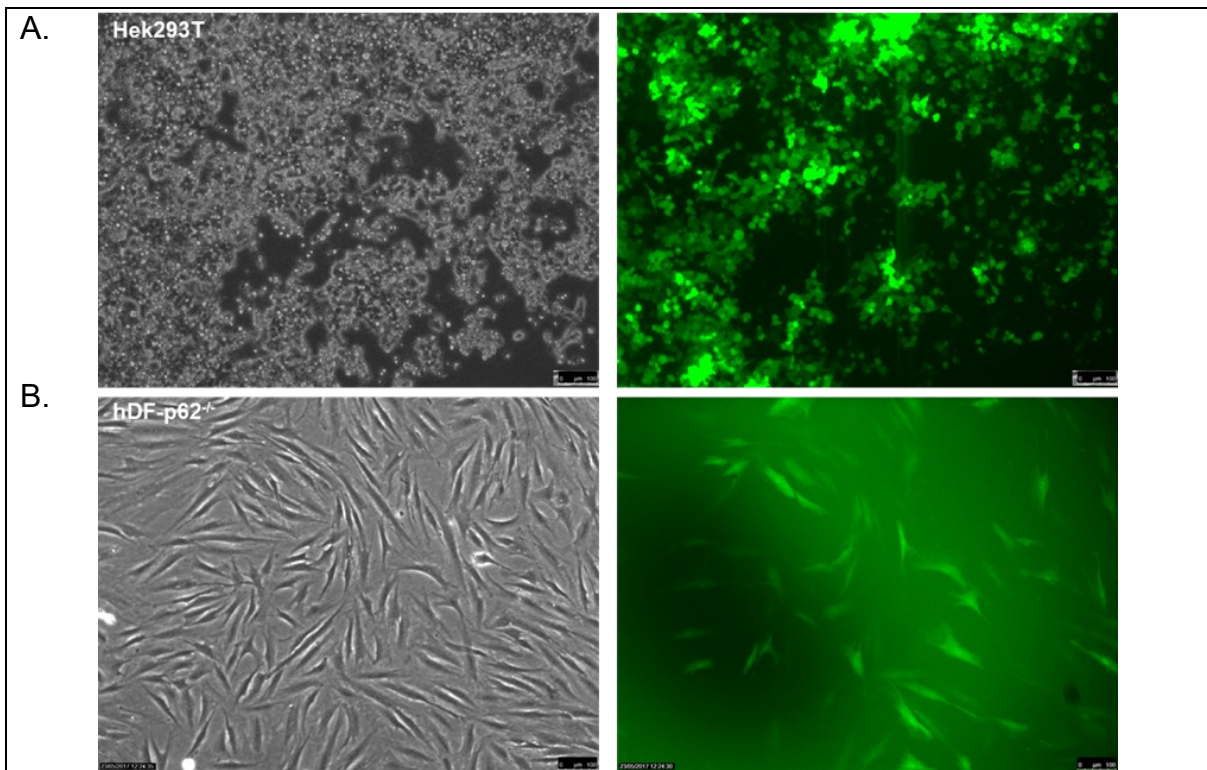


Figure 4.19 hDF-p62^{-/-} transduced with hp62-trunc-GFP lentivirus.

A. Hek293T producer cells transfected with hp62-trunc-GFP lentiviral vector, alongside envelope (pCMVR8.74) and VSV-G packaging expressing (pMD2.G) plasmids and imaged after 72 hours. Transfection efficiency is very high. B. hDF-p62^{-/-} transduced with hp62-trunc-GFP lentivirus containing media 2:1 and imaged after 72 hours. Transduction efficiency is also relatively high. C. Puromycin titration experiment in hDF-p62^{-/-} transduced with hp62-trunc-GFP lentivirus. A range of puromycin concentrations from 0.5-5µg/ml were applied to cells for 48 hours, and allowed to recover for a further 48 hours before imaging. 1µg/ml of puromycin is ideal (as indicated by the red box), and these cells were expanded and cryopreserved for future experiments

5.8. **Mouse p62 cloning**

5.8.1. Introduction

p62 is a highly conserved gene across all species, and study its effects in iPSC reprogramming and the maintenance of pluripotency could provide valuable insight into its biology. As such, I have created a library of genetic manipulation vectors for mouse p62 to compliment those created in human. I have created a mouse p62 shRNA lentiviral vector, in much the same way as the human shRNA. Secondly, I have created a complete p62 overexpression lentivirus and employed state-of-the-art In-Fusion® cloning to create three functional mutants of p62 in key interacting regions.

5.8.2. Mouse shRNA design

A shRNA construct for mousep62 was designed in order to induce p62-knockdown in MEF control cells. shRNA sequences were generated exactly as human shRNA; using the Splash RNA algorithm (Pelossof et al, 2017), which predicts high-potency, miRNA based shRNA sequences (Figure 4.20), whereby a score of over 1.0 suggests a good shRNA sequence. Three sequences can be combined to create a 'triple-hit' effect, thereby increasing efficiency and ensuring a good level of knock-down. Three sequences were selected from the algorithm generated options (in this case sequences 1, 2 and 5 were selected (highlighted in green) as 3 and 4 overlapped with 1 (highlighted in red). Next, sequences and their complimentary strands are aligned to the p62 sequence, with mismatches created in the complimentary strand in order to promote duplex unwinding and passenger strand degradation as previously described. Finally, these sequences are combined with restriction sites added at each end (*HpaI* and *XhoI*) for ease of cloning into our

destination vector of choice (pLL3.7). As with the human shRNA. This shRNA was designed so that each individual sequence could be used separately or together, so restriction sites are also present between each shRNA sequence (*PvuII* between sequences 1 and 2; *SaII* between sequences 2 and 3). Sequences have a stem loop between complementary strands, and approximately 60bp between each sequence for maximum effectiveness.

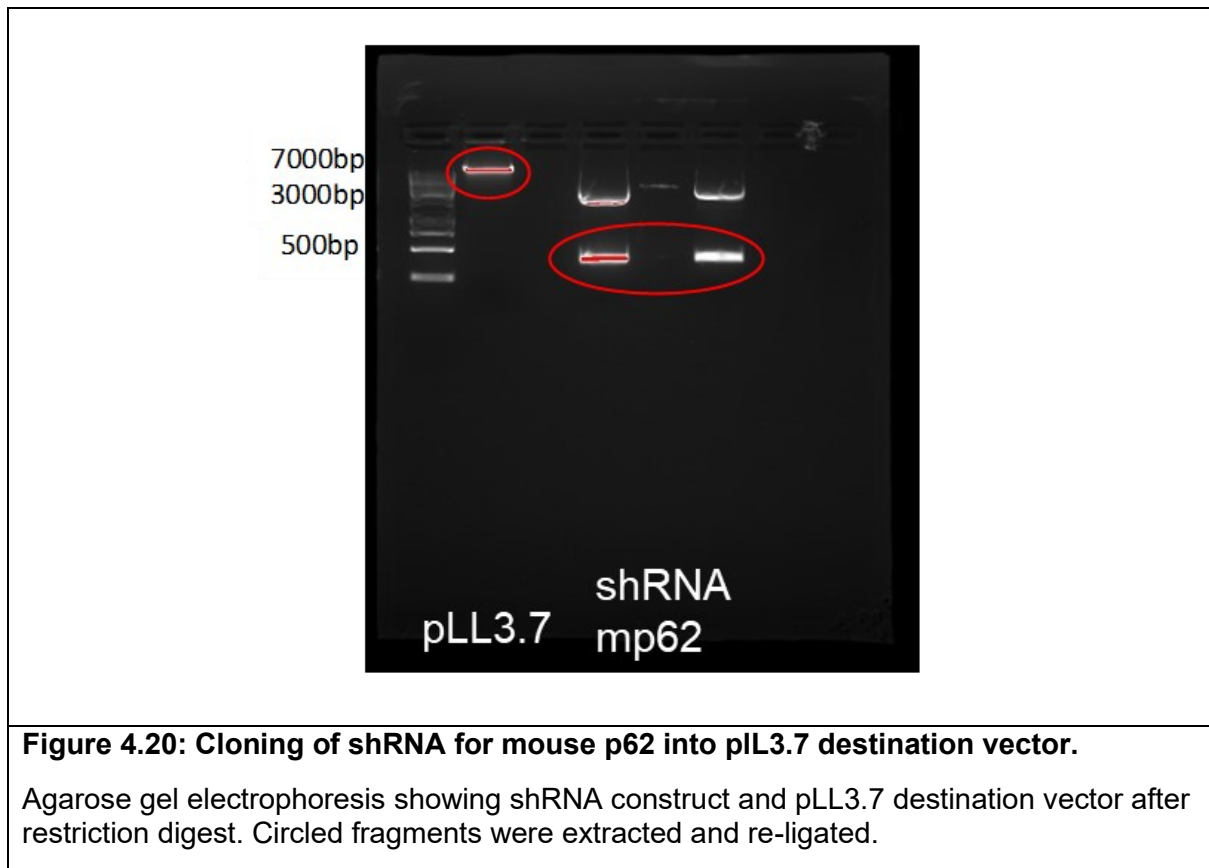
Label	Antisense Guide Sequence	SplashRNA Score
Mouse_SQSTM_1016_v2	TTTTGAAGACAAATGTGTCCAG	1.724
Mouse_SQSTM_283_v2	TTCTCTTTAATGTAGATGCGGA	1.630
Mouse_SQSTM_1015_v2	TTTGAAGACAAATGTGTCCAGT	1.568
Mouse_SQSTM_1019_v2	TTCTTTTGAAGACAAATGTGTC	1.443
Mouse_SQSTM_1288_v2	TTCGAATACTGGATCGTGTCA	1.427

5.8.3. Cloning and validation

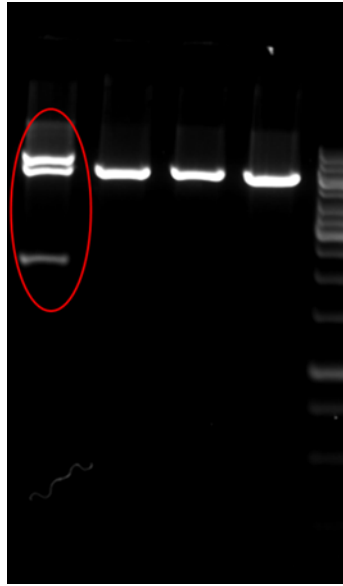
The sh(m)p62 construct was cloned into pLL3.7, whereby both the pLL3.7 destination vector and the originating plasmid containing the shRNA sequence were subject to restriction digest with *HpaI* and *XhoI* enzymes. *HpaI* cuts DNA in a 'blunt' fashion, and *XhoI* leaves a sticky end: this helps to ensure that the shRNA construct is religated into the destination vector in the correct directionality. Digested plasmids are then separated by agarose gel electrophoresis, correct bands are excised and DNA extracted from the gel (Figure 4.20). The linearised pLL3.7 vector and the shRNA construct are then religated and transformed into *Stbl3* competent cells. (See also Materials and Methods). Individual bacterial colonies were then prepped and subjected to restriction digest with *HpaI* and *XhoI* in order to check the success of

the cloning (Figure 4.21.A and sent for Sanger sequencing (Figure 4.21.B)

Unfortunately, several attempts at Sanger sequencing failed to produce readable results despite positive restriction digests, preventing the validation of this construct in cells.



A.



B.

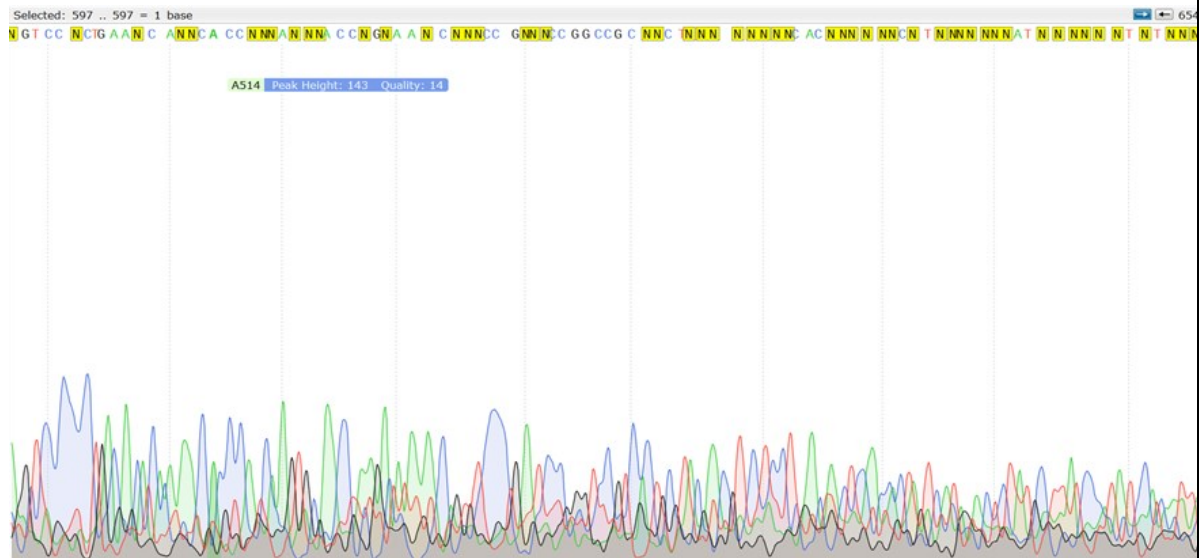


Figure 4.21 Cloning of sh(m)p62 constructs into pLL3.7 lentiviral vector.

A.

First stage colony screening is carried out by restriction digest with *HpaI* and *XhoI*. Lane 1 shows a correct clone, with clean fragments of the correct size. **B.** Clones which appear correct on restriction digest are sent for Sanger sequencing at Source Bioscience, unfortunately Source Bioscience failed to return good sequencing results on multiple occasions

5.9. **Mouse p62 overexpression.**

5.9.1. Design, cloning and validation of mouse p62 overexpression construct.

A construct for the overexpression of mouse p62 (mp62) was designed. The construct was designed as the whole of the mouse p62 coding sequence, which is 1329bp in length and codes for the complete multi-domain p62 protein (443 amino acids in length). This construct was de novo synthesised under my instruction by Origene, and provided in a plasmid with Kanamycin resistance. The mp62 sequence was cloned into the pENTR1A plasmid by PCR cloning. PCR primers were designed for the start and end of the mouse p62 sequence, with the addition of a small 4pb 'buffer' and *EcoRI* restriction site on the forward primer and *BamHI* restriction site on the reverse primer. The mouse p62 sequence was amplified using end-point PCR and the PCR product, alongside pENTR1A minimal cloning vector were digested with *EcoRI* and *BamHI* restriction enzymes. pENTR1A was separated by gel electrophoresis and the correct fragments were extracted from the gel, re-ligated with the mouse p62 sequence and transformed into Stbl3 competent cells as previously described. Individual bacterial clones were prepped, and again subjected to restriction digest with *EcoRI* and *BamHI* as a first line of screening. Correct clones should have two bands on an agarose gel, one at approximately 2200bp (pENTR1a) and one at 1300bp for mouse p62. All three clones appeared to be correct on restriction digest (Figure 4.22).

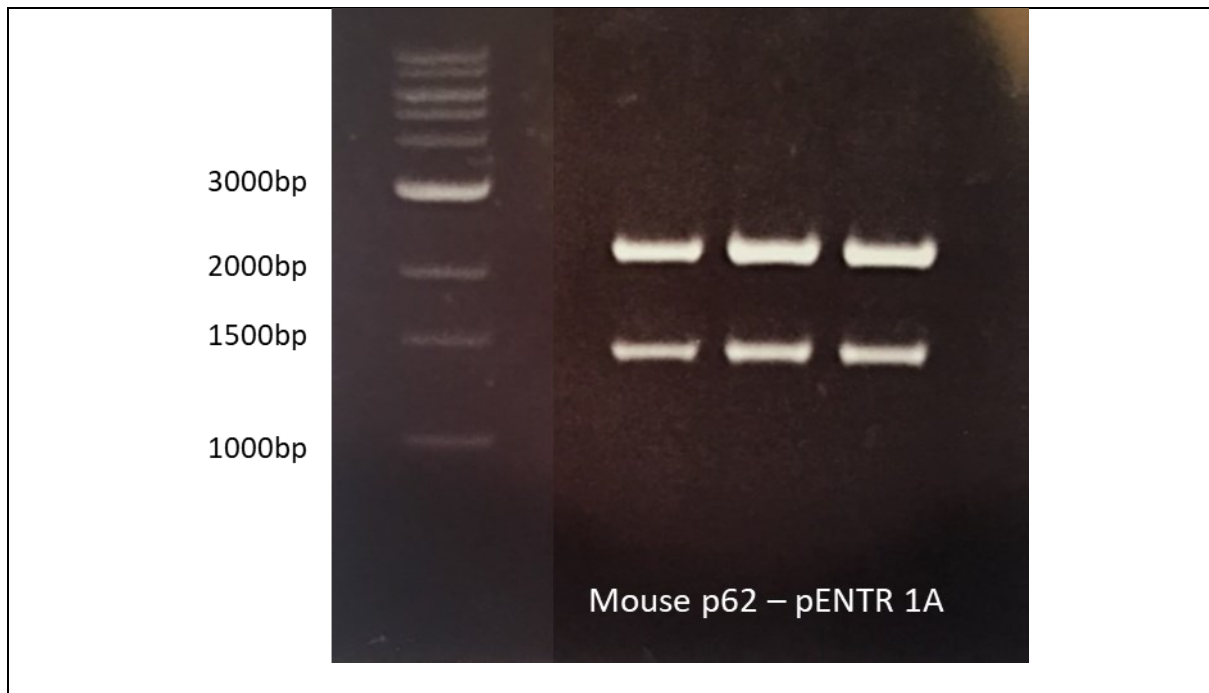
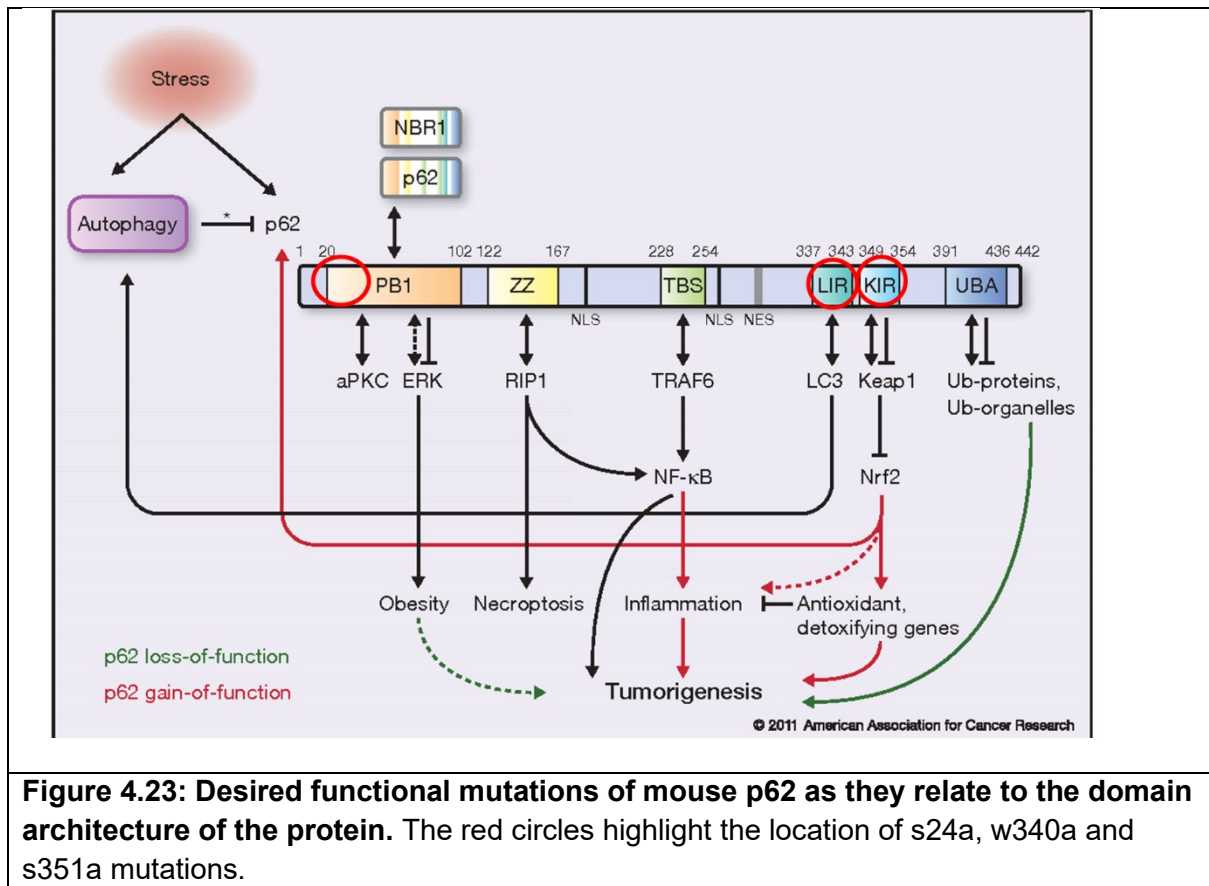


Figure 4.22 Mouse p62 overexpression vector is cloned into pENTR1A minimal cloning vector.

Restriction digest reveals 3 correct clones with fragments of the right size.

5.9.2. Infusion cloning to create specific functional mutants of mouse p62.

In order to study not just if p62 plays a role in iPSC reprogramming but how it exerts these effects, I designed a number of functional mutants to alter the phosphorylation status of a single amino acid, thereby preventing specific p62 interactions. For mouse p62, I designed mutations in three key p62 domains: the PB1 domain, the LIR and the KIR. Figure 4.23 shows the basic domain architecture of mouse p62, with red circles highlighting the location of the proposed mutations: s24a, w340a and s351a.



The In-Fusion® cloning strategy for specific site mutations was similar to the PCR based cloning already described. Mouse p62 sequences were amplified from pENTR1a vectors using primers designed with restriction enzymes as well as the specific base pair mutations we wanted to introduce and 15bp overlap with the desired destination vector. The pENTR1A backbone was then restriction digested using complimentary enzymes and the newly mutated p62 sequence reintroduced into the original vector. Figure 4.24 shows a representative example of an agarose gel showing the PCR amplified mp62 sequence alongside digested and undigested (as control) pENTR1A backbone. After gel extraction, the In-Fusion® reaction is performed and the resulting DNA transformed into Stellar competent cells.

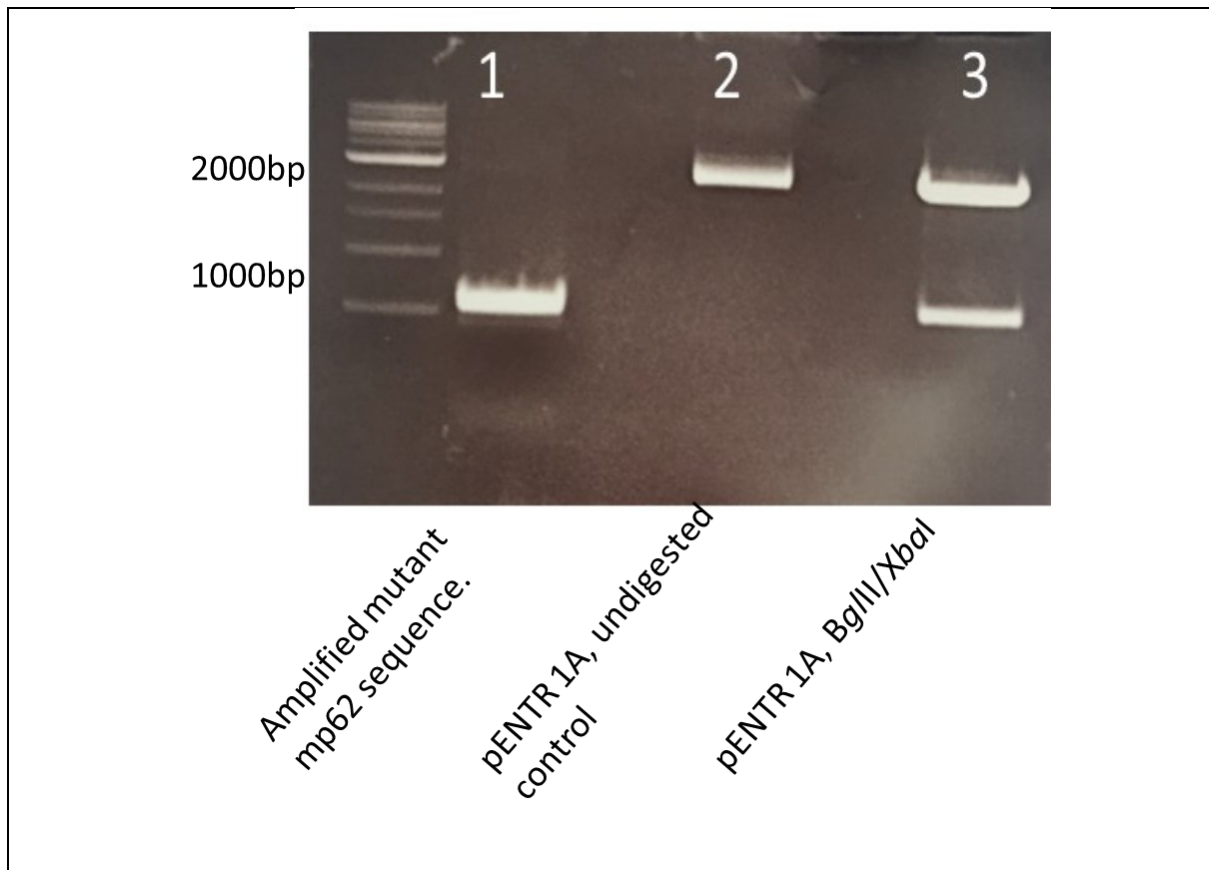


Figure 4.24 Infusion cloning of mp62 mutants in pENTRA1.

mp62 sequence is amplified with primers containing the new mutation to be introduced and restriction sites within the mp62 sequence. pENTRA1 is digested with the same restriction enzymes. pENTR1A backbone and mp62 sequence extracted from the gel, religated and transformed into competent cells.

Clones were sent for sequencing, and sequencing results are shown in Figure 4.25.A, B and C. Correct clones with new mutations were created for mouse p62 as follows: mp62 s24a (PB1 mutation to prevent homodimerisation of p62), w340a (LIR mutation to prevent binding with LC3) and s351a (KIR mutation to prevent interaction with KEAP1), all in pENTR1A minimal cloning vector.

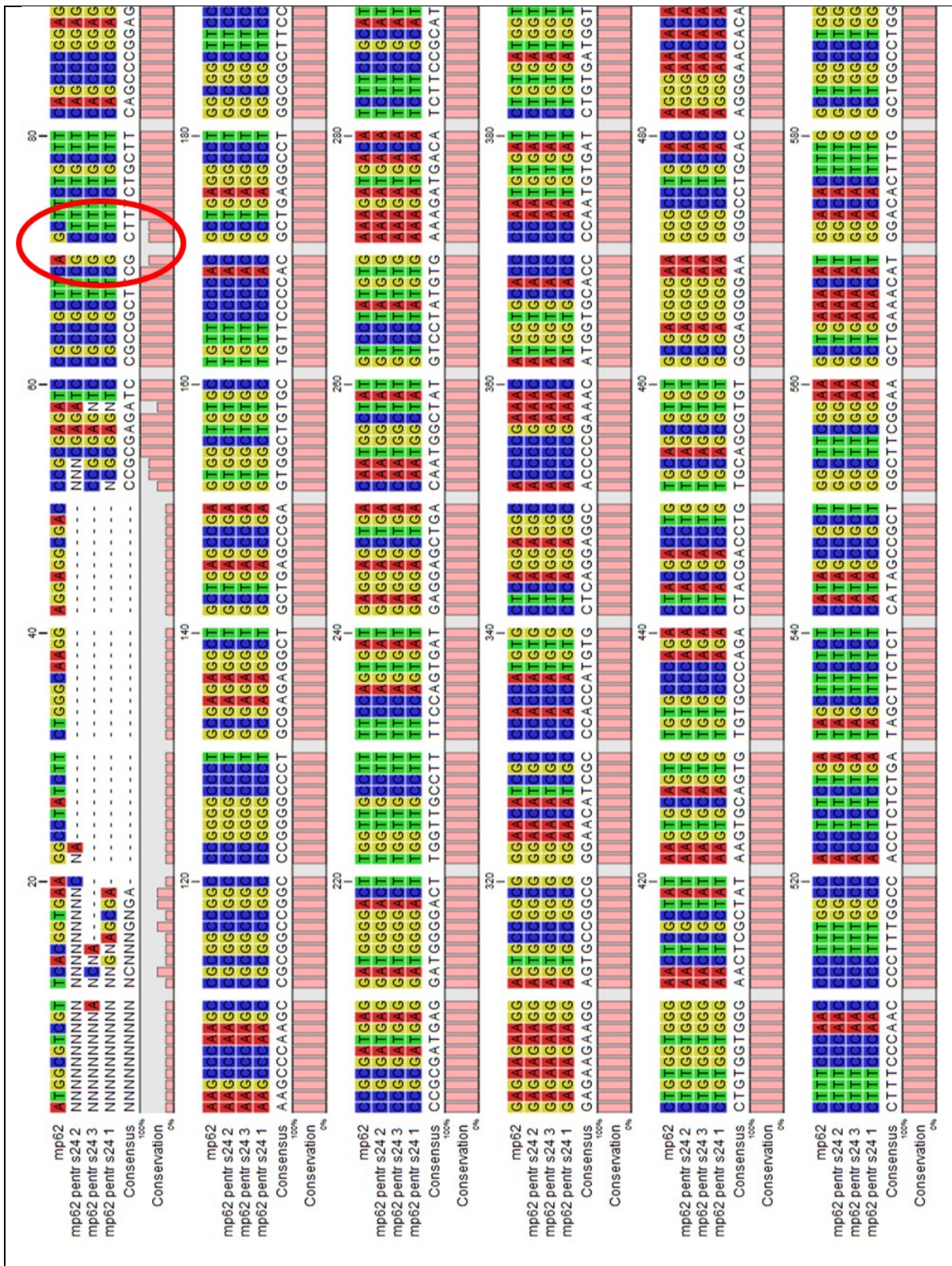


Figure 4.25.A: Successful mouse p62 mutation In-Fusion® cloning in pENTR1A cloning vector- s24a mutation.

Red circle shows that 3 correct clones have the desired mutation, and are otherwise perfectly aligned. Mutation changes AGC (Serine) to GCT (alanine).

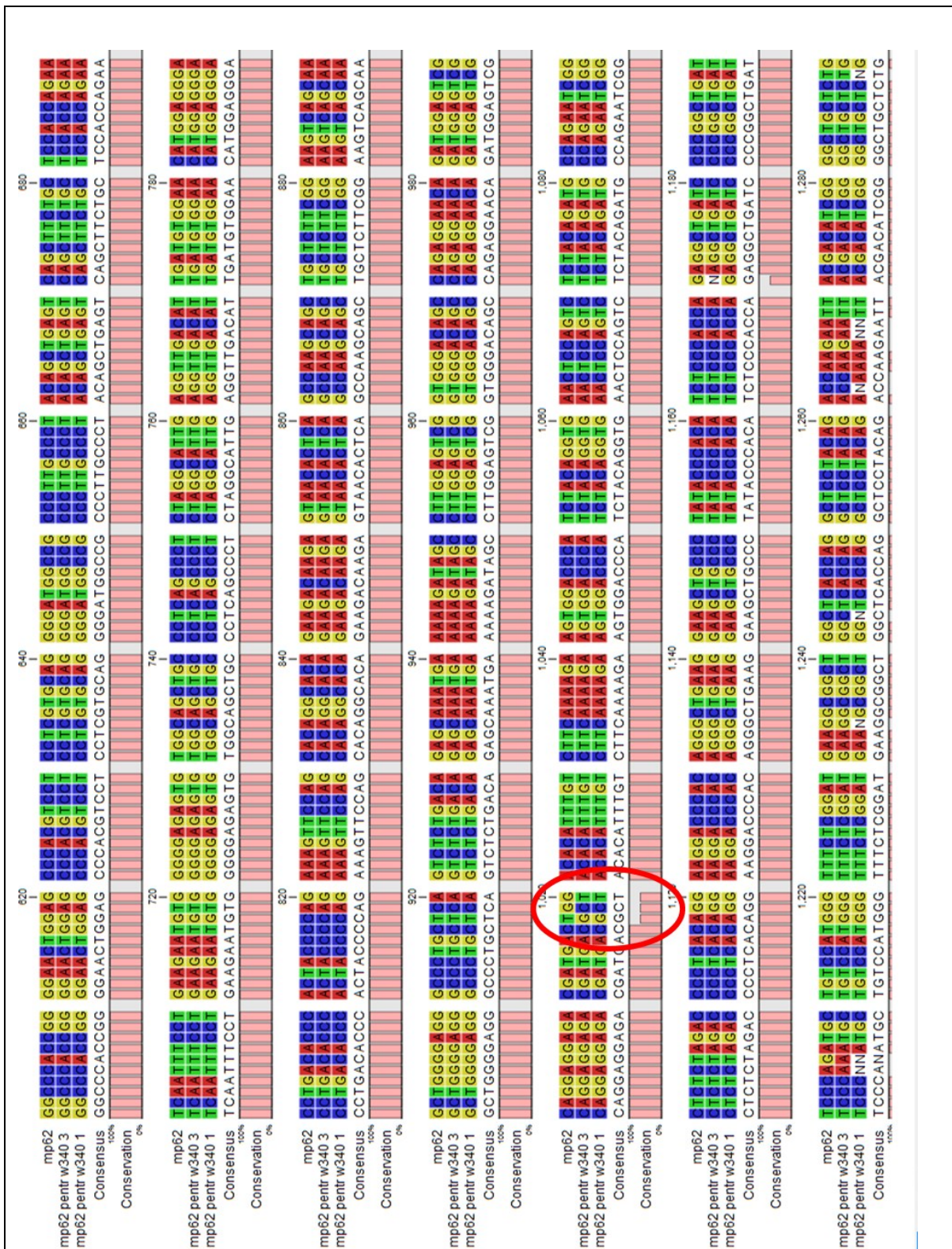


Figure 4.25.B: Successful mouse p62 mutation In-Fusion® cloning in pENTR1A cloning vector- w340a mutation.

Red circle shows 2 correct clones have the desired mutation. The red circle shows DNA base changes from TGG (encoding aspartate) to GCT (alanine).

5.9.3. Recombination into SFFV-lentiviral vector.

As previously described, the pENTR1A minimal vector is an ideal intermediate cloning vector that allows for easy cloning and *attL1* and *attL2* site recombination into a Gateway destination vector of choice containing the *attR1* and *attR2* sites (in this case SFFV-GW). The mp62 pENTR1A complete overexpression cassette and the three new functional mp62 mutants were recombined into SFFV-GW. Individual bacterial colonies prepped and sent to Source bioscience for sequencing. SFFV-mp62 clones were not subjected to screening with restriction enzymes as the SFFV vector is very large (~10.5kb) and contains a huge number of restriction items and on this occasion, it was not possible to find suitable enzymes to screen for the success of the cloning. Figure 4.26.A, B, C and D show multiple sequence alignment of SFFV-mp62 sequencing results for the complete mp62 and the s24a, w340a and s351a mutants correctly aligned and sequenced in the SFFV lentiviral vector.

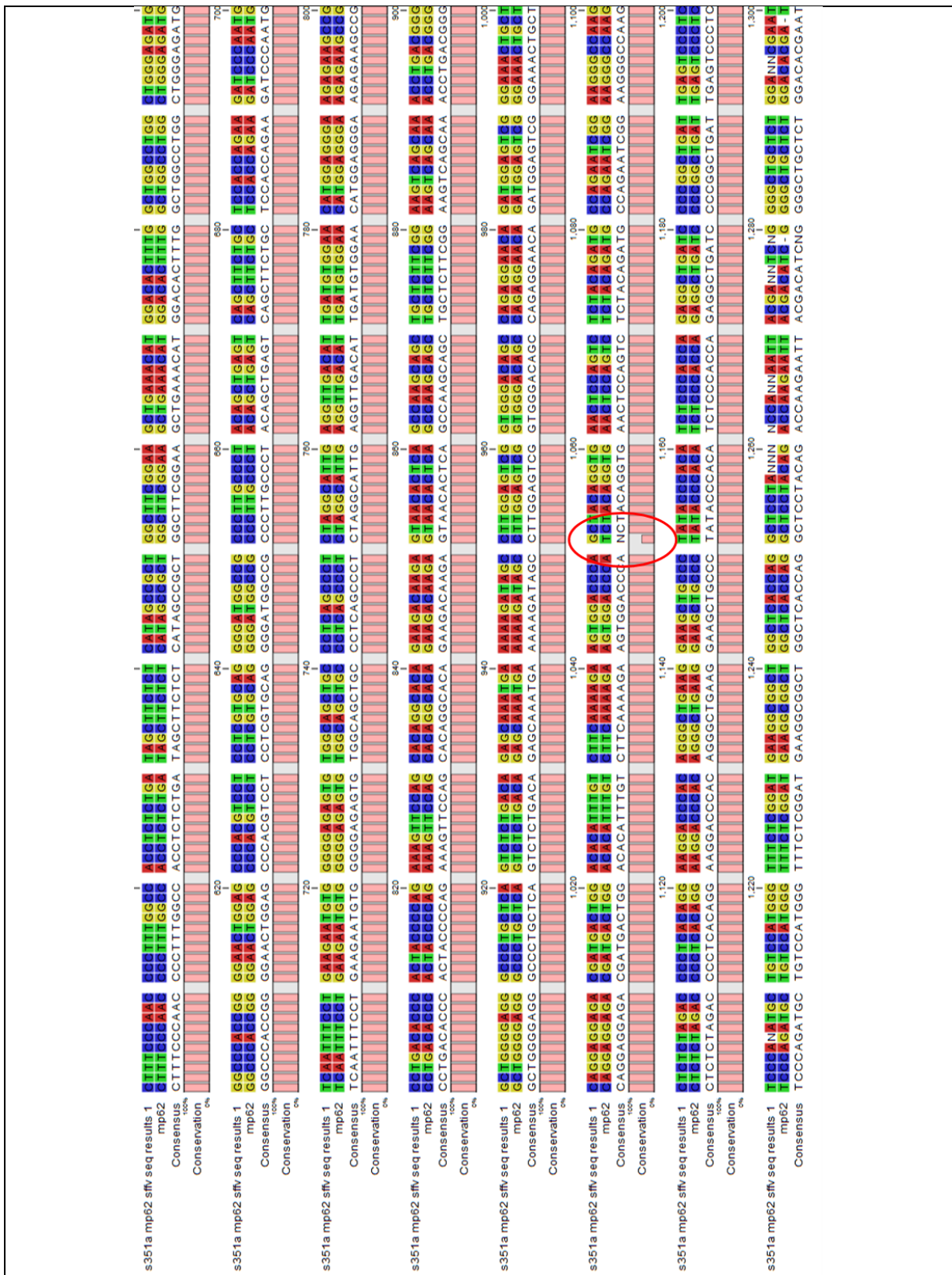


Figure 4.26.D Successful cloning of mp62 in SFFV lentiviral vector- mp62-SFFV-s351a.

s351a mutation in SFF, red circle highlights the mutation.

Unfortunately, because I was unable to confirm the successful cloning of the sh(m)p62 vector, and I did not have access to any other suitable p62 null mouse cells, these vectors could not be implemented. However, these vectors are all available for future works investigating the functional role of p62 in iPSC reprogramming and maintenance of pluripotency in mouse cells: this will be discussed further in the 'Future works' section of this report.

5.10. **Conclusions**

Overall, the data from this chapter demonstrates the ability to create a myriad of tools for the manipulation of genetic and protein expression relating to p62 in both mouse and human cell models. Another element that was not discussed in this chapter was that a range of p62 mutant overexpression plasmids were also designed to create functional mutants in human p62 overexpression in much the same way as the mouse vectors were designed and cloned.

The primary objective for these genetic manipulation vectors was to alter various functions of p62 and interrogate the effects this had on both mouse and human iPSC reprogramming experiments, and on the maintenance of pluripotency. However, alongside I would also have performed numerous analyses on the effects of these functional mutants on important cellular processes to gain a better understanding of the role of p62 in general. For example, Seahorse bioanalysis of energy production would have been invaluable to understand the metabolic and oxidative effects of p62 mutation and loss of function. Immunocytochemistry for p62 and associated interaction partners such as LC3-II or Lamp1, both of which are important markers of lysosomal function. Evidence of an accumulation of p62 in one or more of the mutants could have confirmed or expanded the current understanding of the role of p62 in autophagic processing. For example, would a mutation in the LIR domain of

p62 result in a reduction in autophagic flux and an accumulation of p62?

Alternatively, would another autophagy adaptor such as NBR1 be able to fully compensate for the loss of function in p62? In addition, mitochondrial staining could have revealed a failure of mitochondrial clearance or remodelling, especially if assessed during the iPSC reprogramming process. qPCR analyses could have looked at a wider network of associated genes. In fact, some very preliminary qPCR analyses on p70S6K, NFκB, LC3-II, NRF2 and mTOR indicated that there might be some significant differences in the expression levels of these genes in the presence or absence of p62. Future works should definitely include qPCR or even RNA sequencing analysis to understand the wide gene regulatory networks involved in p62 signalling.

Despite not being able to utilise the entire genetic manipulation toolbox to the full extent hoped during this project, I did have some key cellular models and the fully validated sh(h)p62 with which to interrogate the role of p62 in iPSC reprogramming and the maintenance of pluripotency, including p62 null patient fibroblasts.

Chapter 6. Validation and iPSC reprogramming of p62 null patient fibroblast.

Chapter 5: Results 3: Validation and iPSC reprogramming of p62 null patient fibroblast.

6.1. Introduction

In order to assess the importance and role for p62 in iPSC reprogramming and the maintenance of pluripotency, we acquired two vials of P8 patient fibroblasts from Dr Christopher Carroll (SGUL). These fibroblasts were isolated from patients with a rare neurodegenerative phenotype, characterised by gait problems, cognitive decline and gaze palsy, among other symptoms. Individuals from four families with similar presenting phenotypes were identified, and exome sequencing of these individuals found three different bi-allelic loss of function mutations in the p62 gene. Fibroblasts from these individuals have a complete absence of p62 protein (Haack et al, 2016). For this study, these patient derived p62 null fibroblasts have been named hDF-p62^{-/-}.

6.2. Objectives

- Confirm phenotype of hDF-p62^{-/-} by immunocytochemistry and western blot
- Characterisation of hDF-p62^{-/-} cells by immunocytochemistry with known interacting partners such as mitochondria and lysosomes
- Successful iPSC reprogramming of hDF-p62^{-/-} cells
- Comparison of the efficiency of iPSC reprogramming between hDF-p62^{-/-} and nHDF controls
- Comparison of the morphology of resultant iPSC colonies between hDF-p62^{-/-} and nHDF controls
- Comparison of the ability to maintain pluripotency between hDF-p62^{-/-} and nHDF controls

- Comparison of the ability to differentiate into all three germ layers between hDF-p62^{-/-} and nHDF controls
- Comparison of pluripotency gene expression levels between hDF-p62^{-/-} and nHDF controls

6.3. Characterisation of hDF-p62^{-/-}

Before beginning iPSC reprogramming experiments on hDF-p62^{-/-} cells a number of characterisation experiments were carried out. As with the iPSC reprogramming experiments detailed in the previous chapter, some refining of experimental procedures was necessary before investigating the hDF-p62^{-/-} fibroblasts. p62 plays a key role in selective autophagy, targeting ubiquitin tagged proteins to the lysosome for degradation via the LC3 interacting region (LIR). LAMP1 is a lysosomal membrane protein and is responsible for maintaining the integrity of lysosomal membranes (Cohen-Dvashi et al, 2016), LAMP1 is ubiquitously expressed and is commonly used as a lysosomal marker (Andrejewski et al, 1999) therefore the distribution and potential association of p62 and LAMP1 was assessed by immunofluorescent cell staining and visualised using confocal microscopy.

Firstly, WT-MEFs were plated on gelatin-coated glass-bottomed plates, and fixed with 4% PFA before immunocytochemical staining for p62 and LAMP1 (Figures 5.1 and 5.2). Figures and show WT-MEFs stained for p62 (RED) and Lamp1 (GREEN) and visualised using a confocal microscope, at 40x and 63x magnification, respectively. MEFs are positive for both p62 and LAMP1, although there is no clear evidence of colocalisation of the two. It is difficult to truly assess colocalisation in the images and ideally a much higher magnification, or preferably an electron microscope would be used. Unfortunately, this was the best microscope that was available to me. However, even at this magnification it is possible to see that there is

abundant, diffuse p62 signalling across the cytoplasm, and there are large lysosomal vesicles visible in WT-MEFs, particularly centered around the nucleus.

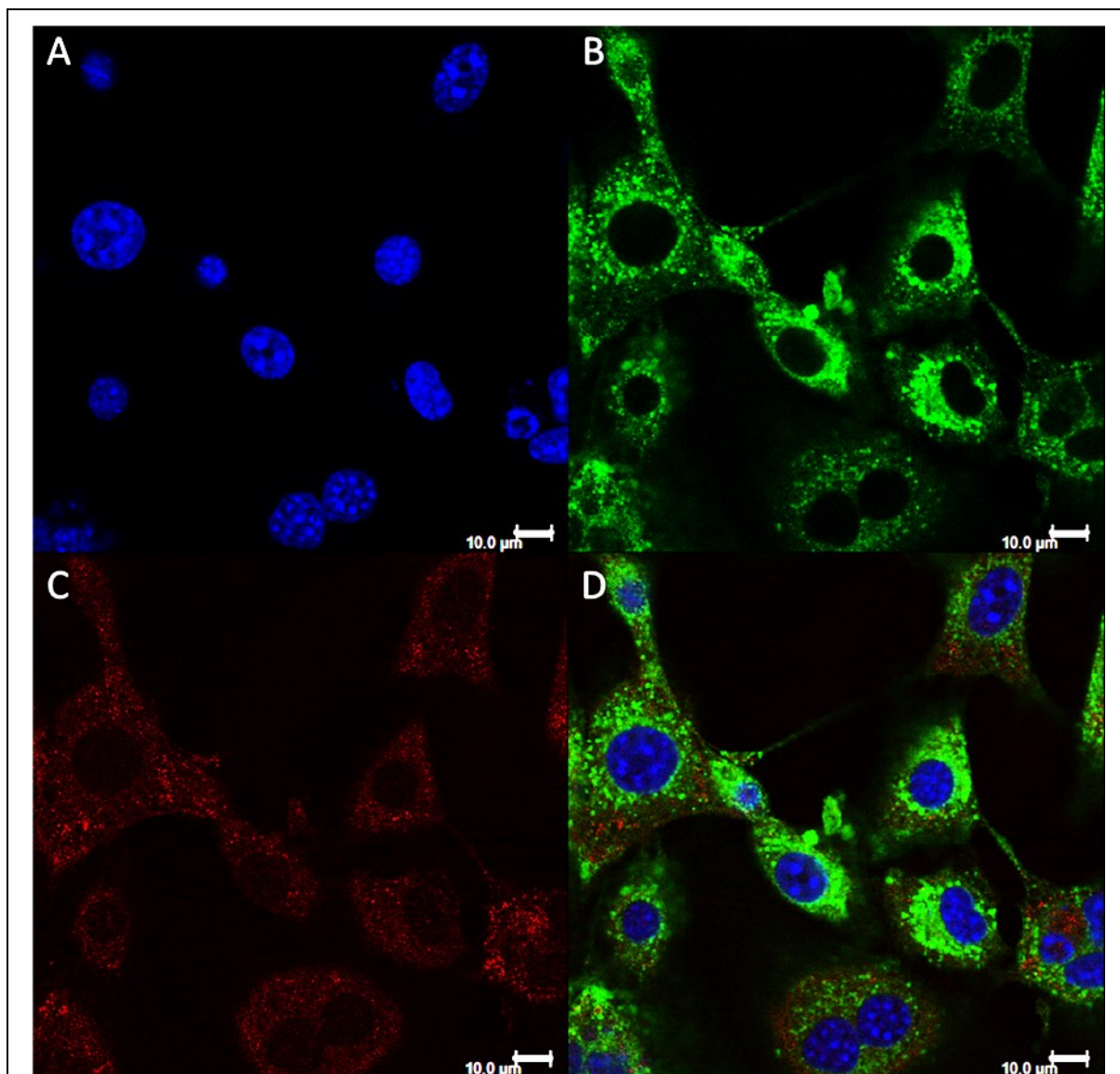
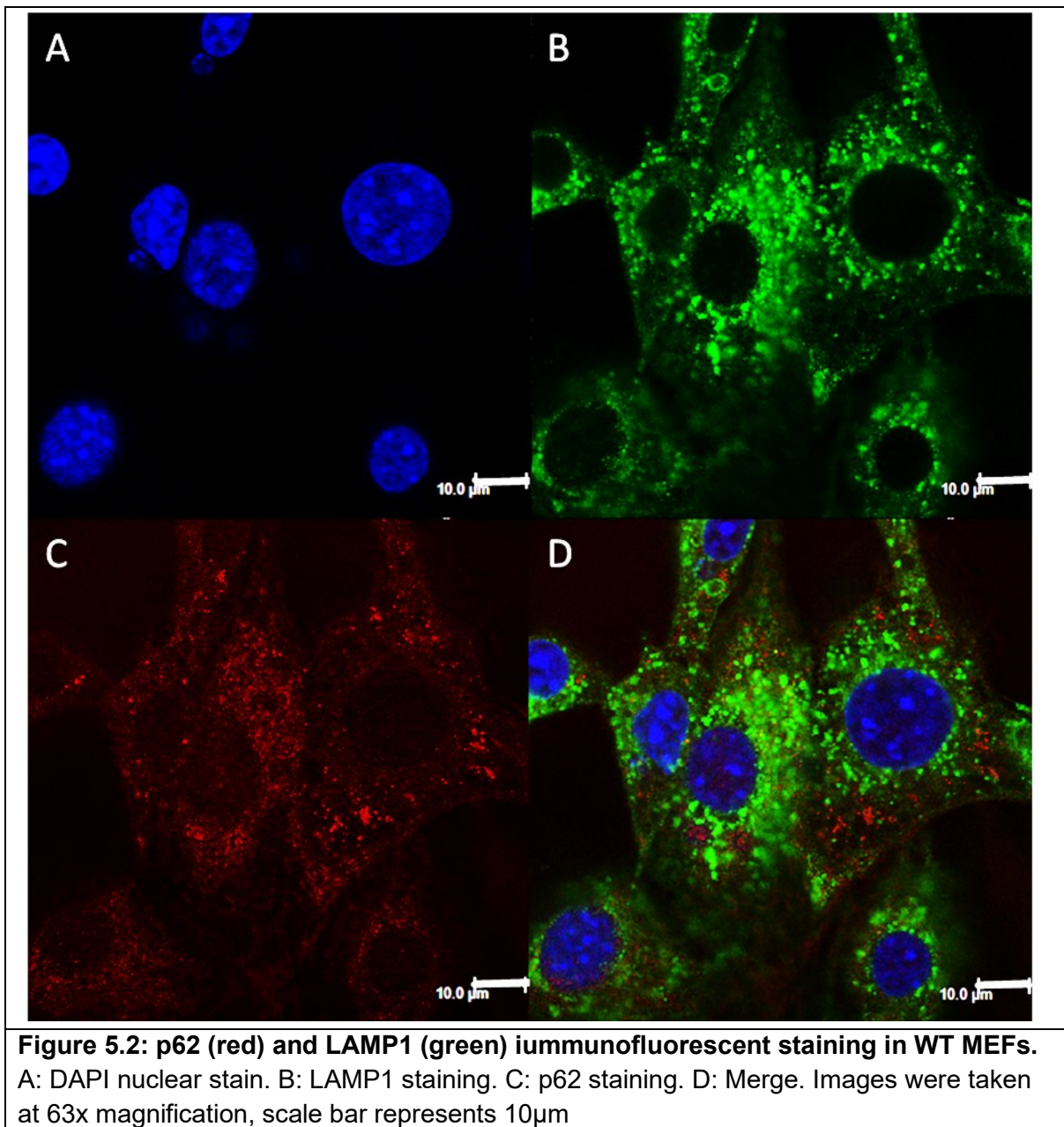


Figure 5.1 p62 (red) and LAMP1 (green) immunofluorescent staining in WT-MEFs.

A: DAPI nuclear stain. B: LAMP1 staining. C: p62 staining. D: Merge. WT-MEFs are strongly positive for both p62 and LAMP1. 40x magnification, scale bar represents 10 μm



Once confident with the use of the confocal microscope, hDF-p62^{-/-} and nhDF cells were seeded on gelatin-coated glass-bottomed plates and allowed to grow until confluent before being fixed with 4% PFA. Immunocytochemical cell staining for anti-p62 and anti-LAMP1 was carried out in order to assess the distribution and potential co-localisation of the two proteins in nhDFs and to confirm the absence of p62 protein in the hDF-p62^{-/-} cells; while assessing the localisation of LAMP1.

Figure 5.3 and Figure 5.4 show hDF-p62^{-/-} cells stained for p62 (or its absence) and LAMP1, with DAPI nuclear stain. As expected, the hDF-p62^{-/-} cells are negative for p62 (Panel C in both Figures) but there is strong positive staining of lysosomal vesicles (Panel B). Figure 5.3 shows images taken at 40x magnification with a 2.5x digital zoom; Figure 5.4 shows images taken at 63x magnification with a 2.5x digital zoom.

Figures 5.5 and Figure 5.6 show nhDFs stained for p62 and LAMP1, with DAPI nuclear stain at 40x magnification with 2.5x digital zoom and 63x magnification with 2.5x digital zoom, respectively. nhDFs are strongly positive for both p62 (RED, Panel C) and LAMP1 (GREEN, Panel B.) There are also several clear areas that appear bright yellow: this could potentially (although not definitely) signal co-localisation (Panel D, Yellow areas), and an association between p62 and LAMP1 in nhDFs. nhDF cells have large lysosomes, and apparently co-localised areas are likely larger autophagosomal aggregates. However, further analyses would be needed to confirm this co-localisation such as the use of Co-Immunoprecipitation whereby p62 could be 'pulled-down' along with its interacting partners (such as LAMP1) by an anti-p62 antibody and bound to agarose or magnetic beads before separating and analysing. This is less prominent in MEFs. Lysosomes in hDF-p62^{-/-} cells are generally smaller than those found in nhDF control cells, likely due to reduced fusion with autophagosomes, indicating a level of defective autophagy in these cells. Figure 5.7 shows no primary antibody negative controls in hDF-p62^{-/-} and nhDFs.

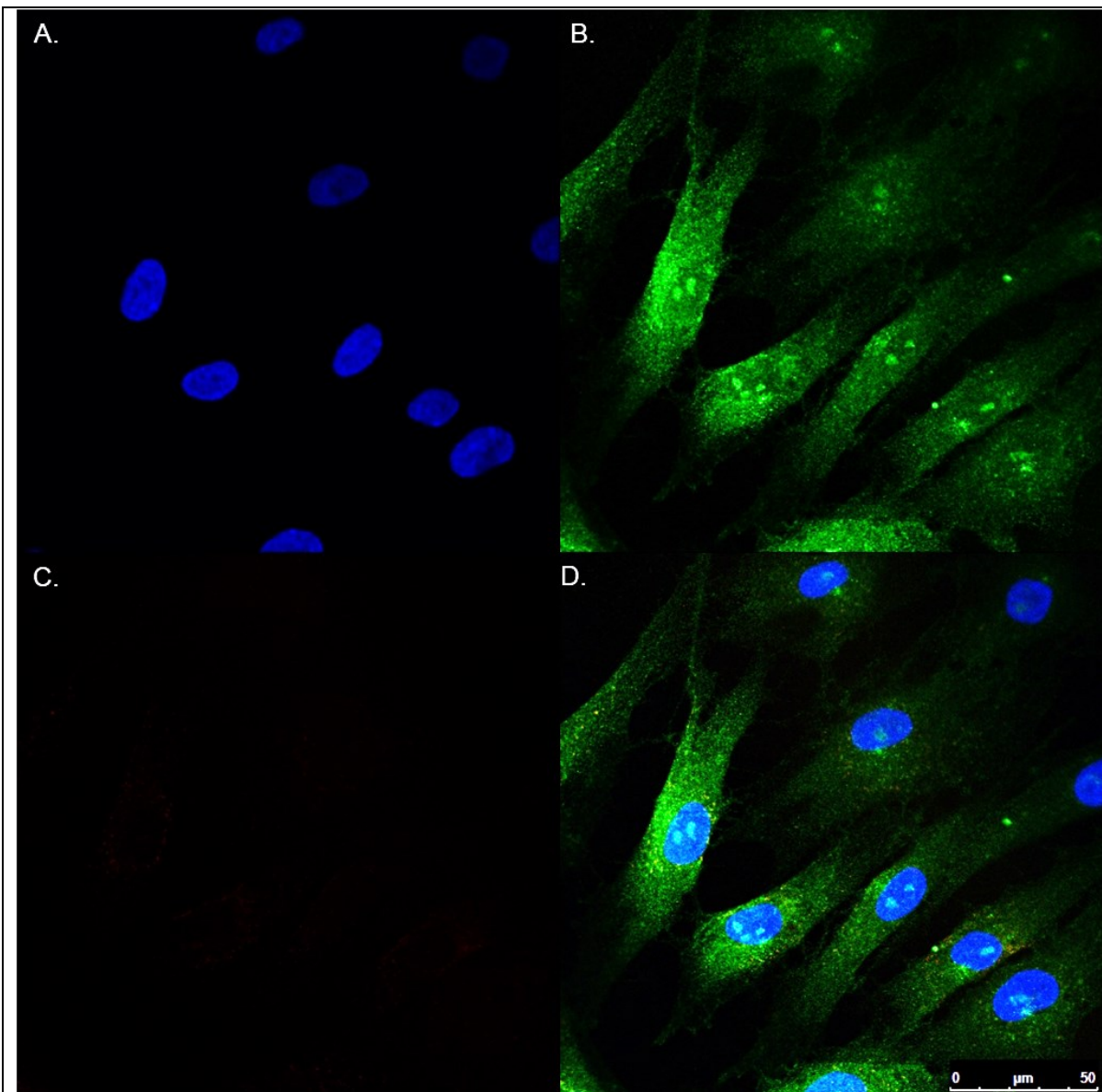


Figure 5.3: p62 (red) and LAMP1 (green) immunofluorescent cell staining in hDF-p62^{-/-} cells.

As expected, hDF-p62^{-/-} cells are negative for p62, confirming the phenotype. A: DAPI nuclear stain. B: LAMP1 staining. C: p62 staining. D: Merge. Images taken at 40x magnification with 2.5x digital zoom, scale bar represents 50μm

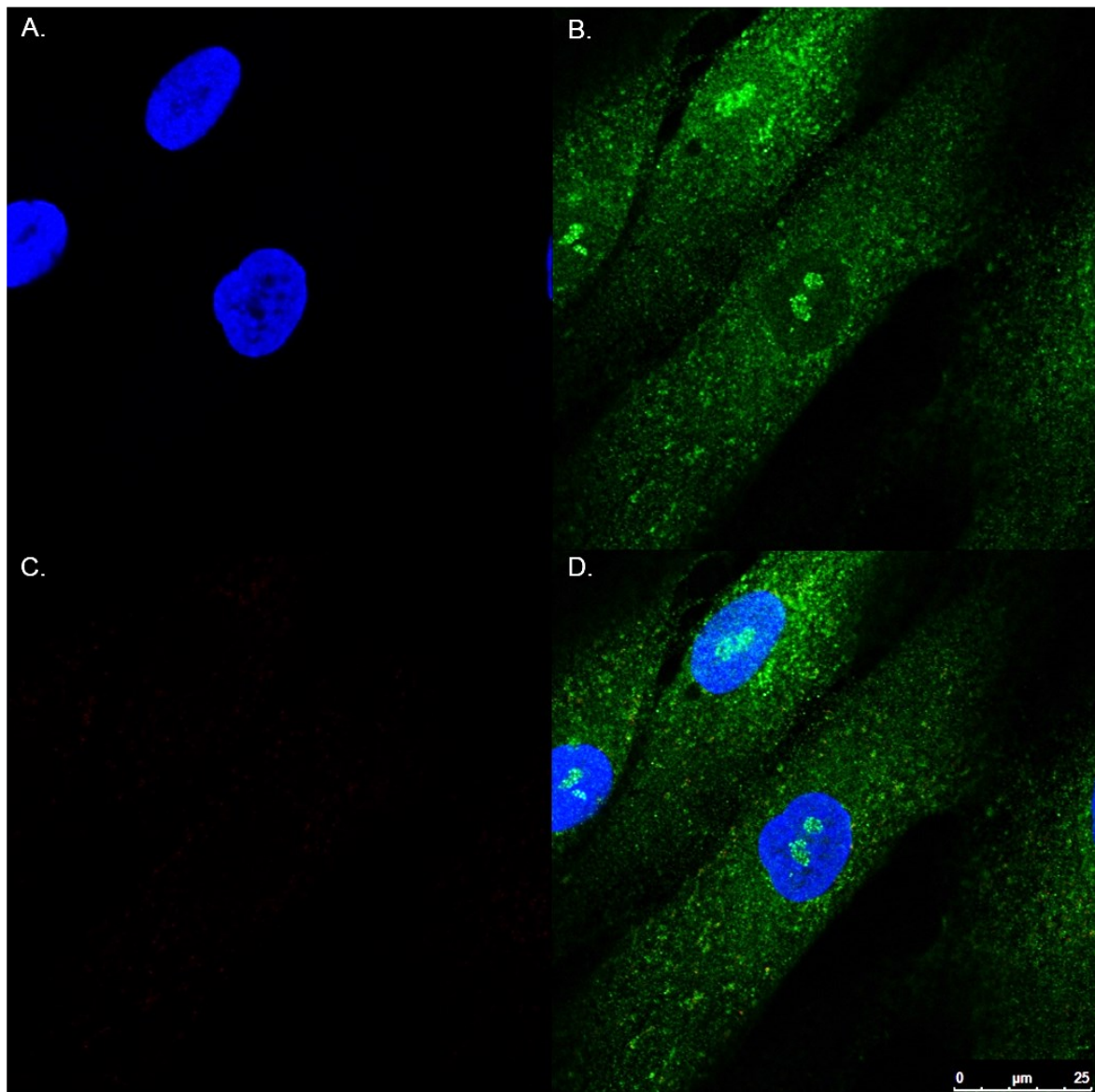


Figure 5.4: p62 (red) and LAMP1 (green) immunofluorescent cell staining in hDF-p62^{-/-} cells. As expected, hDF-p62^{-/-} cells are negative for p62, confirming the phenotype. A: DAPI nuclear stain. B: LAMP1 staining. C: p62 staining. D: Merge. Images taken at 63x magnification with 2.5x digital zoom, scale bar represents 25 μ m

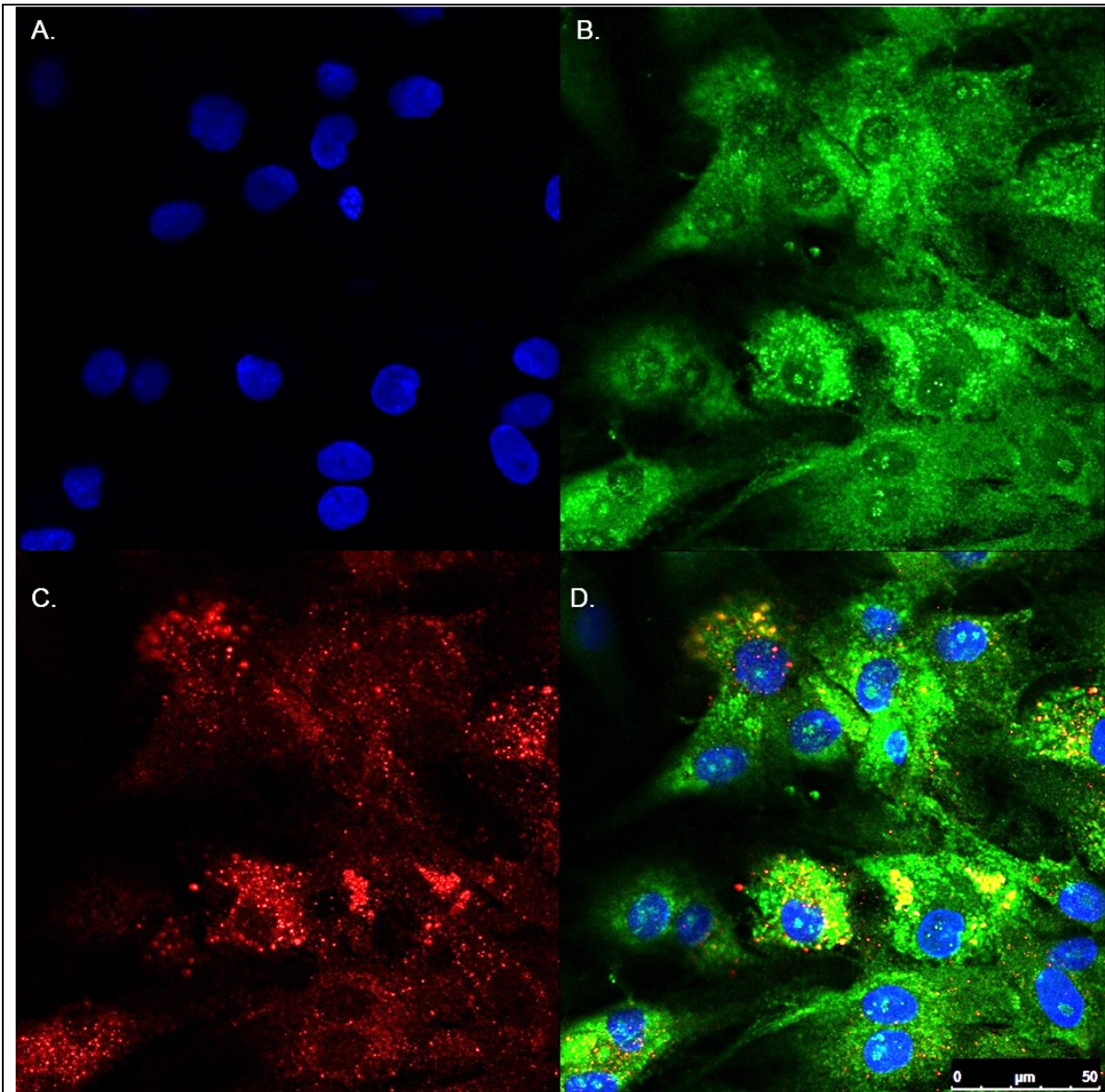
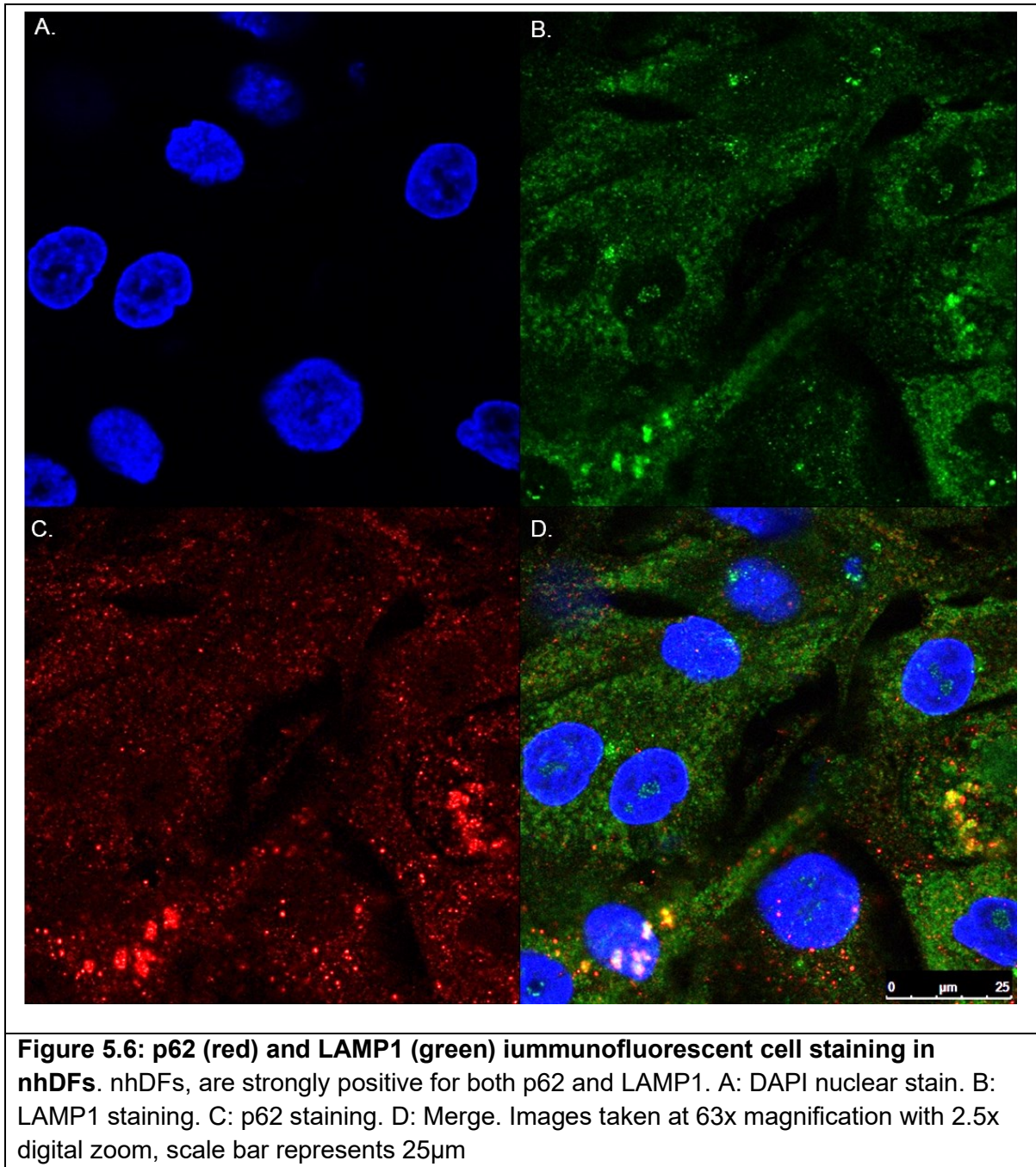


Figure 5.5: p62 (red) and LAMP1 (green) immunofluorescent cell staining in nhDFs. nhDFs, are strongly positive for both p62 and LAMP1 and there are some bright yellow areas, which could indicate a co-localisation, although this cannot be confirmed at this magnification. A: DAPI nuclear stain. B: LAMP1 staining. C: p62 staining. D: Merge. Images taken at 40x magnification with 2.5x digital zoom, scale bar represents 50μm



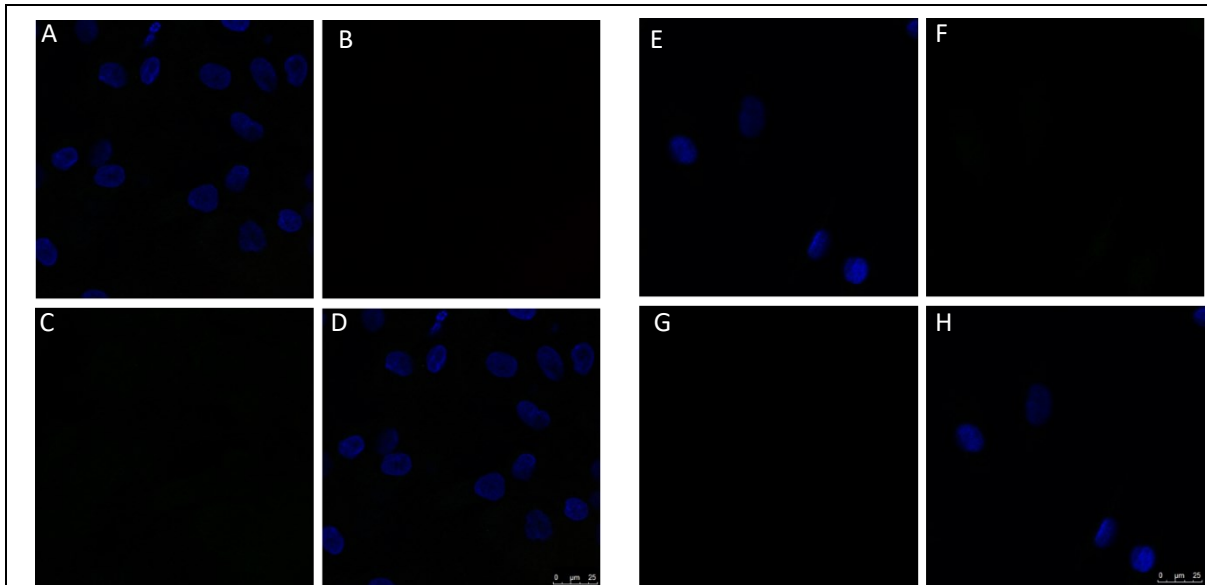


Figure 5.7 No primary antibody negative controls confirm the results of Figures 5.3-5.6. **A-D:** nhDF control cells **E-H:** hDF-p62^{-/-}. The secondary antibody to the anti-p62 antibody is anti-mouse; the secondary antibody to the anti-LAMP1 antibody is anti-rabbit.

hDF-p62^{-/-}, nhDfs, CLN6-hDFs and CLN7-hDFs were also assessed for the presence of p62 protein by western blot (Figure 5.8). Figure 5.8,A shows 20µg of CLN6-hDF and nhDF protein, analysed for p62 with β-actin loading control. Figure 5.8,B shows 20ug of nhDF, hDF-p62^{-/-}, and CLN7-hDF protein analysed for p62 with β-actin loading control. As expected, and confirming that seen in the immunocytochemical staining images, hDF-p62^{-/-} cell express no p62 protein.

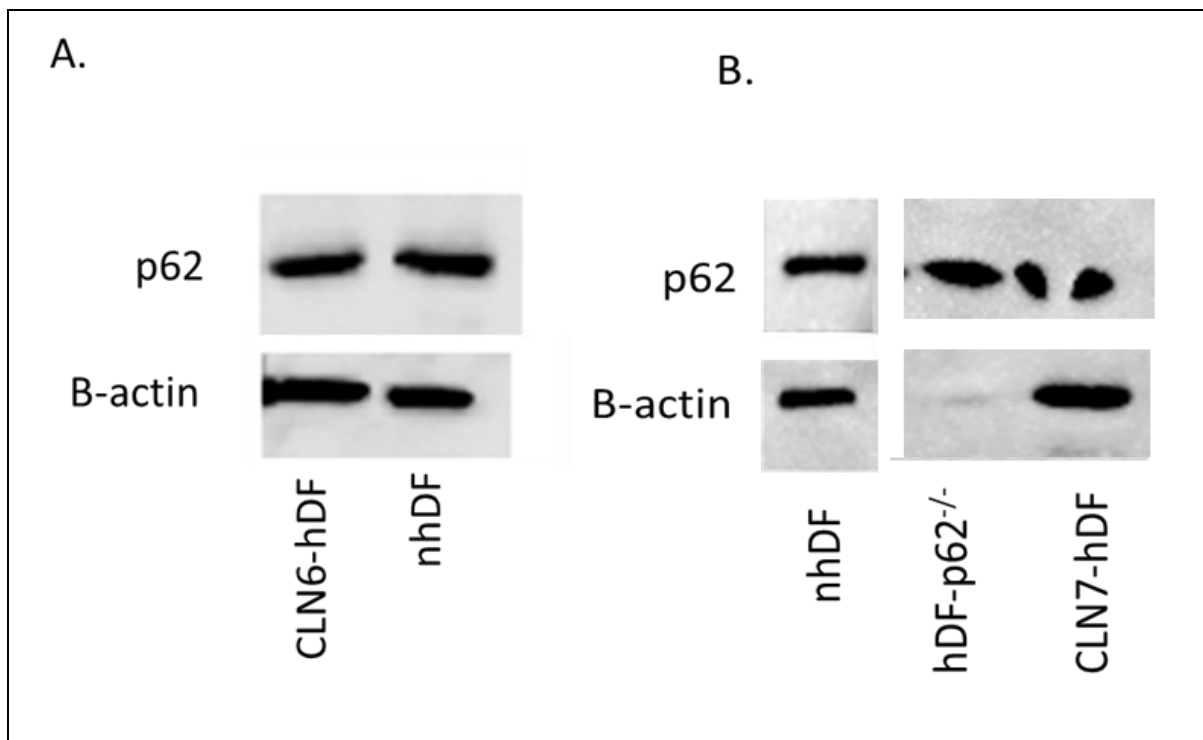


Figure 5.8: Western blot analysis of various fibroblasts for p62 protein.

A. CLN6-hDFs and nhDFs analysed for p62 protein by western blot, with β -actin loading control. 20 μ g of protein was added to wells. p62 antibody was used at a dilution of 1:2000; β -actin antibody was used at a dilution of 1:10,000. An HRP-conjugated secondary antibody was used at a dilution of 1:2000. B. nhDF, hDF-p62^{-/-} and CLN7-hDFs analysed for p62 protein by western blot, with β -actin loading control. 20 μ g of protein was added to wells. p62 antibody was used at a dilution of 1:2000 β -actin antibody was used at a dilution of 1:10,000. An HRP-conjugated secondary antibody was used at a dilution of 1:2000. NB Blots were all performed on the same day, extra irrelevant cell types (Hek293Ts) have been removed from this analysis.

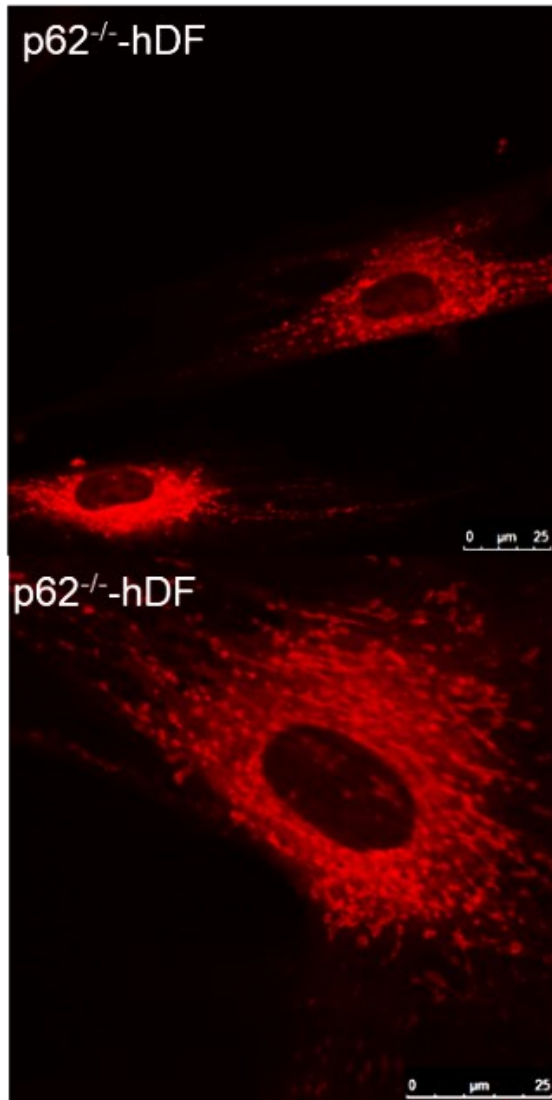
As discussed, p62 is known to have important roles in autophagy, metabolism and anti-oxidant responses. Autophagy has myriad time and context dependent roles in iPSC reprogramming including the regulation of mitochondrial remodelling and mitochondrial clearance, and so I wanted to determine if there different levels of p62 would have an impact on mitochondrial number, localisation or morphology. During selective autophagy, mitochondria are specifically targeted for break down in a process called mitophagy (Wang and Klionsky 2011). In addition, p62 has been shown to target mitochondria for ubiquitination via KEAP1 in a process that is NRF2

independent (Yamada et al, 2019) and to aggregate damaged mitochondria via the PB1 domain (Narenda et al, 2010).

hDF-p62^{-/-} cells were analysed for the presence, number and localisation of mitochondria, using MitoTrackerTM. MitoTrackerTM stains mitochondria in live cells, but it also well retained after fixation. MitoTrackerTM staining was optimised using wild-type MEFs and it was determined that a concentration of 25nM and an incubation time of 20-25 minutes was optimal (not shown). A low concentration of MitoTrackerTM is crucial to ensure that only mitochondria are stained.

hDF-p62^{-/-}, nhDF, CLN6-hDF and CLN7-hDF cells were live stained for MitoTrackerTM at a concentration of 25nM for 20 minutes before imaging on a confocal microscope (Figure 5.9). All cell types are strongly positive for MitoTrackerTM, and some obvious elongation of the mitochondria can be seen in some areas. There does not appear to be any discernible difference in mitochondria number or localisation between the cell types.

A.



B.

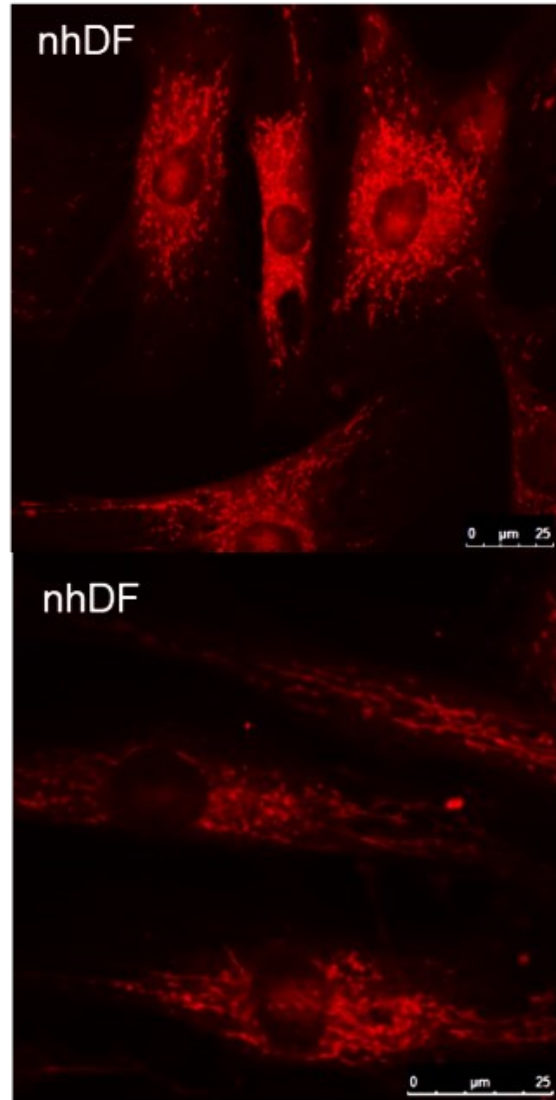


Figure 5.9 MitoTracker™ staining on early passage hDFs.

MitoTracker was applied to live cells in standard hDF maintenance media at concentration of 25nM for 20-25 minutes before visualisation on a Leica Confocal Microscope. **A.** p62^{-/-}-hDF 40x mag. (top image) and 63x mag (bottom image). **B.** nhDF 40x mag (top image) and 63x mag (bottom image).

Scale bars represent 25μM

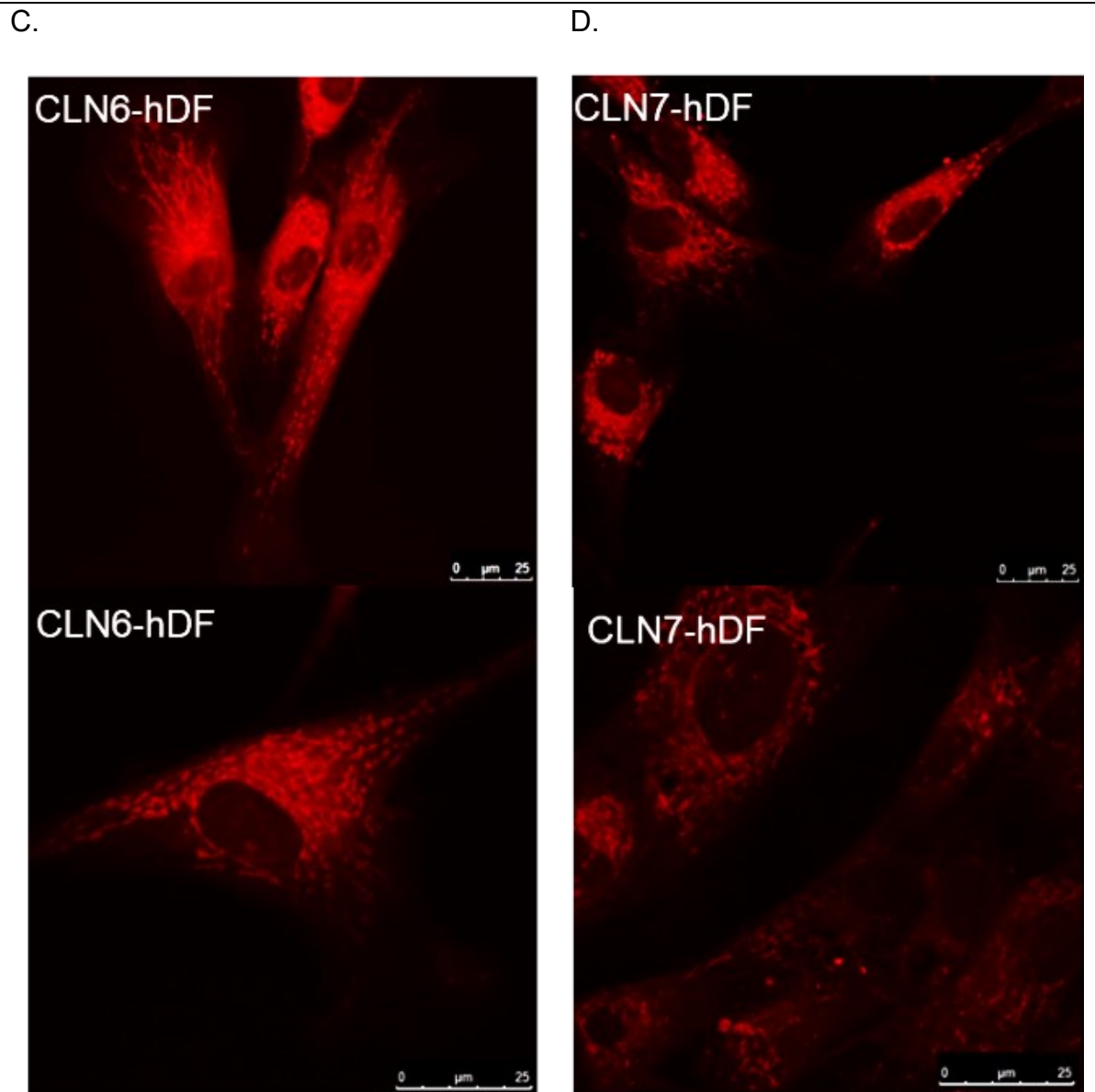


Figure 5.9 MitoTracker™ staining on early passage hDFs.

MitoTracker was applied to live cells in standard hDF maintenance media at concentration of 25nM for 20-25 minutes before visualisation on a Leica Confocal Microscope. **C.** CLN6-hDF 40x mag (top image) and 63x mag (bottom image). **D.** CLN7-hDF 40x mag (top image) and 63x mag (bottom image). Scale bar represents 25μm

Finally, hDF-p62^{-/-}, nhDF, CLN6-hDF and CLN7-hDFs were live stained for MitoTracker™ (RED) as previously described, before being fixed with 4% PFA and immunocytochemically stained with anti-p62 antibody (GREEN) (Figure 5.10), to determine any associations between presence or absence of p62 and the

mitochondria as well as to gain insight into the mitochondrial morphology of the hDFs.

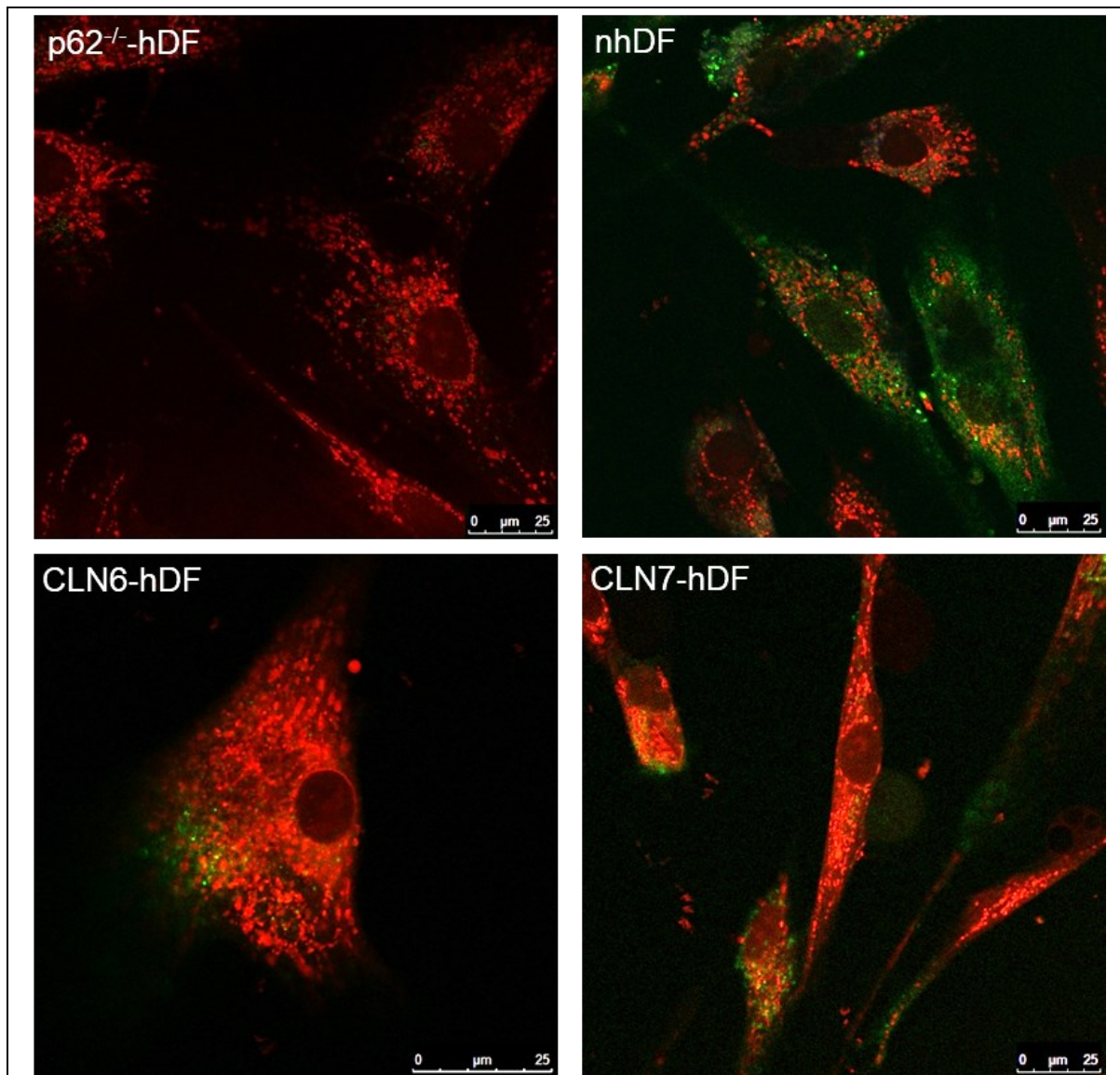


Figure 5.10: MitoTracker™ (RED) and p62 (GREEN) staining on early passage hDFs. MitoTracker was applied to live cells in growth media at concentration of 25nM for 20-25 minutes before fixation and immunocytochemical staining with anti-p62 antibody and visualisation on Leica Confocal Microscope. All images are 43x magnification, scale bar represents 25μm

Images of MitoTracker™ staining show some interesting differences in mitochondrial morphology in nhDF and hDF-p62^{-/-} cells. In hDF-p62^{-/-} cells the majority of mitochondria appear to have a tubular structure, and are distributed across the whole cell. In contrast, in nhDF cells, there are a mixture of tubular and fragmented mitochondria, and the more fragmented mitochondria are clustered in the perinuclear region whereas the more elongated mitochondria are towards the outer edges of the cell bodies. CLN6-hDF and CLN7-hDF mitochondria are broadly similar to those seen in nhDF controls. It is impossible to draw any conclusions from these images as the magnifications and resolution would both need to be higher to truly analyse organelle morphology and images would need to be taken multiple times and quantification applied. However, this would be an interesting avenue to explore further given the literature that already supports a key role for p62 in the regulation of mitochondria. As previously shown, hDF-p62^{-/-} cells do not express any p62 protein but nhDFs appear to display a higher ratio of p62 to mitochondria than CLN6 and CLN7-hDFs.

6.4. **5.4 iPSC reprogramming**

Once hDF-p62^{-/-} fibroblasts had been characterised alongside nhDFs, as well as CLN6 and CLN7 patient fibroblasts, iPSC reprogramming experiments could be undertaken. Because no significant differences had been observed in CLN6 or CLN7 hDFs in terms of p62 protein expression, or in the reprogramming efficiency of these patient cells, the decision was made to focus further experiments on just the hDF-p62^{-/-} cells. In order to compare the efficiency and stability of iPSC reprogramming and the resultant quality of iPSC cells between hDF-p62^{-/-} and nhDF control cells, a large number of reprogramming experiments were conducted.

To recap, reprogramming experiments take 25-30 days from nucleofection with OriP/EBNA episomal reprogramming plasmids to the first manual passage of colonies. The process of reprogramming adult somatic cells such as fibroblasts to iPSCs consists of three main phases, initiation, maturation and stabilisation. During the initiation phase, cells undergo a range of changes including the loss of somatic cell programming; increased proliferation rate; metabolic changes from oxidative to glycolic energy production; and clear and easily visible morphological changes from a mesenchymal to epithelial phenotype. During the maturation phase, cells begin to 'switch on' a programme of pluripotency genes such as Nanog and OCT4 in preparation for independence from transgenes. Finally, in the stabilisation phase cells gain this independence and achieve stable pluripotency. Throughout the ~25-day reprogramming process, two key stages are used to assess visually the success of the first two phases of iPS reprogramming, initiation and maturation.

Parallel iPSC reprogramming experiments were set up with either hDF-p62^{-/-} or nhDF. At ~7-8d, clear evidence of morphological change from a mesenchymal phenotype to an epithelial phenotype can be seen, with cells becoming smaller, more clustered together and less elongated. At ~8d in three independent reprogramming experiments, nhDF and hDF-p62^{-/-} cells appear morphologically alike, with no distinguishable differences between the two cell types at this early stage of the reprogramming process (Figure 5.11A.). At D8, cells are then passaged onto MEF feeder layers, meaning that any morphological changes cannot be assessed for several days during culture acclimatisation.

Between D14-18, early colony formation starts to occur, with small clusters of tightly packed cells beginning to appear. These colonies do not yet have the clearly defined borders and circular appearance of true, established iPS colonies but individual cells

do appear morphologically similar to iPS cells. At D16 of three independent reprogramming experiments, nhDF and hDF-p62^{-/-} cells look morphologically very similar, with no discernible differences at this maturation stage (Figure 5.11.B.). These results suggest that there is no morphological evidence of differences between nhDF and hDF-p62^{-/-} cells in the initiation and maturation phases of iPS reprogramming.

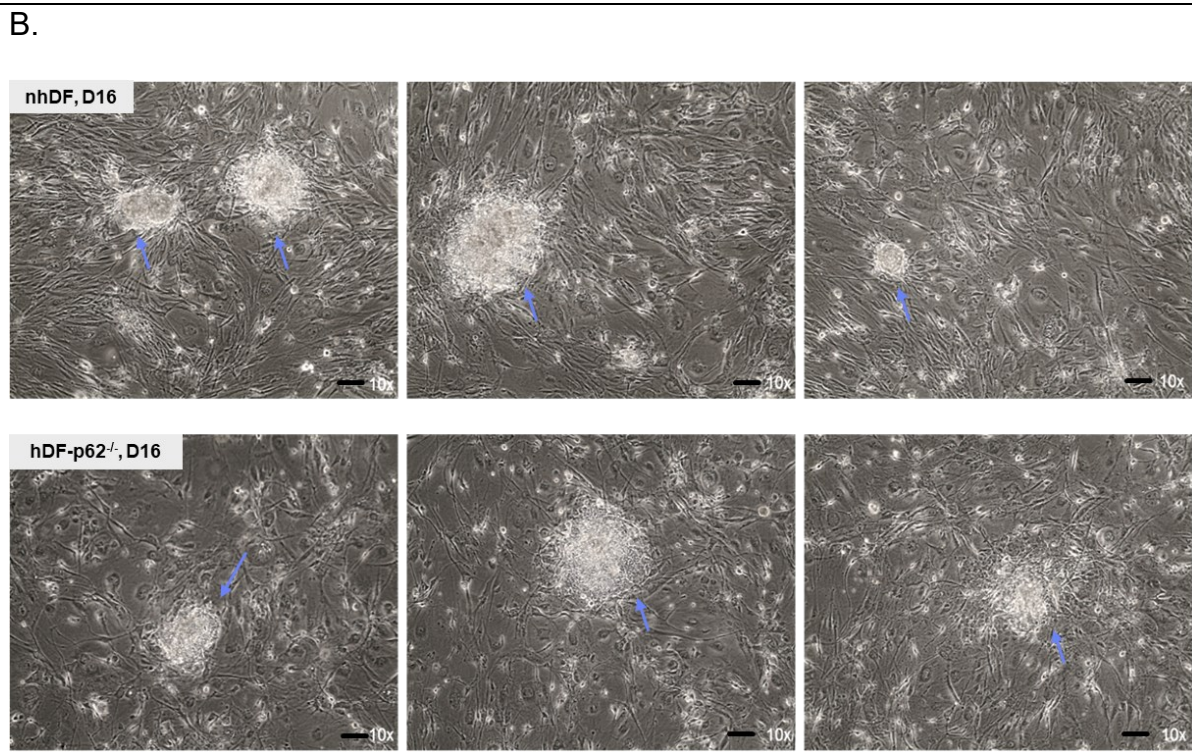
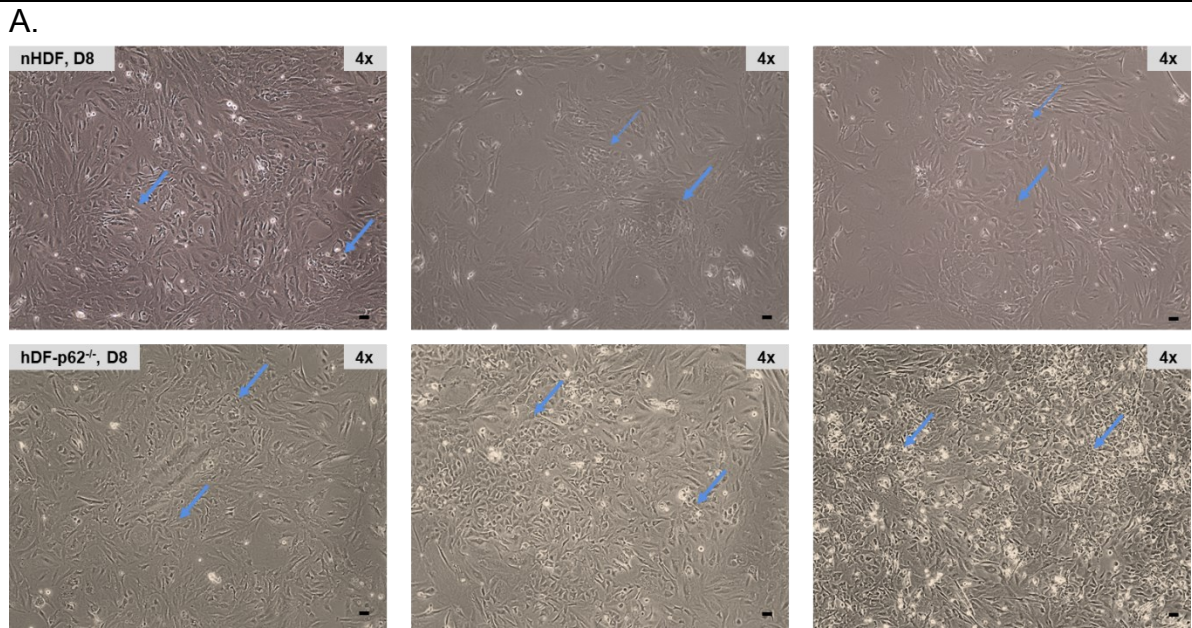


Figure 5.11: nhDF vs hDF-p62^{-/-} iPSC reprogramming.
 A. Day 8 of reprogramming experiments on MEF feeder layers. Visible MET in both cell types (blue arrows), nhDF and hDF-p62^{-/-} hDF cells looks morphologically very similar at day 8. B. Day 16 of three independent reprogramming experiments, where early colony formation is visible (blue arrows). Both nhDF control and hDF-p62^{-/-} cells look morphologically very similar at this stage of the iPSC reprogramming experiment (images are representative of three independent experiments).

At D25, newly established iPS colonies are routinely stained for Alkaline Phosphatase (AP). Alkaline phosphatase activity is upregulated in embryonic stem cells and induced pluripotent stem cells, and staining for AP is a useful and commonly used marker of emerging pluripotency in early passage or newly formed iPS cells. AP staining also allows for easy analysis of colony number, size, shape and uniformity.

At D25 in three independent iPSC reprogramming experiments, cells were stained for AP and both macroscopic and 4x magnification images were taken. In 4x magnification, it is clear that nhDF AP positive iPSC colonies are largely uniform in shape, with clearly defined borders. In contrast, hDF-p62^{-/-} cell colonies are much more irregular, with many smaller colonies and colonies with varying levels of AP staining density (Figure 5.12.A.). Several areas of partial reprogramming or early spontaneous differentiation can also be seen in the images of hDF-p62^{-/-} AP staining. Globally, it is clear that in the hDF-p62^{-/-} cell containing wells there are many smaller, irregular areas of AP positive staining and that the process of reprogramming has been less controlled in hDF-p62^{-/-} cells compared to nhDF controls (Figure 5.12.B).

A.

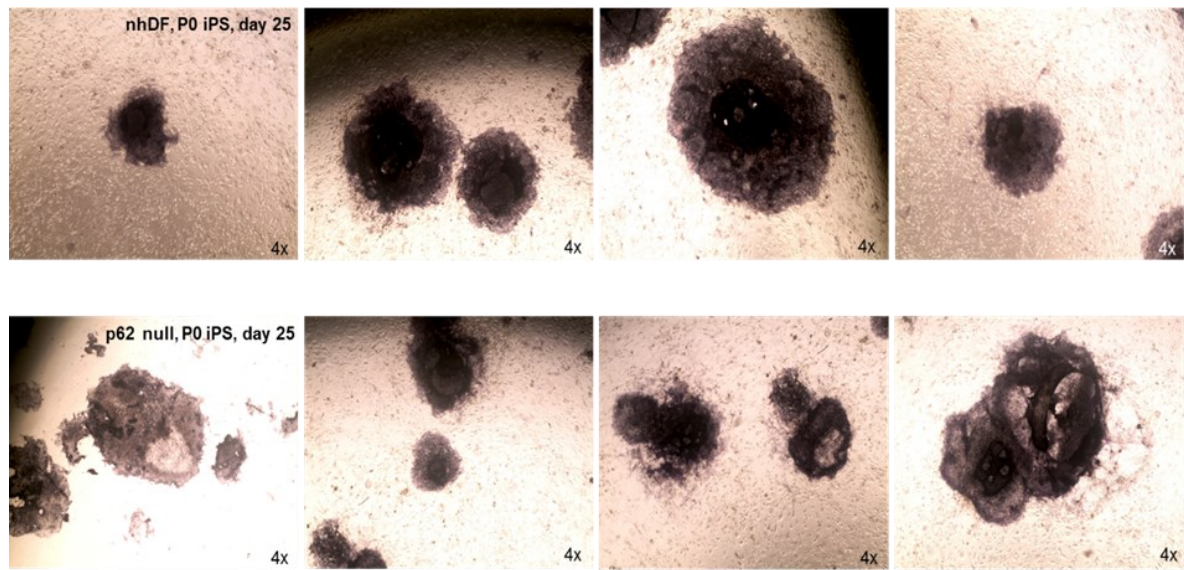


Figure 5.12.A: Primary colony analysis of hDF-p62^{-/-} reprogramming.

A. nhDF compared with hDF-p62^{-/-} during iPSC reprogramming. Day 25, primary (P0) iPSC colonies stained with Alkaline Phosphatase (AP), 4x magnification. nhDF colonies appear morphologically more uniform and circular than hDF-p62^{-/-} colonies. B. Macroscopic images of iPSC reprogramming comparisons of nhDf and hDF-p62^{-/-} iPSC P0, day 25 of reprogramming. The hDF-p62^{-/-} colonies are generally smaller, and less uniform, with many colonies that appear partially reprogrammed, or partially differentiated. Experiments were repeated on three independent occasions.

B.

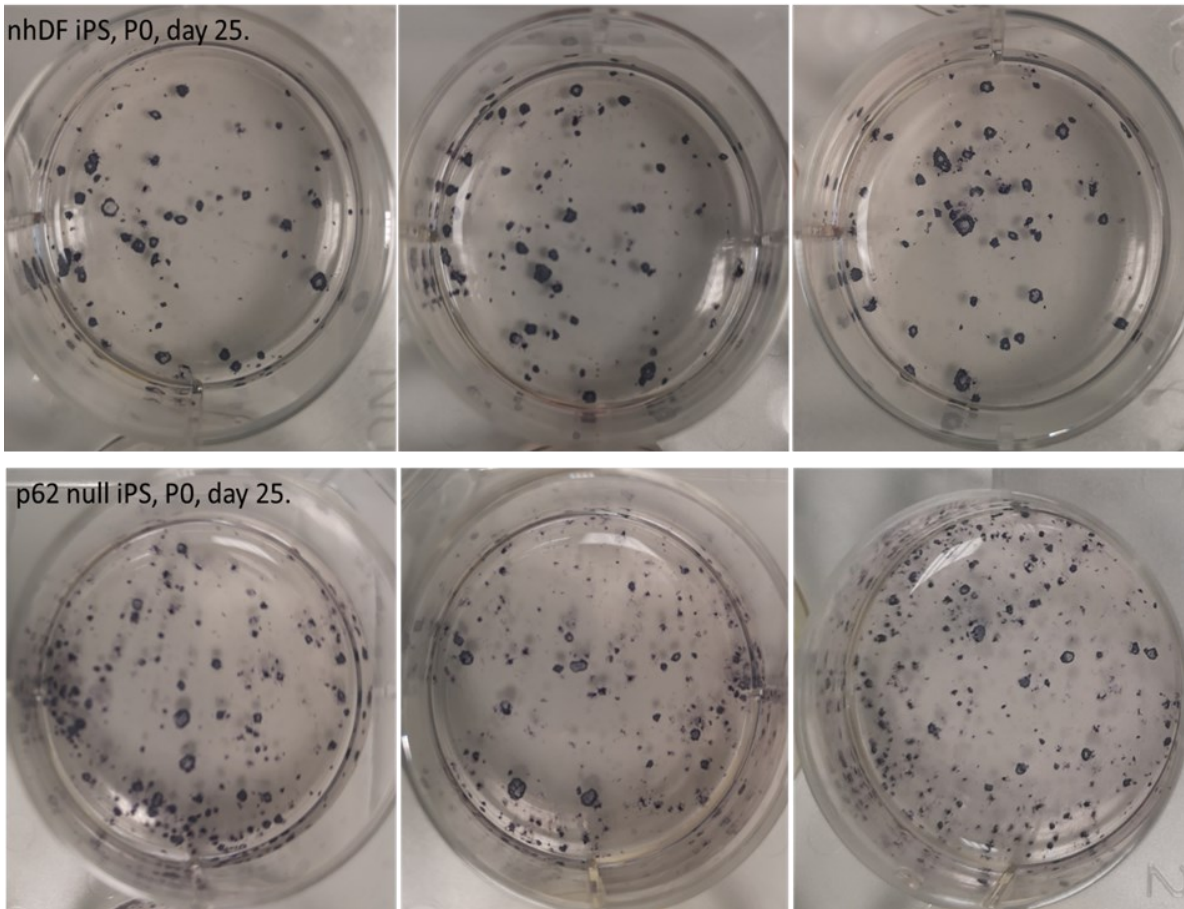


Figure 5.12.B: Primary colony analysis of hDF-p62^{-/-} reprogramming.

B. Macroscopic images of iPSC reprogramming comparisons of nhDf and hDF-p62^{-/-} iPSC P0, day 25 of reprogramming. The hDF-p62^{-/-} colonies are generally smaller, and less uniform, with many colonies, which appear partially reprogrammed, or partially differentiated. Experiments were repeated on three independent occasions.

Macroscopic images of AP stained colony containing wells were then analysed using ImageJ for colony number, size and shape (Figure 5.13). Figure 5.13.A shows a comparison of the number of AP positive primary (P0) colonies at D25 of three independent reprogramming experiments in nhDF control and hDF-p62^{-/-} cells. On average, there were 95 (± 8.49 S.E.M) primary (P0) nhDF iPS colonies at D25 of three independent reprogramming experiments, whereas there were 234 (± 15.69 S.E.M) AP positive hDF-p62^{-/-} colonies at D25 of reprogramming. Across three

independent experiments, as shown in Figure 5.13.A the number of areas stained positive for AP are significantly higher for hDF-p62^{-/-} cells than for comparative nhDF control cells (Figure 5.13, A.) (n=3, p= 0.0336). The software counted all areas stained positive with AP, regardless of size or shape. The experimental variation (S.E.M) in hDF-p62^{-/-} is also much larger than across nhDF control experiments, showing a greater level of variation in reprogramming in hDF-p62^{-/-} cells (S.E.M = 8.498 in nhDF experiments and 15.694 in hDF-p62^{-/-} experiments).

hDF-p62^{-/-} AP positive colonies are also significantly smaller than those in nhDF controls (Figure 5.13.B.) (n=3, p= 0.0113). On average, the size of nhDF iPS colonies is 87.53 pixels² (± 8.0194 S.E.M), whereas the size of hDF-p62^{-/-} colonies is 38pixels² (± 7.747 S.E.M). ImageJ measures size as number of pixels² in images that have been converted to binary and threshold adjusted (see materials and methods).

Thirdly, primary (P0) colonies were analysed for circularity (Figure 5.13.C.). Circularity is measured by ImageJ using $4\pi(\text{area}/\text{perimeter}^2)$ and a score of 1.0 represents a perfect circle. The percentage of colonies that score between 0.5 and 1.0 in circularity is significantly lower in hDF-p62^{-/-} experiments than in nhDF controls (n=3, p= 0.00583). On average, 95.1% (± 0.95 S.E.M) of nhDF colonies have a circularity score above 0.5, whereas only 74.4% (± 2.31 S.E.M) of hDF-p62^{-/-} colonies have a circularity score between 0.5 and 1.0. There is also a greater experimental variation (S.E.M in nhDF experiments = 0.95, S.E.M in hDF-p62^{-/-} experiments = 2.31) in these circularity scores between hDF-p62^{-/-} experiments than between nhDF experiments, suggesting that overall, iPSC reprogramming in hDF-p62^{-/-} cells is less well regulated than nhDF controls.

A.

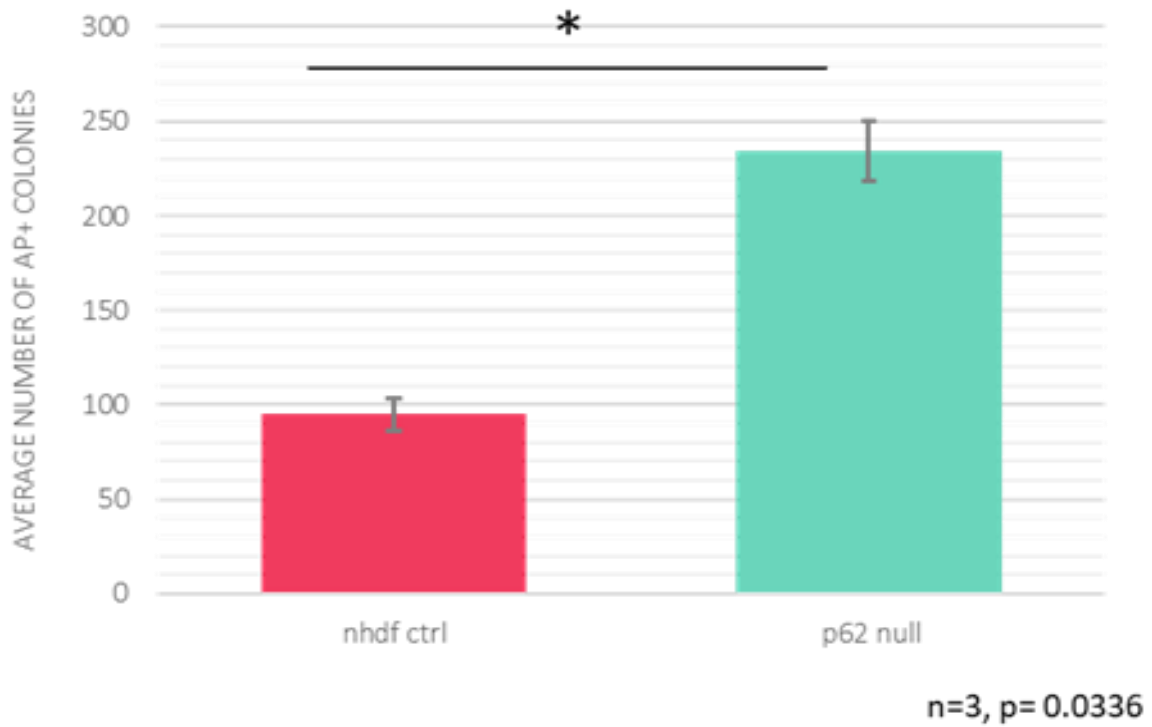


Figure 5.13.A: Comparison of nhDF and hDF-p62^{-/-} iPSC primary colony formation (P0).

Total 'colony' count, analysed using ImageJ and including all areas stained with AP across the entire well of a 6-well plate. Average colony number in nhDF = 95±8.498, hDF-p62^{-/-} = 234.33±15.694. (n=3, p= 0.0336)

B.

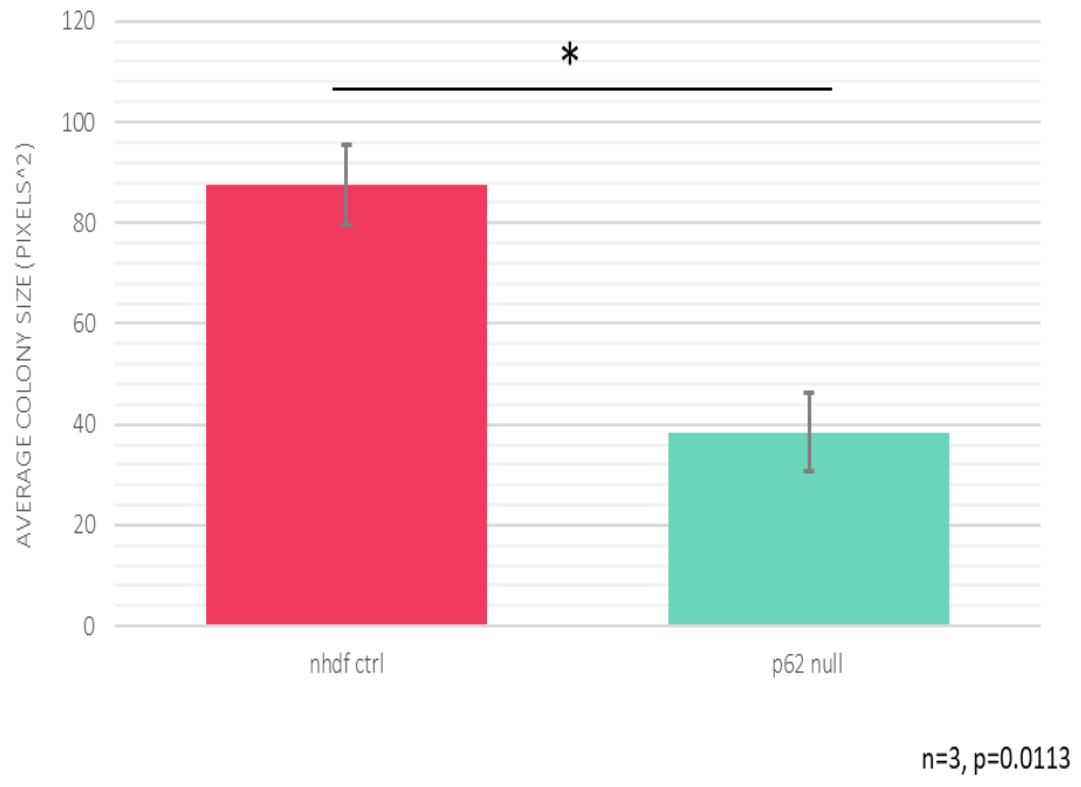


Figure 5.13.B: Comparison of nhDF and hDF-p62^{-/-} iPSC primary colony formation (P0).

Average colony size, analysed using ImageJ and including all areas stained with AP across the entire well of a 6-well plate. Average colony size in nhDF = 87.53 ± 8.0194 pixels² \pm , hDF-p62^{-/-} experiments = 38.41 pixels² ± 15.694 (n=3, p= 0.0113).

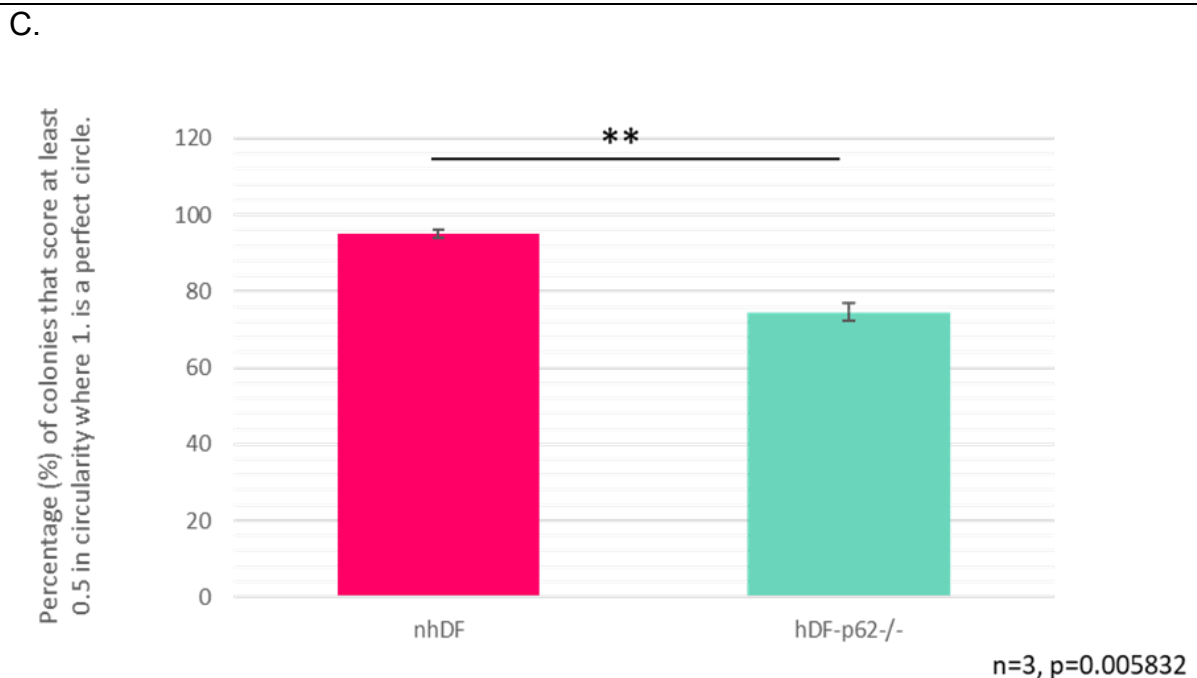


Figure 5.13.C: Comparison of nhDF and hDF-p62^{-/-} iPSC primary colony formation (P0). Percentage of colonies recorded in ImageJ as at least 0.5 in circularity where 1.0 is a perfect circle. Average percentage of ≥ 0.5 circularity colonies in nhDF = $95.1\% \pm 0.95$

,hDF-p62^{-/-} = 74.4% ± 2.31 (n=3, p= 0.0494). Data are collated from 3 independent experiments. p-values obtained by performing an unpaired t-test.

nhDF control and hDF-p62^{-/-} primary (P0) pre-iPSC colonies were manually passaged and the shape and uniformity assessed and analysed visually at P1 (Figure 5.14). All colonies were counted across three independent experiments in nhDF control and hDF-p62^{-/-} cells. Typical iPSC colonies have a clear and well-defined border around the whole circumference. True iPSC colonies in the stabilisation phase and beyond are generally close to circular in shape and cells have a largely uniform appearance with minimal spontaneous differentiation. Figure 5.14.A. shows an example of nhDF control iPSC colonies at P1 and Figure 5.14.B shows an example of hDF-p62^{-/-} colonies at P1. Clear morphological differences can be seen between the two cell types. nhDF colonies are largely uniform in shape, close to circular and have minimal amounts of spontaneous differentiation. In contrast, the hDF-p62^{-/-} colonies are generally smaller, more irregular in shape and have lots of spontaneous differentiation visible.

A.

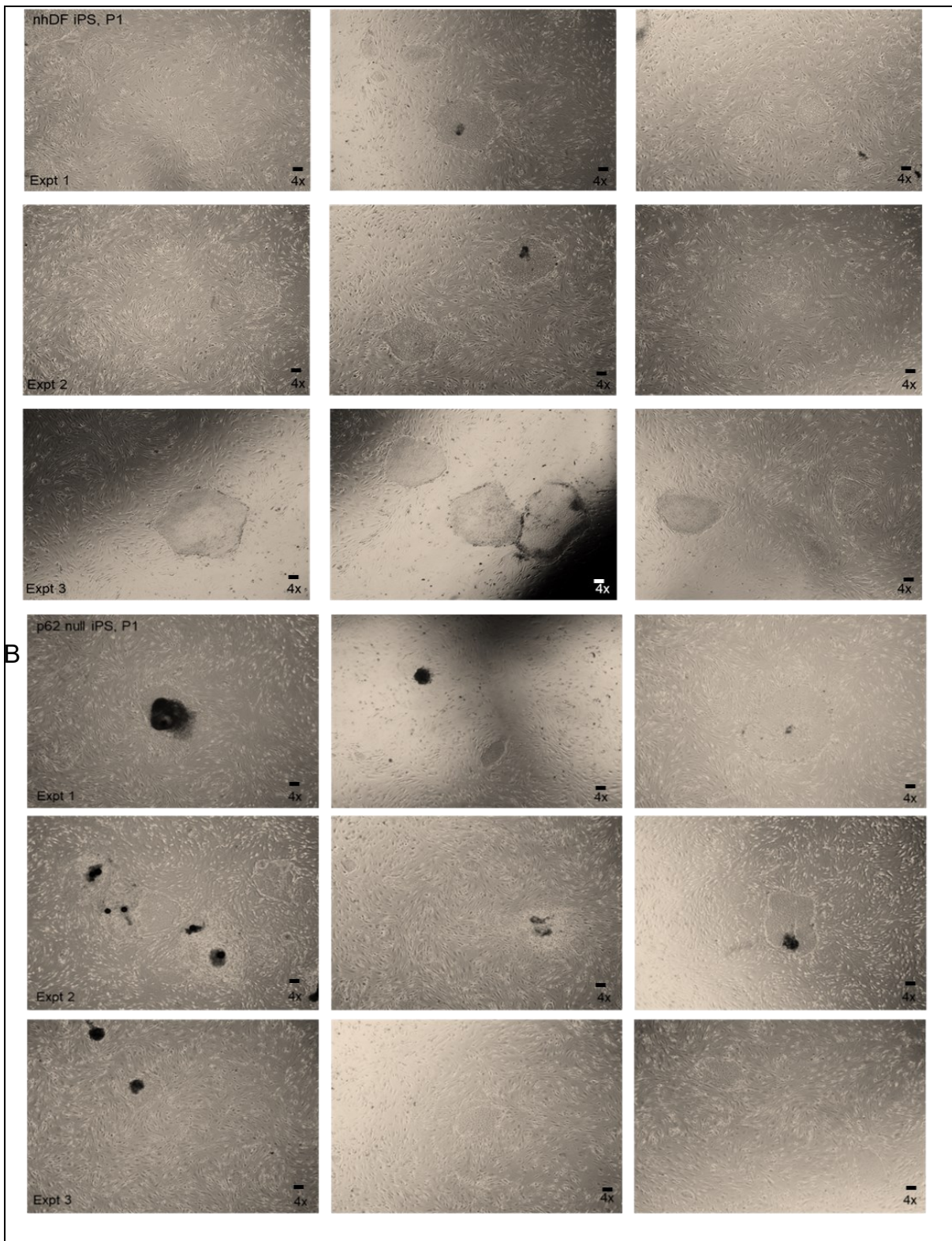
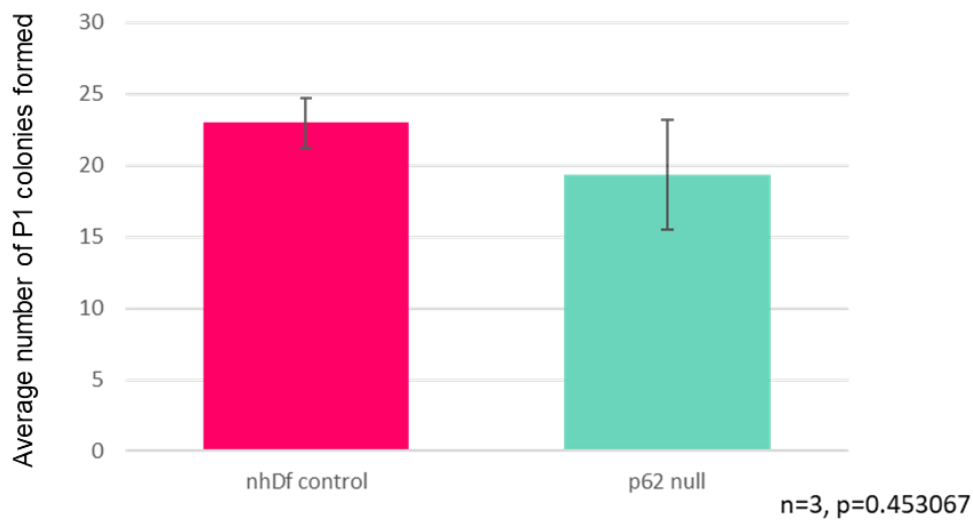


Figure 5.14 iPSC reprogramming of nhDF and hDF-p62^{-/-}, Passage 1 A. Representative examples of nhDF iPS on MEFs, P1. Three independent experiments. **B.** Representative examples of hDF-p62^{-/-} iPS on MEFs, P1. Three independent experiments. Clear morphological differences can be seen between the two cell types, with a higher level of spontaneous differentiation and irregularity in the colonies visible in hDF-p62^{-/-} cells. Images were at 4x magnification, scale bars represent 10µM

The number of P1 colonies were counted and compared in nhDF controls and hDF-p62^{-/-} cells across three independent experiments. There was no significant difference in the number of colonies formed at P1 (Figure 5.15.A) (nhDF average colony number = 23 ± 1.73 , hDF-p62^{-/-} average colony number = 19 ± 3.84 . n=3, p= 0.759). Next, the number and percentage of intact borders in nhDF and hDF-p62^{-/-} colonies was compared (Figure 5.15, B.). P1 colonies were defined as having either a completely intact border or not, in three independent experiments in both nhDF controls and hDF-p62^{-/-}. All images were randomised and blinded before being analysed in order to avoid any bias. Anywhere that a clear break in the colony border was visible where spontaneous differentiation had occurred was counted as not having an intact border. Significantly fewer hDF-p62^{-/-} colonies have complete, intact borders compared to nhDF controls across three independent experiments. 89.1% \pm 2.49 of nhDF control P1 colonies have complete, intact borders, compared to just 49.1% \pm 4.59 of hDF-p62^{-/-} colonies (n=3, p= 0.00682). Of note, the standard error of the mean is also larger in the hDF-p62^{-/-} experiments (4.59 in hDF-p62^{-/-} compared to 2.49 in nhDF experiments), showing a larger variation and a greater degree of dysregulation in hDF-p62^{-/-} cells.

A.



B.

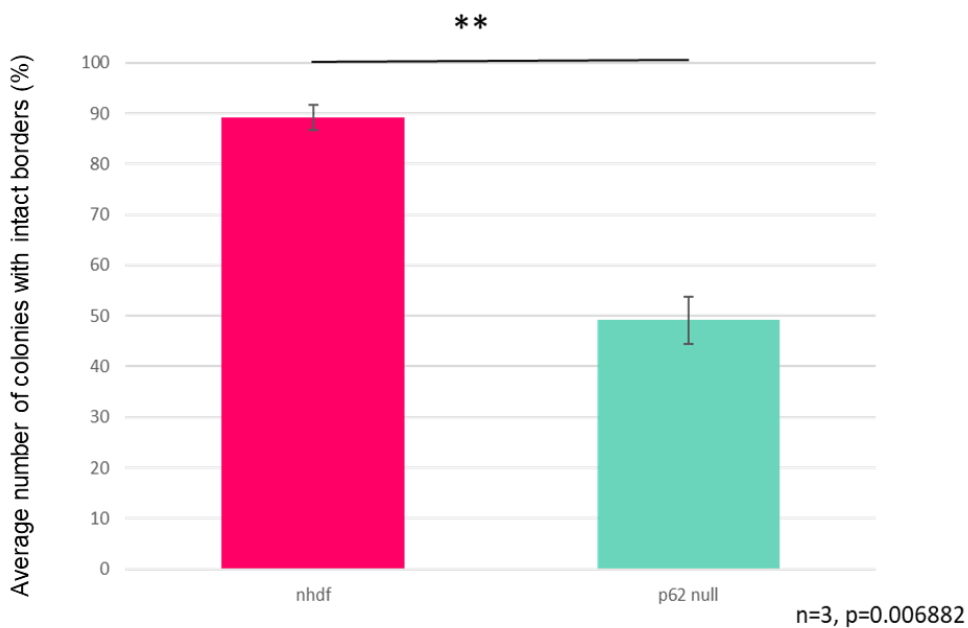
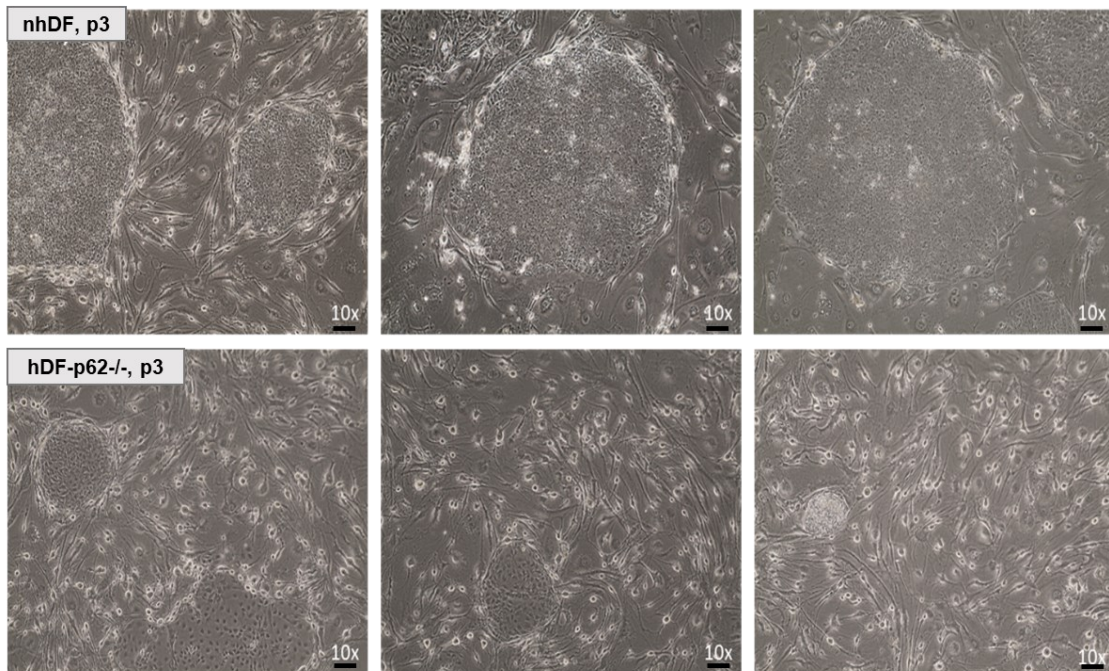


Figure 5.15 Analysis of P1 nhDF and hDF-p62^{-/-} iPSC colonies

A. Average P1 colony number after manual passage of an equal number of P0 colonies in nhDF controls and hDF-p62^{-/-}. There is no significant difference in the number of P1 colonies formed (n=3, p= 0.759). B. Average number of P1 colonies with complete, intact borders in nhDF and hDF-p62^{-/-} colonies across 3 independent experiments. Significantly fewer hDF-p62^{-/-} colonies have complete, intact borders without spontaneous differentiation compared to nhDF controls. An average of 89.1%±2.49 of nhDF colonies have complete intact borders compared to 49.1%±4.59 of hDF-p62^{-/-} colonies (n=3, p= 0.0069). Data collated from 3 independent experiments and analysed by unpaired, two-tailed t-test.

As shown in Figure 5.16, at P3 there are clear morphological differences between nhDF and hDF-p62^{-/-} cells (5.16.A), and by P6 there are virtually no remaining iPSC colonies in the hDF-p62^{-/-} (5.16.B). Across >10 repeat experiments, all evidence of pluripotency and colony formation capacity has been lost by P6 at the latest, often much earlier in hDF-p62^{-/-} cells. In comparison and as expected, nhDF colonies continue to get more uniform and more stable as they reach transgene independency, displaying unlimited capacity for self-renewal. In contrast, hDF-p62^{-/-} cells decrease in number with every passage due to spontaneous differentiation and the failure to proliferate and stabilise into true transgene independent iPS cell lines.

A.



B.

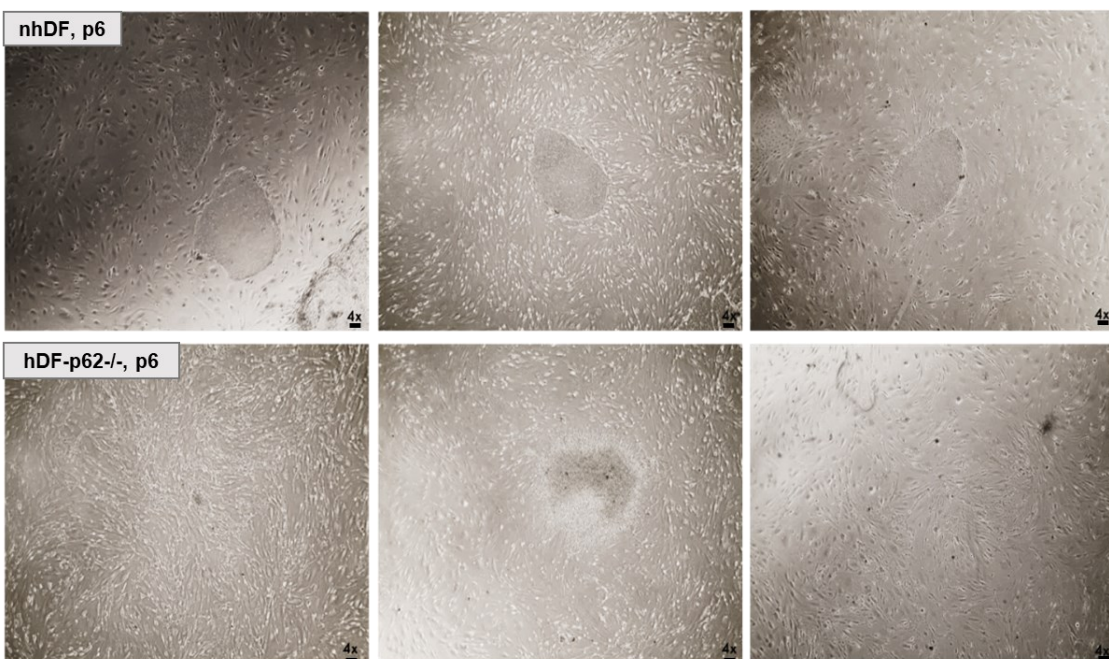


Figure 5.16: hDF-p62^{-/-} colonies rapidly lose pluripotency.

A. nhDF and hDF-p62^{-/-} iPS colonies at P3. nhDF colonies are well defined, circular, with small, tightly clustered cells. p62 colonies are smaller, more irregular and less morphologically similar to typical iPS or ES colonies. B. nhDF and hDF-p62^{-/-} 'iPS' colonies at P6. hDF-p62^{-/-} cells have almost entirely lost all pluripotency related morphology by P6 while nhDF iPS cells maintain pluripotency.

6.5. **Conclusions**

Overall, these data indicate that p62 could play an important role the stabilisation, maturation and maintenance of pluripotency. hDF-p62^{-/-} fibroblasts lack any p62 protein, but appear otherwise broadly similar to control nhDFs. hDF-p62^{-/-} fibroblasts grow slightly more slowly than nhDFs (anecdotal observation only, although this could be quantified in future works). hDF-p62^{-/-} cells show generally a less efficient and less well regulated iPSC reprogramming process than control nhDFs, and cannot maintain pluripotency beyond P6 at the latest. It is not yet clear how p62 may exert these effects on cells. If p62 is essential for successful reprogramming of stable iPSC cell lines, this could help to elucidate further the mechanisms behind iPSC reprogramming and therefore go towards improving iPSC reprogramming efficiency and iPSC stability, thereby increasing the opportunities for safe and stable iPSC therapeutic products to make it in to clinical practise.

Chapter 7. Reprogramming of nhDF-shp62 cells.

Chapter 6: Results -4: Reprogramming of nhDF-shp62 cells.

7.1. Introduction

The successful cloning and validation of an shRNA for human p62, and the creation of a stably transduced GFP-positive cell line (nhDF-shp62) with significantly reduced p62 protein level could then be implemented in reprogramming experiments as previously carried in hDF-p62^{-/-} cells. These experiments would seek to confirm that the effects on reprogramming seen in hDF-p62^{-/-} cells were due to the absence of p62 itself and not due to some other unknown genetic difference. Comparing nhDFs to nhDF-shp62 cells allows for comparison of cells from the same genetic background with the only difference being knock-down of p62 protein.

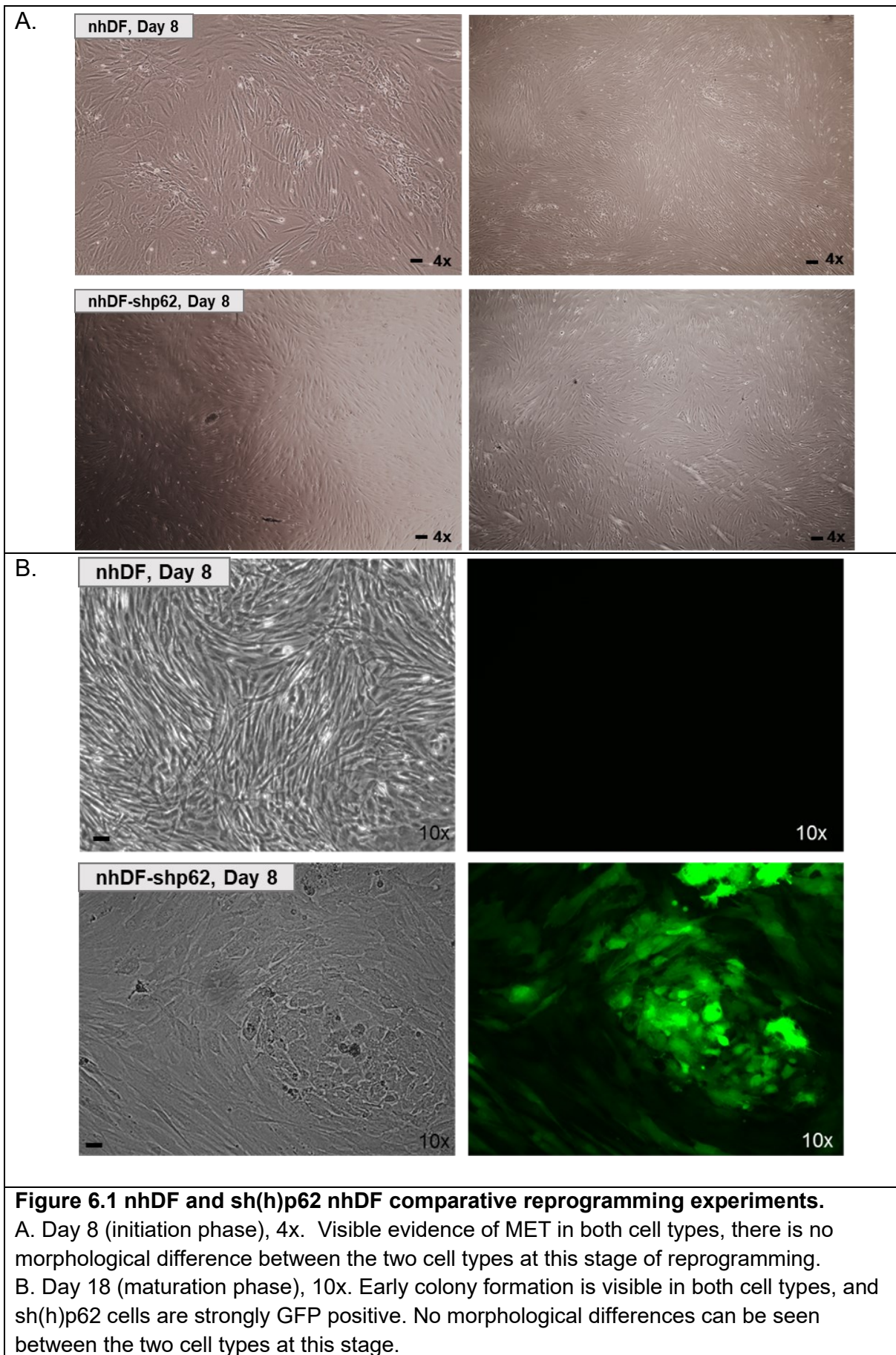
7.2. Objectives

- Successful iPSC reprogramming of nhDF-sh(h)p62 fibroblasts
- Comparison of the efficiency of iPSC reprogramming between nhDF-sh(h)p62 and nhDF controls
- Comparison of the morphology of resultant iPSC colonies between nhDF-sh(h)p62 and nhDF controls
- Comparison of the ability to maintain pluripotency between nhDF-sh(h)p62 and nhDF controls
- Comparison of the ability to differentiate into all three germ layers between nhDF-sh(h)p62 and nhDF controls
- Comparison of pluripotency gene expression levels between nhDF-sh(h)p62 and nhDF controls

nhDFs transduced with shp62 were sorted using fluorescence activated cell sorting (FACS) for GFP expression to create a homogenous population of 100% transduced cells before beginning iPSC reprogramming. This shRNA construct causes approximately 85% knock-down of the p62 protein, as previously demonstrated. Figure 6.1 shows a representative example of nhDF compared to nhDF-shp62 throughout a reprogramming experiment.

7.3. **iPSC reprogramming and colony analysis**

Figure 6.1.A. shows nhDF and nhDF-shp62 reprogramming at D8, when clear signs of the initiation phase of reprogramming, particularly mesenchymal to epithelial transition (MET), can usually be seen. MET can be seen in both the nhDF (top panel) and nhDF-shp62 (bottom panel) examples with no discernible differences between the two. Figure 6.1.B shows D18 for the same reprogramming experiment. During D14-20 the maturation phase of iPSC reprogramming typically occurs. Early colony formation can be seen in both nhDF (top panel) and nhDF-shp62 examples. nhDF-shp62 are also strongly GFP positive at this stage of reprogramming and show colony forming and non-colony forming cells across the well. MEFs are not GFP positive.



After D25 of three independent iPS reprogramming experiments, cells were stained for AP and macroscopic images were taken. It is clear that in the nhDF-shp62 containing wells there are many more small and irregular areas of AP positive staining and that the process of reprogramming has been less controlled in nhDF-shp62 cells compared to nhDF controls (Figure 6.2). AP staining also appears less dense in the nhDF-shp62 compared to nhDF controls.

Macroscopic images of AP stained wells were analysed using ImageJ for colony number, size and shape. Figure 2.6.C shows a comparison of the number of AP positive primary (P0) colonies after 25d of three independent reprogramming experiments in nhDF control and stably transduced nhDF-shp62 cells. On average there were 16 ± 1.00 primary (P0) nhDF iPS colonies after 25d of three independent reprogramming experiments, whereas there were 89 ± 4.70 AP positive nhDF-shp62 colonies after 25d of reprogramming on average. Across three independent experiments, as shown in Figure 6.2.C, the number of areas stained positive for AP are significantly higher in nhDF-shp62 than in comparative nhDF controls ($n=3$, $p=0.0029$) The software counted all areas stained positive with AP, regardless of size or shape. The S.E.M for nhDF-shp62 experiments is also much larger than across nhDF control experiments (S.E.M 4.70 across nhDF-shp62 experiments compared to 1.0 across nhDF experiments) showing a greater level of variation in reprogramming the nhDF-shp62 cells.

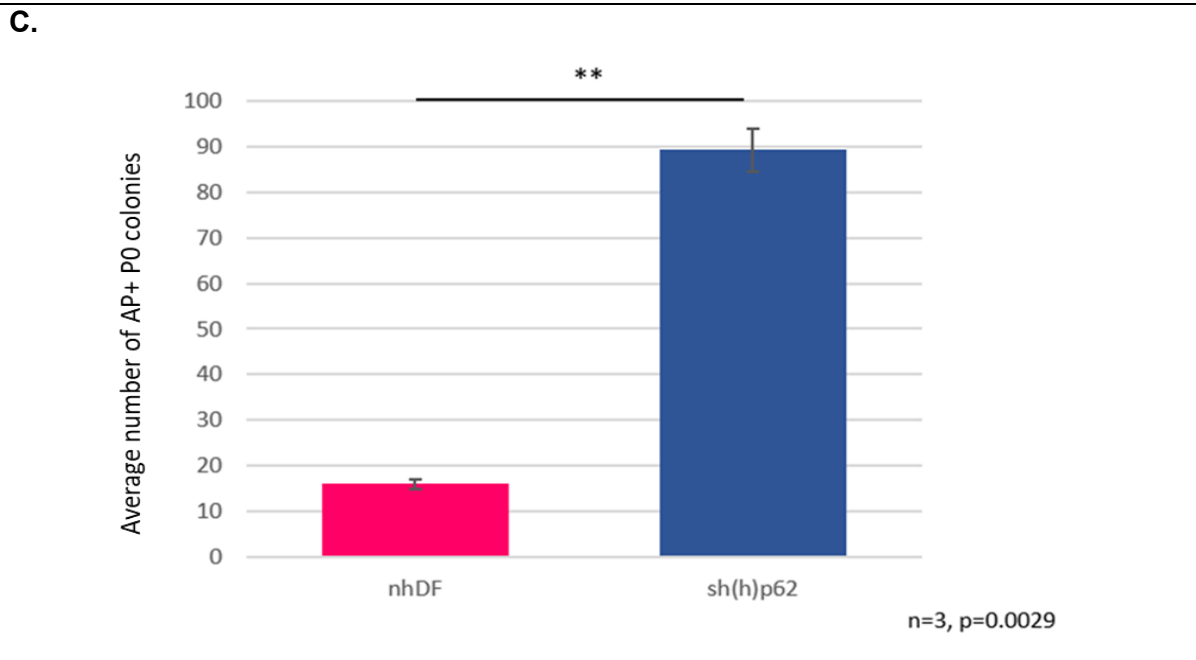
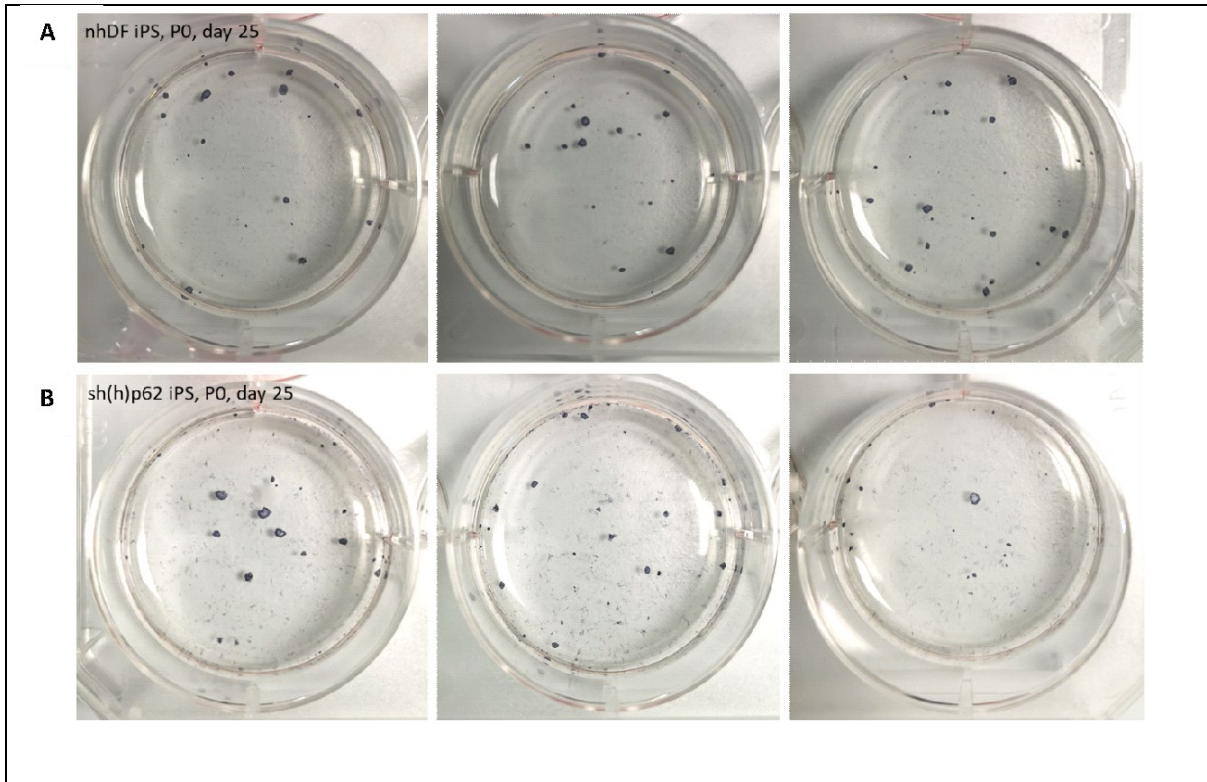


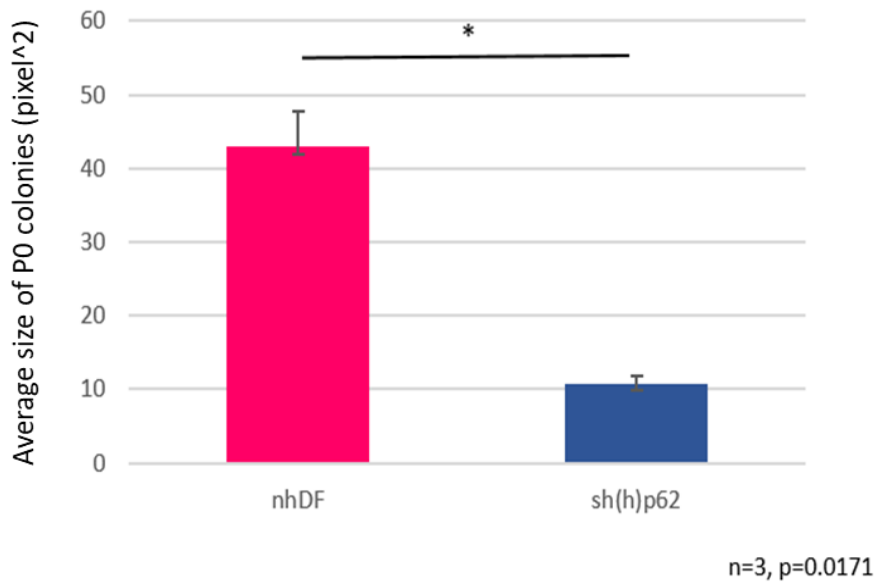
Figure 6.2 nhDF vs p62 null hDF reprogramming. Day 25, primary (P0) iPS colonies stained with Alkaline Phosphatase (AP).

Macroscopic images of three independent experiments nhDF (A) and sh(h)p62 (B) iPS P0, at day 25 of reprogramming. sh(h)p62 colonies are generally less densely stained, and less uniform, with many colonies that appear partially reprogrammed, or partially differentiated and many tiny areas of AP positive staining which are not colonies. C. Total 'colony' count, analysed using ImageJ and including all areas stained with AP across the entire well of a 6-well plate. Average colony number in nhDF experiments = 16±1.00. Average colony number in sh(h)p62 hDF experiments = 89.33±4.70.(n=3, p= 0.0029)

nhDF-shp62 AP positive colonies are also significantly smaller than those in nhDF controls (Figure 6.3.A) ($n=3$, $p= 0.0171$). ImageJ measures size as number of pixels² in images that have been converted to binary and threshold adjusted (see materials and methods). On average the size of nhDF iPS colonies are $42.914 \text{ pixels}^2 \pm 4.74$, whereas the size of nhDF-shp62 colonies is $10.771 \text{ pixels}^2 \pm 1.08$.

Primary (P0) colonies were analysed for circularity (Figure 6.3.B). Circularity is measured by ImageJ using $4\pi(\text{area}/\text{perimeter}^2)$ and a score of 1.0 represents a perfect circle. On average, nhDF-shp62 colonies are significantly less circular than nhDF controls. Across three independent experiments nhDF colonies have an average circularity of 0.897 ± 0.02 whereas nhDF-shp62 colonies only score 0.780 ± 0.1 in circularity ($n=3$, $p=0.0422$).

A.



B.

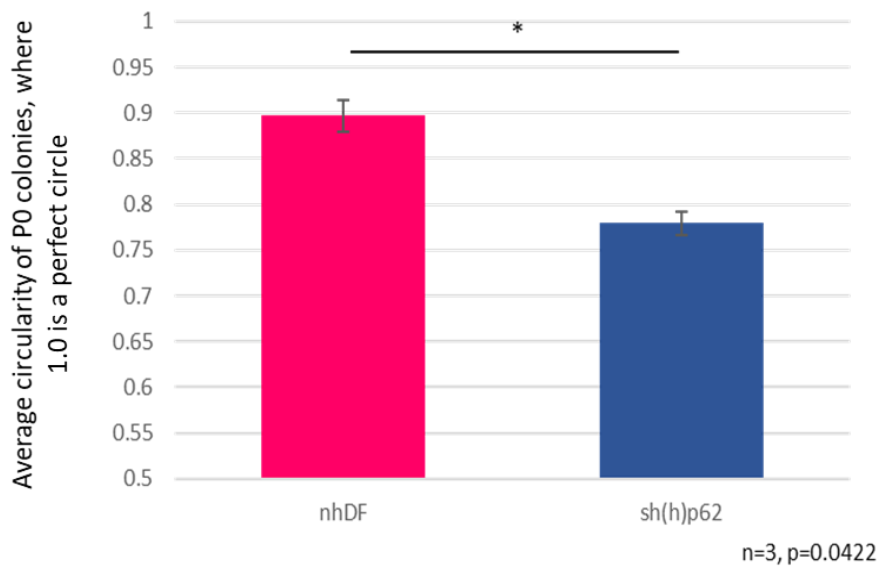
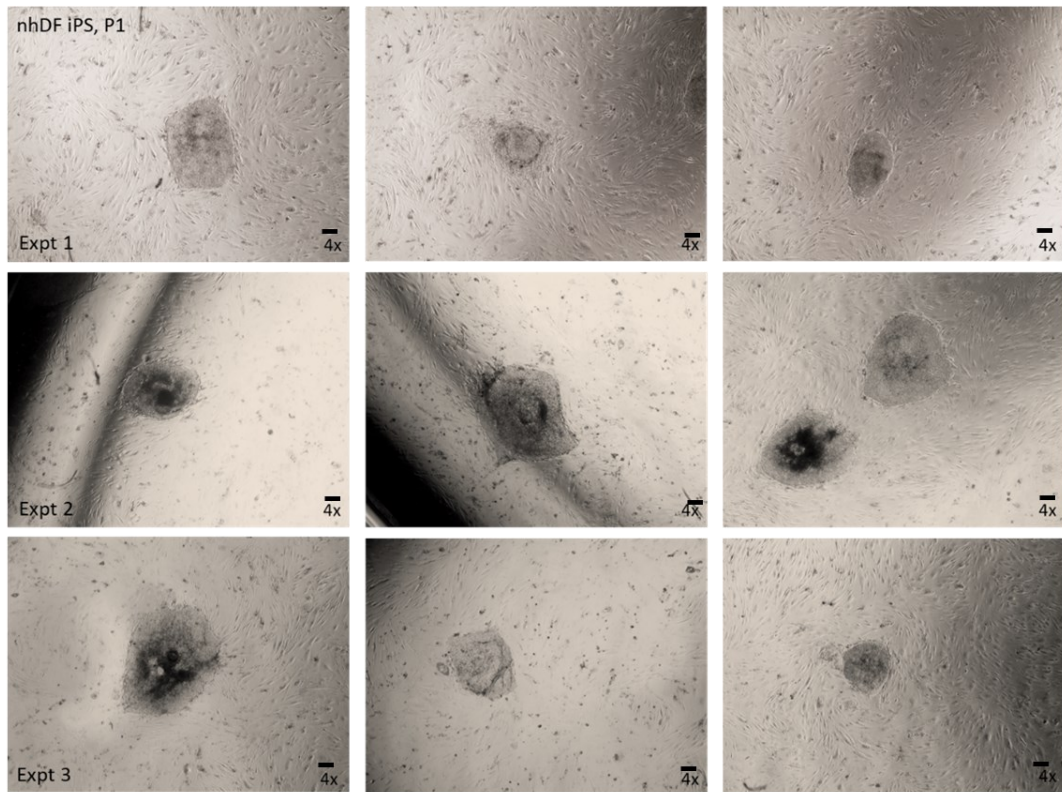


Figure 6.3 nhDF and nhDF-shp62 comparative reprogramming experiments (P0)

A. Average colony size analysed using ImageJ and including all areas stained with AP across the entire well of a 6-well plate. Average colony size in nhDF experiments = 42.914 pixels² ± 4.74, average colony size in nhDF-shp62 experiments = 10.771 pixels² ± 1.08 (n=3, p= 0.0171). B. Average circularity on day 25 of reprogramming (P0), across three independent experiments. ImageJ analyses particles on a scale of 0.0-1.0 where 1.0 is a perfect circle. There is a significant difference in average circularity scores in nhDFs compared to nhDF-shp62 cells. Average colony circularity in nhDf controls is 0.897±0.02 whereas average colony circularity in nhDF-shp62 cells is 0.780±0.01. (n=3, p= 0.0422). Data collated from three independent experiments, p-values calculated by two-tailed unpaired t-test.

nhDF control and nhDF-shp62 primary (P0) colonies were manually passaged and the shape and uniformity assessed and analysed visually at P1 (Figure 6.4). All colonies were counted across three independent experiments in nhDF control and nhDF-shp62. Typical iPS colonies have a clear and well defined border around the whole circumference. True iPS colonies in the stabilisation phase and beyond are generally close to circular in shape and cells have a largely uniform appearance with minimal spontaneous differentiation. Figure 6.4.A. shows an example of nhDF control iPS colonies at P1 and B. shows an example of nhDF-shp62 colonies at P1. Clear morphological differences can be seen between the two cell types. nhDF colonies are largely quite uniform in shape, close to circular and have minimal amounts of spontaneous differentiation. In contrast, the nhDF-shp62 colonies are generally more irregular in shape and have lots of spontaneous differentiation visible.

A.



B.

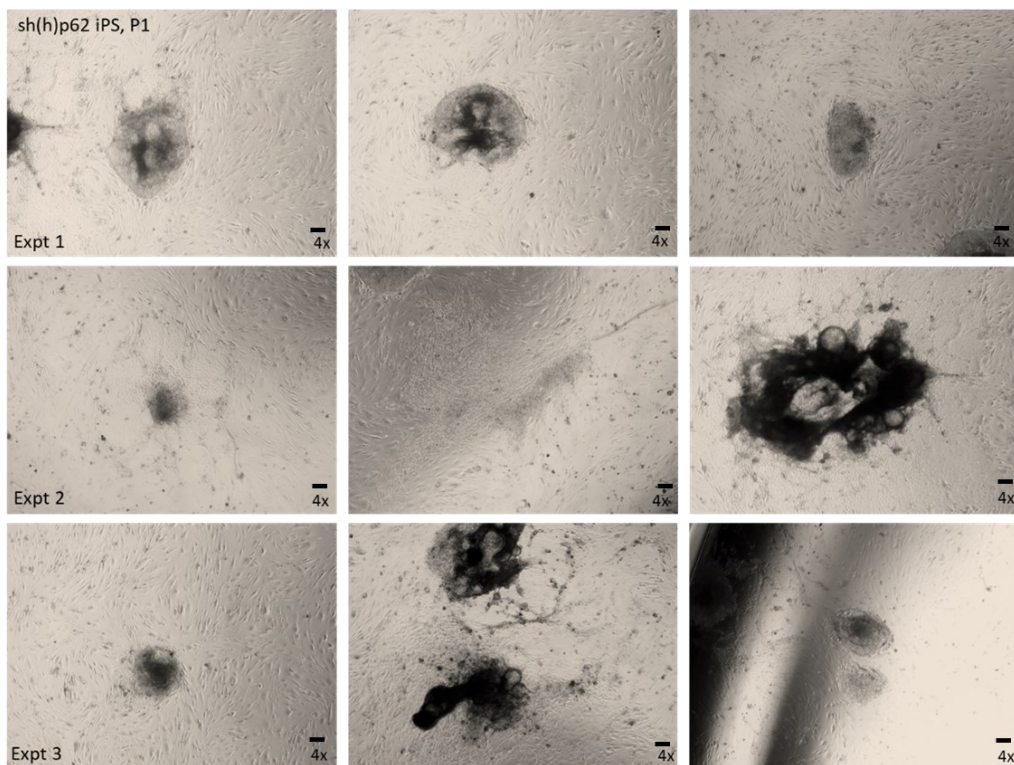


Figure 6.4 iPS reprogramming of nhDF-shp62 cells and nhDF controls, P1.

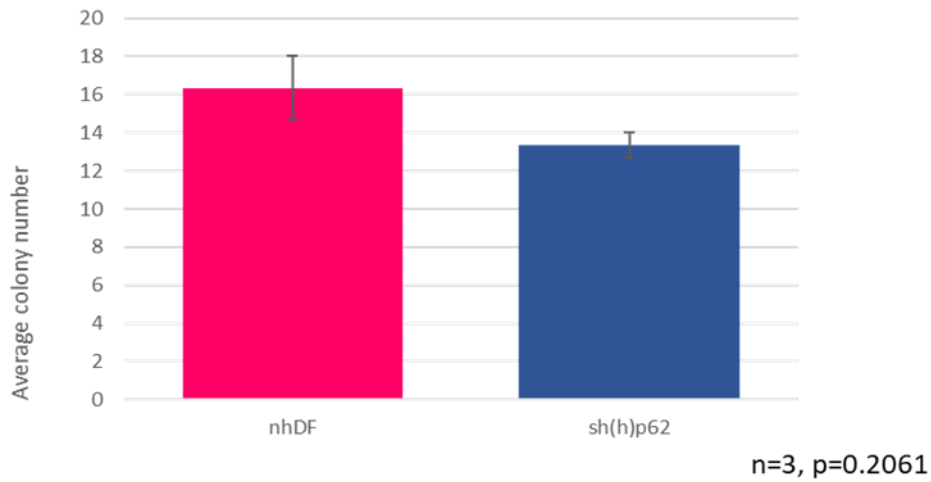
A. Representative examples of nhDF iPS on MEFs, P1. B. Representative examples of nhDF-shp62 iPS on MEFs, P1. Clear morphological differences can be seen between the

two cell types, with a higher level of spontaneous differentiation and irregularity in the colonies visible in nhDF-shp62 cells. Three independent experiments, 4x magnification

First, the number of P1 colonies were counted and compared in nhDF controls and nhDF-shp62 cells across three independent experiments. There was no significant difference in the number of 'colonies' formed at P1 (Figure 6.5.A.) (nhDF average colony number = 16.333 ± 1.67 , nhDF-shp62 average colony number = 13.333 ± 0.67 (n=3, p= 0.2061).

Next, the number and percentage of intact borders in nhDF and nhDF-shp62 colonies was compared (Figure 6.5.B). P1 colonies were defined as having either a completely intact border or not, in three independent experiments in both nhDF controls and nhDF-shp62. All images were randomised and blinded before being analysed in order to avoid any bias. Anywhere that a clear break in the colony border was visible where spontaneous differentiation had occurred was counted as not having an intact border. Significantly fewer nhDF-shp62 have complete, intact borders compared to nhDF controls across three independent experiments. 68.33% \pm 4.67 of nhDF control P1 colonies have complete, intact borders, compared to just 35% \pm 4.16 of nhDF-shp62 colonies (n=3, p= 0.00618).

A.



B.

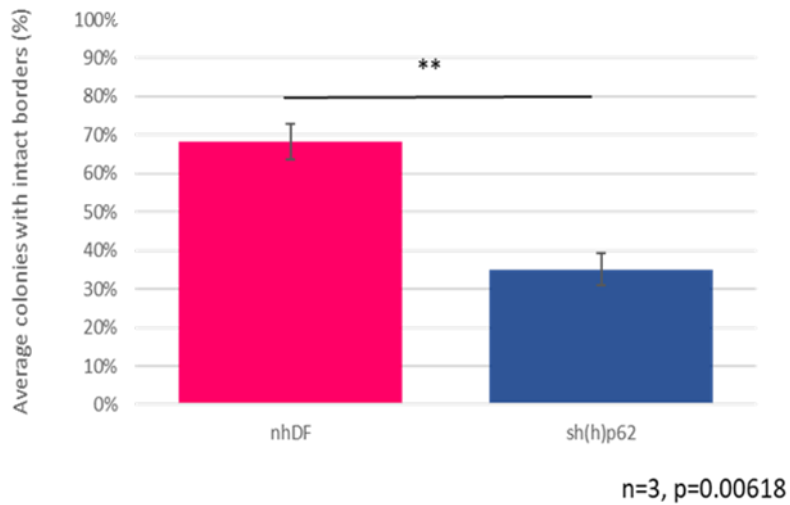


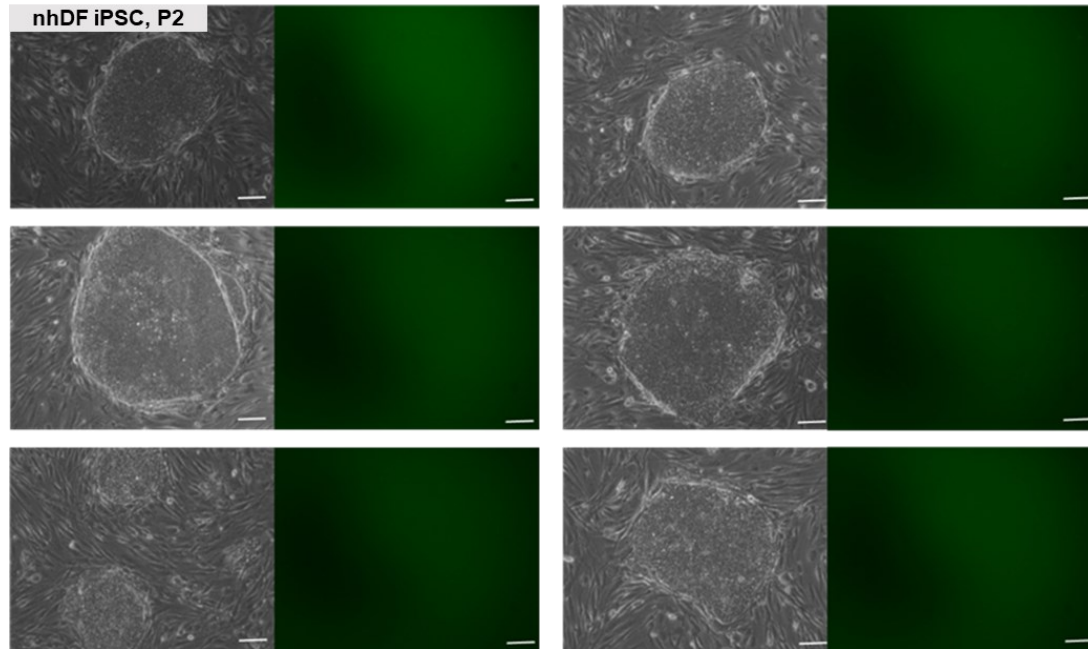
Figure 6.5: nhDF and nhDF-shp62 comparative reprogramming experiments (P1)

A. Average P1 colony number after manual passage of an equal number of P0 colonies in nhDF controls and nhDF-shp62 s. There is no significant difference in the number of P1 colonies formed (16.33 ± 1.67 in nhDF experiments compared to 13.33 ± 0.67 in nhDF-shp62 experiments ($n=3$, $p=0.2061$)). B. Average number of P1 colonies with complete, intact borders in nhDF and nhDF-shp62 across 3 independent experiments. Significantly fewer nhDF-shp62 colonies have complete, intact borders without spontaneous differentiation compared to nhDF controls. An average of 68.3% (S.E.M 4.67)) of nhDF colonies have complete intact borders compared to just 35% (S.E.M 4.16) of nhDF-shp62

colonies (n=3, p= 0.00618). Data collated for 3 independent experiments, p values calculated using unpaired t-test.

nhDF and nhDF-shp62 iPS cells were manually passaged weekly. nhDF colonies, as expected became more uniform and less likely to spontaneously differentiate with each passage (Figures 6.6, 6.7 and 6.8) nhDF-shp62, do not become stabilised in the same way and showed clear similarities with the behaviour of hDF-p62^{-/-} colonies. Large amounts of spontaneous differentiation continues to occur with passaging, and any surviving colonies do not have the typical uniformity of stable iPSC colonies. Most cells were not morphologically similar to the hDFs from which they were derived, but do not appear like true iPSCs either, suggesting an intermediate phenotype. At early passages (P2/3) some iPS-like cells remain (see white arrows on Figures 6.6 and 6.7), with others not resembling iPS cells at all (red arrows).

A.



B.

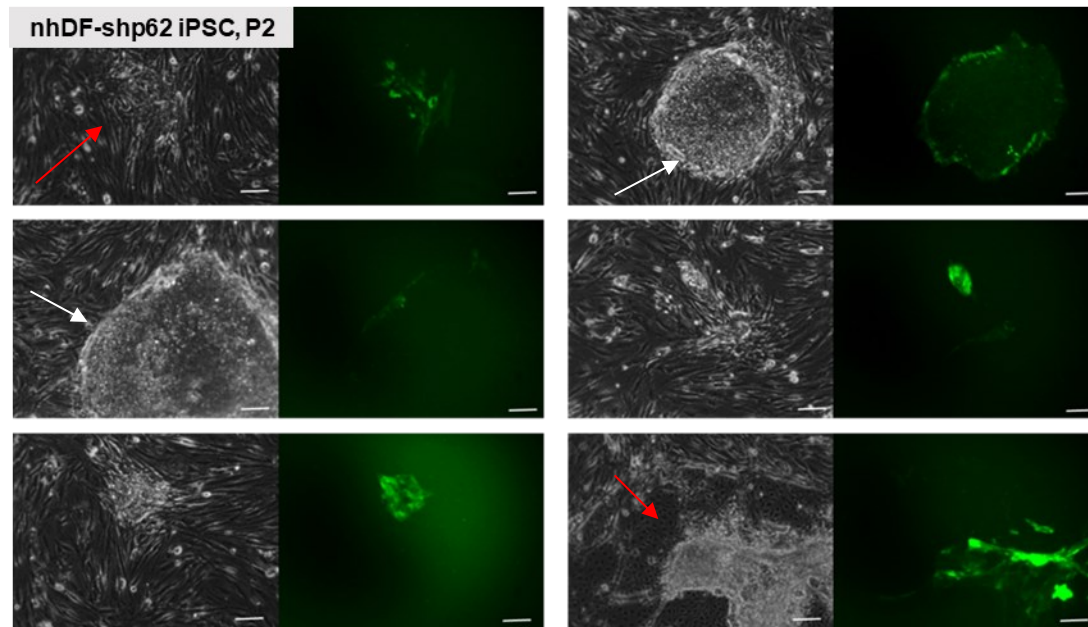
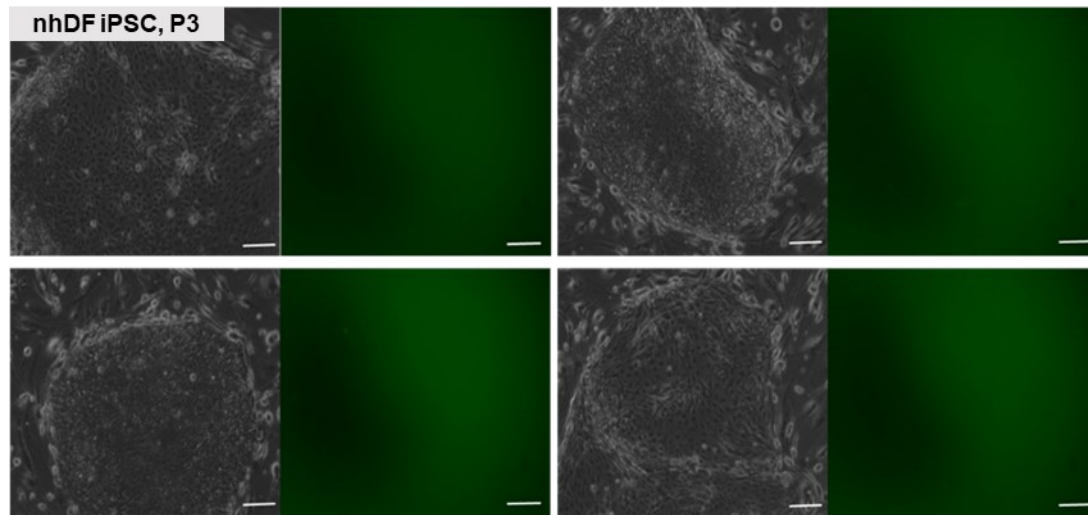


Figure 6.6: Phase and fluorescence imaging of nhDF and nhDF-shp62 derived iPS cells at passage 2.

A. nhDF derived iPS controls: all colonies are uniform, well defined and morphologically typical of iPS colonies as well as being GFP negative. B. nhDF-shp62 'iPS' cells. Large

amounts of spontaneous differentiation can be seen at this early passage, and cells have lost much GFP expression, indicating a repression of the sh(h)p62 construct. Cells that are morphologically iPS-like have the lowest levels of GFP expression. All images taken at 4x magnification, scale bars represent 100µm

A.



B.

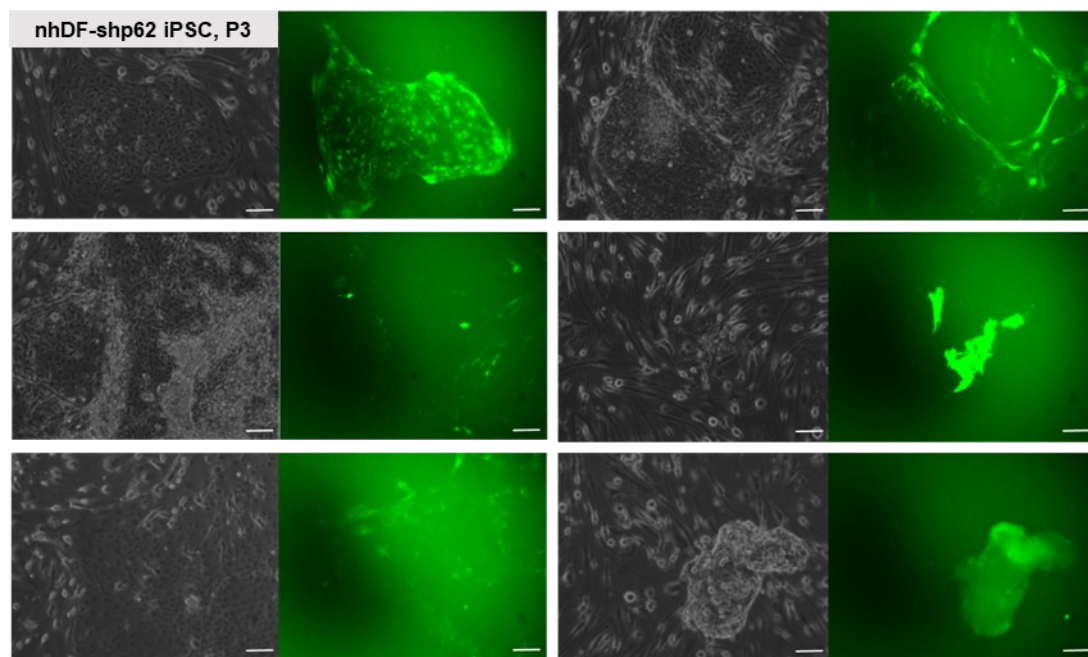


Figure 6.7: Phase and fluorescence imaging of nhDF and nhDF-shp62 derived iPS cells at passage 3. **A.** nhDF derived iPS controls: all colonies are uniform, well defined and morphologically typical of iPS colonies as well as being GFP negative. **B.** nhDF-shp62 'iPS' cells. Even further amounts of spontaneous differentiation can be seen, Cells that are morphologically iPS-like have the lowest levels of GFP expression. With higher levels of spontaneous expression results in a return towards strong levels of GFP expression in these cells. All images taken at 4x magnification, scale bars represent 100µm. **A.** nhDF derived iPS controls: all colonies are uniform, well defined and morphologically typical of iPS colonies as well as being GFP negative. **B.** nhDF-shp62 'iPS' cells. Even further amounts of spontaneous differentiation can be seen, Cells that

are morphologically iPS-like have the lowest levels of GFP expression. With higher levels of spontaneous expression results in a return towards strong levels of GFP expression in these cells. All images taken at 4x magnification, scale bars represent 100µm.

At later passages (P5-9) (Figures 6.8 and 6.9) almost no iPS-like cells remain, with all cells having differentiated or lost for nhDF-shp62, while nhDF controls continue indefinitely. nhDF-shp62 colonies have never survived beyond P9. This is slightly longer than the hDF-p62^{-/-} cells, which could not be passaged beyond P6. In some reprogramming experiments, nhDF-shp62 have been lost or differentiated entirely at earlier passages.

The sh(h)p62 construct also contains a GFP cassette. As shown in Figure 6.1, the hDFs that underwent reprogramming were 100% transduced with this construct and all cells were GFP expressing. However, as the cells undergo the later stages of the reprogramming process the GFP expression is partially lost, suggesting that the sh(h)p62 construct is being repressed in the iPS cells or that a small number of sh(h)p62/GFP negative cells overcome nhDF-shp62. Irrespective, these iPSC-like colonies are unable to persist long-term, suggesting that p62 is crucial in the stabilisation phase of iPS reprogramming and long-term colony maintenance. Our assessment of the shp62 knockdown shows that some residual p62 expression persists which may explain why nhDF-shp62 cells survive for slightly longer than p62 null cells.

In particular, it is notable that in fluorescence imaging of nhDF-shp62 cells at P2, 3 and 9, the cells that are most stem-like morphologically tend to have little to no GFP expression at all. In contrast, cells that have clearly differentiated and possess markedly different morphologies have the highest level of GFP expression and therefore, potentially the lowest level of p62 expression. The shp62 cassette and

eGFP cassettes are controlled by two different promoters though, and p62 expression levels have not been assessed in these cells.

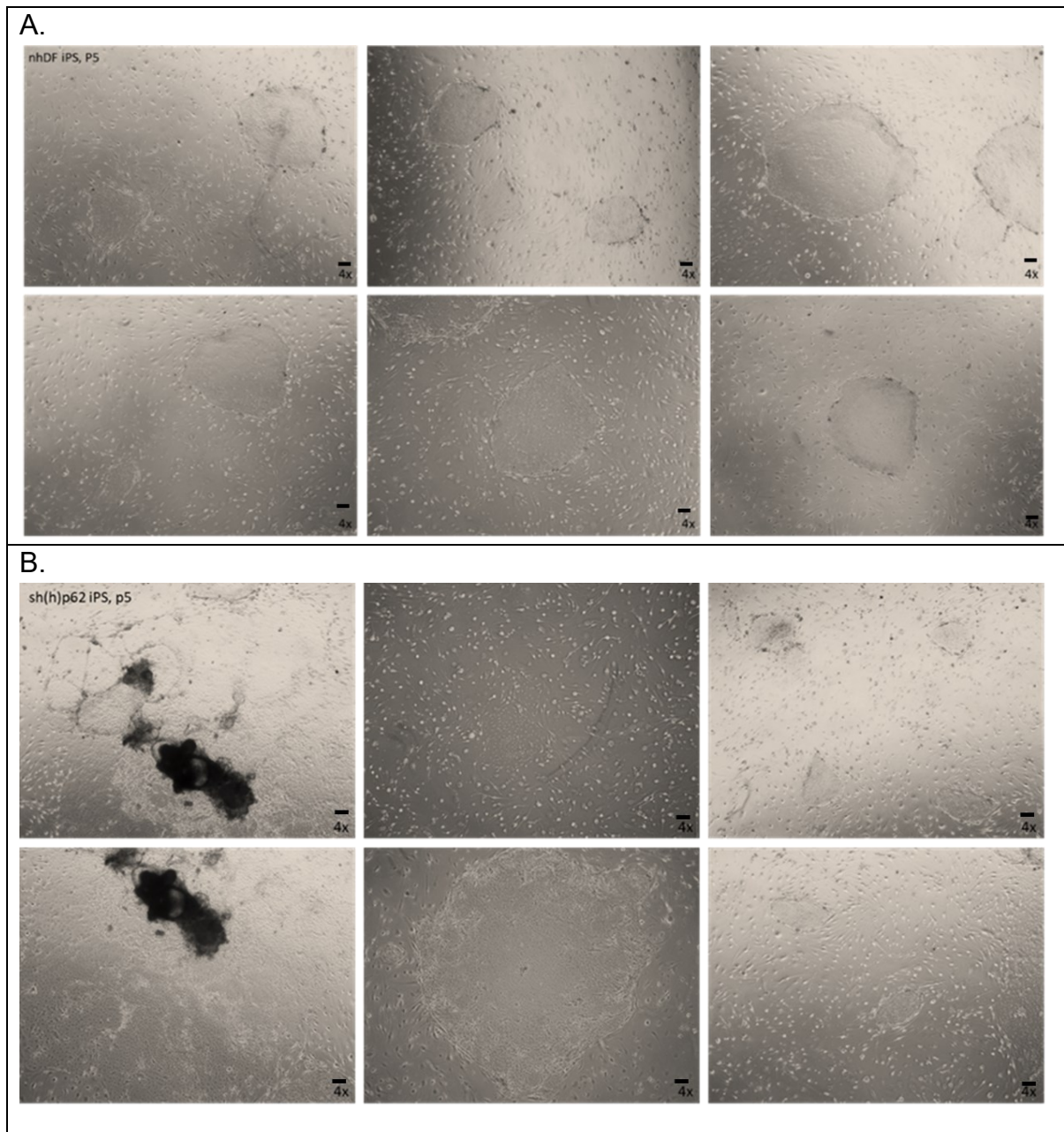
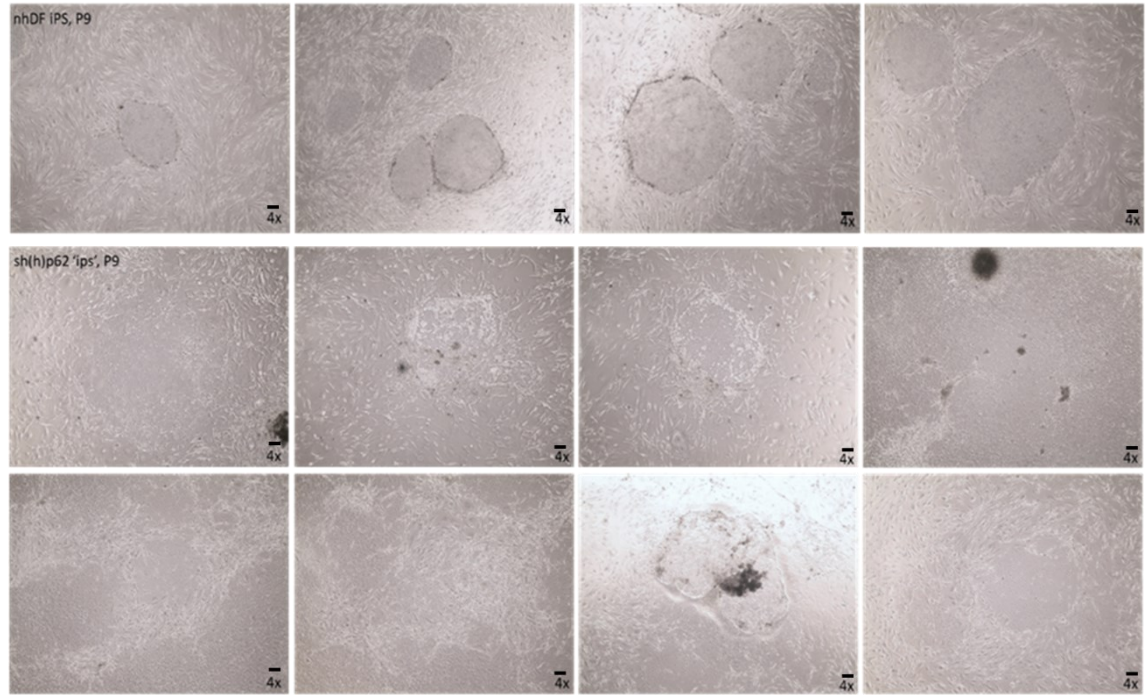


Figure 6.8: Phase imaging of nhDF and nhDF-shp62 derived iPS cells at passage 5. A. nhDF derived iPS controls: all colonies are uniform, well defined and morphologically typical of established, stable iPS lines. B. nhDF-shp62 'iPS' cells. Even further amounts of spontaneous differentiation can be seen with almost no cells resembling true iPS by this passage. All images taken at 4x magnification, scale bars represent 100 μ M

A.



B.

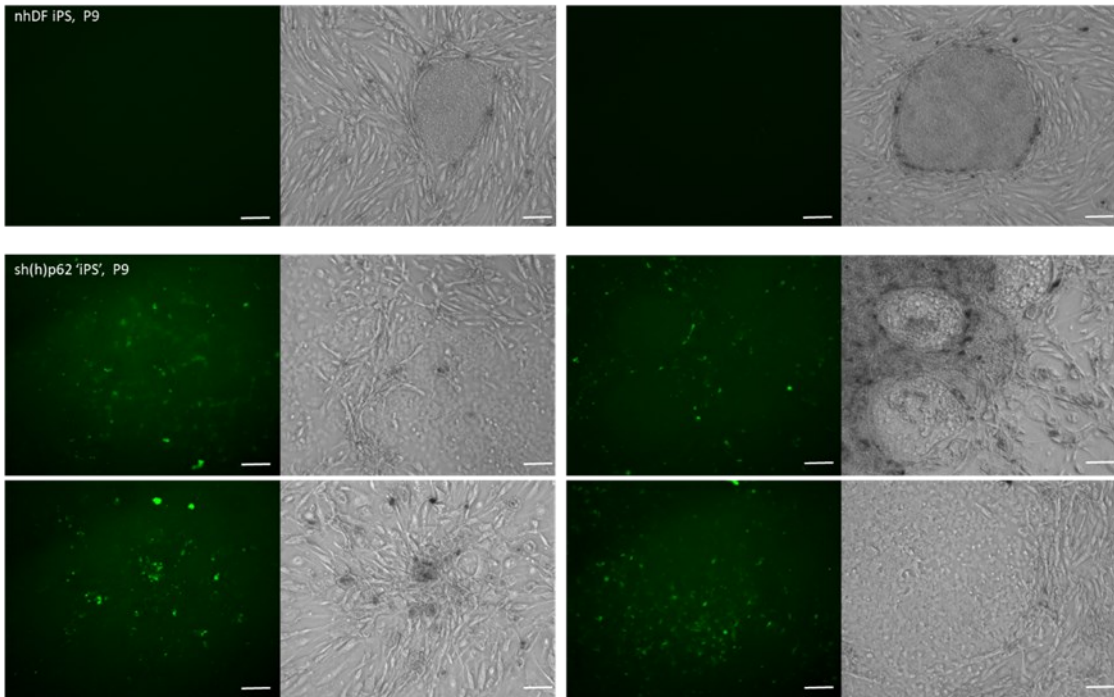


Figure 6.9 Phase and fluorescence imaging of nhDF and nhDF-shp62 derived iPS cells at passage 9.

A. Phase images of nhDF (top panel) and nhDF-shp62 (bottom panel) 'iPS' at passage 9. nhDF iPS colonies by passage 9 are well established and stabilised. B. Fluorescence imaging of passage 9 nhDF and nhDF-shp62 'iPS' cells. By passage 9 little to no cells that are morphologically iPS like remain in the nhDF-shp62 experiments. All images taken at 4x magnification, scale bars represent 100µm.

7.4. **Tri-lineage differentiation**

It is clear that nhDF-shp62 cells have a clear propensity for spontaneous differentiation, and as such, they were subjected to an established embryoid body (EB) spontaneous differentiation protocol. By removing media components essential for the maintenance of pluripotency (FGF) and subjecting cells to a serum containing media, cells are encouraged to differentiate without any specific directionality. As one of the key hallmarks of pluripotency is the ability for cells to be differentiated into cells from all three germ layers (endoderm, mesoderm and ectoderm); it is expected that established iPSC will spontaneously differentiate in this manner. Cells were imaged after 8d in suspension culture (Figure 6.10), before being re-plated in adherent cell culture plates and allowed to grow and differentiate for a further 8d (Figure 6.11). At day eight, nhDF-shp62 EBs are heterogeneously GFP positive, while cells that have grown out from these do not express the same levels of GFP (Figure 6.10). hDF-p62^{-/-} cells were not subjected to this spontaneous differentiation experiment because it was not possible to amplify iPSC colonies to sufficient cell numbers.

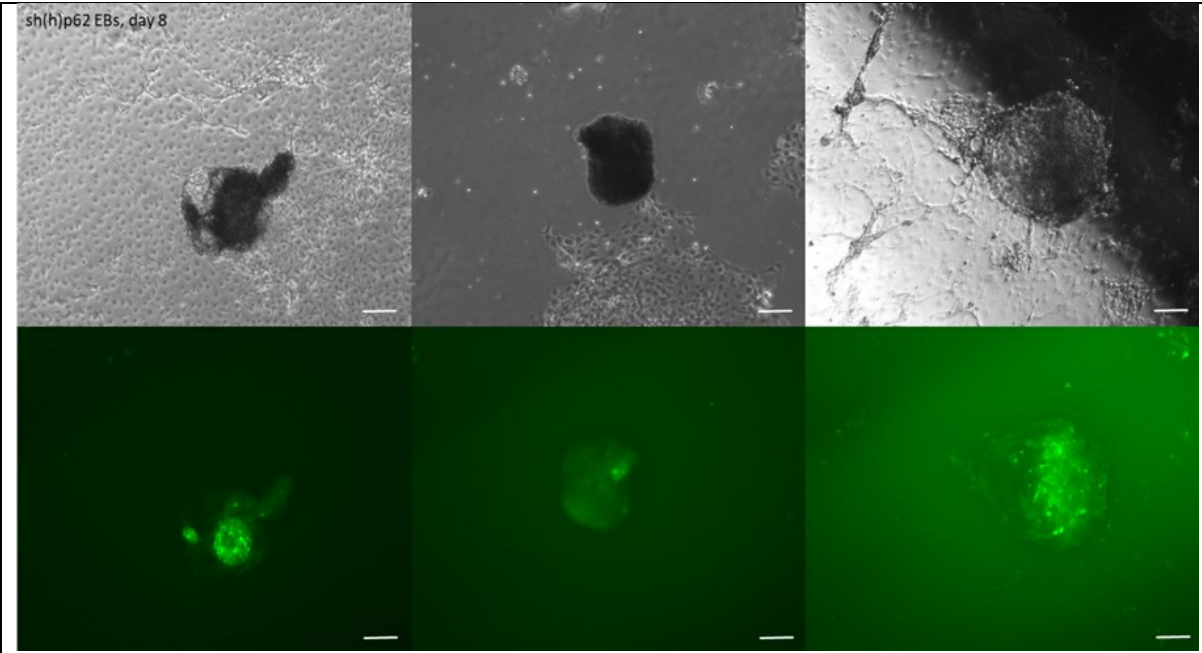


Figure 6.10: Phase and fluorescence imaging of nhDF-shp62 embryoid bodies (EBs) after 8 days in suspension culture. EBs are GFP positive, but cells grown out from EBs are not. All images taken at 4x magnification, scale bars represent 100 μ m.

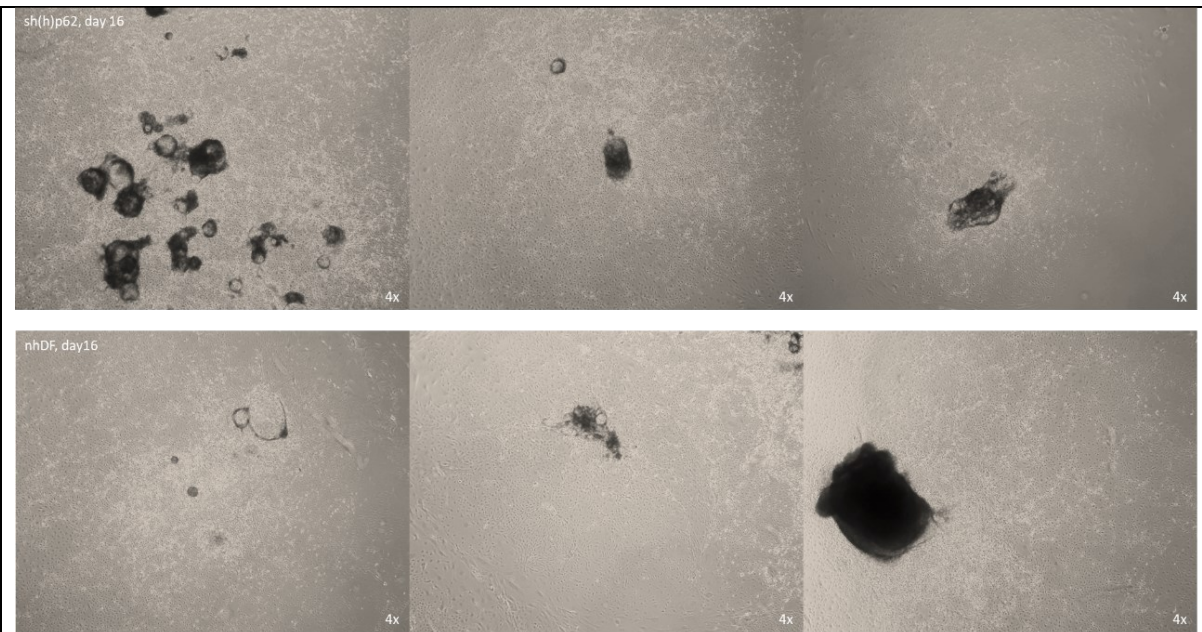


Figure 6.11 Phase imaging of nhDF-shp62 embryoid bodies (EBs) after replating onto adherent plates and 8 days of outgrowth. A wide range of cell types and morphologies can be seen. All images taken at 4x magnification.

After 16d of spontaneous differentiation, cells were fixed and stained for β III-tubulin and Sox17, two early differentiation markers for ectodermal and endodermal lineage, respectively. The nhDF-shp62 derived iPSCs subjected to this spontaneous differentiation protocol appeared to show a high level of proximity between sh(h)p62-GFP and β III-tubulin (Figure 6.12). In contrast, there was no visible co-localisation between sh(h)p62-GFP and Sox17 (Figure 6.13). nhDF derived control iPSCs subjected to spontaneous differentiation stained positive for both β III-tubulin and Sox17 (Figure 6.14). Although this is preliminary data, it does suggest that nhDF-shp62-derived iPS cells may have a propensity to differentiate towards a neural lineage. Interestingly, neuroectoderm is considered the “default” differentiation lineage when exiting pluripotency (Kamiya et al, 2011) meaning that loss of p62 could be either promoting exit from pluripotency or neuroectodermal differentiation.

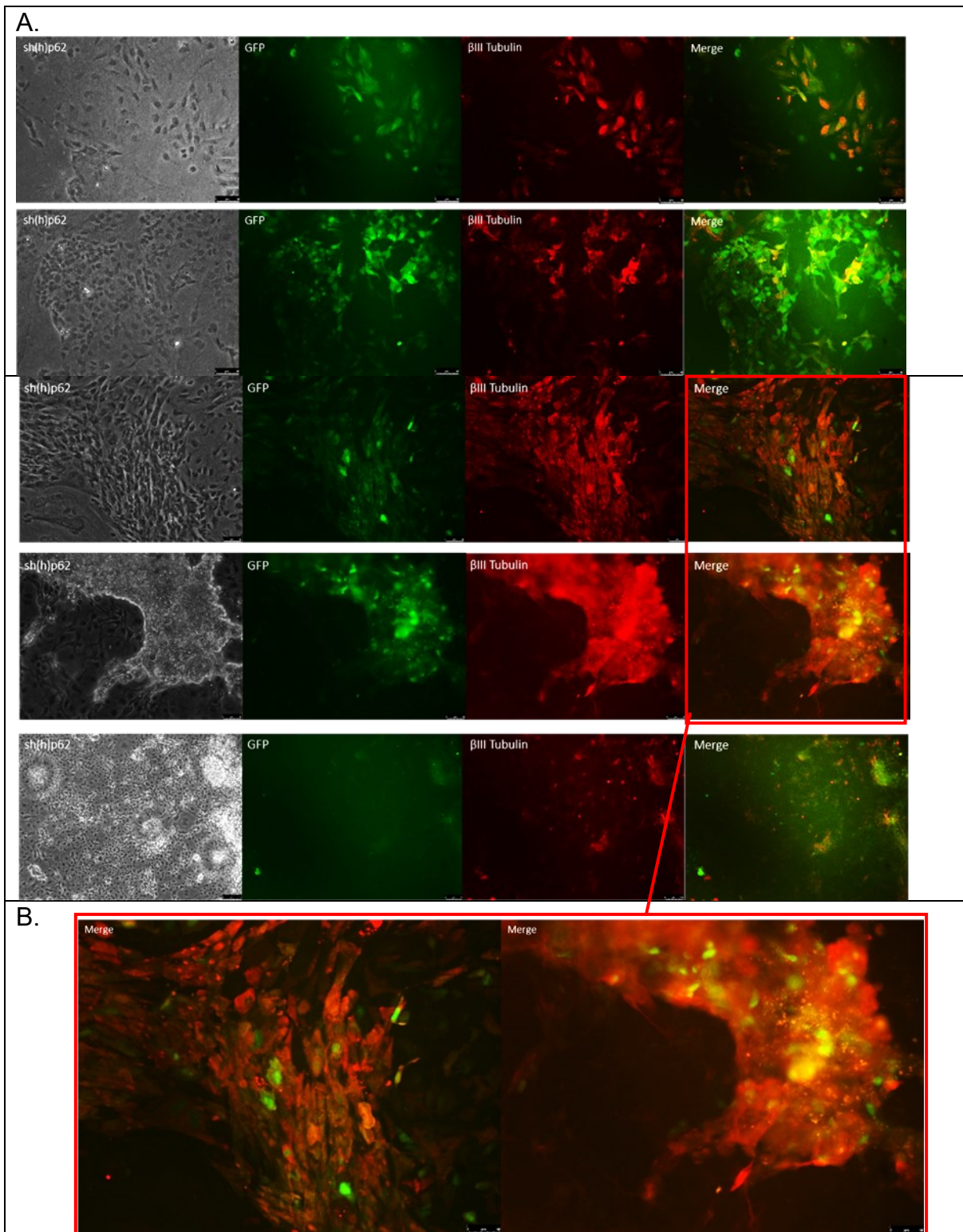


Figure 6.12 nhDF-shp62 'iPS' cells subjected to 16 days of a spontaneous differentiation protocol and stained for β III-Tubulin, an early neural specification marker A. High levels of co-expression can be seen with cells both sh(h)p62-GFP positive and positive for β III-Tubulin, bright yellow areas suggest possible co-localisation, although a higher magnification would be required to confirm this. Panels highlighted by the red box are enlarged in B. All images taken at 4x magnification, with scale bars representing 100 μ m.

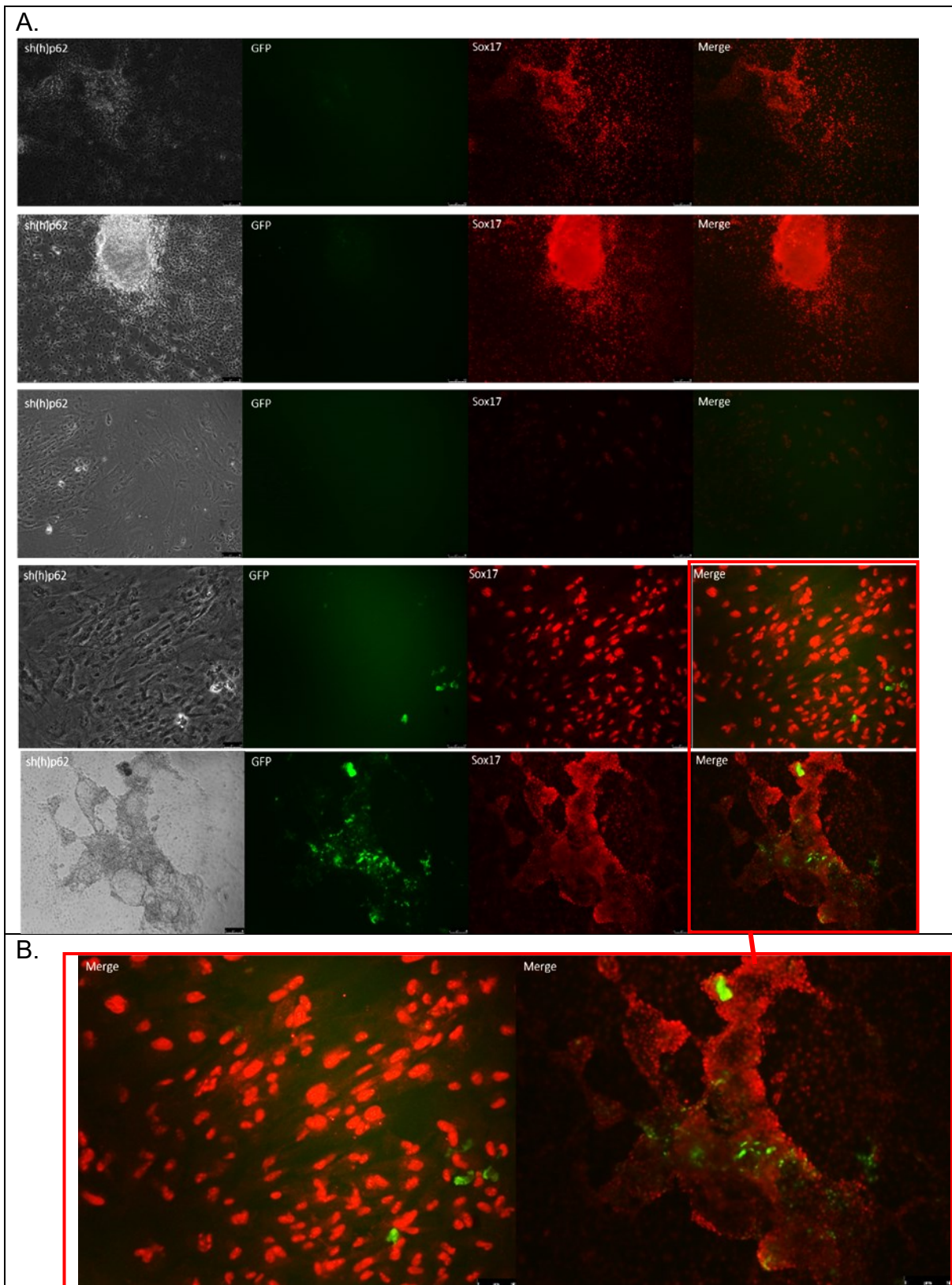


Figure 6.13: nhDF-shp62 ‘iPS’ cells subjected to 16 days of a spontaneous differentiation protocol and then stained for Sox17, an early endoderm marker. A. nhDF-shp62 are positive for both shp62-GFP and Sox17, Cells do not appear to co-express sh(h)p62 and Sox 17, although a higher magnification would be required to

confirm. B. Panels highlighted in the red box are enlarged. All images were taken at 4x magnification, with scale bars representing 100 μ m.

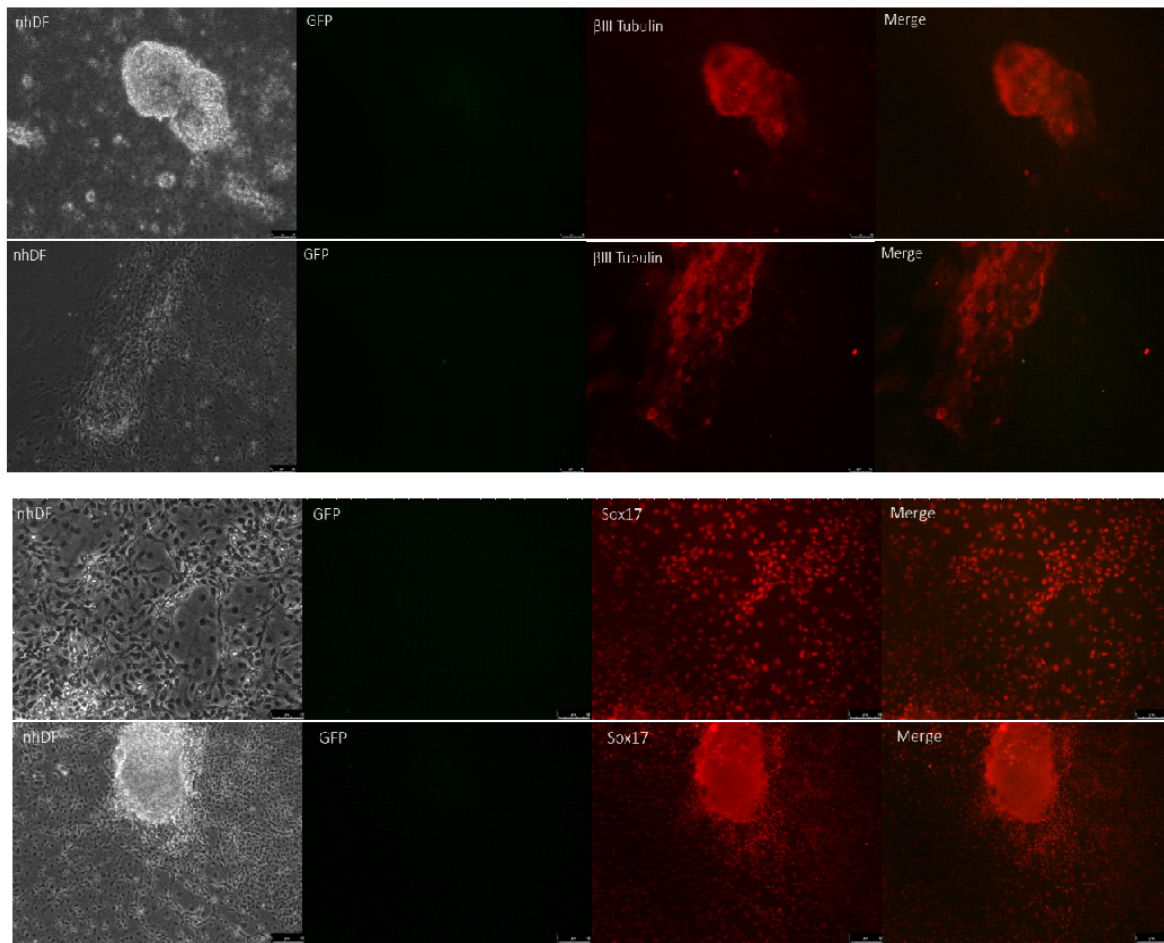


Figure 6.14 nhDF control iPSC were subjected to 16 day spontaneous differentiation protocol stained positive for both β III-Tubulin and Sox17 but negative for GFP, as expected. All images taken at 4x magnification, with scale bars representing 100 μ m

7.5. Discussion

Overall, these results provide good evidence to support the hypothesis that p62 plays a key role in the stabilisation phase of iPS reprogramming and in the maintenance of pluripotency. Both hDF-p62^{-/-} and nhDF-shp62 cells form primary colonies, although these are significantly less uniform, smaller and generally dysregulated compared to nhDF derived controls. hDF-p62^{-/-} and nhDF-shp62 derived iPSC lines become more and more dysregulated with each subsequent

passage, with extremely high levels of spontaneous differentiation occurring. In addition, neither hDF-p62^{-/-} and nhDF-shp62 derived iPSC lines have maintained pluripotent colonies beyond P6-9, respectively. nhDF derived control iPS lines have been passaged to beyond 30 passages within this project.

It is possible that nhDF-shp62 derived iPS cells appear to repress the sh(RNA) construct once a level of pluripotency has been reached. This is a credible hypothesis due to the enormous number of genetic, epigenetic, metabolic and morphological changes that cells undergo throughout this process. Interestingly, I present preliminary data that suggests the nhDF-shp62 derived iPS cells begin to rapidly differentiate the construct appears to be switched back on. However, it is worth noting that the shp62 cassette and eGFP cassette are expressed under the control of two different promoters, and I have not assessed the level of p62 expression in these differentiated cells. However, this lentiviral vector is commonly used in iPSC and differentiating cells with eGFP being used as a marker for expression of the inserted transgene (Singovski et al, 2015; Zhang et al, 2016; Zhang et al, 2017).

Further, when subjected to an established spontaneous differentiation protocol, nhDF-shp62 derived iPSC lines may show a propensity to differentiate towards an ectodermal/neural lineage either as a targeted differentiation or as an exit from pluripotency signal in the absence of other differentiation cues.

Chapter 8. Discussion, future works and conclusions.

Chapter 7: Discussion and future works.

The ability to reprogram adult somatic cells to an embryonic-like state known as induced pluripotency is an exciting and not yet fully realised technology for use in regenerative medicine, drug screening and disease modelling. Current gold-standard methods for iPSC reprogramming are highly inefficient, with much still unknown about the mechanisms by which it occurs, although a level of autophagic recycling, mitochondrial remodelling, bioenergetics and transcription level changes occur.

p62 is a multi-domain, multi-functional protein with roles in autophagy, nutrient sensing, mitochondrial degradation and energetics and the anti-oxidant response.

Until now, the potential role of p62 in iPSC reprogramming or the maintenance of the pluripotent state has been unknown. The data presented in this report suggest that p62 may play a role in iPSC reprogramming or the maintenance of pluripotency.

Throughout this project I was able to successfully reprogram a number of fibroblast cells from mouse and human to pluripotency including Harvard doxycycline inducible MEFs, WT MEFs, control nhDFs, Batten disease CLN6 and CLN7 mutation patient fibroblasts, p62 null patient fibroblasts and shRNA mediated p62 knock-down fibroblasts. The McKay lab iPSC reprogramming protocol is robust and allows for the efficient iPSC reprogramming of any fibroblast using episomal OriP/EBNA reprogramming plasmids.

Initial development of iPSC reprogramming skills and methodologies were carried out on the Harvard inducible MEFs, which reprogram to pluripotency at extremely high efficiency, in order to understand the practical processes involved in iPSC reprogramming within a robust and efficient system, and with the simple addition of doxycycline all that was required to induce reprogramming. In analysing primary

colonies, it was impossible to count colony number as individual iPSC colonies were too close together to be distinguished on a macro scale manually or in ImageJ software; this is compounded by the fact that mouse iPSC and ESC colonies are much smaller than their human counterparts are. Far more colonies were formed in JB7 (homozygous for OKSM and Oct4-GFP) cells than JB8 (homozygous for OKSM but heterozygous for Oct4-GFP), possibly because JB7 MEFs were reprogrammed at P3 whereas JB8 MEFs were reprogrammed at P5. Notably, the polycistronic OKSM reprogramming cassette in these cells does not contain shp53, unlike the OriP/EBNA plasmids used for other reprogramming experiments in this study. This could mean that the later passage JB8 MEFs had undergone some level of cell senescence, resulting in a lower reprogramming efficiency in these cells compared to the JB7.

It is common to observe elevated levels of p62 in Batten disease neurons (Brandenstein et al, 2016) and fibroblasts, in fact other members of the McKay lab have observed higher levels of p62 expression in CLN7 neural progenitor cells. Other members of the McKay lab had previously found that CLN6 and CLN7 Batten disease patient fibroblasts reprogrammed with higher efficiency than our control cells (anecdotal, not quantified), although this was never the case in my hands. A statistical analysis was never carried out in these particular experiments, but a basic assessment of primary colony number did not suggest any difference in reprogramming efficiency between CLN6 or CLN7 fibroblasts compared to nhDF. Secondly, although significant p62 elevation has previously been reported in CLN7 mutant mouse fibroblasts (Brandenstein et al, 2016), this has not been observed in human fibroblasts or iPSC within the McKay group (unpublished observations).

Collated across all iPSC reprogramming experiments I conducted on all cell sources, there was less evidence of MET occurring in cells seeded at a lower density. The reason for this difference in density is simply that some cells and some individual experiments take longer to recover from the stress induced at nucleofection; although the reasons for this disparity are not known. hDF-p62^{-/-} cells grow more slowly than nhDF controls, so when the same number of cells are nucleofected they will take slightly longer to reach confluence than nhDF controls. However, this lack of visible MET is certainly not unique to the hDF-p62^{-/-}. Importantly, I observed no correlation between a lack of visible MET and reprogramming success at P0, as evidenced by nhDF and CLN6 reprogramming experiments.

CLN7-iPSC showed positive staining for a range of key pluripotency markers alongside hESC positive controls, including marker that aren't in the OriP/EBNA reprogramming plasmids, suggesting that the cells own pluripotency maintenance regulatory gene network had been 'switched-on'. Furthermore, CLN7-iPSC, CLN6-iPSC and nhDF-iPSC were all cultured for many passages (up to 30) throughout the length of this project; far beyond the period for which episomal plasmids are retained and thus the cells are expected to be completely transgene independent.

Throughout this project, I have created a wide range of tools in order to genetically modulate p62 expression in both mouse and human cells. Several genetically modified stable cell lines have been created, and some of these have been utilised in iPSC reprogramming experiments. This toolkit was not utilised as fully as hoped, but their potential for future use is enormous. The limitations of this study, as well as future works will be discussed later in this section.

Firstly, I designed, cloned, validated and implemented an shRNA for human p62 in order to create a cell line with p62 knock-down. Sequences were validated using Sanger sequencing, tested, and validated in a Hek293T cell line. Hek293T cells are useful for their rapid growth and proliferation as well as their high transfection efficiency and virus production (Thomas and Smart, 2005).

In these initial Hek293T experiments, levels of p62 protein expression were only reduced a small amount. However, these cells were lysed only 48hours after transduction. With shRNA taking up to 22 hours to have its effects on transcription (O'Keefe, 2013) and studies suggesting that the half-life of p62 protein is up to 24 hours (Lerner et al, 2013); it is possible that there had not been enough time to see sufficient reduction of p62 protein levels. In addition, a heterogeneous population of cells were lysed. Nevertheless, a sufficiently encouraging level of p62 protein reduction was achieved to carry out further experiments. Cells were clonally expanded to create a homogenous population of cells, and on analysis with western blot in three independent experiments, an average of 85.21% reduction in protein levels was achieved. When nhDFs were transduced with sh(h)p62, the time taken to expand these cells for sorting by FACS eliminated any concern over p62 protein half-life.

A human p62 overexpression plasmid was designed and *de novo* synthesised in a minimal promoterless vector. I designed this construct with restriction enzymes for ease of cloning into the pENTR-1a minimal cloning vector. This was done successfully, and confirmed by Sanger sequencing, as was subsequent recombination into the SFFV-GW lentivector. However, it was later decided that the addition of either a puromycin selection marker or GFP cassette or similar would be vital in ensuring transduction efficiency, the creation of a homogeneous cell line and

further analyses. Within the McKay lab we had a further lentiviral vector, which contains both puromycin resistance selection and a GFP cassette: I attempted to clone the hp62 cassette into the vector (IRES-GFP-PGK-PURO) however, unfortunately the proximity of suitable restriction sites within the multiple cloning site (MCS) of the destination vector made this unfeasible. Ultimately, in order to maximise time and opportunity to carry out further experiments, the decision to purchase a complete human p62 overexpression plasmid was made. However, this lentiviral vector may be useful in future works where a homogeneous population of cells is less important, or a more suitable vector may become available to clone the construct into.

pBABE-puro-HA-p62 and pBABE-puro-HA-p62-LIR were created by the Jayanta Debnath lab (Chen et al, 2013) and purchased from Addgene. pBABE-puro-HA-p62 is a retroviral expression plasmid for complete human p62. pBABE-puro-HA-p62-LIR has a mutation causing a single amino acid change from a tryptophan (W) to an alanine (A). The W338A mutation prevents p62 from recognising or being able to interact with LC3, and therefore the breakdown of p62 by autophagy (Chen et al, 2013; Bertrand et al, 2015; Yan et al, 2018). pBABE-puro-HA-p62 and pBABE-puro-HA-p62-LIR retroviral plasmids were successfully transfected into Hek293T cells, and subsequently stably transduced into hDF-p62^{-/-} cells. Homogeneous lines of hDF-p62^{-/-} cells transduced with either pBABE-puro-HA-p62 or pBABE-puro-HA-p62 were created with puromycin selection. In future experiments, the downstream effects of W338A mutation could be validated by analysing the levels of p62-LC3 interaction.

pBMN-mCherry-p62(Δ UBD) and pBMN-mCherry-p62(UBD/W340A) retroviral plasmids were created by the Michael Lazarou lab (Padman et al, 2019) and

purchased from Addgene. pBMN-mCherry-p62(Δ UBD) is truncated to omit the UBA domain from amino acid 385 onwards, thereby preventing any interaction with ubiquitinated proteins or organelles such as mitochondria targeted for degradation. pBMN-mCherry-p62(UBD/W340A) is truncated at amino acid 385 and has an additional mutation leading to an amino acid change from tryptophan to alanine at 340 (W340A). Sequences were confirmed with Sanger sequencing. Both W338A and W340A mutations work in the same way to prevent LC3 binding. Of course, other proteins besides p62 do contain UBD domains (e.g. OPTN, NBR1 and NDP52) (Padman et al, 2019), so this does not prevent that targeting of ubiquitin tagged proteins to autophagosome in general, merely, the ability of p62 specifically to enact this function. In addition, p62 is degraded by autophagy itself and both LC3 and UBA interactions are essential for this (Pankiv et al, 2007). Furthermore, autophagy can be initiated without p62 (Itakura and Mizushima, 2011) as other proteins with PB1, LIR and UBA domains exist.

pBMN retroviruses were produced using Hek293T cells and hDF-p62^{-/-} that were on D1 of iPSC reprogramming were stably transduced thereby introducing mutant p62 protein expression on a null background at the very beginning of iPSC reprogramming. To my knowledge, and interrogation of iPSC reprogramming on cell lines expressing mutant p62 have not been carried out previously. Unfortunately, these experiments also had to be curtailed at day 6 of iPSC reprogramming. In this case, it was determined that it was not necessary to create a homogeneous population of cells for iPSC reprogramming experiments. Instead, the hope was that because the pBMN plasmids contain mCherry, the experiments would have an 'internal control' whereby we could assess in real time any differences in efficiency of iPSC reprogramming and the maintenance of pluripotency between hDF-p62^{-/-}

(untransduced cells) and cells stably transduced with the p62 overexpression mutant viruses. It would also be interesting in the future to create a pure population of the cells and carry out iPSC reprogramming, however, as we only have hDF-p62^{-/-} fibroblasts from P8 onwards, the time taken to transduce, expand and sort these would likely render them too old and senescent to be effectively reprogrammed. Perhaps a small molecule to inhibit p62, or specific p62 functions could be utilised to transiently reduce p62 expression at certain time points during the iPSC reprogramming process in order to assess the effects in a time and context dependent manner. For example, LP1-006 and XRK3F2 are both inhibitors of the p62-zz domain (Adamik et al, 2018; Li et al, 2019) which could be utilised to interrogate the specific function of the ZZ-domain during iPSC reprogramming or pluripotency.

I also cloned a truncated version of human p62 which only contains a small central portion of human p62 encompassing just the ZZ-type zinc finger region and TB domain. This truncated mutant of human p62 was successfully cloned into SFFV-lentivirus and could be used in future experiments to examine the effect of p62 in iPSC reprogramming in the absence of the PB1, KIR, LIR and UBA domains. By preventing dimerisation at the PB1 domain, autophagy targets would not be aggregated and targeted for break down (Lane et al, 2017). This could, hypothetically, lead to an accumulation of organelles and proteins in cells, which could ultimately trigger apoptosis. Apoptosis has been demonstrated as a key event in early iPSC reprogramming (Li et al, 2011). Caspases involved in apoptosis are activated by Oct4 expression and the inhibition of this process prevents iPSC reprogramming (Li et al, 2011). However, an excess of apoptosis or cell senescence can cause cell death and prevent iPSC reprogramming (Cheung et al, 2012).

Perhaps apoptosis is required in the early initiation and induction of iPSC reprogramming but can be detrimental in later stages.

In addition to the suite of human p62 genetic manipulation tools I created, I also designed and cloned a range of tools for the genetic manipulation of mouse p62 expression. Human and mouse p62 are very similar, with the same basic domain architecture and many similar phosphorylation sites. Mouse p62 shRNA was designed and cloned into pLL3.7 lentiviral vector. A mouse p62 overexpression cassette was successfully cloned into SFFV-lentiviral vector. In addition, I utilised state-of-the-art InFusion® cloning to create 3 functional mutants s24a, w340a and s351a to prevent phosphorylation occurring at these sites and therefore curbing binding interactions between p62 and itself (s24a PB1 domain mutation), LC3 (w340a LIR mutation) and KEAP1 (s351A KIR mutation). These unique mouse p62 functional mutant lentiviral vectors can be utilised in future mouse iPSC reprogramming experiments.

hDF-p62^{-/-} were characterised alongside nhDF controls using confocal microscopy of immunocytochemical staining for p62 and Lamp1. As expected, hDF-p62^{-/-} cells express no p62 protein, whereas MEFs and nhDFs are both strongly positive for p62 and Lamp1 by immunocytochemistry. Interestingly, I observed strong co-localisation between p62 and Lamp1 in nhDFs, in large aggregates suggesting fusion of autophagolysosomes containing p62 to be degraded. In contrast, in WT MEFs this co-localisation does not occur. One possible reason for this is that potentially the nhDFs were stressed at the time of PFA fixation; however, nhDFs and MEFs were cultured in the same media for the same amount of time and treated identically throughout culturing and fixing. Furthermore, in the hDF-p62^{-/-} cells, lysosomes

appeared morphologically smaller, likely due to an absence or reduction of fusion with autophagosomes because of the absence of p62.

Western blot analysis of p62 protein levels in hDF-CLN6, hDF-CLN7, nhDF and hDF-p62^{-/-} cells revealed, as expected a complete absence of p62 protein in hDF-p62^{-/-} fibroblasts. Importantly, p62 protein levels were not elevated in CLN6 or CLN7 mutant fibroblasts compared to nhDF controls in contrast to that observed in neural cell types in these Batten disease sub-types (Brandenstein et al, 2016).

hDF-p62^{-/-} fibroblasts were also assessed using MitoTracker™ compared to nhDF controls. It has previously been reported that an absence of p62 can lead to a reduction in perinuclear clustering of damaged and fragmented mitochondria (Okatsu et al, 2010), and this can be seen when comparing nhDFs to hDF-p62^{-/-}.

Mitochondrial function is dependent on a continuously changing balance of fission and fusion to manage the number and size of mitochondria based on the cells energetic needs (Seibenhener et al, 2013). When mitochondria are damaged they can lose mitochondrial membrane potential and become depolarised (Zorova et al, 2017) and fusion of mitochondria to form longer, tubular mitochondrial structures is reported to be a mechanism of recovering these damaged mitochondria and preserving their function (Twig et al, 2008). Furthermore, the fragmentation of mitochondria is directly related to dysfunctional mitochondrial bioenergetics. Alternatively, depolarised or fragmented mitochondria are also targeted for degradation by autophagy (Twig et al, 2008). Mitochondria were reported to be more fragmented in the absence of p62 in mouse fibroblasts, neurons and astrocytes and mitochondria returned to a tubular morphology when p62 was reintroduced (Seibenhener et al, 2013). However, hDF-p62^{-/-} cells appeared to display the opposite morphology, with a high number of elongated, fused mitochondria,

particularly around the nucleus compared to controls. This was intriguing, given what is reported in the literature, however, it is possible that due to impaired autophagic processing in hDF-p62^{-/-} cells damaged mitochondria are fused with healthy ones because they are not being degraded by autophagy to the same extent. Finally, Yamada et al (2018) found that mitochondria size was not altered by p62 knock-out in mouse hepatic cells, and this was true of cells in my experiments too.

Further analysis would be necessary in order to fully assess differences in mitochondria in hDF-p62^{-/-} cells compared to nhDF controls, including analysis of a much greater number of cells over multiple experiments, assessment of mitochondrial membrane potential using TMRM (Tetramethylrhodamine, Methyl Ester) and analysis of bioenergetics of both cell types using Seahorse bioanalyser. There is some debate over whether or not p62 is essential for mitochondrial clearance (Geisler et al, 2010; Okatsu et al, 2010; Arduíno et al, 2011): p62 is hypothesised to be important in the process of mitochondrial clearance, but it is possible that other similar proteins can compensate for p62 in its absence (Geisler et al, 2010). Interestingly, p62 induced degradation of mitochondria is mediated by PARKIN, and human fibroblasts express very low levels of PARKIN (Calvo-Garrido et al, 2019) which could explain the lack of mitochondrial fragmentation seen in my hDF-p62^{-/-} cells. It is necessary for the targeting of mitochondria both for ubiquitination and translocation to the autophagosome once ubiquitinated (Ni et al, 2015).

When assessing mitochondrial number size and morphology in association with p62 staining nhDFs, CLN6 and CLN7-hDFs do not appear to show a high level of co-localisation between mitochondria and p62. Intriguingly, CLN6 and CLN7-hDFs

appear to have a high number of mitochondria than nhDF control cells and hDF-p62^{-/-}, and this could be an interesting line of further investigation.

iPSC reprogramming experiments were carried out in hDF-p62^{-/-} fibroblasts compared to nhDF controls. At ~8d cells were assessed by microscopy and appeared morphologically similar: both nhDF controls and hDF-p62^{-/-} cells display clear evidence of MET, an early event in the initiation phase of iPSC reprogramming. This suggests that hDF-p62^{-/-} cells are able to initiate iPS reprogramming in the same way as nhDF control cells. Equally, when assessing very early colony formation, which generally starts to happen between ~14-18d, there are no discernible differences between hDF-p62^{-/-} cells and nhDF controls. Early colony formation is indicative of the second phase of iPSC reprogramming, maturation, during which a programme of endogenous pluripotency regulating genes begin to be 'switched-on' as a result of the forced over-expression of a select few of these genes supplied by the reprogramming plasmids (or virus/mRNA).

However, upon analysis on primary (P0) 'iPSC' colonies at day 25, clear morphological and behavioural differences became apparent. nhDF primary colonies were largely round, well-defined, strongly positive for AP and show limited amounts of partial reprogramming or early spontaneous differentiation. Of course, when reprogramming to induced pluripotency there was always some level of differentiation or incomplete reprogramming, particularly at early passages because iPSC reprogramming is a multi-step process reliant on multiple successful phases. iPSC reprogramming, as discussed in the introduction, is highly inefficient and there are multiple points during the process during which the process can falter. Even the use of four separate plasmids for iPSC reprogramming means that the chances of

cells receiving equal amounts of each one are very slim. However, in nhDF cells the appearance of incompletely reprogrammed colonies or spontaneous differentiation is low, because conditions are such that true iPSC colonies flourish. In contrast, in reprogramming experiments with hDF-p62^{-/-} cells, most primary (P0) colonies displayed signs of partial reprogramming or spontaneous differentiation. hDF-p62^{-/-} primary 'iPSC' colonies are irregular in shape, have areas where AP staining is much weaker, and there was a high level of differentiation visible. In addition, there were multiple much smaller areas of AP positive staining, possibly suggesting a high level of partial reprogramming. It seems unlikely that it is simply that hDF-p62^{-/-} cells reprogram more slowly than nhDF controls because the two cell types are so similar in the early stages of the experiments.

Macroscopic images of P0 colonies stained with AP show many more AP positive areas in the hDF-p62^{-/-} experiments than in the nhDF controls. This must not be assumed to mean a higher reprogramming efficiency in hDF-p62^{-/-}, on the contrary, most of these areas do not morphologically resemble iPSC colonies. Analysis of AP positive areas using ImageJ revealed a significantly higher number of AP+ areas in hDF-p62^{-/-} cells compared to nhDF controls. On average, there were 95 (± 8.498 S.E.M) primary (P0) nhDF iPSC colonies at 25d of three independent reprogramming experiments, whereas there were 234 (± 15.694 S.E.M) primary (P0) hDF-p62^{-/-} 'colonies'. Furthermore, the standard error of the mean was also much higher in hDF-p62^{-/-} experiments compared to control (± 15.694 compared to ± 8.498 , respectively), suggesting a higher level a variation between experiments.

hDF-p62^{-/-} 'colonies' were also significantly smaller than nhDF controls: hDF-p62^{-/-} colonies were on average 38pixels² (± 7.747 S.E.M) compared to nhDF colonies which were on average 87.53 pixels² (± 8.0194 S.E.M). Finally, P0 hDF-p62^{-/-} were

more irregular in shape than nhDF controls: only 74.4% of hDF-p62^{-/-} colonies scored higher than 0.5 for circularity compared to 95.1% on nhDF P0 colonies. All that being said, a small number of colonies (or parts of colonies) that resembled iPSC colonies were present in hDF-p62^{-/-} experiments and so these cells were passaged by manual excision in equal number to nhDF colonies. After approximately one week in culture, with daily media replenishment P1 'iPSC' colonies were again analysed for number and colony regularity. P1 colonies were analysed visually, but all images were unlabelled at the time of analysis to avoid any confirmation bias. Colony number was similar across both nhDF control and hDF-p62^{-/-} experiments, but there was a significant difference in the regularity and morphology of the colonies. In three independent nhDF derived iPSC experiments, 89.1% of colonies had the well-defined boundary surrounding the entirety of the colony that is typical of true pluripotent stem cell colonies. In contrast, only 49.1% of hDF-p62^{-/-} colonies had complete borders. All other colonies had either no well-defined border at all or at least one area where spontaneous differentiation had occurred thereby 'breaking' this border. Further passages of hDF-p62^{-/-} revealed that hDF-p62^{-/-} derived colonies were unable to retain any level of pluripotency they once had. In the representative examples shown in Chapter 5, all signs of pluripotency had been entirely lost by passage 6, but this was actually the best-case scenario achieved throughout this project. Other reprogramming experiments with hDF-p62^{-/-} cells did not survive past passage 3 (data not shown). In contrast, nhDF derived iPS colonies have been passaged upwards of 30 times during this project.

Overall these data show, for the very first time (to the best of my knowledge), that cells are unable to complete the 3rd stabilisation phase of iPSC reprogramming, achieve transgene independency or maintain pluripotency in the absence of p62.

Cells can initiate iPSC reprogramming and appear to go through the earlier phases of iPSC reprogramming in a similar fashion to nhDF controls. p62 expression has been shown to promote cell proliferation in cancer stem cells in multiple cancer types via both NFκB and NRF2 signalling (Duran et al, 2008; Komatsu et al, 2010; Duran et al; 2011; Nihira et al 2014). Further, the inhibition of p62 suppressed cell proliferation by preventing the correct formation of autophagosomes and inducing autophagic cell death (Nihira et al; 2014). These works indicate that rapid cell proliferation (as is necessary in both iPSC reprogramming, and in tumourigenesis) relies on the signalling of p62. However, a thorough literature review failed to show any published works on the effects of p62 specifically in pluripotency or iPSC reprogramming.

Further studies are needed to understand why this is and the exact mechanistic role of p62 in regulating the maintenance of pluripotency. Many planned analyses on these particular cells were made almost impossible by the fact that cells were lost or differentiated so rapidly. Firstly, just having enough cells for protein or RNA extraction made qPCR of gene transcription levels or western blot analysis extremely difficult. Secondly, if cells are not true iPSC, as it is clear they are not, then what is the value in comparing them to nhDF derived iPSC controls and does a more suitable control exist? Some analyses that would have been possible and insightful if time had allowed include analysis of gene transcription levels, bioenergetics using Seahorse bioanalyser and the use of transcription factor activated reporters throughout the iPSC process, for example at ~8d, 16d, and 22d (just before primary colony analysis). This may have provided some insight into the exact point at which iPSC reprogramming faltered in hDF-p62^{-/-} cells.

Furthermore, I had planned to gain crucial insight into the pathways and interacting partners involved in this p62-related failure to reach or maintain pluripotency by utilising the mutant overexpression vectors for human p62, which I created and validated. This would have told us whether the effect on pluripotency was due to the ability of p62 to induce autophagy (via its PB1, and LC3 domains); because of its involvement in mitochondrial remodelling and targeting for degradation; due to its UBA domain and the targeting of proteins for degradation by autophagy or a combination of these interactions. Multiple experiments had to be abandoned at short notice due to Covid-19 and the closure of the university: Dozens of iPSC reprogramming experiments (pBMN-mcherry-p62(Δ UBD) and pBMN (Δ UBD/W340A compared to controls) and several more flasks of cells which were ready to begin iPSC reprogramming (hp62-trunc overexpression; pBABE-pur-HA-p62 and pBABE-puro-HA-p62-LIR) were unfortunately never able to come to fruition. However, all of the tools I have created for the manipulation of p62 can now be utilised in future experiments both in the context of iPSC reprogramming and pluripotency, and further afield; for example in studying neurodegenerative disease.

hDF-p62^{-/-} patient cells were a kind gift from Dr Chris Carroll. The work of his research group describing and characterising these cells shows that he has looked at cells from multiple patients: however, I am unaware which of these patients the cells I have come from and therefore have no other information about the genetic profile of these cells. In order to ensure that any effect on iPSC reprogramming seen in these cells is definitely the result of an absence of p62 and not some other genetic difference in the patient cells, I designed, cloned, validated and implemented an shRNA for human p62 (sh(h)p62).

This shRNA construct contained three individual mir-based hairpins, predicted by SplashRNA algorithm to provide at least 80% knock-down as previously described. Validation experiments in Hek293T cells confirmed that sh(h)p62 resulted in an 85.21% reduction in p62 protein levels. A novel cell line (nhDF-shp62) was subjected to iPSC reprogramming alongside nhDF controls in the same manner as hDF-p62^{-/-}. hDF-p62^{-/-} cells were derived from a single patient and we did not have an isogenic control. By creating the nhDF-shp62 cell line it was possible to have cell line with significantly reduced p62 expression on the same genetic background as the nhDF control cells. Further, interrogating the effects of p62 knock-down on these cells confirmed that the results in hDF-p62^{-/-} cells were due to their lack of p62 and not some other unknown genetic differences. Further, the hDF-p62^{-/-} cells were primary fibroblasts of which only a very small number were available. Utilising the sh(h)p62 lentivirus to create nhDF-shp62 cells could be repeated at any time, providing more source material.

Much like hDF-p62^{-/-} cells, nhDF-shp62 cells appear morphologically similar to nhDF controls at both ~8d and ~16d of iPSC reprogramming. nhDF-shp62 and nhDF controls both show clear signs of MET at 8d, confirming initiation of iPSC reprogramming. Furthermore, at 18d early iPSC colony formation can be seen suggesting that cells have successfully reached the maturation phase of iPSC reprogramming. In addition, because the sh(h)p62 construct also has a GFP cassette, nhDF-shp62 cells at 18d reprogramming are strongly positive for GFP, suggesting that p62 knock-down is in effect (although it is worth remembering that the shRNA cassette and the GFP cassette are under the control of two separate promoters).

However, at 25d, much like in hDF-p62^{-/-} experiments, there are clear differences between nhDF control and nhDF-shp62 cells. Once again, primary (P0) colonies were analysed in ImageJ for number, size and shape. There were significantly more AP+ areas in nhDF-shp62 experiments than nhDF controls. On average, there were 16 P0 nhDF iPSC colonies, whereas there were 89 AP positive nhDF-shp62 'iPSC' colonies after 25d of reprogramming on average. In addition, nhDF-shp62 colonies were significantly smaller than the nhDF controls: on average nhDF derived iPSC colonies are 42.914 pixels², whereas the size of nhDF-shp62 colonies is 10.771 pixels². Finally, P0 nhDF-shp62 colonies were significantly more irregular in shape than nhDF iPSC colonies. On average nhDF iPSC colonies score 0.897 for circularity, where 1.0 is a perfect circle and nhDF-shp62 colonies score just 0.78. nhDF-shp62 derived 'iPSC' colonies behave extremely similarly to hDF-p62^{-/-} derived iPSC.

As with hDF-p62^{-/-} experiments, nhDF-shp62 derived P0 'iPSC colonies were manually passaged alongside nhDF iPSC controls. Colonies were visually analysed for colony number, regularity and morphology. Again, images were unlabelled at the time of analysis to avoid any bias. As previously described, P1 colony number was similar in both nhDF-shp62 and nhDF controls. 68.3% of nhDF iPSC colonies across three independent experiments had a well-defined border around the whole of the colony whereas only 35% of nhDF-shp62 derived colonies had complete borders. Significantly fewer nhDF-shp62 colonies were morphologically typical of iPSC colonies.

Further passaging of nhDF-shp62 derived colonies revealed a similar profile of rapid spontaneous differentiation and cell loss to that seen in hDF-p62^{-/-} experiments. In addition, analysis of GFP expression in these cells through multiple passages

revealed some very interesting results. As previously described at 18d of iPSC reprogramming, 100% of cells were GFP+. However, with subsequent passages GFP expression was reduced, particularly in those cells that were most morphologically like true iPSC cells. This could indicate that the sh(h)p62 construct was also repressed in these cells, which could explain why nhDF-shp62 derived 'iPSC' colonies survived for slightly longer than hDF-p62^{-/-} (although still never beyond passage 9). Cells that had undergone obvious spontaneous differentiation were, in general, strongly GFP+, suggesting that whatever suppression of expression of sh(h)p62 virus was reversed when cells differentiated or no longer expressed pluripotency genes.

A search of the literature failed to uncover other robust examples of this occurring; however, the Retinoblastoma gene (RB) is known to repress expression of the U6 promoter. p53 regulates expression of Rb (Shiio et al, 1992), and our iPSC reprogramming plasmids contain a shRNA for p53. It is possible, that knock-down of p53 in our reprogramming cells leads to an increase in Rb expression and thereby suppression of the U6 promoter. The sh(h)p62 construct is under control of the U6 promoter, followed by a CMV promoter controlled eGFP cassette. p62 protein levels were not assessed at the time and so it is impossible to know whether or not both GFP and sh(h)p62 expression were repressed. Hypothetically; if the shRNA was repressed and p62 expression levels were returned towards normal, this was able to rescue a pluripotent phenotype in the nhDF-shp62 cells; suggesting that p62 is crucial during the iPSC reprogramming, and that cells cannot reach transgene independency or maintain pluripotency without it. If the shRNA was not repressed, then our results continue to reflect those seen in the hDF-p62^{-/-} cells.

My nhDF-shp62 cells faithfully recapitulated the novel results seen in hDF-p62^{-/-} cells. In the absence of p62, cells are able to initiate iPSC reprogramming, and likely enter the maturation phase as well. However, cells are unable to complete the stabilisation phase of iPSC reprogramming, reach transgene independency or maintain pluripotency in the absence of p62.

Tri-lineage differentiation experiments in nhDF-shp62 derived 'iPSC' cells also indicated that it is possible that cells tend towards a neural lineage in the absence of p62. EBs formed from dissociated nhDF-shp62 'iPSC' were GFP positive and when transferred to adherent culture differentiated into cell types with diverse morphology. Cells were stained for Sox17 (an early endodermal marker) and β -III Tubulin (an early marker of neuroectoderm). Unfortunately, staining for α -smooth muscle actin, a mesodermal marker, was unsuccessful in this particular experiment and could not be repeated. Interestingly, neuroectoderm is considered the "default" differentiation lineage when exiting pluripotency (Kamiya et al, 2011) meaning that loss of p62 could be either promoting exit from pluripotency or neuroectodermal differentiation. Recent studies have shown that p62 is essential for normal neural differentiation, and the switch to oxidative phosphorylation during this process (Calvo-Garrido et al, 2019). This does suggest that perhaps an absence of p62 in my nhDF-shp62 cells is promoting an exit from pluripotency rather than differentiation to a neuronal lineage. In addition, if p62 is essential for a switch from glycolytic to oxidative phosphorylation during neuronal differentiation, it is likely that it is also essential for the switch from oxidative phosphorylation to glycolysis that happens during iPSC reprogramming. Of course, p62 is well known for its role in the response to oxidative stress (Jiang et al, 2015).

Conclusions

- I successfully reprogrammed a range of mouse and human fibroblasts to induced pluripotency using a variety of iPSC reprogramming methods.
- I created a 'tool-box' of genetic manipulation vectors for the study of p62 overexpression and knock-down in both complete and functionally mutated for9hms for use in mouse and human cells.
- sh(h)p62 mediated knockdown achieves >85% reduction in p62 protein levels.
- I characterised hDF-p62^{-/-} cells and undertook extensive iPSC reprogramming experiments and analysis into the efficiency of iPSC reprogramming in these cells as well as their inability to maintain pluripotency.
- The results seen in hDF-p62^{-/-} iPSC reprogramming were faithfully recapitulated in nhDF-shp62 cells transduced with sh(h)p62 lentivirus.
- nhDF-shp62 iPSC reprogramming and tri-lineage differentiation experiments gave some insight into the way that exit from pluripotency may be regulated by p62.

Overall, my results reveal a potential novel role for p62 in the establishment and maintenance of pluripotency as evidenced in patient cells with a complete absence in p62 protein and in nhDFs stably transduced with shRNA to reduce p62 protein levels by 86%. Future works can utilise the genetic manipulation tools I created to elucidate the exact mechanism by which p62 and its downstream interacting partners are essential for iPSC reprogramming and the maintenance of pluripotency.

References

- Abbott DW, Yang Y, Huttli JE., et al. Madhavarapu, S., Kelliher, M. A., Cantley, L. C. (2007) 'Coordinated regulation of Toll-like receptor and NOD2 signaling by K63-linked polyubiquitin chains.' *Mol Cell Biol*, 27 pp. 6012-6025. DOI: [10.1128/MCB.00270-07](https://doi.org/10.1128/MCB.00270-07)
- Aflatoonian, B., Ruban, L., Shamsuddin, S., Baker, D., Andrews, P., & Moore, H. (2010). Generation of Sheffield (Shef) human embryonic stem cell lines using a microdrop culture system. *In vitro cellular & developmental biology. Animal*, 46(3-4), 236–241. <https://doi.org/10.1007/s11626-010-9294-2>
- Alegre, F., Moragrega, Á. B., Polo, M., Marti-Rodrigo, A., Esplugues, J. V., Blas-Garcia, A., & Apostolova, N. (2018). Role of p62/SQSTM1 beyond autophagy: a lesson learned from drug-induced toxicity in vitro. *British journal of pharmacology*, 175(3), 440–455. <https://doi.org/10.1111/bph.14093>
- Andrejewski, N., Punnonen, E. L., Guhde, G., Tanaka, Y., Lüllmann-Rauch, R., Hartmann, D., von Figura, K., & Saftig, P. (1999). Normal lysosomal morphology and function in LAMP-1-deficient mice. *The Journal of biological chemistry*, 274(18), 12692–12701. <https://doi.org/10.1074/jbc.274.18.12692>
- Anokye-Danso, F., Trivedi, C. M., Jühr, D., Gupta, M., Cui, Z., Tian, Y., Zhang, Y., Yang, W., Gruber, P. J., Epstein, J. A. and Morrisey, E. E. (2011) 'Highly Efficient miRNA-Mediated Reprogramming of Mouse and Human Somatic Cells to Pluripotency.' *Cell Stem Cell*, 8(4) pp. 376-338. DOI: [10.1016/j.stem.2011.03.001](https://doi.org/10.1016/j.stem.2011.03.001)
- Arabadjiev, B., Petkova, R., Momchilova, A., Chakarov, S., & Pankov, R. (2012). Of mice and men – differential mechanisms of maintaining the undifferentiated state in mESC and hESC. *BioDiscovery*. doi:10.7750/BioDiscovery.2012.3.1
- Babu, J. R., Seibenhener, M. L., Peng, J., Strom, A.-L., Kempainen, R., Cox, N., Zhu, H., Wooten, M. C., Diaz-Meco, M. T., Moscat, J. and Wooten, M., W. (2008) 'Genetic inactivation of p62 leads to accumulation of hyperphosphorylated tau and neurodegeneration.' *Journal of Neurochemistry*, 106 pp. 107-120. DOI: [10.1111/j.1471-4159.2008.05340.x](https://doi.org/10.1111/j.1471-4159.2008.05340.x)
- Bang, J. S., Choi, N. Y., Lee, M., Ko, K., Lee, H. J., Park, Y. S., Jeong, D., Chung, H. M., & Ko, K. (2018). Optimization of episomal reprogramming for generation of human induced pluripotent stem cells from fibroblasts. *Animal cells and systems*, 22(2), 132–139. <https://doi.org/10.1080/19768354.2018.1451367>
- Barré-Sinoussi, F., & Montgutelli, X. (2015). Animal models are essential to biological research: issues and perspectives. *Future science OA*, 1(4), FSO63. <https://doi.org/10.4155/fso.15.63>
- Bertrand, M., Petit, V., Jain, A., Amsellem, R., Johansen, T., Larue, L., Codogno, P and Beau, I. (2015) 'SQSTM1/p62 regulates the expression of junctional proteins through epithelial-mesenchymal transition factors.' *Cell Cycle*, 14(3) pp. 364-374. DOI: [10.4161/15384101.2014.987619](https://doi.org/10.4161/15384101.2014.987619)
- Borger, D. K., McMahon, B., Roshan Lal, T., Serra-Vinardell, J., Aflaki, E., & Sidransky, E. (2017). Induced pluripotent stem cell models of lysosomal storage disorders. *Disease models & mechanisms*, 10(6), 691–704. <https://doi.org/10.1242/dmm.029009>
- Bragança, J., Lopes, J. A., Mendes-Silva, L. and Santos, J. M. A. (2019) 'Induced pluripotent stem cells, a giant leap for mankind therapeutic applications.' *World J Stem Cells*, 11(7) pp. 421–430. DOI: [10.4252/wjsc.v11.i7.421](https://doi.org/10.4252/wjsc.v11.i7.421)
- Brandenstein, L., Schweizer, M., Sedlacik, J., Fiehler, J. and Storch, S. (2016) 'Lysosomal dysfunction and impaired autophagy in a novel mouse model deficient for the lysosomal membrane protein Cln7.' *Human Molecular Genetics*, 25(4) pp. 777-791. DOI: [10.1093/hmg/ddv615](https://doi.org/10.1093/hmg/ddv615)

- Brown, R. A., Voit, A., Srikanth, M. P., Thayer, J. A., Kingsbury, T. J., Jacobson, M. A., Lipinski, M. M., Feldman, R. A., & Awad, O. (2019). mTOR hyperactivity mediates lysosomal dysfunction in Gaucher's disease iPSC-neuronal cells. *Disease models & mechanisms*, 12(10), dmm038596. <https://doi.org/10.1242/dmm.038596>
- Buckley, S. M., Delhove, J.M., Perocheau, D.P., Karda, R., Rahim, A.A., Howe, R., Ward, N.J., Birrell, M.A., Belvisi, M.A., Arbutnot, P., Johnson, M.R., Waddington, S.N. and McKay, T.R. (2015) 'In vivo bioimaging with tissue-specific transcription factor activated luciferase reporters.' *Scientific Reports*, 5 pp. 11842. DOI: [10.1038/srep11842](https://doi.org/10.1038/srep11842)
- Buganim, Y., Faddah, D. A., Cheng, A. W., Itskovich, E., Markoulaki, S., Ganz, K., Klemm, S. L., Oudenaarden, A. V. and Jaenisch, R. (2012) 'Single-cell gene expression analyses during cellular reprogramming reveal an early stochastic and a late hierarchic phase.' *Cell*, 150(6) pp. 1209–1222. DOI: [10.1016/j.cell.2012.08.023](https://doi.org/10.1016/j.cell.2012.08.023)
- Calvo-Garrido, J., Maffezzini, C., Schober, F., Clemente, P., Uhlin, E., Kele, M., Stranneheim, H., Lesko, N., Bruhn, H., Svenningsson, P., Falk, A., Wedell, A., Freyer, C. and Wredenberg, A. (2019) 'SQSTM1/p62-Directed Metabolic Reprogramming Is Essential for Normal Neurodifferentiation.' *Stem cell reports*. 12(4) pp. 696-711. DOI: [10.1016/j.stemcr.2019.01.023](https://doi.org/10.1016/j.stemcr.2019.01.023)
- Chagastelles, P. C. and Nardi, N. B. (2011) 'Biology of stem cells: an overview.' *Kidney Int Suppl* 1(3) pp. 63-67.
- Chandra, R. B., Ahmed, I., Ramalingam, S., Jala, V., Haribabu, B., Ramamoorthy, P., Ashcraft, J., Valentino, J., et al. (2019) 'Co-localization of autophagy-related protein p62 with cancer stem cell marker dclk1 may hamper dclk1's elimination during colon cancer development and progression.' *Oncotarget*, 10 pp. 2340-2354.
- Chandrachud, U., Walker, M.W., Simas, A.M., Heetveld, S., Petcherski, A., Klein, M., Oh, H., Wolf, P., Zhao, W.N., Norton, S., Haggarty, S.J., Lloyd-Evans, E. and Cotman, S.L. (2015) 'Unbiased Cell-based Screening in a Neuronal Cell Model of Batten Disease Highlights an Interaction between Ca²⁺ Homeostasis, Autophagy, and CLN3 Protein Function.' *Journal of Biological Chemistry*, 290 pp. 14361-14380.
- Chen, N., Eritja, N., Lock, R., & Debnath, J. (2013). Autophagy restricts proliferation driven by oncogenic phosphatidylinositol 3-kinase in three-dimensional culture. *Oncogene*, 32(20), 2543–2554. <https://doi.org/10.1038/onc.2012.277>
- Chen, H.-Y. and White, E. (2011) 'Role of Autophagy in Cancer Prevention.' *Cancer Prev Res* 4(7) pp.973-983
- Chen, Y., Li, Q., Li, Q., Xing, S., Liu, Y., Liu, Y., Chen, Y., Liu, W., et al. 'p62/SQSTM1, a Central but Unexploited Target: Advances in its Physiological/Pathogenic Functions and Small Molecular Modulators.' *Journal of Medicinal Chemistry Article* PMID: 32324396
- Christiana, F., Krause, E., Houslay, M. D. and Baillie, G. S. (2014) 'PKA phosphorylation of p62/SQSTM1 regulates PB1 domain interaction partner binding.' *Biochimica et Biophysica Acta (BBA) - Molecular Cell Research*, 1843(11) pp. 2765-2774.
- Claassen, D. A., Desler, M.M. and Rizzino, A. (2009) 'ROCK Inhibition Enhances the Recovery and Growth of Cryopreserved Human Embryonic Stem Cells and Human Induced Pluripotent Stem Cells.' *Mol Reprod Dev*, 76(8) pp. 722-732.
- Clausen, C. (2014) 'Transient p53 Suppression Increases Reprogramming of Human Fibroblasts without Affecting Apoptosis and DNA Damage.' *Stem Cell Reports*, 3(3) pp. 404–413.
- Cohen-Dvashi, H., Israeli, H., Shani, O., Katz, A., & Diskin, R. (2016). Role of LAMP1 Binding and pH Sensing by the Spike Complex of Lassa Virus. *Journal of virology*, 90(22), 10329–10338. <https://doi.org/10.1128/JVI.01624-16>

Cruvinel, E., Ogasu, I., Cerioni, R., Rodrigues, S., Gonçalves, J., Góes, M. E., Alvim, J. M., Silva, A. C., Lino, V. S., Boccardo, E., Goulart, E., Pereira, A., Dariolli, R., Valadares, M., & Biagi, D. (2020). Long-term single-cell passaging of human iPSC fully supports pluripotency and high-efficient trilineage differentiation capacity. *SAGE open medicine*, 8, 2050312120966456. <https://doi.org/10.1177/2050312120966456>

David, L. and Polo, J. M. (2014) 'Phases of reprogramming.' *Stem Cell Research*, 12(3) pp. 754-761.

Denk, H. S., Conny, Abuja, P. M. and Zatloukal, K. (2019) 'Sequestosome 1/p62-related pathways as therapeutic targets in hepatocellular carcinoma.' *Expert Opinion on Therapeutic Targets*, 23(5) pp. 393-406.

Drozd, A. M., Walczak, M. P., Piaskowski, S., Stoczynska-Fidelus, E., Rieske, P., & Grzela, D. P. (2015). Generation of human iPSCs from cells of fibroblastic and epithelial origin by means of the oriP/EBNA-1 episomal reprogramming system. *Stem cell research & therapy*, 6(1), 122. <https://doi.org/10.1186/s13287-015-0112-3>

Du, Y., Wooten, M. C., Gearing, M. and Wooten, M. W. (2009) 'Age-associated oxidative damage to the p62 promoter: implications for Alzheimer disease.' *Free Radic. Biol. Med.*, 46 pp. 492-501.

Durán, A., Serrano, M., Leitges, M., Flores, J. M., Picard, S., Brown, J. P., Moscat, J., & Diaz-Meco, M. T. (2004). The atypical PKC-interacting protein p62 is an important mediator of RANK-activated osteoclastogenesis. *Developmental cell*, 6(2), 303–309. [https://doi.org/10.1016/s1534-5807\(03\)00403-9](https://doi.org/10.1016/s1534-5807(03)00403-9)

Duran, A., Linares, J. F., Galvez, A. S., Wikenheiser, K., Flores, J. M., Diaz-Meco, M. T., & Moscat, J. (2008). The signaling adaptor p62 is an important NF-kappaB mediator in tumorigenesis. *Cancer cell*, 13(4), 343–354. <https://doi.org/10.1016/j.ccr.2008.02.001>

Duran, A., Amanchy, R., Linares, J. F., Joshi, J., Abu-Baker, S., Porollo, A., Hansen, M., Moscat, J., & Diaz-Meco, M. T. (2011). p62 is a key regulator of nutrient sensing in the mTORC1 pathway. *Molecular cell*, 44(1), 134–146. <https://doi.org/10.1016/j.molcel.2011.06.038>

Elitt, M., Barbar, L. and Tesar, P. (2018) 'Drug screening for human genetic diseases using iPSC models.' *Hum Mol Genet*, 27(R2) pp. 89-98.

Elshazzly, M., Lopez, M.J., Reddy, V., et al. Embryology, Central Nervous System. [Updated 2021 Apr 10]. In: StatPearls [Online]. Treasure Island (FL): StatPearls Publishing; 2021 Jan-. Available from: <https://www.ncbi.nlm.nih.gov/books/NBK526024/>

Ericsson, A. C., Crim, M. J., & Franklin, C. L. (2013). A brief history of animal modeling. *Missouri medicine*, 110(3), 201–205.

Fan, W., Cheng, K., Qin, X., Narsinh, K. H., Wang, S., Hu, S., Wang, Y., Chen, Y., et al. (2013) 'mTORC1 and mTORC2 Play Different Roles in the Functional Survival of Transplanted Adipose-Derived Stromal Cells in Hind Limb Ischemic Mice Via Regulating Inflammation In Vivo.' *Stem Cells*, 31 pp. 203-214.

Farkhondeh, A., Li, R., Gorshkov, K., Chen, K. G., Might, M., Rodems, S., Lo, D. C. and Zheng, W. (2019) 'Induced pluripotent stem cells for neural drug discovery ' *Drug Discovery Today*, 24(4) pp. 992-999. DOI: [10.1016/j.drudis.2019.01.007](https://doi.org/10.1016/j.drudis.2019.01.007)

Feldman, M., Apsel, B., Uotila, A., Loewith, R., Knight, Z. and al., e. (2009) 'Active-Site Inhibitors of mTOR Target Rapamycin-Resistant Outputs of mTORC1 and mTORC2.' *PLOS Biology* 7(2)

Fusaki, N., Ban, H., Nishiyama, A., Saeki, K. and Hasegawa, M. (2009) 'Efficient induction of transgene-free human pluripotent stem cells using a vector based on Sendai virus, an RNA virus that

does not integrate into the host genome.' *Proc Jpn Acad Ser B Phys Biol Sci.* , 85(8) pp. 348-362.
<https://doi.org/10.2183/pjab.85.348>

Galavotti, S. B., S, Faccenda, D., Shaked-Rabi, M., Sanzone, S., McEvoy, A., Dinsdale, D., Condorelli, F., Brandner, S., et al. (2013) 'The autophagy-associated factors DRAM1 and p62 regulate cell migration and invasion in glioblastoma stem cells.' *Oncogene*, 32 pp. pages 699–712.

Garreta, E., Sanchez, S., Lajara, J., Montserrat, N. and Belmonte, J. C. I. (2018) 'Roadblocks in the Path of iPSC to the Clinic.' *Curr Transplant Rep*, 5(1) pp. 14-18.

Geetha, T., Seibenhener, M. L., Babu, J. R., Diaz-Meco, M. T. and Moscat, J. (2005) 'The p62 Scaffold Regulates Nerve Growth Factor-induced NF- κ B Activation by Influencing TRAF6 Polyubiquitination.' *The Journal of Biological Chemistry*, 280 pp. 35625-35629.

Geisler, S., Holmstrom, K. M., Skujat, D., Fiesel, F. C., Rothfuss, O. C., Kahle, P. J. and Springer, W. (2010) 'PINK1/Parkin-mediated mitophagy is dependent on VDAC1 and p62/SQSTM1.' *Nature Cell Biology*, 12(2) pp. 119-131.

Gepstein L. Derivation and potential applications of human embryonic stem cells. *Circ Res*. 2002 Nov 15;91(10):866-76. doi: 10.1161/01.res.0000041435.95082.84.

Ginis, I., Luo, Y., Miura, T., Thies, S., Brandenberger, R., Gerecht-Nir, S., Amit, M., Hoke, A., Carpenter, M. K., Itskovitz-Eldor, J., & Rao, M. S. (2004). Differences between human and mouse embryonic stem cells. *Developmental biology*, 269(2), 360–380.
<https://doi.org/10.1016/j.ydbio.2003.12.034>

Glick, D., Barth, S. and Macleod, K. F. (2010) 'Autophagy: cellular and molecular mechanisms.' *The Journal of Pathology*, 221 pp. 3-12.

Golipour, A., David, L., Liu, Y., Jayakumaran, G., Hirsch, C. L., Trcka, D. and Wrana, J. L. (2012) 'A Late Transition in Somatic Cell Reprogramming Requires Regulators Distinct From the Pluripotency Network.' *Cell Stem Cell*, 7(11)

Ha S, Jeong SH and Yi K, e. a. 'Phosphorylation of p62 by AMP-activated protein kinase mediates autophagic cell death in adult hippocampal neural stem cells.' *J Biol Chem* . 292(33) pp. 13795-13808.

Haack, T. B., Ignatius, E., Calvo-Garrido, J., Iuso, A., Isohanni, P., Maffezzini, C., Lonngvist, T., Suomalainen, A., et al. (2016) 'Absence of the autophagy adaptor SQSTM1.p62 causes childhood-onset neurodegeneration with ataxia, dystonia and gaze palsy.' *American Journal of Human Genetics*. 99(3) pp. 735-743.

Haltia, M. and Goebel, H. H. (2013) "The neuronal ceroid-lipofuscinoses: A historical introduction." *Biochimica et Biophysica Acta (BBA)- Molecular Basis of Disease*, 1832(11) pp. 1795-1800.

Hawkins, K., Joy, S. and McKay, T. (2014) 'Cell signalling pathways underlying induced pluripotent stem cell reprogramming.' *World J Stem Cells* . , 26(5) pp. 620–628.

Hawkins, K. E., Joy, S., Delhove, J. M., Kotiadis, V. N., Fernandez, E., Fitzpatrick, L. M., Whiteford, J. R., King, P. J., Bolanos, J. P., Duchon, M. R., Waddington, S. N., & McKay, T. R. (2016). NRF2 Orchestrates the Metabolic Shift during Induced Pluripotent Stem Cell Reprogramming. *Cell reports*, 14(8), 1883–1891. <https://doi.org/10.1016/j.celrep.2016.02.003>

Ichimura Y, Komatsu M. Activation of p62/SQSTM1-Keap1-Nuclear Factor Erythroid 2-Related Factor 2 Pathway in Cancer. *Front Oncol*. 2018;8:210. Published 2018 Jun 7. doi:10.3389/fonc.2018.00210
Ichimura, Y., Kominami, E., Tanaka, K. and Komatsu, M. (2008) 'Selective turnover of p62/A170/SQSTM1 by autophagy.' *Autophagy*, 4 pp. 1063–1066.

Ichimura, Y., Kumanomidou, T., Sou, Y.-s., Mizushima, T., Ezaki, J., Ueno, T., Kominami, E., Yamane, T., et al. (2008) 'Structural Basis for Sorting Mechanism of p62 in Selective Autophagy.' *The journal of biological chemistry*, 283(33) pp. 22847-22857.

Ichimura, Y., Waguria, S., Sou, Y.-s., Kageyama, S., Hasegawa, J., Ishimura, R., Saito, T., et al. (2013) 'Phosphorylation of p62 Activates the Keap1-Nrf2 Pathway during selective autophagy.' *Molecular Cell*, 51 pp. 618-631.

Inoue, D., Suzuki, T., Mitsuishi, Y., Miki, Y., Suzuki, S., Sugawara, S., Watanabe, M., et al. (2012) 'Accumulation of p62/SQSTM1 is associated with poor prognosis in patients with lung adenocarcinoma.' *Cancer Sci*, 103 pp. 760-766.

Islam, M. A., Sooro Mopa, A. and Zhang, P. (2018) 'Autophagic Regulation of p62 is Critical for Cancer Therapy.' *Int J Mol Sci*, 19(5) p. 1405.

Itakura, E. and Mizushima, N. (2011) 'p62 targeting to the autophagosome formation site requires self-oligomerization but not LC3 binding.' *J Cell Biol.*, 192(1) pp. 17-27.

Jackson, S. A. and Sridharan, R. (2013) 'Peering into the black box of reprogramming to the pluripotent state.' *Current Pathobiology Reports*, 1(2) pp. 129-136.

Jain, A., Lamark, T., Sjøttem, E., Bowitz Larsen, K., Awuh, J. A., Øvervatn, A., McMahon, M., Hayes, J. D., et al. (2010) 'p62/SQSTM1 Is a Target Gene for Transcription Factor NRF2 and Creates a Positive Feedback Loop by Inducing Antioxidant Response Element-Driven Gene Transcription.' *J Biol Chem*, 285(29)

Johansen, T. L., T. (2011) 'Selective autophagy mediated by autophagic adapter proteins' *Autophagy* 7 pp. 279–296.

Kalkan, T., Olova, N., Roode, M., Mulas, C., Lee, H. J., Nett, I., Marks, H., Walker, R., Stunnenberg, H. G., Lilley, K. S., Nichols, J., Reik, W., Bertone, P., & Smith, A. (2017). Tracking the embryonic stem cell transition from ground state pluripotency. *Development (Cambridge, England)*, 144(7), 1221–1234. <https://doi.org/10.1242/dev.142711>

Kamiya, D. B., Satoe Sasai, Noriaki Ohgushi, Masatoshi Inomata, Hidehiko Watanabe, Kiichi Kawada, Masako Yakura, Rieko Kiyonari, Hiroshi Nakao, Kazuki Jakt, Lars Martin Nishikawa, Shin-ichi Sasai, Yoshiki. (2011) 'Intrinsic transition of embryonic stem-cell differentiation into neural progenitors.' 470 pp. 503–509.

Kansanen, E., Kuosmanen, S. M., Leinonen, H. and Levonen, A.-L. 'The Keap1-Nrf2 pathway: Mechanisms of activation and dysregulation in cancer.' *Redox Biology* 1(1) pp. 45-49.

Katsuragi, Y., Ichimura, Y. and Komatsu, M. (2015) 'p62/SQSTM1 functions as a signalling hub and an autophagy adaptor.' *FEBS*, 282(24) pp. 4672-4678.

Kiecker, C., Bates, T., & Bell, E. (2016). Molecular specification of germ layers in vertebrate embryos. *Cellular and molecular life sciences : CMLS*, 73(5), 923–947. <https://doi.org/10.1007/s00018-015-2092-y>

Kim, S.-K., Choe, J.-Y. and Park, K.-Y. (2016) 'Enhanced p62 is responsible for mitochondrial pathway-dependent apoptosis and interleukin-1 β production at the early phase by monosodium urate crystals in murine macrophage.' *Inflammation* 39 pp. 1603-1616.

Kim, J. S., Bae, G. E., Kim, K. H., Lee, S. I., Chung, C., Lee, D., Lee, T. H., Kwon, I. S., & Yeo, M. K. (2019). Prognostic Significance of LC3B and p62/SQSTM1 Expression in Gastric Adenocarcinoma. *Anticancer research*, 39(12), 6711–6722. <https://doi.org/10.21873/anticancer.13886>

Kim D, Choi BH, Ryoo IG and MK., K. (2018) 'High NRF2 level mediates cancer stem cell-like properties of aldehyde dehydrogenase (ALDH)-high ovarian cancer cells: inhibitory role of all-trans retinoic acid in ALDH/NRF2 signaling.' *Cell Death & Disease*, 9(896)

- Kinarivala, N., Morsy, A., Patel, R., Carmona, A. V., Sajib, M. S., Raut, S., Mikelis, C. M., Al-Ahmad, A., & Trippier, P. C. (2020). An iPSC-Derived Neuron Model of CLN3 Disease Facilitates Small Molecule Phenotypic Screening. *ACS pharmacology & translational science*, 3(5), 931–947. <https://doi.org/10.1021/acspsci.0c00077>
- Komatsu, M., Kurokawa, H., Waguri, S., Taguchi, K., Kobayashi, A., Ichimura, Y., Sou, Y.-S., Ueno, I., et al. (2010) 'The selective autophagy substrate p62 activates the stress responsive transcription factor Nrf2 through inactivation of Keap1.' *Nature Cell Biology* 12 pp. 213–223. <https://doi.org/10.1038/ncb2021>
- Kumari, D. (2016) 'Pluripotent stem cells: from the bench to the clinic' Chapter. States of pluripotency: Naïve and Primed Pluripotent Stem Cells DOI: 10.5772/63202
- Lane, J. D., Korolchuk, V. I., Murray, J. T., Lamark, T., Svenning, S. and Johansen, T. (2017) 'Regulation of selective autophagy: the p62/SQSTM1 paradigm.' *Essays Biochem* 61(6) pp. 609-624.
- Lau, A., Wang, X.-J., Zhao, F., Villeneuve, N. F., Wu, T., Jiang, T., Sun, Z., White, E., et al. (2010) 'A Noncanonical Mechanism of Nrf2 Activation by Autophagy Deficiency: Direct Interaction between Keap1 and p62.' *Molecular and Cellular Biology* 30(13) pp. 3275-3285.
- Lerner, C., Bitto, A., Pulliam, D., Nacarelli, T., Konigsberg, M., Van Remmen, H., Torres, C., et al. (2013) 'Reduced mammalian target of rapamycin activity facilitates mitochondrial retrograde signaling and increases life span in normal human fibroblasts.' *Aging Cell*, 12 pp. 966-977.
- Li, L., Shen, C., Nakamura, E., Ando, K., Signoretti, S., Beroukhim, R., Cowley, G. S., Lizotte, P., et al. (2013) 'SQSTM1 Is a Pathogenic Target of 5q Copy Number Gains in Kidney Cancer.' 24(6) pp. 738-750.
- Li, F., He, Z., Shen, J., Huang, Q., Li, W., Liu, X., He, Y., Wolf, F., & Li, C. Y. (2010). Apoptotic caspases regulate induction of iPSCs from human fibroblasts. *Cell stem cell*, 7(4), 508–520. <https://doi.org/10.1016/j.stem.2010.09.003>
- Lim, D., Lee, H. S., Ku, B., Shin, H.-C. and Kim, S. J. (2019) 'Oligomer Model of PB1 Domain of p62/SQSTM1 Based on Crystal Structure of Homo-Dimer and Calculation of Helical Characteristics.' *Mol Cells*, 42(10) pp. 729–738.
- Lim, J., Lachenmayer, M.L., Wu, S., Liu, W., Kundu, M., Wang, R., Komatsu, M., et al. (2015) 'Proteotoxic stress induces phosphorylation of p62/SQSTM1 by ULK1 to regulate selective autophagic clearance of protein aggregates.' *Plos Genetics*, 11(2) p. e1004987.
- Linares, J. F., Duran, A., Reina-Campos, M., Aza-Blanc, P., Campos, A., Moscat, J. and Diaz-Meco, M. T. (2015) 'Amino acid activation of mTORC1 by a PB1-domain-driven kinase complex cascade.' *Cell Rep.*, 12(8) pp. 1339–1352.
- Lippai, M. and Low, P. (2014) 'The role of the selective adaptor p62 and ubiquitin-like proteins in autophagy.' *BioMed Research International*, 2014
- Liu, W. J., Ye, L., Huang, W. F., Guo, L. J., Xu, Z. G., Wu, H. L., Yang, C. and Liu, H. F. (2016) ' p62 links the autophagy pathway and the ubiquitin–proteasome system upon ubiquitinated protein degradation.' *Cellular & Molecular Biology Letters*, 21(29)
- Long, M., Li, X., Li, L., Dodson, M., Zhang, D. D. and Zheng, H. (2017) 'Multifunctional p62 Effects Underlie Diverse Metabolic Diseases.' *Trends Endocrinol Metab*, 28(11) pp. 818-830.
- Long, J., Garner, T. P., Pandya, M. J., Craven, J., Chen, P., Shaw, B., Williamson, M. P., Layfield, R., et al. (2010) 'Dimerisation of the UBA Domain of p62 Inhibits Ubiquitin Binding and Regulates NF-κB Signalling.' 396(1) pp. 178-194.

- Lu, B., Jiao, Y., Wang, Y., Dong, J., Wei, M., Cui, B., Sun, Y., Wang, L., et al. (2017) 'A FKBP5 mutation is associated with Paget's disease of bone and enhances osteoclastogenesis.' *Experimental & Molecular Medicine*, 49 p. page e336.
- Luciani, M., Gritti, A., & Meneghini, V. (2020). Human iPSC-Based Models for the Development of Therapeutics Targeting Neurodegenerative Lysosomal Storage Diseases. *Frontiers in molecular biosciences*, 7, 224. <https://doi.org/10.3389/fmolb.2020.00224>
- Ludwig, E., Kujak, A., Rauti, A., Andrzejewski, S., Langbehn, S., Mayfield, J., Fuller, J., Yashiro, Y., et al. '20 Years of Human Pluripotent Stem Cell Research: It All Started with Five Lines.' *Tenneille* 23(5) pp. 644-648.
- Luo, R.-Z., Yuan, Z.-Y., Li, M., Xi, S.-Y., Fu, J. and He, J. (2013) 'Accumulation of p62 is associated with poor prognosis in patients with triple-negative breast cancer.' *Onco Targets Ther.* , 6 pp. 883–888.
- Ma, S., Attarwala, I. Y. and Xie, X.-Q. (2019) 'SQSTM1/p62: A Potential Target for Neurodegenerative Disease.' *ACS Chemical Neuroscience* 10(5) pp. 2094-2114.
- Ma, T., Li, J., Xu, Y., Yu, C., Xu, T., Wang, H., Liu, K., Cao, N., et al. (2015) 'Atg5-independent autophagy regulates mitochondrial clearance and is essential for iPSC reprogramming.' *Nature Cell Biology* 17 pp. 1379–1387.
- Mandai, M. W., Akira Kurimoto, Yasuo Hiram, Yasuhiko Morinaga, Chikako Daimon, Takashi Fujihara, Masashi Akimaru, Hiroshi Sakai, Noriko Shibata, Y., Terada, M. and Nomiya, Y. (2017) 'Autologous Induced Stem-Cell-Derived Retinal Cells for Macular Degeneration.' *N Engl J Med* 376 pp. 1038-1046.
- Manley, S., Williams, J. A. and Ding, W.-X. (2013) 'The Role of p62/SQSTM1 in Liver Physiology and Pathogenesis.' *Exp Biol Med (Maywood)*, 238(5) pp. 525-538.
- Martin, G.R. (1981) Isolation of a pluripotent cell line from early mouse embryos cultured in medium conditioned by teratocarcinoma stem cells. *Proc Natl Acad Sci USA*. Dec;78(12):7634-8. doi: 10.1073/pnas.78.12.7634
- Matsumoto, G., Wada, K., Okuno, M., Kurosawa, M. and Nukina, N. (2011) 'Serine 403 Phosphorylation of p62/SQSTM1 Regulates Selective Autophagic Clearance of Ubiquitinated Proteins.' *Molecular Cell*, 44 pp. 279-289.
- Menendez, J., Vellon, L., Oliveras-Ferreros, C., Cufí, S. and Vazquez-Martin, A. (2011) 'mTOR-regulated senescence and autophagy during reprogramming of somatic cells to pluripotency: a roadmap from energy metabolism to stem cell renewal and aging.' *CellCycle*, 10(21) pp. 3658-3677.
- Mitsui, S., Otomo, A., Nozaki, M., Ono, S., Sato, K., Shirakawa, R., Adachi, H., Aoki, M., et al. (2018) 'Systemic overexpression of SQSTM1/p62 accelerates disease onset in a SOD1 H46R -expressing ALS mouse model.' *Molecular Brain* 11(30)
- Mizushima, N. (2007) 'Autophagy: Process and Function.' *Genes and Development*, 21 pp. 2861-2873.
- Modo, M. (2008) 'Brain Repair How Stem Cells Are Changing Neurology.' *Bull Soc Sci Med Grand Duche Luxemb*, 2 pp. 217-257.
- Moradi, S., Mahdizadeh, H., Šarić, T., Kim, J., Harati, J., Shahsavarani, H., Greber, B. and Moore IV, J. B. (2019) 'Research and therapy with induced pluripotent stem cells (iPSCs): social, legal, and ethical considerations.' *Stem Cell Research & Therapy* 10(341)
- Moscat, J., Diaz-Meco, M. T. and Wooten, M. W. (2007) 'Signal integration and diversification through the p62 scaffold protein.' 32(2) pp. 95-100.

MRC.UKRI. (2021) UK Stem Cell Bank steering committee [Online] [Accessed 19.05.2021] <https://mrc.ukri.org/research/policies-and-guidance-for-researchers/uk-stem-cell-bank-steering-committee/>

National Academy of Sciences (US) and Institute of Medicine (US) Committee on the Use of Animals in Research. Science, Medicine, and Animals. Washington (DC): National Academies Press (US); 1991. SCIENCE, MEDICINE, AND ANIMALS. Available from: <https://www.ncbi.nlm.nih.gov/books/NBK223354/>

Nakamura, K., Kimple, A. J., Siderovski, D. P. and Johnson, G. L. (2010) 'PB1 domain Interaction of p62/Sequestosome 1 and MEKK3 Regulates NF- κ B Activation.' *Journal of Biological chemistry*, 285(3) pp. 2077-2089.

Ni, H.-M., Williams, J. A. and Ding, W.-X. (2015) 'Mitochondrial dynamics and mitochondrial quality control.' *Redox Biology*, 4 pp. 6-13.

Nihira, K., Miki, Y., Ono, K., Suzuki, T., & Sasano, H. (2014). An inhibition of p62/SQSTM1 caused autophagic cell death of several human carcinoma cells. *Cancer science*, 105(5), 568–575. <https://doi.org/10.1111/cas.12396>

Nita, D. A., Mole, S. E., & Minassian, B. A. (2016). Neuronal ceroid lipofuscinoses. *Epileptic disorders: international epilepsy journal with videotape*, 18(S2), 73–88. <https://doi.org/10.1684/epd.2016.0844>

O'Keefe, E. P. (2013) 'siRNAs and shRNAs: Tools for Protein Knockdown by Gene Silencing.' *MATER METHODS* 3(197)

Okatsu, K., Saisho, K., Shimanuki, M., Nakada, K., Shitara, H., Sou, Y. s., Kimura, M., Sato, S., et al. (2010) 'p62/SQSTM1 cooperates with Parkin for perinuclear clustering of depolarized mitochondria.' *Genes to Cells*, 15 pp. 887-900.

Okita K,M.Y., Sato Y, Okada A, Morizane A, Okamoto S, Hong H, Nakagawa M, Tanabe K, Tezuka KI, Shibata T, Kunisada T, Takahashi M, Takahashi J, Saji H, Yamanaka S. (2011) 'A more efficient method to generate integration-free human iPS cells.' *Nature Methods*, April 3 2011,

Okita, K., Yamakawa, T., Matsumura, Y., Sato, Y., Amano, N., Watanabe, A., Goshima, N., & Yamanaka, S. (2013). An efficient nonviral method to generate integration-free human-induced pluripotent stem cells from cord blood and peripheral blood cells. *Stem cells*, 1(3), 458–466. <https://doi.org/10.1002/stem.1293>

Padman, B. S. N., Thanh Ngoc Uoselis, Louise Skulsuppaisarn, Marvin Nguyen, Lan K. Lazarou, Michael. (2019) 'LC3/GABARAPs drive ubiquitin-independent recruitment of Optineurin and NDP52 to amplify mitophagy.' *Nat Commun.* , 10(408).

Pankiv, S. C., T.H. Lamark, T. Brech, A. Bruun, J. A. and Outzen, H. e. a. (2007) 'p62/SQSTM1 binds directly to Atg8/ LC3 to facilitate degradation of ubiquitinated protein aggregates by autophagy.' *J Biol Chem* 282 pp. 24131–24145.

Pankiv, S., Lamark, T., Bruun, J., Øvervatn, A., Bjørkøy, G. and Johansen, T. (2010) 'Nucleocytoplasmic shuttling of p62/SQSTM1 and its role in recruitment of nuclear polyubiquitinated proteins to promyelocytic leukemia bodies.' *J Biol Chem.*, 285(8) pp. 5941-5953.

Peng, H., Yang, J., Li, G., You, Q., Han, W., Li, T., Gao, D., Xie, X., et al. (2017) 'Ubiquitylation of p62/sequestosome1 activates its autophagy receptor function and controls selective autophagy upon ubiquitin stress.' *Cell Research*, 27 pp. 657 -674.

Pollizzi, K. N., Patel, C. H., Sun, I.-H., Oh, M.-H., Waickman, A. T., Wen, J., Delgoffe, G. M. and Powell, J. D. (2015) 'mTORC1 and mTORC2 selectively regulate CD8+ T cell differentiation.' *J Clin Invest.* , 125(5) pp. 2090-2108.

- Pölönen, P., Deen, A. J., Leinonen, H. M., Jyrkkänen, H.-K., Kuosmanen, S., Mononen, M., Jain, A., Tuomainen, T., et al. (2019) 'Nrf2 and SQSTM1/p62 Jointly Contribute to Mesenchymal Transition and Invasion in Glioblastoma.' *Oncogene*, 38(50)
- Pun, N. J., Park and P-H. (2017) 'Role of p62 in the suppression of inflammatory cytokine production by adiponectin in macrophages: involvement of autophagy and p21/Nrf2 axis.' *Scientific Reports*, 393
- Rahman, M., Jamil, H., Akhtar, N., Rahman, K., Islam, R. and Asaduzzaman, S. (2016) 'STEM CELL AND CANCER STEM CELL: A Tale of Two Cells.' *Progress in Stem Cell*, 3(2) pp. 97-108.
- Pelossof, R., Fairchild, L., Huang, CH. et al. Prediction of potent shRNAs with a sequential classification algorithm. *Nat Biotechnol* 35, 350–353 (2017). <https://doi.org/10.1038/nbt.3807>
- Ras, T., Jere, W., Parinya, N., Taneli, R. and Timo, O. 'Combined negative effect of donor age and time in culture on the reprogramming efficiency into induced pluripotent stem cells.' *Stem Cell Research*, 15(1) pp. 254-262.
- Richard, S., Yu, D., Blumer, K. J., Hausladen, D., Olszowy, M. W., Connelly, P. A., & Shaw, A. S. (1995). Association of p62, a multifunctional SH2- and SH3-domain-binding protein, with src family tyrosine kinases, Grb2, and phospholipase C gamma-1. *Molecular and cellular biology*, 15(1), 186–197. <https://doi.org/10.1128/MCB.15.1.186>
- Riz, I., Hawley, T. S., Marsal, J. W. and Hawley, R. G. 'Noncanonical SQSTM1/p62-Nrf2 pathway activation mediates proteasome inhibitor resistance in multiple myeloma cells via redox, metabolic and translational reprogramming.' *Oncotarget*, 7 pp. 66360-66385.
- Rodriguez, A., Durán, A., Selloum, M., Champy, M.-F., Diez-Guerra, F., J. , Flores, J. M., Serrano, M., et al. (2006) 'Mature-onset obesity and insulin resistance in mice deficient in the signaling adapter p62.' *Cell Metab*, 3 pp. 211-222.
- Rossant, J., & Tam, P. (2017). New Insights into Early Human Development: Lessons for Stem Cell Derivation and Differentiation. *Cell stem cell*, 20(1), 18–28. <https://doi.org/10.1016/j.stem.2016.12.004>
- Roy BC, A. I., Ramalingam S, et al. (2019) 'Co-localization of autophagy-related protein p62 with cancer stem cell marker dclk1 may hamper dclk1's elimination during colon cancer development and progression.' *Oncotarget* . , 10(24) pp. 2340–2354.
- Rubinson DA, D. C., Kwiatkowski AV, Sievers C, Yang L, Kopinja J, Rooney DL, Ihrig MM, McManus MT, Gertler FB, Scott ML, Van Parijs L. . (2003) 'A lentivirus-based system to functionally silence genes in primary mammalian cells, stem cells and transgenic mice by RNA interference. . ' *Nature Genetics*, 33(3) pp. 401-406.
- Ryoo, I.-g. C., Bo-hyun, Ku, S.-K. and Kwak, M.-K. (2018) 'expression mediates p62-associated NFE2L2/NRF2 activation in breast cancer stem cell-like cells: Implications for cancer stem cell resistance.' *Redox Biol*. 17 pp. 246–258.
- Saito, T., Ichimura, Y., Taguchi, K., Suzuki, T., Mizushima, T., Takagi, K., Hirose, Y., Nagahashi, M., et al. (2016) 'p62/Sqstm1 Promotes Malignancy of HCV-positive Hepatocellular Carcinoma Through Nrf2-dependent Metabolic Reprogramming.' *Nat Commun*, 27(7:12030)
- Salminen, A., Kaarniranta, K., Haapasalo, A., Hiltunen, M., Soininen, H. and Alafuzoffbe, I. (2012) 'Emerging role of p62/sequestosome-1 in the pathogenesis of Alzheimer's disease.' *Progress in Neurobiology*, 96(1) pp. Pages 87-95.
- Samavarchi-Tehrani, P., Golipour, A., David, L., Sung, H.-K., Beyer, T. A., Datti, A., Woltjen, K., Nagy, A., et al. (2010) 'Functional Genomics Reveals a BMP-driven Mesenchymal-To-Epithelial Transition in the Initiation of Somatic Cell Reprogramming.' *Cell Stem Cell*, 7(1) pp. 64-77.
- Sánchez-Martín , P. K., Masaaki. (2018) 'p62/SQSTM1 – steering the cell through health and disease.' *Journal of Cell Science* 131(jcs222836)

- Sánchez-Martín, P., Saito, T. and Komatsu, M. (2019) 'p62/SQSTM 1: 'Jack of all trades' in health and cancer. ' *FEBS J*, 286 pp. 8-23.
- Sanz, L., Diaz-Meco, M. T., Nakano, H., & Moscat, J. (2000). The atypical PKC-interacting protein p62 channels NF-kappaB activation by the IL-1-TRAF6 pathway. *The EMBO journal*, 19(7), 1576–1586. <https://doi.org/10.1093/emboj/19.7.1576>
- Schlaeger, T. M., Daheron, L., Brickler, T. R., Entwisle, S., Chan, K., Cianci, A., DeVine, A., Ettenger, A., Fitzgerald, K., Godfrey, M., Gupta, D., McPherson, J., Malwadkar, P., Gupta, M., Bell, B., Doi, A., Jung, N., Li, X., Lynes, M. S., Brookes, E., ... Daley, G. Q. (2015). A comparison of non-integrating reprogramming methods. *Nature biotechnology*, 33(1), 58–63. <https://doi.org/10.1038/nbt.3070>
- Schimmack, G., Schorpp, K., Kutzner, K., Gehring, T., Brenke, J. K., Hadian, K. and Krappmann, D. 'YOD1/TRAF6 association balances p62-dependent IL-1 signaling to NF-κB.' *Institute of Molecular Toxicology and Pharmacology, Helmholtz Zentrum München – German Research Center for Environmental Health, Germany*,
- Schnerch, A., Cerdan, C., & Bhatia, M. (2010). Distinguishing between mouse and human pluripotent stem cell regulation: the best laid plans of mice and men. *Stem cells (Dayton, Ohio)*, 28(3), 419–430. <https://doi.org/10.1002/stem.298>
- Sergin, I., Bhattacharya, S., Emanuel, R., Esen, E., Stokes, C. J., Evans, T. D., Arif, B., Curci, J. A., & Razani, B. (2016). Inclusion bodies enriched for p62 and polyubiquitinated proteins in macrophages protect against atherosclerosis. *Science signaling*, 9(409), ra2. <https://doi.org/10.1126/scisignal.aad5614>
- Shackleton, M. (2010) 'Normal stem cells and cancer stem cells: similar and different.' *Seminars in Cancer Biology*, 20(2)
- Shaw, B., Burrell, C. L., Darrell Green, Navarro-Martinez, A., Scott, D., Daroszewska, A., Hof, R. v. t., Smith, L., et al. (2019) 'Molecular insights into an ancient form of Paget's disease of bone.' *Proc Natl Acad Sci USA*, 116(21) pp. 10463-10472.
- Shiio, Y., Yamamoto, T. and Yamaguchi, N. (1992) 'Negative regulation of Rb expression by the p53 gene product. ' *Proc Natl Acad Sci U S A* , 12 pp. 5206-5210.
- Short, B. (2016) 'p62 aggregation is a problem for neural stem cells.' *J Cell Biol* 212(5) p. 482.
- Singh, V. K., Kalsan, M., Kumar, N., Saini, A., & Chandra, R. (2015). Induced pluripotent stem cells: applications in regenerative medicine, disease modeling, and drug discovery. *Frontiers in cell and developmental biology*, 3, 2. <https://doi.org/10.3389/fcell.2015.00002>
- Singovski, G., Bernal, C., Kuciak, M., Siegl-Cachedenier, I., Conod, A., & Ruiz i Altaba, A. (2016). In vivo epigenetic reprogramming of primary human colon cancer cells enhances metastases. *Journal of molecular cell biology*, 8(2), 157–173. <https://doi.org/10.1093/jmcb/mjv034>
- Sommer, C. A., Stadtfeld, M., Murphy, G. J., Hochedlinger, K., Kotton, D. N. and Mostoslavsky, G. (2009) 'Induced Pluripotent Stem Cell Generation Using a Single Lentiviral Stem Cell Cassette.' *Stem Cells*, 27(3) pp. 543-549.
- Stadtfeld, M., Nagaya, M., Utikal, J., Weir, G. and Hochedlinger, K. (2008) 'Induced Pluripotent Stem Cells Generated Without Viral Integration.' *Science*, 7(322) pp. 945-949.
- Stadtfeld, M., Maherali, N., Borkent, M., & Hochedlinger, K. (2010). A reprogrammable mouse strain from gene-targeted embryonic stem cells. *Nature methods*, 7(1), 53–55. <https://doi.org/10.1038/nmeth.1409>

Stewart SA, D. D., Palliser D, Mizuno H, Yu EY, An DS, Sabatini DM, Chen IS, Hahn WC, Sharp PA, Weinberg RA, Novina CD. (2003) 'Lentivirus-delivered stable gene silencing by RNAi in primary cells.' *RNA*, 9(4) pp. 493-501.

Sugiyama M, Yoshizumi T and Yoshida Y, e. a. (2016) 'p62 Promotes Amino Acid Sensitivity of mTOR Pathway and Hepatic Differentiation in Adult Liver Stem/Progenitor Cells: p62 regulates liver stem cell differentiation.' *Journal of Cellular Physiology*, 232(10)

Sumimoto, H., Kamakura, S. and Ito, T. (2007) 'Structure and Function of the PB1 Domain, a Protein Interaction Module Conserved in Animals, Fungi, Amoebas, and Plants.' *Science's STKE* 401(6)

Sun A. (2018). Lysosomal storage disease overview. *Annals of translational medicine*, 6(24), 476. <https://doi.org/10.21037/atm.2018.11.39>

Takahashi K, Y. S. (2006) 'Induction of pluripotent stem cells from mouse embryonic and adult fibroblast cultures by defined factors.' *Cell*, 126, 2006 Aug 25, Epub 2006 Aug 10., pp. 663-676.

Takahashi K, T. K., Ohnuki M, Narita M, Ichisaka T, Tomoda K, Yamanaka S. (2007) 'Induction of pluripotent stem cells from adult human fibroblasts by defined factors.' *Cell.*, 131 2007 Nov 30;, pp. 861-872.

Thomas, P and TG, S. (2005) 'HEK293 cell line: a vehicle for the expression of recombinant proteins.' *Pharmacol Toxicol Methods*, 51(3) pp. 187-200.

Thomson, J. A., Itskovitz-Eldor, J., Shapiro, S. S., Waknitz, M. A., Swiergiel, J. J., Marshall, V. S. and Jones, J. M. (1998) 'Embryonic Stem Cell Lines Derived from Human Blastocysts.' *Science*, 282(5391) pp. 1145-1147.

Twig, G., Elorza, A., Molina, A. J. A., Mohamed, H., Wikstrom, J. D., Walzer, G., Stiles, L., Haigh, S. E., et al. (2008) 'Fission and selective fusion govern mitochondrial segregation and elimination by autophagy.' *EMBO J* 27 pp. 433-446.

Umemura, A., He, F., Taniguchi, K., Nakagawa, H., Yamachika, S., Font-Burgada, J., Zhong, Z., Subramaniam, S., et al. (2016) 'p62, Upregulated during Preneoplasia, Induces Hepatocellular Carcinogenesis by Maintaining Survival of Stressed HCC-Initiating Cells.' 29(6) pp. Pages 935-948.

Vadlamudi, R.K. and Shin, J. (1998) 'Genomic structure and promoter analysis of the p62 gene encoding a non-proteasomal multiubiquitin chain binding protein.' *FEBS Letters*, 435

Valencia, T., Kim, J. Y., Abu-Baker, S., Moscat-Pardos, J., Ahn, C. S., Reina-Campos, M., Duran, A., Castilla, E. A., et al. (2014) 'Metabolic Reprogramming of Stromal Fibroblasts through p62-mTORC1 Signaling Promotes Inflammation and Tumorigenesis.' 26(1) pp. 121-135.

Vanneaux, V. (2019) 'Induced Pluripotent Stem Cells for Clinical Use.' *Open access peer-reviewed chapter*,

Vazin, T. and Freed, W. J. (2010) 'Human embryonic stem cells: Derivation, culture, and differentiation: A review.' *Restor Neurol Neurosci.* , 28(4) pp. 589–603.

Wang, S., Xia, P., Ye, B., Huang, G., Liu, J. and Fan, Z. (2013) 'Transient Activation of Autophagy via Sox2-Mediated Suppression of mTOR Is an Important Early Step in Reprogramming to Pluripotency.' *Cell Stem Cell*, 13(5) pp. 617-625.

Wang C, Chen S and Yeo S, e. a. (2016) ' p62/SQSTM1 determines the fate of autophagy-deficient neural stem cells by increasing superoxide.' 212(5) pp. 545-560.

Wang, K., & Klionsky, D. J. (2011). Mitochondria removal by autophagy. *Autophagy*, 7(3), 297–300. <https://doi.org/10.4161/auto.7.3.14502>

Warren, L., Manos, P. D., Ahfeldt, T., Loh, Y. H., Li, H., Lau, F., Ebina, W., Mandal, P. K., Smith, Z. D., Meissner, A., Daley, G. Q., Brack, A. S., Collins, J. J., Cowan, C., Schlaeger, T. M., & Rossi, D. J. (2010). Highly efficient reprogramming to pluripotency and directed differentiation of human cells with synthetic modified mRNA. *Cell stem cell*, 7(5), 618–630. <https://doi.org/10.1016/j.stem.2010.08.012>

Wiegand, C. and Banerjee, I. (2019) 'Recent advances in the applications of iPSC technology.' *Current Opinion in Biotechnology*, 60 pp. 250-258.

Woltjen, K., Michael, I., Mohseni, P. et al. (2009) 'piggyBac transposition reprograms fibroblasts to induced pluripotent stem cells'. *Nature* 458, 766–770. <https://doi.org/10.1038/nature07863>

Wong, P. K., Chapman, E. and Zhang, D. D. 'p62 links autophagy and Nrf2 signaling.' *Free Radical Biology and Medicine*, 88(B) pp. 199-204.

Wu, Y., Li, Y., Zhang, H., Huang, Y., Zhao, P., Tang, Y., Qiu, X., et al. (2015) 'Autophagy and mTORC1 regulate the stochastic phase of somatic cell reprogramming.' *Nature Cell Biology*, 17(6) pp. 715-725.

Xia, M. p. c. M. s. m.-t. c., Yu, H., et al. (2014) 'p62/SQSTM1 is involved in cisplatin resistance in human ovarian cancer cells via the Keap1-Nrf2-ARE system.' *Journal of Oncology*, pp. 2341-2348.

Xiaolong, L., Shuang, L., Yue, Z., Xiaofeng, M., Kai, Z., Xinglan, H. and Zuo, W. 'Interaction Domains of p62: A Bridge Between p62 and Selective Autophagy.' *DNA AND CELL BIOLOGY*, 32(5) pp. 220-227.

Xu, L.-Z., Li, S.-S., Zhou, W., Kang, Z.-J., Zhang, Q.-X., Kamran, M., Xu, J., Liang, D.-P., et al. (2017) 'p62/SQSTM1 enhances breast cancer stem-like properties by stabilizing MYC mRNA.' *Oncogene* 36 pp. 304-317.

Yamada, T., Murata, D., Adachi, Y., Kieltoh, Kameoka, Atsushilgarashi, S., Kato, T., Araki, Y., et al. (2018) 'Mitochondrial Stasis Reveals p62-Mediated Ubiquitination in Parkin-Independent Mitophagy and Mitigates Nonalcoholic Fatty Liver Disease.' 28(4) pp. 588-604.e585.

Yan, X. Y., Zhong, X. R., Yu, S. H., Zhang, L. C., Liu, Y. N., Zhang, Y., Sun, L. K., & Su, J. (2019). p62 aggregates mediated Caspase 8 activation is responsible for progression of ovarian cancer. *Journal of cellular and molecular medicine*, 23(6), 4030–4042. <https://doi.org/10.1111/jcmm.14288>

Yu, J., Vodyanik, M., Smuga-Otto, K. and al., e. (2007) 'Induced pluripotent stem cell lines derived from human somatic cells.' *Science*, 318(5858) pp. 1917-1920.

Yu, Z., Pestell, T. G., Lisanti, M. P. and Pestell, R. G. (2012) 'Cancer Stem Cells.' *Int J Biochem Cell Biol.*, 4(12) pp. 2144–2151.

Yu, J., Hu, K., Smuga-Otto, K., Tian, S., Stewart, R., Slukvin, I. I. and Thomson, J. A. (2009) 'Human Induced Pluripotent Stem Cells Free of Vector and Transgene Sequences.' *Science*, 324(5928) pp. 797–801.

Zach, F., Polzer, F., Mueller, A. and Gessner, A. (2018) 'p62/sequestosome1 deficiency accelerates osteoclastogenesis *in vitro* and leads to Paget's disease-like bone phenotypes in mice.' *The Journal of Biological Chemistry*, 293 pp. 9530-9541.

Zakrzewski, W., Dobrzyński, M., Szymonowicz, M., & Rybak, Z. (2019). Stem cells: past, present, and future. *Stem cell research & therapy*, 10(1), 68. <https://doi.org/10.1186/s13287-019-1165-5>

Zhang, Y., Mun, S. R., Linares, J. F., Ahn, J., Towers, C. G., Ji, C. H., Fitzwalter, B. E., Holden, M. R., Mi, W., Shi, X., Moscat, J., Thorburn, A., Diaz-Meco, M. T., Kwon, Y. T., & Kutateladze, T. G. (2018). ZZ-dependent regulation of p62/SQSTM1 in autophagy. *Nature communications*, 9(1), 4373. <https://doi.org/10.1038/s41467-018-06878-8>

Zhang, Y., Yu, Z., Jiang, D., Liang, X., Liao, S., Zhang, Z., Yue, W., Li, X., Chiu, S. M., Chai, Y. H., Liang, Y., Chow, Y., Han, S., Xu, A., Tse, H. F., & Lian, Q. (2016). iPSC-MSCs with High Intrinsic

MIRO1 and Sensitivity to TNF- α Yield Efficacious Mitochondrial Transfer to Rescue Anthracycline-Induced Cardiomyopathy. *Stem cell reports*, 7(4), 749–763.
<https://doi.org/10.1016/j.stemcr.2016.08.009>

Zhang, S., Xie, Y., Cao, H. et al. (2017) 'Common microRNA–mRNA interactions exist among distinct porcine iPSC lines independent of their metastable pluripotent states.' *Cell Death Dis* 8, e3027 (2017). <https://doi.org/10.1038/cddis.2017.426>

Zhou, H., Wu, S., Joo, J. Y., Zhu, S., Han, D. W., Lin, T., Trauger, S., Bien, G., et al. (2009) 'Generation of Induced Pluripotent Stem Cells Using Recombinant Proteins.' 4(5)

Zorova, L., Popkov, V., Plotnikov, E. and al., e. (2018) 'Mitochondrial membrane potential.' *Anal Biochem.* , 552 pp. 50-59.

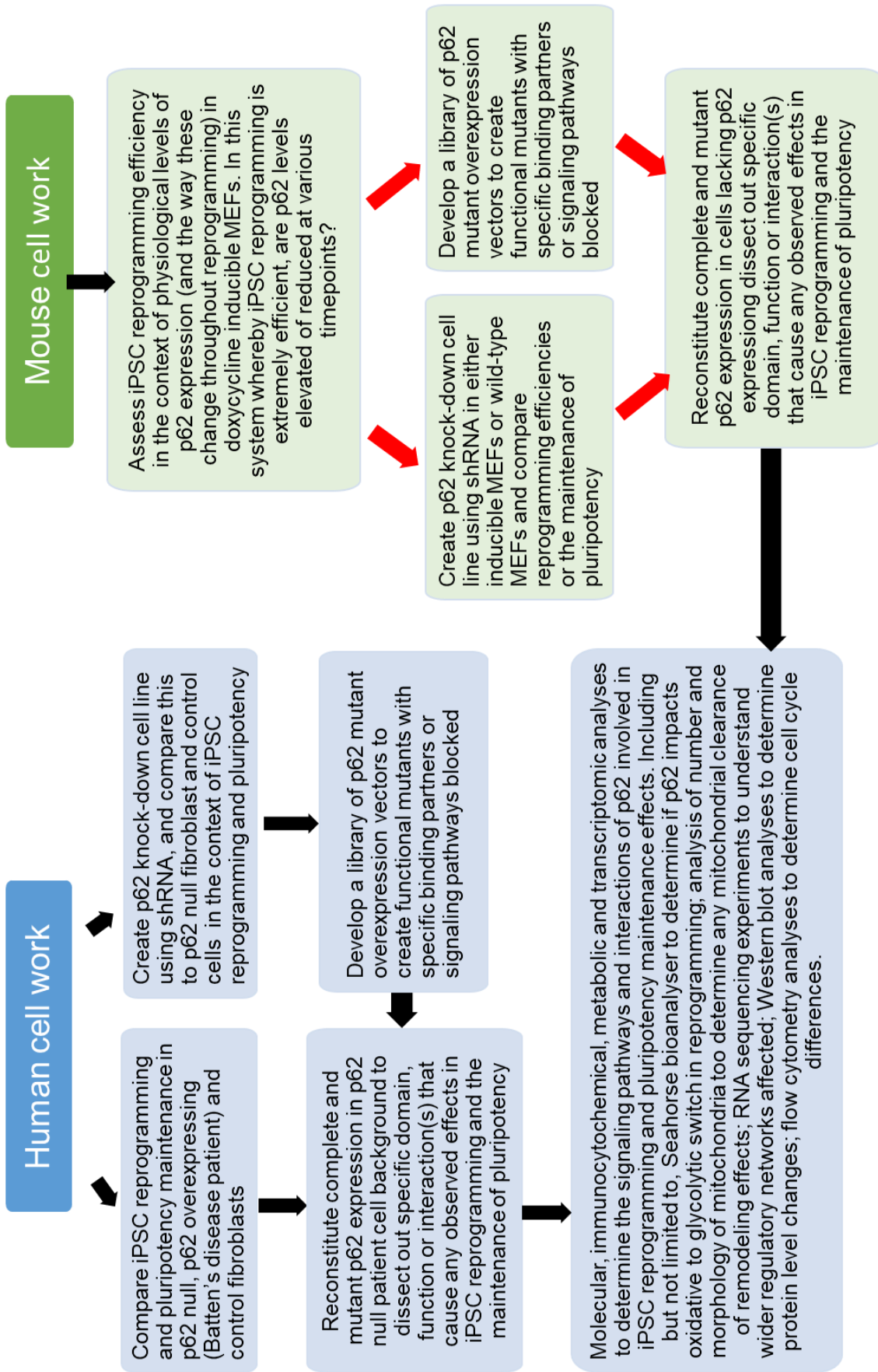
Zottia, T., Scudiero, I., Settembre, P., Ferravante, A., Mazzone, P., Andrea, L., Reale, C., Vitob, P., et al. (2014) 'TRAF6-mediated ubiquitination of NEMO requires p62/sequestosome-1.' *Molecular Immunology*, 58(1) pp. 27-31.

Appendix 1: List of Abbreviations

ALS:	Amyotrophic Lateral Sclerosis
AMPK:	AMP-activated protein kinase
aPKC:	atypical protein kinase C
Atg:	autophagy related genes
Cas9:.....	CRISPR associated protein 9
CD44:	cluster of differentiation
CK2:	Casein Kinase 2
CRISPR:	Clustered regularly interspaced short palindromic repeats
CSC:	Cancer stem cells
ERK:	extracellular signal related kinase
ESCs:	Embryonic stem cells
GMP:	Good Manufacturing Practise
hESCs:	human ESCs
ICM:	inner cell mass
IL-1:	Interleukin-1
iPSC:	induced pluripotent stem cells
IRS-1:	insulin receptor substrate 1
KIR:	Keap1 interacting region
KLF4:	Kruppel-like factor
LC3-II:	microtubule-associated protein light chain 3
LIR:	LC3 interacting region
LRS:	LC3 recognition sequence
LSD:.....	Lysosomal storage disorders
MEKK3:	Mitogen Activated protein kinase 3
MET:	mesenchymal to epithelial
mRNA:	messenger RNA
mTORC1:	mechanistic target of rapamycin complex 1
NBR1:	Neighbour of BRCA 1
NCL:	neuronal ceroid lipofuscinosis
NES:	nuclear export signal
NF-KB:	Nuclear Factor kappa-light-chain-enhancer of activated B cells
NGF:	nerve growth factor
NLS:	nuclear localisation signals
NRF2-Keap1:	nuclear factor erythroid 2–related factor 2, Kelch Like ECH Associated Protein 1
NSC:	neural stem cells
Oct4:	octamer-binding transcription factor 4
PB1:	Phox-BEM1
PDE4:	Phosphodiesterase-4
PKA:	cAMP dependent protein kinase

PKC: atypical protein kinase C
 RANKL: Receptor Activator of NF- κ B ligand
 RIP1: Receptor-interacting serine/threonine-protein kinase 1
 ROS: neutralisation of reactive oxygen species, 35; reactive oxygen species
 RPE:Retinal pigment epithelium
 shRNA: short hairpin RNA
 SOX2: sex determining region Y-box 2
 TALENS.....Transcription activator like effector nuclease
 TB: binding region, 28; TRAF6 binding region
 TFAR:.....Transcription factor activated reporter
 TFEB:.....Transcription factor EB
 TNBC: triple-negative breast cancer
 TNF: Tumour necrosis factor
 Traf6: TNF receptor-associated factor 6
 UBA: Ubiquitin associated
 ULK: Unc-51 like kinase
 ZZ: zinc finger region

Appendix 2: Summary of project aims and objectives in human and mouse cells.



Appendix 3: Cell culture media components

Media	Components	Amount/Final concentration	Supplier
hDF/MEF media	Dulbecco's Modified Eagle's Medium (DMEM) with 4.5 g/L Glucose, without L-Glutamine	450 mL	Lonza, BE12-614F
	FBS	10% (50 mL)	Gibco™ 10270106
	L-glutamine	2 mM	Lonza, BE17-605E
	Penicillin/Streptomycin	50 µg/mL	Lonza, DE17-603E
	Plasmocin or Mycozap	10 µM	Invivogen, ant-mpp Lonza, VZA-2032
hESC/hiPSC feeder culture media	DMEM/F12	45 mL	Gibco, 10565-018
	Knock-Out serum replacement	20% (9 mL)	Fisher Scientific UK, 11520366
	Fibroblast growth factor (FGF)	5 µg/ mL	Peprotech, 100-18B
	Penicillin/Streptomycin	50 µg/mL	Lonza, DE17-603E
	β- Mercaptoethanol (BME)	0.1 mM	Gibco, 31350-010
	Non-essential amino acids (NEAA)	1 mL / 100 mL of media	Gibco, 11140-050
hESC/hiPSC feeder free culture media	mTeSR™1 + Supplement	As supplied	Stem cell technologies, 85850
Inducible MEF maintenance media	DMEM with 4.5 g/L Glucose, without L-Glutamine	450 mL	Lonza, BE12-614F
	FBS	10% (50 mL)	Gibco™ 10270106
	L-glutamine	2 mM	Lonza, BE17-605E
	NEAA	1 mL / 100 mL of media	Gibco, 11140-050
	BME	55 µM	Gibco, 31350-010
Inducible MEF reprogramming media	Knock-out DMEM	400 mL	
	FBS	20% (100 mL)	Gibco™ 10270106
	L-glutamine	2 mM	Lonza, BE17-605E
	NEAA	1 mL / 100 mL of media	Gibco, 11140-050
	Ascorbic Acid	5 µg/ mL	
	mLIF	1000 units/ mL	
	Doxycycline	2 µg/ mL	
Induced miPS maintenance media	Knock-out DMEM	400 mL	
	FBS	20% (100 mL)	Gibco™ 10270106
	L-glutamine	2 mM	Lonza, BE17-605E
	NEAA	1 mL / 100 mL of media	Gibco, 11140-050
	mLIF	1000 units/ mL	
mESC/miPSC maintenance media	DMEM with 4.5 g/L Glucose, without L-Glutamine	42.5 mL	Lonza, BE12-614F
	FBS	15%	Gibco™ 10270106
	L-glutamine	2 mM	Lonza, BE17-605E
	Penicillin/Streptomycin	50 µg/mL	Lonza, DE17-603E
	NEAA	1 mL / 100 mL of media	Gibco, 11140-050
	β- Mercaptoethanol (BME)	0.1 mM	Gibco, 31350-010
	mLIF	1000 units/ mL	
Freeze media	DMSO	90%	Fisher Scientific, BP231-100
	FBS	10%	Gibco™ 10270106

Appendix 4: anti-p62 antibody data sheet

Product datasheet

Anti-SQSTM1 / p62 antibody - Autophagosome Marker ab56416

KO VALIDATED

★★★★★ 31 Abreviews 434 References 4 Images

Overview

Product name	Anti-SQSTM1 / p62 antibody - Autophagosome Marker
Description	Mouse monoclonal to SQSTM1 / p62 - Autophagosome Marker
Host species	Mouse
Tested applications	Suitable for: IHC-P, WB, ICC/IF, Flow Cyt, IHC-Fr
Species reactivity	Reacts with: Mouse, Rat, Human, Rhesus monkey
Immunogen	Recombinant full length protein corresponding to Human SQSTM1/ p62 aa 1-440. Database link: Q13501
Positive control	WB: HeLa, Hap1. Flow Cyt: HeLa. IHC-P: Human lymph node. ICC/IF: HeLa
General notes	This product was changed from ascites to tissue culture supernatant on 28 th May 2019. Please note that the dilutions may need to be adjusted accordingly. If you have any questions, please do not hesitate to contact our scientific support team.

Appendix 5: PCR and cloning primers. Orange portions represent restriction sites.

Mouse p62 forward primer	TATCGGATTCATGGCGTCGTTACGGTGAAG
Mouse p62 reverse primer 1	GATCGAATTCCTAAACCTTATCGGTCGTCATCCTTG
Mouse p62 reverse primer 2	GATCGAATTCCTAAACCTTATCGGTCGTCATCCTTGTAATCC
Human p62 forward primer	GATCGGTACCGATCATGGCGTCGC
Human p62 reverse primer	GATCGAATTCGATCTCACAACGGCGGGGGATGCT

Appendix 6: In-Fusion® cloning primers. Orange portions represent key mutation sites

Human p62	
<i>KpnI</i> .hP62.Forward	AGTCGACTGGATCCGGTACCATGGCGTCGCTC
<i>EcoRI</i> .hP62.Reverse	GTGCGGCCGCGAATTCTCACAACGGCGG
K7A.Forward	AGTCGACTGGATCCGGTACCATGGCGTCGCTCACCGTGgcgGCCTACCTTCTGGG
<i>ClaI</i> .T269A.Forward	TTGAAGTTGATATCGATGTGGAGCACGGAGGGAAAAGAAGCCGCC TGgcgCCCGTCTCTCC
S403.Reverse	TCAGAGAAGCCCATGGcCAGCATCTGG
Mouse p62	
<i>BglII</i> .P62.Forward	GGTACCGAGGAGATCTATGGCGTCGTTACG
<i>MluI</i> .P62.Reverse	GCGGCCGCGTACGCGTCAATGGTGGAGGGTGCTTCGAATACTGG
<i>BglII</i> .S024.Forward	GGTACCGAGGAGATCTATGGCGTCGTTACGGTGaagGCCTATCTTCTGGGC AAGGAGGAGGCGACCCGCGAGATCCGCCGCTTCGCTTTCTGCTTCAGCCCG GA
<i>XbaI</i> .W340.Reverse	CTGTGAGGGGTCTAGAGAGCTTGGCCCTTCGATTCTGGCATCTGTAGAGA CTGGAGTTCACCTGTAGaTGGGTCCACTTCTTTGAAGACAAATGTGTagcGT CATCGTCTC
<i>XbaI</i> .S351.Reverse	CTGTGAGGGGTCTAGAGAGCTTGGCCCTTCGATTCTGGCATCTGTAGAGA CTGGAGTTCACCTGTAGcTGGGTCCACTTC
mP62.subclone.Forward	ATCCGGTACCGAATTATGGCGTCGTTACGGTGAAGGC
mp62.subclone.Reverse	GTGCGGCCGCGAATTCAGGAAACAGCTATGACCGCG